Toward Safe Control under Uncertainty: Adaptation and Prediction for Control Barrier Functions

by

Mitchell K. Black, Jr.

A dissertation submitted in partial fulfillment
of the requirements for the degree of
Doctor of Philosophy
(Aerospace Engineering)
in the University of Michigan
2023

Doctoral Committee:

Professor Dimitra Panagou, Chair
Professor Anouck Girard
Professor Ilya Kolmanovsky
Professor Vasileios Tzoumas

Mitchell K. Black, Jr.
mblackjr@umich.edu
ORCID iD: 0000-0002-3857-1146

DEDICATION

To my family, in the broadest sense of the word.

ACKNOWLEDGMENTS

Sometimes a finished product is greater than the sum of its parts, but in this case no amount of late nights in the lab or hours spent editing could have produced a thesis that does justice to the efforts, to the support, or to the kindness of the people who have made writing it possible. Between advisors and colleagues, family and friends, the number who have made an impact on the content of this dissertation is vast. None, however, compares to that of my advisor, Professor Dimitra Panagou. From the first day I walked into her office, she set expectations high and never shied away from letting me know if I had not met them. Quite honestly, it was very much a trial-by-fire experience. But it forced me to grow as a student and a researcher in ways I never thought possible, and it instilled in me a confidence derived from knowing that she would not ask of her students that of which she did not believe them to be capable. Even when I gave her evidence to contradict these beliefs, she was supportive and considerate of me as a person first and a researcher second, and ultimately was instrumental in helping me get through a version of the dark period that many graduate students encounter. I will be forever grateful for her patience and her wisdom.

Serendipitously, two of my other committee members, Professor Anouck Girard and Professor Ilya Kolmanovsky, were actually my co-advisors before I was advised by Professor Panagou. I have them to thank for my initial opportunity to attend the University of Michigan as a graduate student in 2016. Although for reasons relating to my own maturity I was not in a place to continue as a Ph.D. student at that time, I am thankful both for the lessons they taught me then and for their grace in agreeing to serve on my committee this time around. Their time and insight, in addition to that given by my fourth committee member, Professor Vasileios Tzoumas, greatly improved the quality of this dissertation. I have also Dr. Bardh Hoxha, Dr. Georgios Fainekos and Dr. Danil Prokhorov of Toyota Motor North America to thank for serving as advisors by proxy during my internship in the summer of 2022. Their mentorship was directly responsible for one of the main technical results in this dissertation, and there is no doubt in my mind that it would not have been possible without them. Similarly, Dr. Mrdjan Jankovic and Abhishek Sharma of Ford Motor Company were instrumental in the development of another major result that was used in a variety of the case studies contained in this dissertation. I would be remiss if I did not further acknowledge the hard work of Dr. Kunal Garg and Dr. Ehsan Arabi, without whom several of the papers contributing to this dissertation would not have been possible. Many of the remaining

results stemmed from ideas generated during conversations with my fellow lab members. Dr. James Usevitch, Dev Agrawal, and Hardik Parwana, despite the fullness of their plates, so to speak, never seemed too busy to turn down an opportunity to discuss interesting ideas. I can say the same for Joseph Breeden, whose research interests often overlapped with mine, and for Alia Gilbert and Kaleb Ben Naveed, though the intersection of our research was often an empty set.

It is no secret that here in Michigan the sun rarely graces us with its presence during the winter months, yet my family never failed to shine a light for me in the dark. As the first of them to pursue a Ph.D., I cannot say with certainty that they always understood my motivation. But their support never wavered, and to me that meant more than if I was the very last of them to take this journey. I could always count on my mom, Martha, to offer encouragement when I got down, and on my Dad, Mitchell Sr., to remind me to enjoy life, because success is never final and failure is not fatal. Despite neglecting many of my brotherly duties these last few years, my siblings, Ryan, Emily, and Holly, kept the jokes flowing even if they were made at my, or more likely Emily's, expense. The Hughes family kept me grounded; my cousins Meghan, Katie, and Allison, and my aunt Nancy and uncle Greg, made sure I knew that even if I could do graduate school, there were many other things that I could *not* do (like play "smart" chess). Many other cousins, including Christian, Evan, and Andrew, expressed their support through attendance at Michigan football games, and I'll always be thankful for the respite brought by those Saturdays. I am exceedingly fortunate to have all four grandparents, Lyford and Holly, and Ken and Barbara, with me to this day. They always expressed wonder at the nature of my research and its many applications to autonomous driving, especially considering how they have seen the automobile evolve throughout their lifetimes. For my soon-to-be family, I am thankful for the guidance and insight offered by Dr. Sridhar Kota. Nobody helped me navigate the ins and outs of being a graduate student more than he did, and it is likely that I would have become further lost along the way without his wisdom and generosity. Not to be outdone by her husband, Usha Kota was a constant source of joy in my life. I cherish our petite (or not) post-dinner bowls of ice cream, and if there is anyone in the world more deserving of an honorary doctorate in culinary science, I have yet to meet that person.

Apart from research, I have probably spent more time running these last few years than anything else. So thank you to Connor, my day 1; to George, my partner-in-crime; to Ian, Griffin, and Parker, the boys; to Avi, a kindred spirit if there ever was one; to Mason, a very large bird; to Austin Lin, the guru of swol; to Nick and the entire Willis family, Sierra, Lachlan, Darcy, and Wesley; to Phil and Geoff, the ultimate conversationalists; to Mike, who would have been faster in his day than his son Hobbs with the right shoes; and many, many others for the miles and the memories. And to Ron Warhurst, thank you for believing in me as a runner and more importantly as a person, and for the endless zingers and one-liners. To other friends and roommates including Jonny, Veronica, Austin de Spirito, Pat, AJ, Chris, Alex, Trent, Garrett, Kaiti, Katie, Catherine, Amanda; thanks for

making home wherever you were: Ann Arbor, Boston, Maine, and beyond.

And most importantly, to the love of my life. Thank you, Shalini, for walking with me every step of the way; for shouldering my burdens; for giving me your heart; and for keeping mine safe.

TABLE OF CONTENTS

LIST OF FIGURES

FIGURE

LIST OF TABLES

TABLE

LIST OF APPENDICES

LIST OF ACRONYMS

aCBF Adaptive Control Barrier Function

ADAS Autonomous Driver Assistance Systems

APFs Artificial Potential Fields

C-CBF Consolidated Control Barrier Function

CBF Control Barrier Function

CCM Control Contraction Metric

CLF Control Lyapunov Function

EDMD Extended dynamic mode decomposition

FF-CBF Future-Focused Control Barrier Function

FTS Finite-Time Stability

FxT Fixed-Time

FxTS Fixed-Time Stable

KOT Koopman operator theory

LQR Linear-Quadratic Regulator

MPC Model Predictive Control

NN Neural Network

PE Persistence of Excitation

PID Proportional-Integral-Derivative

PRM Probabilistic Roadmap Method

QP Quadratic Program

R-CBF Robust Control Barrier Function

RA-CBF Risk-Aware Control Barrier Function

RFF-CBF Relaxed Future-Focused Control Barrier Function

RG Reference Governor

RL Reinforcement Learning

RRT Rapidly-exploring Random Tree

S-CBF Stochastic Control Barrier Function

SDE Stochastic Differential Equation

UAV Unmanned Aerial Vehicle

LIST OF SYMBOLS

$\mathbb{R}$ Set of real numbers

$\mathbb{R}^n$ Set of n-tuples of real numbers

$\mathbb{R}^{m\times n}$ Set of real matrices with m rows and n columns

$\left[n\right]$ Set of integers $\{1,\ldots,n\}$

$\mathcal{C}^r$ Set of r-times continuously differentiable functions

$\|\cdot\|$ Euclidean norm (2-norm) of $(\cdot)$

$\|\cdot\|_\infty$ Infinity norm (sup-norm) of $(\cdot)$

$\mathrm{Tr}(\boldsymbol{M})$ Trace of a square matrix $\boldsymbol{M}$

$\lambda_{min}(\boldsymbol{M})$ Minimum eigenvalue of square matrix $\boldsymbol{M}$

$\lambda_{max}(\boldsymbol{M})$ Maximum eigenvalue of square matrix $\boldsymbol{M}$

$\sigma_r(\boldsymbol{M})$ r^{th} singular value of matrix $\boldsymbol{M}$

$\mathrm{col}_i(\boldsymbol{M})$ i^{th} column of matrix $\boldsymbol{M}$

$\mathrm{row}(\boldsymbol{M})$ Row space of matrix $\boldsymbol{M}$

$\mathcal{N}(\boldsymbol{M})$ Null space of matrix $\boldsymbol{M}$

$\mathrm{Int}(\mathcal{S})$ Interior of the set $\mathcal{S}$

$\partial\mathcal{S}$ Boundary of the closed set $\mathcal{S}$

$\emptyset$ Empty set

$\mathbf{0}$ Zero vector of appropriate dimensions

$\mathbf{1}$ Ones vector of appropriate dimensions

$\mathcal{K}_\infty$ Set of extended class-$\mathcal{K}$ functions

$L_f h(\boldsymbol{x})$ Lie derivative of $h\in\mathcal{C}^1$ along f defined as $\frac{\partial h}{\partial \boldsymbol{x}} f(\boldsymbol{x})$

$U\left[a,b\right]$ Uniform distribution supported from below by a and above by b

ABSTRACT

Control design for nonlinear dynamical systems is an essential field of study in a world growing ever more reliant on autonomous system technologies. In practical applications, it is often desirable for the state of the system to converge to some target point or region; however, it is *critical* that the system remain *safe*, i.e., that the system trajectories satisfy a collection of spatiotemporal constraints over the operational lifetime. While generally difficult for nonlinear systems, guaranteeing safety via control design is further complicated under uncertainty introduced by confounding phenomena such as incomplete or inaccurate system information (e.g., unmodelled dynamics), exogenous disturbances (e.g., wind gusts), measurement noise, or the presence of sovereign agents whose actions may be unpredictable. Offline tools for policy learning and system verification may be able to account for some of these effects, but their utility is diminished by the tendency of dynamic, real-world environments to change. It is of paramount importance, therefore to investigate viable options for online safe control. Toward this objective, much attention in recent years has been paid to CBFs as a tool for state-feedback control that certifies the satisfaction of spatiotemporal constraints at all times. This dissertation studies the theory and viability of CBF-based safe control synthesis for nonlinear systems under various classes of system uncertainty.

First, the problem of encoding future state prediction into CBF-based control for nonlinear, control-affine, multi-agent systems is studied. A novel class of future-focused CBFs is developed for autonomous vehicle control under the foundational presumption that vehicles seek to minimize unnecessary acceleration or braking. Centralized and decentralized control laws are proposed for multi-agent systems with varying degrees of communicability, and it is shown how satisfaction of the newly developed CBF conditions via control design guarantees collision avoidance.

Then, the problem of safe control design is studied for a dynamical system subject to an additive, parameter-affine perturbation to the system dynamics. Parameter adaptation laws are proposed to learn the unknown parameters within fixed time, i.e., within a finite time independent of the initial parameter estimates, when a system identifiability condition is met, and to learn the true perturbation when it is not. It is shown that the proposed adaptation framework may be used to learn a more generic class of additive, unmodelled dynamics within fixed-time via application to Koopman operator theory, by which a nonlinear system admits an analogous, infinite-dimensional, linear representation. A robust, adaptive CBF controller is then proposed to guarantee spatiotem-

poral constraint adherence under parameter adaptation despite the considered model uncertainty.

Next, control design for probabilistic safety over a finite time interval is studied for a class of nonlinear, control-affine, *stochastic* systems, i.e., systems subject to additive Brownian motion noise. A novel form of risk-aware CBFs is developed, the use of which for control design results in the satisfaction of a user-specified upper bound on the probability that the system becomes unsafe within the considered (finite) time interval. Conditions are derived under which the proposed risk-aware CBF controller reduces conservatism introduced by an existing method.

Finally, the problem of online, certifiably safe control for nonlinear, control-affine systems is addressed under a collection of arbitrarily many spatiotemporal constraints and input constraints. An approach to synthesizing one consolidated CBF candidate from the collection of constraints is proposed, and online parameter adaptation laws are introduced to vary the relative weightings of the individual constraint functions such that, under certain assumptions, the consolidated CBF is rendered valid despite limited control authority.

CHAPTER 1

Introduction

This dissertation addresses open problems in control design for safety-critical systems under various classes of model uncertainty through the lens of online parameter adaptation and future safety forecasting. This chapter serves to introduce the motivation guiding this line of research, to highlight the problems considered and contributions made herein, to survey the literature and situate said contributions, and to provide an outline for the remainder of the dissertation.

1.1 Motivation

A safe autonomous system is the gate to a fully autonomous system, and the prevalence of and desire for autonomy in robotic and aerospace systems has grown rapidly in recent years. From Autonomous Driver Assistance Systems (ADAS) in vehicles traversing our roadways and autopilots commanding extensive portions of commercial flights, to automated exploratory missions roving across the dusty red landscape of Mars and Unmanned Aerial Vehicle (UAV) package delivery direct to our doorsteps, humans have demonstrated an interest in using autonomous systems both to solve complex problems and to perform tasks that are otherwise repetitive or mundane. Critical, however, to the deployment of these autonomous systems in real-world scenarios is their ability to remain safe throughout their operating lifetime. In other words, many autonomous systems are safety-critical.

The best interpretation of the term safety-critical system is perhaps the literal one; however, a more precise and commonly accepted definition is a system whose failure may lead to loss of life, loss of economic value, or damage to the surrounding environment [1]. For a safety-critical system, the autonomy pipeline may be viewed as consisting of four components, each constituting an important piece of the autonomy puzzle: sensing, the system must be able to extract information related to the state of itself and its surrounding environment; perception, the system must be able to understand and make inferences on the sensed data in order to form a foundation on which to base its actions; planning, the system must be able to generate a plan to achieve its desired outcome; and

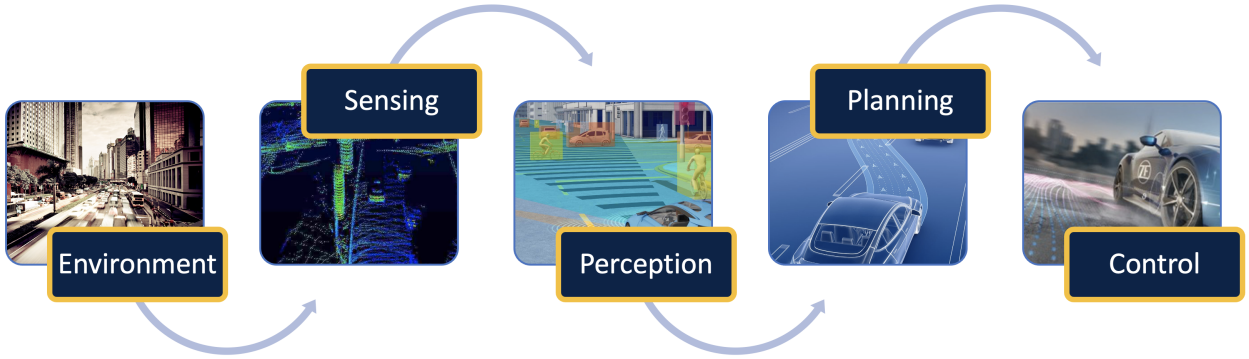

Figure 1.1: A visualization of the autonomy pipeline.

control, the system must be able to carry out the plan using its available actions. The chart shown in Figure 1.1 highlights the interconnectedness of these elements of the autonomy pipeline. It is beyond the scope of any one thesis, however, to develop a complete framework for realizing safe autonomy; thus, in this dissertation, the primary focus is on safe planning and control predicated on assumptions regarding the environment and the quality (or lack thereof) of the preceding sensing and perception systems.

Central to the field of safe control is the notion of set invariance. In recent years, Control Barrier Functions (CBFs) have emerged as a viable tool for rendering a constraint set forward invariant. First introduced in [2] and popularized by [3], CBFs belong to a class of model-based approaches to constrained control design and require that the control input to the system satisfies an inequality condition. For classes of nonlinear, control-affine dynamical systems it has become common to include this CBF condition as a linear inequality in an optimization-based control law, most frequently taking the form of a Quadratic Program (QP). Thus, the CBF may be interpreted as a means of filtering out control inputs that lead to constraint violations. One drawback that has been observed with this class of CBF-QP controllers, however, is that while the control solution is computed pointwise-in-time (and is thus optimal for the present time instance) optimality is not guaranteed over any operating period. In this sense, CBF control laws have been called myopic: the evaluation of a present input as acceptable or not is based entirely on the present time and state and notably does not take any prediction of future system trajectories into account. An example scenario encountered due to this property is an autonomous vehicle executing an aggressive evasive maneuver shortly before a colliding with an obstacle when a smooth deviation from the nominal path would have steered it clear well in advance of any collision. In that sense, not only may this myopic tendency produce sub-optimal behavior but it may also lead to more dangerous situations. An advantage offered by CBF-based controllers over some predictive control architectures, (e.g. Model Predictive Control (MPC)) however, is that they may be computed efficiently and used

online in real-time even for nonlinear dynamical systems. This motivates the study of future-focused CBFs for efficient, predictive, QP-based control in this dissertation.

As a model-based approach to constrained control design, CBFs require the availability of an accurate system model in order to preserve forward invariance of the constraint set. For complicated dynamical systems such a model may be difficult to obtain in practice, but even for simple systems there may be exogenous disturbances from the environment that perturb the system dynamics. Under such circumstances, modifications must be made to the CBF condition in order to account for the error associated with the uncertainty in the model. For example, under a class of additive, bounded perturbations to a set of deterministic system dynamics the CBF condition may include a term which protects against the worst-case disturbance. While this approach guarantees that constraint satisfaction is achieved, the resulting controller may be over-conservative if the true perturbation rarely attains this worst-case bound. One way of reducing this conservatism is to identify the true system model online from data. With the explosion of recent advances in machine learning, there are many options for performing such a task. In contrast to offline learning methods, which require collecting large amounts of training data and cannot account for live perturbations, online learning methods offer a level of real-time adaptivity and responsiveness to unmodeled disturbances that can significantly reduce conservatism in CBF-based control design. And whereas approaches to online system identification may guarantee convergence asymptotically or exponentially as time tends to infinity, it has been shown that convergence in fixed-time, i.e. within a finite time independent of the initial condition, offers stronger disturbance rejection properties and thus may be more suitable for use in CBF-based control. With respect to this dissertation, the preceding discussion motivates the study of Fixed-Time Stable (FxTS) parameter adaptation for system identification and its application for safe control design.

In reality, however, the sensors used to collect data in pursuit of an accurate system model are inherently noisy. Even with ideal sensors, imperfections present in real systems and perturbations to the environment inject a level of randomness into the system dynamics. In many applications, including robot navigation and autonomous vehicle control, it is reasonable to treat this random noise as an additive, Brownian motion perturbation and thus to model the dynamical system as a Stochastic Differential Equation (SDE). In leaving the deterministic modeling regime, however, it is no longer possible to certify that CBF-based control results in constraint satisfaction with probability 1. Rather, there is now a non-zero risk of incurring constraint violations associated with taking actions that in the deterministic regime guarantee constraint satisfaction. In theory, the probability of constraint violations ought to tend toward 1 as the system operating time tends toward infinity, i.e., it is impossible to protect indefinitely against disturbances sampled from unbounded probability distributions over infinite time. Therefore, beginning with [4] and the stochastic barrier certificate, CBF development in the stochastic setting has leaned heavily on martingale theory for

both discrete- and continuous-time stochastic processes to bound the probability that a given constraint is violated over a *finite time interval*. While useful in theory, these methods do not consider the magnitude of the diffusion term in the SDE and therefore have been shown to lead to conservative behavior in practice. This motivates the study in this dissertation of a new class of risk-aware CBFs that confer a more accurate bound on the risk that the system incurs constraint violations over a finite time interval.

To this point, the discussion on CBF-based control design has operated on the assumption that the CBF is *valid*, i.e. that the CBF condition is met at all times even under input constraints. If that is not the case, then the CBF-QP control law will become infeasible and some other safe control policy must be activated, i.e., the CBF-QP controller is no longer viable. Further, the prior assertions on CBFs have held only for a single constraint function. Although for a single candidate CBF there exist guarantees of validity under certain conditions, these results do not generally extend to control systems seeking to satisfy multiple constraints simultaneously, and is significantly more difficult in the presence of input constraints. For the viability of implementing this class of controllers on real systems, this is a major deficiency. Some recent work has sought to address this open problem by considering only the constraint closest incurring violations at any given time, but this may introduce undesirable oscillatory behavior or chattering of the control input, which may lead to the loss of uniqueness of solutions. If, however, it were possible to consolidate the many constraint functions into one candidate CBF and subsequently verify it as valid, then existing approaches to CBF-based control could be employed to satisfy all constraints jointly in perpetuity. This motivates the study of constraint function weight adaptation for the purpose of certifying a consolidated CBF as valid even under input constraints.

1.2 Problem Statements and Summary of Contributions

This dissertation addresses open problems in CBF-based control design for safety-critical systems using parameter adaptation and predictions of future safety. In what follows, each sub-problem considered herein is introduced and a summary of the solution proposed by this dissertation is provided.

1.2.1 Safe, Predictive Control with Future-Focused CBFs

CBF-based controllers are known to introduce present-focused, myopic behavior at the system level which may lead to dangerous future situations, loss of a viable control input, or sub-optimality. To address this problem, Chapter 2 of this dissertation introduces a novel class of Future-Focused Control Barrier Functions (FF-CBFs) (and a relaxed version thereof) for a form

of computationally efficient, predictive control for safety-critical systems. The fundamental underlying intuition is that systems seek minimum-effort control laws, e.g., an autonomous vehicle would seek to minimize unnecessary acceleration and braking, and as such the FF-CBF seeks to preserve safety of predicted zero-control trajectories over an arbitrarily long future time interval. It is shown that safety is preserved under FF-CBF-based control with unlimited control authority and perfect state measurements regardless of whether the predicted zero-control trajectories are realized, such that it is a suitable policy for a collection of autonomous vehicles seeking to traverse a busy intersection. The efficacy of the proposed approach is studied in the context of this intersection crossing problem for (car-like) autonomous vehicles, where it is observed that the new CBFs decrease the occurrence of intersection deadlocks while preserving favorable safety and control feasibility properties.

1.2.2 Fixed-Time System Identification for Safe Control

Belonging to a class of model-based approaches to safe control design, CBFs require the availability of an accurate system model in order to provide guarantees of safety. In the absence of such a model, many existing works assume that a nominal system model is correct to within some bounded error and use a robust control law assuming a worst-case effect of the model uncertainty on system-level safety. This introduces conservatism in the control design, especially so when the bound on the unknown disturbance grows very large. The work presented in Chapters 3 and 4 address this problem by identifying classes of model uncertainty within fixed-time.

In Chapter 3, two proposed FxTS parameter adaptation laws are introduced for identifying unknown parameters appearing linearly in a class of unknown, nonlinear, control-affine systems. More specifically, the parameter adaptation laws guarantee that model uncertainty represented by an additive, parameter-affine perturbation is learned within fixed-time under the assumption that the unknown parameters belong to a known polytope and perfect state measurements are available. As a result, a robust, adaptive control framework is then proposed for safe control design at all stages of the parameter adaptation process.

Chapter 4 relaxes the perfect measurement requirement from above by investigating the robustness properties of one of the adaptation laws proposed in Chapter 3 to measurement noise and/or time-varying parameters. New conditions on FxTS are derived to support the accompanying analysis. Then, a further generalization of the fixed-time system identification problem is studied in the context of learning a bounded, additive, nonlinear perturbation to the system dynamics and using a robust, adaptive CBF condition to preserve safety.

1.2.3 Risk-Aware Control of Stochastic, Safety-Critical Systems

In practice, random phenomena often perturb even a known system model in the form of, e.g., exogenous disturbances. When modelling such randomness by distributions with infinite support, e.g., Gaussians, Poissons, etc., it is no longer possible to guarantee with 100% certainty that a system will remain safe within an operating period, i.e., there is a non-zero chance that a random perturbation will cause the system to exit the safe set. For systems modeled according to a class of nonlinear, control-affine, SDEs it is therefore necessary to understand how control actions taken affect the probability of the system becoming unsafe over a finite time interval. While existing work has studied this problem, the resulting controllers tend to be extremely conservative.

As such, Chapter 5 of this dissertation introduces a novel class of Risk-Aware Control Barrier Functions (RA-CBFs) for the control of nonlinear, control-affine, stochastic, safety-critical systems with unlimited control authority and derives conditions under which, given perfect state measurements, the resulting control actions are less conservative than the state-of-the-art. Bounds are then derived for the probability that the system will become unsafe within a specified finite time interval under the proposed control law, and an algorithm for further tightening the risk bound is presented.

1.2.4 Safe Control under Multiple Spatiotemporal and Input Constraints

Two challenging open problems in CBF-based control design are verifying that a CBF candidate is valid and synthesizing a viable control law in the presence of multiple CBF candidates, which may represent a collection of spatiotemporal constraints, especially under limited control authority. Chapter 6 of this dissertation seeks to jointly address both of these problems by introducing the notion of a Consolidated Control Barrier Function (C-CBF), i.e., a function that synthesizes multiple spatiotemporal constraint functions into one candidate CBF, and by rendering it valid for a class of nonlinear, control-affine systems via online adaptation of its constituent functions' weights. Given that the work of Chapters 3 and 4 address the problem of nonlinear system identification, this work assumes a perfectly known system model. Cases of unbounded and limited control authority are considered separately, and it is shown that a class of CBF-QP control laws is guaranteed to be feasible whenever the underlying adaptation-based optimization problem has a feasible solution.

In the following section, a survey of the literature is conducted in order to place the stated contributions within a broader context.

1.3 Literature Review

1.3.1 Safe Control and Motion Planning

1.3.1.1 Safety via Motion Planning

Motion planning and control design for safety-critical systems has become an active field of research in recent years. Significant attention has been paid to the development of motion planning algorithms belonging to classes of both sampling-based [5, 6, 7] and sample-free [8, 9] approaches. Many sampling-based methods search over the state and action spaces (e.g., A* [10, 11], Rapidly-exploring Random Tree (RRT) [12, 13]) in order to generate feasible, safe trajectories efficiently online at the expense of scaling poorly with the state dimension and number of agents in the system. A further known disadvantage to these methods is possibly slow convergence to optimality dependent on the initial guess. Sample-free methods like MPC [14, 15] typically solve an optimal control problem (or approximation thereof) in pursuit of the same goal. For nonlinear dynamical systems, however, obtaining even locally optimal solutions may 1) be computationally burdensome, 2) provide little robustness to disturbances or unmodelled phenomena, or 3) scale poorly, similar to sampling-based methods. In practice, the use of these methods typically requires either considering some simplified (i.e., linear) dynamics model and accounting for disturbances via enlarging unsafe regions, or learning optimal policies offline [16, 17, 18]. Specific to MPC, a further difficulty is in choosing control parameters, for example in cost function design or look-ahead horizon, that guarantee certain desirable properties in the closed-loop system response. Thus, while recent advances in numerical methods and available tools (e.g., CasADI [19]) have diminished the disadvantages of these types of methods, tractability concerns and loss of guarantees due to problem simplifications often weaken the feasibility of these methods for use in online control, i.e., in real-time applications.

1.3.1.2 Safety via Feedback Control

Due to these drawbacks, there has been an increased interest in the development of safe state-feedback control policies, which typically may be computed very efficiently online. Recent advances along these lines include (i) Reference Governors (RGs) [20, 21], which rectify unsafe reference signals fed into an existing closed-loop dynamical system, (ii) Control Contraction Metrics (CCMs), which imply the existence of a tracking controller capable of contracting the system trajectories toward any reference [22, 23], (iii) CBFs [3, 24], which filter unsafe nominal control inputs to ensure that system trajectories evolve within a particular set of states, and (iv) learned policies (even relating to (i) [25], (ii) [26], or (iii) [27]). Methods from each of the above classes have achieved favorable results both in theory and practice; however, none is a panacea. RGs

have succeeded in providing formal guarantees of safety [28], but preserving these guarantees for systems with either dynamics or constraints that are nonlinear may require linearization and/or polyhedral set approximation and thus introduce conservatism in the system's emergent behavior [29]. CCMs, though able to guarantee that system trajectories remain within some tube surrounding a reference trajectory even under uncertainty [30], typically still require a high-level planner to generate such a safe reference. CBFs, unlike RGs, are straightforward to use for safe control of classes of nonlinear systems subject to nonlinear constraints, even under perturbations [31, 32], but synthesizing a *valid* CBF, i.e., one for which a derivative condition holds over the system trajectories everywhere within a given set, is akin to synthesizing a valid (control) Lyapunov function. It is a difficult problem. In fact, in each of the first three classes of methods (RGs, CCMs, and CBFs) validity is both required to obtain the promised behavior and difficult to verify. Learned control policies circumvent this challenge to some extent, i.e., the objective is to learn a policy that meets the criteria for validity (for e.g., a RG [33], CCM [26], or CBF [34]); however, they frequently require extensive offline training (e.g., from expert demonstration [27], reinforcement learning [35], etc.) and thus generally both lack guarantees and suffer performance degradation due to disturbances in real-time.

1.3.1.3 Safe Control with Control Barrier Functions

Despite these challenges, the recent arrival of CBFs has ushered in a new era in constrained, nonlinear control design. First appearing concurrently in [2] for deterministic systems and [4] for stochastic systems, and popularized as an ingredient to QP-based control by [3], a valid CBF serves as a formal certificate that system trajectories beginning within some set will evolve within that set for all future time. In this way, a CBF may be used to certify that a set of safe states is *forward invariant*, thereby guaranteeing safety. For classes of continuous-time, nonlinear, control-affine dynamical systems the class of CBF-QP controllers behaves in a similar fashion to reference governors in that they filter out nominally unsafe legacy inputs [36, 37, 24]; but CBFs overcome challenges faced by using reference governors for classes of nonlinear systems with nonlinear state constraints due to the CBF condition being affine in the control input. From a performance perspective, one deficiency in CBF-based control is the tendency to consider safety only in the present, possibly to the detriment of future liveness. In this sense, they work similarly in practice to artificial potential fields (APFs) [38, 39], which administer repulsive forces to obstacles and attractive forces to goal regions by modifying some desired or nominal action only when neglecting to do so is deemed unsafe. Many works have referred to this emergent behavior as *myopic*, and the same is done in this dissertation. Unfortunately, myopic tendencies may cause problems with the existence of a feasible input [40], convergence to an undesirable equilibrium [41], or sub-optimal behavior. Many authors have sought to improve the pointwise feasibility of the CBF-QP controller by

e.g., solving a (penalized) optimal control problem via approximate dynamic programming [42], adapting the class $\mathcal{K}$ parameter in the CBF condition [43, 44], or by adding additional feasibility constraints that further restrict the admissible control space in the QP [45, 46]. Solutions to avoiding undesirable equilibria include rotating Control Lyapunov Function (CLF) level sets [47], or using auxiliary control inputs activated when falling toward such equilibria [41, 48]. Ensuring optimality (in whatever sense) of the trajectories resulting from a CBF-QP controller, however, is difficult without the use of predictive control. For this reason, various works have investigated how to incorporate CBF constraints into MPC controllers [49, 50, 51], though as noted previously for real-time applications these methods may require modifications that invalidate the formal guarantees provided by CBF methods. Recent studies have sought to circumvent this limitation with multi-rate controllers, which synthesize simplified high-level MPC planners with low-level CBF controllers [52, 53]. While often usable for single-agent systems, the demands of re-planning may diminish the efficacy of these approaches in the context of multi-agent systems. The work in this dissertation addresses the problem of computationally efficient, *future-focused* (i.e., predictive) control for safety-critical multi-agent systems under both centralized and decentralized control architectures.

1.3.2 Safety under Uncertainty: Deterministic Setting

1.3.2.1 Robustly Safe Control Design under Model Uncertainty

Model-based tools for constrained, nonlinear control design, of which CBFs are one, rely on the availability of an accurate system model. In the absence of such a model, the field of robust nonlinear control offers protection against classes of bounded disturbances. Traditional approaches to robust control include backstepping [54, 55], feedback linearization [56, 57], and sliding mode control [58, 59], and have been shown to achieve success in such applications as quadrotor waypoint tracking [54] and bi-pedal robots [59], among others. What these methods typically lack, however, is any consideration of the notion of safety in the control framework. Recently, various so-called safety-embedded control techniques have been proposed to address this problem, e.g., the addition of barrier functions in backstepping control design [60, 61] or by augmenting the closed-loop system with barrier states [62, 63] and using stabilizing controllers (like pole-placement). Unfortunately, finding acceptable control parameters for these methods may require solving nonlinear optimization problems (as in [60]) and the inclusion of barrier states may lead to loss of system controllability [62]. Additional recent work derives a safe sliding mode controller for a generic class of systems with both matched and unmatched uncertainty [64], but uses CBFs explicitly in the design of a transient time function (i.e., for control prior to reaching the sliding manifold). In contrast, various works began investigating the robustness properties of CBFs for deterministic

systems shortly after their introduction to the literature. First, it was shown in [65] for systems with (sufficiently small) bounded, additive perturbations to the dynamics that (small) constraint violations may be incurred; this notion of input-to-state safety was given a more rigorous treatment in [66, 67], whereas the Robust Control Barrier Function (R-CBF) was introduced in [31] to preserve constraint set invariance in the presence of a broader class of additive, non-vanishing disturbances. In the interim, R-CBFs have been used in control design to protect against bounded measurement noise [68], state estimation error [69], and unknown actions taken by multi-agent systems [70], among other applications (see e.g., [71, 72, 73, 74]).

A major practical limitation to this class of robust controllers is that they become highly conservative as the known (or assumed) disturbance bound grows: predicated on the assumption that a worst-case perturbation acts on the system at all times, R-CBFs and the aforementioned robust control techniques require actions that guarantee protection against such a disturbance even when the true system disturbance may be very small or even assist the closed-loop response. In the context of CBF methods, the authors of [32] introduced the Adaptive Control Barrier Function (aCBF) to relax this worst-case consideration away from the boundary of the constraint set for a class of additive, parameter-affine perturbations to the system dynamics. Due to assumptions on the compactness and convexity of the admissible parameter set, it turns out that the aCBF condition is equivalent to the R-CBF condition on the boundary of the constraint set, and is a relaxation thereof over the interior. Other proposed approaches to relaxing R-CBFs in this way include tunable CBFs [67], though it is worth noting that these works adapt the safety condition purely on the basis of proximity to the barrier of the safe set, and notably not according to updated information regarding the system model as do techniques in the fields of adaptive and machine learning-based control. For safety-critical applications, various works in model reference adaptive control adapt parameters in response to disturbances in real-time to track the trajectories of some nominal reference model [75, 76], but require that safety is encoded in the planning stage (e.g., via trajectory tubes [77]). Traditional adaptive controllers refer to safety in the context of preventing transient instability [78], and as a result the line between adaptive and learning-based approaches to safe control has become blurred in recent years, with many works using machine learning algorithms such as Bayesian optimization [79, 80], Gaussian processes [81, 82], etc. or so-called neuro-adaptive schemes [83, 84] to recover representations of unmodelled dynamics. For example, in [85], the authors use a neuro-adaptive scheme for updating the weights of a feedforward Neural Network (NN) modelling the system disturbance. These methods typically lack guarantees on estimation error bounds, however, unlike other classes of set-membership methods, e.g., [86] in which the authors proposed a data-driven set-membership identification algorithm for tightening an admissible set for unknown parameters and more accurately estimating the system disturbance. These works inspired a variety in the vein of so-called robust, adaptive CBF control, i.e. methods that both *adapt* to estimated

perturbations to the system while remaining *robust* to estimation error (see e.g., [87, 88, 89, 90]).

1.3.2.2 Reducing Model Uncertainty via Nonlinear System Identification

Owing to the complexity and richness of behavior exhibited by nonlinear systems, e.g., multiple equilibria, finite escape-time, chaos, etc., the field of nonlinear system identification is vast. Optimization-based methods seek a locally (e.g., nonlinear least-squares regression [91, 92], sequential quadratic programming [93, 94], etc.) or globally (e.g., genetic algorithms [95, 96], particle swarm [97, 98], etc.) optimal parametric representation of the system model. Convergence to a global optimum is typically very slow, however, and locally optimal solutions may be insufficiently descriptive for use in control design. Other methods include frequency-domain methods like Volterra series [99], i.e., the nonlinear analog to the convolutional description of linear systems, though the number of free parameters tends to be very large, and statistical methods like Markov chain Monte Carlo [100, 101] and particle filters [102, 103], though these tend to necessitate many offline simulations of the system of interest. Moreover, the above approaches may struggle if the choice of candidate models is poorly parameterized [104]; therefore, many works rely on "black-box" methods for generating a representation of the system, the most popular class of which is (deep) learning [105, 106, 107, 108]. As powerful function approximators, deep learning methods have demonstrated potential for identifying complex dynamical systems like rotorcraft [109, 110], ocean currents [111, 112], financial markets [113, 114], etc. In practice, however, the identification process for all of the above methods is computationally intensive due to some combination of number of free parameters (e.g., NVIDIA language model uses $>$8 billion parameters), time to solve optimization problem, and amount of required data, all of which make these approaches to nonlinear system identification unfit for online control synthesis.

Unknown linear systems, i.e., systems for which unknown parameters appear linearly in the system dynamics, are much easier to identify. Classes of batch estimators, like least-squares, and recursive parameter estimation laws (see e.g., [115, 116, 117]) have both been shown to perform well even under noisy measurements. For these classes of methods, it is well-known that parameter estimates are guaranteed to converge to the true parameters (or neighborhood thereof) as either the number of samples or time tends toward infinity. In recent years, developments in Koopman operator theory (KOT) have demonstrated that related linear identification schemes may in some cases be applied to identify unknown nonlinear systems. The semigroup of Koopman operators describes the evolution of scalar output functions of the nonlinear system of interest, frequently called *observables*, in an analogous, infinite-dimensional, and importantly linear (Banach) space. In theory, the main idea is that knowing the Koopman operator in the space of observables allows for the exact reconstruction of the dynamics of the original nonlinear system. As such, much attention of late has been paid to data-driven methods for constructing a finite-dimensional matrix representation

of the infinite-dimensional Koopman operator. Extended dynamic mode decomposition (EDMD), first introduced in [118], has emerged as a valuable tool for carrying out such an approximation [119, 120, 121, 122, 123, 124], etc. Intuitively, EDMD computes a finite-dimensional Koopman matrix algorithmically by lifting input/output measurements to the space of observables via user-specified basis functions and then computing the matrix using batched least-squares. While first introduced for Koopman-based identification specifically for discrete-time dynamical systems, EDMD has also successfully been used to learn a matrix representation of the Koopman generator[1] [122, 123], i.e., the operator describing the evolution of observables for continuous-time systems. It has been shown by various works (e.g., [125, 126]) that learning the Koopman matrix via EDMD leads to exact reconstruction of the Koopman operator as the number of samples tends to infinity, and error bounds have been derived with respect to finite-data [127, 128]; however, these results require the assumption that data is either independently, identically distributed or ergodic in nature. In its absence, these methods lack formal guarantees regarding approximation error bounds and thus may be detrimental to safe control design. As such, while studies have demonstrated the use of Koopman-based system identification in a variety of control applications including soft robotics [119, 121], motor control [129], and quadrotors [130], to this point the existing literature has not used Koopman-based system identification for control of safety-critical systems. Further reviews of KOT for control may be found in [131, 132].

While EDMD uses least-squares regression to compute an approximation of the Koopman matrix (or generator), some recent work has investigated the use of recursive parameter estimation schemes for Koopman-based nonlinear system identification [133]. But whereas this and other works in linear parameter estimation guarantee asymptotic or exponential convergence to the Koopman matrix, the notions of Finite-Time Stability (FTS) and FxTS are stronger in the sense that they guarantee convergence to an equilibrium point within a finite time. In addition to faster rates of convergence, it has been shown by [134] and [135] that systems perturbed by additive, vanishing disturbances maintain the FTS and FxTS properties of the equilibrium of the unperturbed system, and that under additive, bounded disturbances the system trajectories converge to a smaller neighborhood of the equilibrium than if the original equilibrium were asymptotically or exponentially stable. In addition to the above properties, the finite settling time for a FxTS equilibrium is uniformly bounded for all initial conditions, which makes it an attractive candidate for study in the context of system identification for safe control design. This dissertation addresses the problem of safe control for unknown, nonlinear, control-affine dynamical systems using Fixed-Time (FxT) parameter adaptation laws to identify 1) a class of additive, parameter-affine perturbations to the system and 2) a more generic class of additive, bounded, but possibly nonlinear perturbations, i.e.

[1]The Koopman operator is to the Koopman generator as the state-transition matrix e^{At} is to the matrix A for continuous-time linear systems of the form $\dot{x} = Ax$.

to identify classes of additive disturbances to the system within fixed-time.

1.3.3 Safety under Uncertainty: Probabilistic Setting

It is reasonable to question the practical relevance of approaches to system identification predicated on the assumption that available output measurements are noise-free. The value in this line of work, however, lies in the ability to further analyze such results under conditions related to the quality of measurements. Many studies consider the effect of parameter estimation schemes under an assumed bounded perturbation (e.g., [115]); however, sensor noise may be more accurately modeled as a random signal [136]. As such, significant attention has been paid to the use of Gaussian processes (GPs), a tool by which unknown dynamics may be represented as a distribution over random functions, for learning in safe control via reachability-based methods [137], online parameter tuning [138], Lyapunov methods [139], and CBFs [140]. The goal is to learn a distributional representation of the unknown system model such that safety may be certified with some probability p, an objective that theoretically plays well with CBF-based approaches to control design. As such, a wide variety of work has studied the problem of synthesizing a probabilistically safe control law using GPs and CBFs [141, 142, 143, 144], etc. The misconception, however, is that safety may be guaranteed with probability p by learning a GP model of the system dynamics and using that model for CBF-based control design. Instead, the result is a CBF constraint that is guaranteed to hold *pointwise-in-time* with probability p, which does not certify safety with probability p over any measurable time interval. Methods of this form have been proposed in a number of works under different names, e.g., probabilistic CBFs [145, 146], chance-constrained CBFs [147, 148], among others, though to-date in the survey of works no study has derived a relation between instantaneous safety and safety over some operating time. Similar to chance-constrained CBF methods are so-called risk-aware controllers. Of late, a particular focus has been using the notion of Conditional Value-at-Risk, a coherent risk measure, in control design [149, 150]. These approaches seek to encode that the controller protects against the mean of some specified fraction of the tail of worst-case outcomes in a given distribution, and have been proposed for planning [151, 152, 153] in addition to control, though typically lack guarantees of safety over time like their probabilistic CBF relatives.

Stochastic system theory, in contrast, is specifically amenable to this form of analysis, i.e., safety over a finite time interval. Traditional models of SDEs take the form of a difference equation, necessitated by non-differentiability of the class of additive, random processes (namely, Brownian motion) perturbing the nominal (ordinary differential equation) system model. Beginning with the introduction of the stochastic barrier certificate by [4], which formulated an affine condition predicated on the notion of the barrier function as a stochastic martingale, a major focus in control for

stochastic safety-critical systems in recent years has been barrier function based methods. The notion of the Stochastic Control Barrier Function (S-CBF), the effect of which was shown to bound the probability of the system becoming unsafe within a specified finite time, was first introduced by [154]. Several works have advanced S-CBF theory since then, in particular [155] for adapting the failure probability on the fly and further robustifying the method under measurement noise via Kalman filtering in [156], and in [157] for constraints with higher relative-degree; however, it has been shown that the probability of preserving safety decays exponentially with the length of the time interval and that the conditions are often restrictive in practice [158]. In [159] this problem is addressed via reciprocal and zeroing CBFs for stochastic systems with claims of safety with probability one over infinite time intervals, though the required level of conservatism is unclear despite assumed access to unbounded control authority. Other works address this problem of conservatism by sampling predicted trajectories of a SDE for use in MPC [160], but lose the theoretical guarantees of probabilistic safety over time in doing so. This dissertation studies the problem of reducing conservatism in risk-aware control design for stochastic safety-critical systems, i.e., how to design a state-feedback controller such that the probability that the system becomes unsafe over a finite time interval is bounded, and bounded less conservatively than in existing methods.

1.3.4 Verification in Safe Control

A challenging remaining problem in online control synthesis for safety-critical systems is the one concerning verification, i.e., does the specified control law *guarantee* safety given the system under consideration, which may be subject to unknown perturbations or actuation limits. Various methods treat the problem in an offline setting by, for example, computing robustly controlled invariant sets via linear matrix inequalities [161, 162, 163], sum-of-squares programming [164, 165], etc., or by generating controllers for which the forward-reachable set remains safe using Hamilton-Jacobi analysis [166, 167]. In general, computational demands necessitate that these methods are applied offline. Even if somehow Moore's law were to persist and advancements in computing power were able to support the online implementation of such approaches, in practice controlled invariant sets are typically under-approximated and forward-reachable sets are over-approximated, and thus the above methods introduce conservatism.

Similar to guarantees of stability and convergence conferred by control Lyapunov functions, results for CBFs on certified controlled set invariance only hold if the function is shown to be *valid*, i.e., if a condition on the rate of change of the CBF over the trajectories of the system dynamics holds everywhere in the safe set. For systems with unbounded control authority subject to one state constraint, the authors of [3] show that the CBF-QP control law is guaranteed to preserve safety; however, generally the certification of *candidate* CBFs as valid is a challenging problem compli-

cated by the presence of input constraints. This is addressed for high-order CBFs constructively in [168] and through parameter adaptation in [169], but the results break down with the addition of even a second state constraint. This is a problem that has only undergone consideration in the recent past, during which time proposed solutions have mainly skirted the underlying issue either by assuming that only one constraint is relevant at once [170], or by synthesizing switching functions to address the most dangerous constraint [171, 172]. These non-smooth approaches may induce undesirable oscillatory system behavior or violate regularity conditions required for existence and uniqueness of solutions.

It has been proposed by several works (e.g., [173, 174]) that one constraint function be synthesized smoothly from the arbitrarily many under consideration by the system. This is done, for example, in [173] by smoothly approximating the minimum of all CBF candidate functions with a log-sum of exponentials. The advantage is then that the existing CBF-QP controller could be used to enforce safety. Thus far, however, the above works have made no attempt to validate their unified CBF as valid, and therefore it is unknown whether forward invariance is ensured. For validation, sum-of-squares programming has been used to verify CBFs for a class of polynomial systems in [175, 176], whereas similar methods were used to achieve this objective with linear programming in [177]. What remains challenging with those methods, however, is in finding a suitable CBF if the proposed function fails the verification. In contrast, other solutions propose the offline learning of valid CBFs [27] or policies directly [178, 179]. What is problematic about these offline approaches, however, is that any guarantees may be rendered invalid for systems deployed in dynamic, uncertain, or simply different environments. This dissertation studies the problem of synthesizing a *valid* CBF from arbitrarily many constraint functions and certifying it as such via parameter adaptation *online* despite the presence of input constraints.

1.4 Outline

In what follows, an outline of the remaining chapters is provided along with a brief overview of the contributions made therein.

- Chapter 2 introduces future-focused CBFs for predictive control of safety-critical systems. The results in this chapter are based on the work in [180].
- Chapter 3 presents two FxTS parameter adaptation laws for identification and safe control of nonlinear, control-affine systems subject to a class of additive, parameter-affine disturbances. The results in this chapter are based partially on the work in [181, 182].
- Chapter 4 analyzes the robustness of results in Chapter 3 and proposes a Koopman-based parameter adaptation law for fixed-time identification of a more generic class of additive,

nonlinear disturbances. The results in this chapter are based partially on the work in [182, 183].

- Chapter 5 introduces risk-aware CBFs for probabilistic safety via control for stochastic systems. The results in this chapter are based on the work in [184].
- Chapter 6 introduces a consolidated CBF-based adaptive control framework for control of nonlinear, control-affine systems subject to multiple spatiotemporal and input constraints. The results in this chapter are based on the work in [185, 186].

To conclude, Chapter 7 summarizes the above contributions and closes with remarks on future research directions.

1.5 Additional Notation

In the remainder, scalar quantities and functions will be denoted as lower-case variables (e.g. scalar $a \in \mathbb{R}$, function $f : \mathbb{R} \to \mathbb{R}$), vectors as bold lower-case variables (e.g. $\boldsymbol{v} \in \mathbb{R}^n$), and matrices as bold upper-case variables (e.g. $\boldsymbol{M} \in \mathbb{R}^{m \times n}$).

CHAPTER 2

Future-Focused Control Barrier Functions

In this chapter, the problem of control design for the simultaneous safety of both present and predicted future state trajectories is considered for a collection of autonomous vehicles described by a (car-like) dynamic bicycle model. Motivated by the tendency of existing methods for online safe control design to rectify desired control actions only when deemed to infringe upon *present* safety, a class of Future-Focused Control Barrier Functions (FF-CBFs) is introduced to reorient the notion of safety to account for *future* constraint violations *predicted* under a zero-control policy acting over an arbitrarily large future time interval. Supported by the popularity of minimum-norm control laws (e.g., [187]), the predicted zero-control policy is founded on the assumption that vehicles seek to minimize unnecessary acceleration in their control design. Notably, however, it is shown that safety of the actual system trajectories is preserved under the effect of FF-CBF-based control even when the predictions on how the future states will evolve do not come true.

After reviewing preliminaries and defining the problem in Section 2.1, an unsignaled autonomous vehicle intersection crossing problem is introduced to motivate the class of FF-CBFs proposed in Section 2.2. It is shown how, in the case where all vehicles seek to proceed straight through the intersection, the FF-CBF admits an analytical solution to the minimum predicted future inter-vehicle distance and may thus be synthesized in a computationally efficient FF-CBF-Quadratic Program (QP)-based control law for online predictive control. For the more general case where vehicles may be turning, an optimization framework is proposed for identifying the predicted minimum distance. Taking into account that the FF-CBF defines a virtual barrier in the sense that violations do not imply that a collision has occurred (or is inevitable in the future), a Relaxed Future-Focused Control Barrier Function (RFF-CBF) is then proposed to permit such violations away from the physical barrier between vehicles and, in doing so, to ease the feasibility burden of the proposed QP control law. A set of comparative numerical trials is undertaken for the unsignaled intersection crossing problem in Section 2.3, in which the success of the proposed FF-CBF and RFF-CBF control laws are contrasted with limitations of an existing method. A hardware experiment is then used to demonstrate the use of a RFF-CBF controller in a real-time application. The results of this chapter are based on [180]. The author wishes to acknowledge the

contributions of co-authors Dr. Mrdjan Jankovic and Abhishek Sharma to the development of the ensuing work.

2.1 Mathematical Preliminaries

2.1.1 System Model

Under consideration in this chapter is a collection of agents, $\mathcal{A}$, each of whose dynamics is governed by the following class of nonlinear, control-affine systems

$$\dot{\boldsymbol{x}}_i = f_i(\boldsymbol{x}_i(t)) + g_i(\boldsymbol{x}_i(t))\boldsymbol{u}_i(t), \quad \boldsymbol{x}_i(0) = \boldsymbol{x}_{i0}, \tag{2.1}$$

where $\boldsymbol{x}_i \in \mathbb{R}^n$ and $\boldsymbol{u}_i \in \mathcal{U}_i \subset \mathbb{R}^m$ denote the state and control vectors respectively for agent $i \in \mathcal{A}$, and where $f_i : \mathbb{R}^n \to \mathbb{R}^n$ and $g_i : \mathbb{R}^n \to \mathbb{R}^{n\times m}$ are locally Lipschitz in their arguments and not necessarily homogeneous across agents. The set $\mathcal{U}_i$ denotes the set of admissible control inputs, often referred to as the input constraint set. It is further assumed that $\mathcal{A}$ has cardinality $p > 1$, i.e., that there are p agents in the system. A subset of agents $\mathcal{A}_c \subseteq \mathcal{A}$ is assumed to be communicating in that they share information (e.g., control inputs) and thus may use centralized control laws computed by a common node. The remaining agents $\mathcal{A}_n = \mathcal{A} \setminus \mathcal{A}_c$ are non-communicating and must resort to decentralized control laws.

2.1.2 Set Invariance with Control Barrier Functions (CBFs)

Consider a continuously differentiable constraint function $h_i : \mathbb{R}^n \to \mathbb{R}$, and assume that its zero super-level set is known to be the set of safe states, denoted by $\mathcal{S}_i$. For example, if the function h_i encodes collision avoidance with respect to a given obstacle then the set $\mathcal{S}_i$ is the set of collision-free states for that obstacle. The set $\mathcal{S}_i$ is defined as

$$\mathcal{S}_i = \{\boldsymbol{x} \in \mathbb{R}^n \mid h_i(\boldsymbol{x}_i) \geq 0\}, \tag{2.2a}$$

$$\text{int}(\mathcal{S}_i) = \{\boldsymbol{x} \in \mathbb{R}^n \mid h_i(\boldsymbol{x}_i) > 0\}, \tag{2.2b}$$

$$\partial\mathcal{S}_i = \{\boldsymbol{x} \in \mathbb{R}^n \mid h_i(\boldsymbol{x}_i) = 0\}. \tag{2.2c}$$

The notions of safety and forward invariance are used interchangeably throughout this chapter, and thus the latter is defined as follows.

Definition 2.1 (Forward-Invariant Set). *A set $\mathcal{S}_i$ is **forward invariant** if the trajectories of* (2.1) *evolve within $\mathcal{S}_i$ at all times, i.e., if $\boldsymbol{x}_i(0) \in \mathcal{S}_i \implies \boldsymbol{x}_i(t) \in \mathcal{S}_i$. $\forall t \geq 0$.*

The following constitutes a necessary and sufficient condition for forward invariance of a set [188].

Lemma 2.1 (**Nagumo's Theorem**). *Suppose that there exists $\boldsymbol{u}_i \in \mathcal{U}_i$ such that* (2.1) *admits a globally unique solution for each $\boldsymbol{x}_i(0) \in \mathcal{S}_i$, and that $\frac{\partial h_i}{\partial \boldsymbol{x}_i} \neq 0$, $\forall \boldsymbol{x}_i \in \partial\mathcal{S}_i$. Then, the set $\mathcal{S}_i$ is forward invariant for the controlled system* (2.1) *if and only if*

$$L_{f_i} h_i(\boldsymbol{x_i}) + L_{g_i} h_i(\boldsymbol{x_i})\boldsymbol{u}_i \geq 0, \ \forall \boldsymbol{x}_i \in \partial\mathcal{S}_i. \tag{2.3}$$

The condition (2.3) states that the time-derivative of the function h_i over the trajectories of (2.1) must be non-negative on the boundary of the set $\mathcal{S}_i$. With h_i then non-decreasing whenever $\boldsymbol{x}_i \in \partial\mathcal{S}_i$, it will always hold that $h_i(\boldsymbol{x}_i) \geq 0$ and thus the set S_i is forward invariant. One way to render a set forward invariant is to use CBFs in the control design. Before formally introducing the notion of a CBF, the following definition is required.

Definition 2.2 (**Extended Class $\mathcal{K}_\infty$ Function**). *A function $\alpha : \mathbb{R} \to \mathbb{R}$ belongs to extended class $\mathcal{K}_\infty$ if $\alpha(0) = 0$ and α is strictly increasing over $(-\infty, \infty)$.*

Definition 2.3 (**Control Barrier Function (CBF)**). *Given a set $\mathcal{S}_i \subset \mathbb{R}^n$ defined by* (2.2) *for a continuously differentiable function $h_i : \mathbb{R}^n \to \mathbb{R}$, the function h_i is a **control barrier function** defined on a set $\mathcal{D}_i$, where $\mathcal{S}_i \subseteq \mathcal{D}_i \subset \mathbb{R}^n$, if there exists a Lipschitz continuous extended class $\mathcal{K}_\infty$ function α such that*

$$\sup_{\boldsymbol{u}_i \in \mathcal{U}_i} \left[L_{f_i} h_i(\boldsymbol{x_i}) + L_{g_i} h_i(\boldsymbol{x_i})\boldsymbol{u}_i \right] \geq -\alpha(h_i(\boldsymbol{x_i})), \ \forall \boldsymbol{x}_i \in \mathcal{D}_i. \tag{2.4}$$

It is evident that (2.4) reduces to (2.3) when $\boldsymbol{x}_i \in \partial\mathcal{S}_i$, thus if $h_i(\boldsymbol{x}(0)) \geq 0$ and h_i is a CBF on $\mathcal{D}_i$ then $\mathcal{S}_i$ can be rendered forward invariant. Note that the CBF is defined over a larger set $\mathcal{D}_i$ to encode asymptotic convergence of the set $\mathcal{S}_i$ if ever the trajectories of (2.1) were to leave $\mathcal{S}_i$. Due to (2.4) being affine in the control input, many works include CBF conditions (2.4) as linear constraints in a quadratic program (QP) based control law [3, 189], etc. When agents in the system are cooperative and communicating, a centralized controller may be deployed as follows

$$\boldsymbol{u}^* = \arg\min_{\boldsymbol{u} \in \mathcal{U}} \frac{1}{2}\|\boldsymbol{u} - \boldsymbol{u}^0\|^2 \tag{2.5a}$$

$$\text{s.t.} \quad \forall i, j = 1, \ldots, p, \ i \neq j$$

$$\phi_i + \boldsymbol{\gamma}_i \boldsymbol{u}_i \geq 0, \tag{2.5b}$$

$$\phi_{ij} + \boldsymbol{\gamma}_{ij} \boldsymbol{u} \geq 0, \tag{2.5c}$$

where $\boldsymbol{u} = [\boldsymbol{u}_1, \ldots, \boldsymbol{u}_p]^\top$ and $\boldsymbol{u}^0 = [\boldsymbol{u}_1^0, \ldots, \boldsymbol{u}_p^0]^\top$ denote concatenations of the input and nominal input vectors respectively, and

$$\phi_i = L_{f_i} h_i(\boldsymbol{x}_i) + \alpha_i(h_i(\boldsymbol{x}_i)), \tag{2.6a}$$

$$\phi_{ij} = L_{f_i} h_{ij}(\boldsymbol{x}_i, \boldsymbol{x}_j) + L_{f_j} h_{ij}(\boldsymbol{x}_i, \boldsymbol{x}_j) + \alpha_{ij}(h_{ij}(\boldsymbol{x}_i, \boldsymbol{x}_j)), \tag{2.6b}$$

$$\boldsymbol{\gamma}_i = L_{g_i} h_i(\boldsymbol{x}_i), \tag{2.6c}$$

$$\boldsymbol{\gamma}_{ij} = [L_{g_1} h_{ij}(\boldsymbol{x}_i, \boldsymbol{x}_j) \ldots L_{g_p} h_{ij}(\boldsymbol{x}_i, \boldsymbol{x}_j)], \tag{2.6d}$$

where each $\alpha_i, \alpha_{ij} \in \mathcal{K}_\infty$ such that (2.5b) represents an agent-specific constraint (e.g., speed limit) and (2.5c) represents an inter-agent constraint (e.g., collision avoidance). Note that $\boldsymbol{\gamma}_{ij}$ is a row vector of all zeros except indices i and j, denoted $\boldsymbol{\gamma}_{ij,[i]}$ and $\boldsymbol{\gamma}_{ij,[j]}$ respectively. If the agents are non-communicating, however, then a decentralized control law of the following form may be used:

$$\boldsymbol{u}_i^* = \underset{\boldsymbol{u}_i \in \mathcal{U}_i}{\arg\min} \frac{1}{2} \|\boldsymbol{u}_i - \boldsymbol{u}_i^0\|^2 \tag{2.7a}$$

$$\text{s.t. } \forall j = 1, \ldots, p,\ i \neq j$$

$$\phi_i + \boldsymbol{\gamma}_i \boldsymbol{u}_i \geq 0, \tag{2.7b}$$

$$\phi_{ij} + \boldsymbol{\gamma}_{ij,[i]} \boldsymbol{u}_i \geq 0, \tag{2.7c}$$

where (2.7b) and (2.7c) represent agent-specific and inter-agent constraints similar to (2.5b) and (2.5c). As noted by [190], collision avoidance is guaranteed under the centralized control scheme (2.5) whenever it is feasible, unlike the decentralized controller (2.7) under which (for a generic CBF h_{ij}) no such guarantee exists even when used uniformly by all agents. In Section 2.3, forms of (2.5) and (2.7) are used to solve versions of the intersection crossing problem outlined in Section 2.1.3.

2.1.3 Problem Formulation

Let $\mathcal{F}$ be an inertial frame with a point s_0 denoting its origin. Consider a collection of vehicles $\mathcal{A}$ approaching an unsignaled four-way intersection, where the dynamics of the i^{th} vehicle are

modeled as

$$\dot{x}_i = v_i \left(\cos \psi_i - \sin \psi_i \tan \beta_i\right), \tag{2.8a}$$

$$\dot{y}_i = v_i \left(\sin \psi_i + \cos \psi_i \tan \beta_i\right), \tag{2.8b}$$

$$\dot{\psi}_i = \frac{v_i}{l_r} \tan \beta_i, \tag{2.8c}$$

$$\dot{\beta}_i = \omega_i, \tag{2.8d}$$

$$\dot{v}_i = a_i, \tag{2.8e}$$

where x_i and y_i denote the position of the center of gravity (c.g.) of the vehicle with respect to s_0, ψ_i is the orientation of the body-fixed frame, $\mathcal{B}_i$, with respect to $\mathcal{F}$, β_i is the slip angle[1] of the vehicle c.g. relative to $\mathcal{B}_i$ (we assume $|\beta_i| < \frac{\pi}{2}$), and v_i is the velocity of the rear wheel with respect to $\mathcal{F}$. The state of vehicle i is denoted by $\boldsymbol{z}_i = [x_i \ y_i \ \psi_i \ \beta_i \ v_i]^\top$, and the full state is $\boldsymbol{z} = [\boldsymbol{z}_1 \dots \boldsymbol{z}_p]^\top$. The control input of the ith vehicle is $\boldsymbol{u}_i = [\omega_i \ a_i]^\top$, where a_i is the linear acceleration of the rear wheel and ω_i the angular velocity of the slip angle, β_i, which is related to the steering angle, δ_i, via $\tan \beta_i = \frac{l_r}{l_r + l_f} \tan \delta_i$, where $l_f + l_r$ is the wheelbase with l_f (resp. l_r) the distance from the c.g. to the center of the front (resp. rear) wheel. The model, depicted in Figure 2.1, is a dynamic extension of the kinematic bicycle model described in [191, Chapter 2], and is often used for autonomous vehicles [192].

For safety, consider that each vehicle must 1) obey the road speed limit and drive only in the forward direction, 2) remain inside the road boundaries, and 3) avoid collisions with all vehicles. The satisfaction of requirement 2) can be handled via nominal design of ω_i, whereas 1) and 3) may be encoded with the following candidate CBFs:

$$h_{s,i}(\boldsymbol{z}_i) = (v_{max} - v_{r,i})(v_{r,i}), \tag{2.9}$$

$$h_{0,ij}(\boldsymbol{z}_i, \boldsymbol{z}_j) = (x_i - x_j)^2 + (y_i - y_j)^2 - (2R)^2, \tag{2.10}$$

where v_{max} denotes the speed limit (in m/s) and R is a safe radius in m. Note that (2.10) is widely used in the literature to encode collision avoidance [193, 190]. Thus, $h_{s,i}$ and $h_{0,ij}$ define the following sets at time t:

$$\mathcal{S}_{s,i}(t) = \{\boldsymbol{z}_i(t) \in \mathbb{R}^5 : h_{s,i}(\boldsymbol{z}_i(t)) \geq 0\},$$
$$\mathcal{S}_{0,ij}(t) = \{(\boldsymbol{z}_i(t), \boldsymbol{z}_j(t)) \in \mathbb{R}^5 \times \mathbb{R}^5 : h_{0,ij}(\boldsymbol{z}_i(t), \boldsymbol{z}_j(t)) \geq 0\},$$

[1]The slip angle is the angle between the velocity vector associated with a point in a frame and the orientation of the frame.

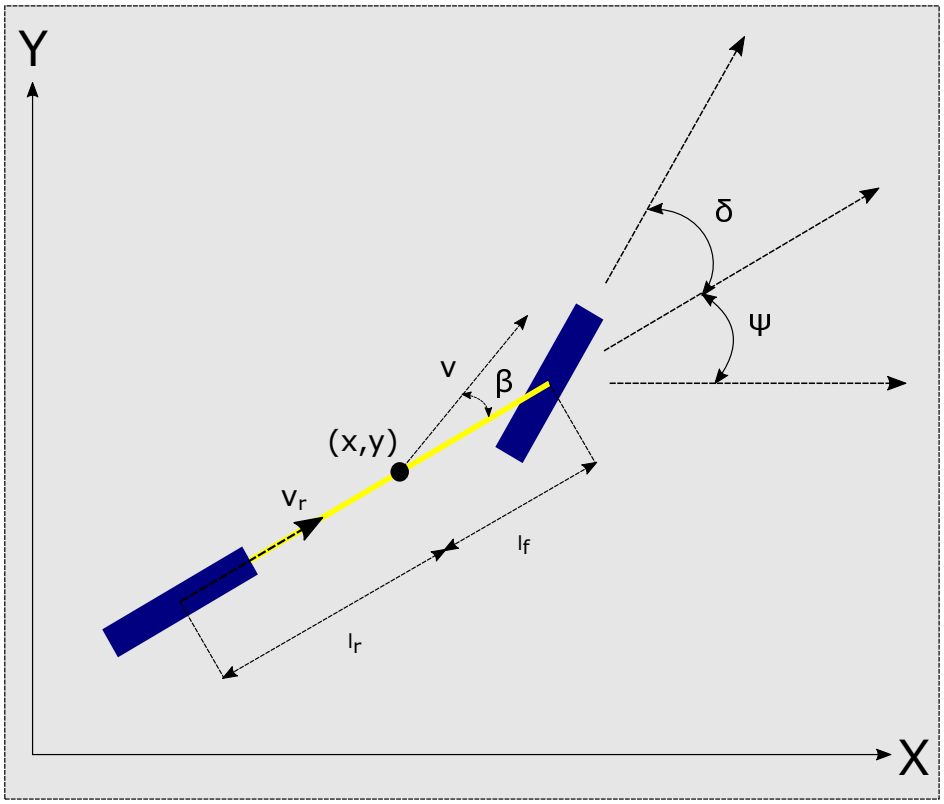

Figure 2.1: Diagram of bicycle model described in (2.8).

the intersection of which constitutes the safe set for a given vehicle, i.e.

$$\mathcal{S}_i(t) = \{\mathcal{S}_{s,i}(t) \cap \mathcal{S}_{0,i}(t)\}, \tag{2.11}$$

where $\mathcal{S}_{0,i}(t) = \bigcap_{j=1,j\neq i}^{N} \mathcal{S}_{0,ij}(t)$.

Before the problem under consideration can be formally introduced, it must be pointed out that the dynamics (2.8) under some predicted control policy $\hat{\boldsymbol{u}}_i$ may be expressed as

$$\dot{\hat{\boldsymbol{z}}}_i = f_i(\hat{\boldsymbol{z}}_i(\tau)) + g_i(\hat{\boldsymbol{z}}_i(\tau))\hat{\boldsymbol{u}}_i,\ \hat{\boldsymbol{z}}_i(t_0) = \boldsymbol{z}_i(t_0), \tag{2.12}$$

where $\hat{\boldsymbol{z}}_i \in \mathbb{R}^n$ denotes the state predicted under the policy $\hat{\boldsymbol{u}}_i$, t_0 is the beginning of the prediction interval $\mathcal{T}(t_0) = [t_0, t_0+\bar{\tau}]$ with look-ahead time $0 < \bar{\tau} < \infty$, and $\tau \in \mathcal{T}(t_0)$. At any time instance, the predicted dynamics (2.12) may be propagated forward in time to determine the predicted state $\hat{\boldsymbol{z}}_i(\tau)$ at some future time $\tau \in \mathcal{T}(t_0)$. Motivated by the popularity of minimum-norm controllers (e.g., [187]), in this chapter the predicted control policy $\hat{\boldsymbol{u}}_i$ is taken to be the zero-control policy, defined as $\hat{\boldsymbol{u}}_i \triangleq [\hat{\omega}_i\ \hat{a}_i]^\top = [0\ 0]^\top$.

Assumption 2.1 (Collision-Free Initial Predicted Trajectories). *For all vehicles $i \in \mathcal{A}$ with*

dynamics governed by (2.8)*, assume that the predicted closed-loop trajectories of* (2.12) *under the zero-control policy* $\hat{\boldsymbol{u}}_i$ *beginning at* $t_0 = 0$ *are safe over the interval* $\tau \in [0, \bar{\tau}]$*, i.e.* $\hat{\boldsymbol{z}}_i(\tau) \in \mathcal{S}_i(\tau)$ *for all* $\tau \in [0, \bar{\tau}]$, $\forall i \in \mathcal{A}$*.*

Assumption 2.1 states that no collisions shall occur between vehicles traveling with constant velocity within a time $\bar{\tau}$ of the initial time instant, i.e. no vehicles are on a collision course at the outset. The following remark highlights how this may be restrictive, and thus serves as one of the motivating factors behind the RFF-CBF introduced in Section 2.2.4.

Remark 2.1. *The look-ahead time* $\bar{\tau}$ *directly influences the set of allowable initial conditions, and vice versa: given* $\bar{\tau}$*, the set of allowable initial conditions is restricted to* $\mathcal{Z}_0(\bar{\tau}) = \{\boldsymbol{z} \in \mathbb{R}^{pn} : F(\boldsymbol{z}, \bar{\tau}) \geq 0\}$*, where* $F : \mathbb{R}^{pn} \times \mathbb{R}_{\geq 0} \to \mathbb{R}$ *is negative if vehicles are predicted to collide under* $\hat{\boldsymbol{u}}_i$ *and non-negative otherwise. On the other hand, given the set of initial states* $\mathcal{Z}_0$*, the allowable values of* $\bar{\tau}$ *are those for which no collisions occur under* $\hat{\boldsymbol{u}}_i$ *over the initial time interval* $[0, \bar{\tau}]$*.*

The problem under consideration in this chapter is now introduced.

Problem 2.1. *Consider a set of vehicles (*$i \in \mathcal{A}$*) whose dynamics are described by* (2.8)*. Given Assumption 2.1, design a control law,* $\boldsymbol{u}_i^*(t) = [\omega_i^*(t)\ a_i^*(t)]^\top$*, such that,* $\forall i \in \mathcal{A}$*,*

1. *the closed-loop trajectories of* (2.8) *remain safe for all time (*$\boldsymbol{z}_i(t) \in \mathcal{S}_i(t)$, $\forall t \geq 0$*), and*
2. *at every time* $t \geq 0$ *the closed-loop trajectories of* (2.12) *over the interval* $\tau \in [t, t + \bar{\tau}]$ *remain safe under the zero-control policy* $\hat{\boldsymbol{u}}_i$*, i.e.* $\hat{\boldsymbol{z}}_i(\tau) \in \mathcal{S}_i(\tau)$, $\forall \tau \in [t, t + \bar{\tau}]$, $\forall t \geq 0$ *under* $\hat{\boldsymbol{u}}_i(\tau)$*.*

The second element of Problem 2.1 requires that the trajectories of (2.12), i.e., the trajectories of (2.1) under the zero-control control policy $\hat{\boldsymbol{u}}_i$, remain safe for all time. In the following section, a function that serves as a facet of the proposed solution to Problem 2.1 is introduced: a FF-CBF suitable for QP-based controllers.

2.2 Future-Focused Control Barrier Functions

Recall the nominal CBF for inter-agent safety given by (2.10), and note that for two agents i and j it may be rewritten as

$$h_{0,ij}(\boldsymbol{z}_i, \boldsymbol{z}_j) = D_{ij}^2(\boldsymbol{z}_i, \boldsymbol{z}_j) - (2R)^2, \tag{2.13}$$

where $D_{ij}(\boldsymbol{z}_i, \boldsymbol{z}_j) = \sqrt{(x_i - x_j)^2 + (y_i - y_j)^2}$ defines the distance between two agents in the XY plane. Let the differential inter-agent position, $\boldsymbol{\xi}_{ij}$, velocity, $\boldsymbol{\nu}_{ij}$, and acceleration, $\boldsymbol{\alpha}_{ij}$, vectors be

$$\begin{aligned}
\boldsymbol{\xi}_{ij} &= [\xi_{x,ij},\ \xi_{y,ij}]^\top = [x_i - x_j,\ y_i - y_j]^\top, \\
\boldsymbol{\nu}_{ij} &= [\nu_{x,ij},\ \nu_{y,ij}]^\top = [\dot{x}_i - \dot{x}_j,\ \dot{y}_i - \dot{y}_j]^\top, \\
\boldsymbol{\alpha}_{ij} &= [\alpha_{x,ij},\ \alpha_{y,ij}]^\top = [\ddot{x}_i - \ddot{x}_j,\ \ddot{y}_i - \ddot{y}_j]^\top,
\end{aligned}$$

where the argument t has been omitted for conciseness. In what follows, the subscript ij is also dropped from D, ξ, ν, and α. The critical observation is that the inter-agent distance at any arbitrary time, T, is $D(\boldsymbol{z}_i(T), \boldsymbol{z}_j(T)) = \|\boldsymbol{\xi}(T)\|$. In what follows, forms of the minimum value for the inter-agent distance are given for two different cases under the zero-control control policy $\hat{\boldsymbol{u}}_i$: in Section 2.2.1, the case where all agents have a zero slip angle (and thus are not turning) is studied, i.e., for $\beta_i = 0$, $\forall i \in \mathcal{A}$, and in Section 2.2.2 the case where one or more agents may be turning is considered, i.e., for when $\exists i \in \mathcal{A}$ such that $\beta_i \neq 0$.

2.2.1 Zero Slip-Angle: No Turning Agents

For the case where $\beta_i = 0$, $\forall i \in \mathcal{A}$, under the zero-control control policy $\hat{\boldsymbol{u}}_i$ all agents have zero acceleration in the XY plane (i.e., $\ddot{x}_i = \ddot{y}_i = \ddot{x}_j = \ddot{y}_j = 0$). As such, a linear model predicts the following at time $T = t + \tau$: $\boldsymbol{\xi}(t + \tau) = \boldsymbol{\xi}(t) + \boldsymbol{\nu}(t)\tau$. Under such circumstances, the predicted distance at a time of $t + \tau$ is

$$D\big(\hat{\boldsymbol{z}}_i(t + \tau), \hat{\boldsymbol{z}}_j(t + \tau)\big) = \sqrt{\xi_x^2 + \xi_y^2 + 2\tau(\xi_x\nu_x + \xi_y\nu_y) + \tau^2(\nu_x^2 + \nu_y^2)}.$$

As such, the minimum predicted future distance between agents under the zero-control policy may be defined as

$$D\big(\hat{\boldsymbol{z}}_i(t + \tau^*), \hat{\boldsymbol{z}}_j(t + \tau^*)\big) = \|\boldsymbol{\xi}(t) + \boldsymbol{\nu}(t)\tau^*\|, \tag{2.14}$$

where

$$\tau^* = \underset{\tau \in \mathbb{R}}{\arg\min}\, D^2\big(\hat{\boldsymbol{z}}_i(t + \tau), \hat{\boldsymbol{z}}_j(t + \tau)\big) = -\frac{\xi_x\nu_x + \xi_y\nu_y}{\nu_x^2 + \nu_y^2}. \tag{2.15}$$

2.2.2 Non-Zero Slip-Angle: Turning Agents

In this section, the case where $\exists i \in \mathcal{A}$ such that $\beta_i \neq 0$ is addressed. It is worth noting that while the simulation results presented in Section 2.3 do not use controllers derived using the method presented in this section, it is provided nevertheless for completeness. In this case, all agents i with $\beta_i \neq 0$ have non-zero acceleration in the XY plane even under the zero-control control policy $\hat{\boldsymbol{u}}_i$ (i.e., $\ddot{x}_i \neq 0, \ddot{y}_i \neq 0$). Additionally, the linear model used for future state prediction in the

prior scenario is no longer accurate due to the constant rate of (2.8c) under the zero-control policy. As such, a nonlinear model is required to predict the minimum inter-agent distance D^* at time $T = t + \tau$:

$$D^*(\hat{\boldsymbol{z}}_i(t+\tau^*), \hat{\boldsymbol{z}}_j(t+\tau^*)) = \left\| \boldsymbol{\xi}(t) + \boldsymbol{\nu}(t)\tau^* + \int_0^{\tau^*} \boldsymbol{\alpha}(s)ds \right\|,$$

where

$$\begin{aligned}
\alpha_x(s) = v_j\dot{\psi}_j\Big(&\cos\big(\psi_j(t) + \dot{\psi}_j s\big) - \sin\big(\psi_j(t) + \dot{\psi}_j s\big)\tan(\beta_j)\Big) \\
&- v_i\dot{\psi}_i\Big(\cos\big(\psi_i(t) + \dot{\psi}_i s\big) - \sin\big(\psi_i(t) + \dot{\psi}_i s\big)\tan(\beta_i)\Big), \\
\alpha_y(s) = v_i\dot{\psi}_i\Big(&\sin\big(\psi_i(t) + \dot{\psi}_i s\big) + \cos\big(\psi_i(t) + \dot{\psi}_i s\big)\tan(\beta_i)\Big) \\
&- v_j\dot{\psi}_j\Big(\sin\big(\psi_j(t) + \dot{\psi}_j s\big) + \cos\big(\psi_j(t) + \dot{\psi}_j s\big)\tan(\beta_j)\Big),
\end{aligned}$$

such that $\boldsymbol{\alpha}(s) = [\alpha_x(s)\ \alpha_y(s)]^\top$, and

$$\tau^* = \min \mathcal{M} = \arg\min_{\tau \geq 0} D^2\big(\hat{\boldsymbol{z}}_i(t+\tau), \hat{\boldsymbol{z}}_j(t+\tau)\big). \tag{2.16}$$

Note that in (2.16) it is specified that τ^* is the minimum element of the set $\mathcal{M}$ consisting of minimizers of D^2. With D^2 being nonlinear in τ due to the non-zero acceleration of vehicles in the XY plane, numerical tools are used to compute the solutions to (2.16).

2.2.3 FF-CBF for Collision Avoidance

It goes without saying that the true trajectories of (2.1) will often evolve without deploying the predicted zero-control policy $\hat{\boldsymbol{u}}_i$, just as a maximum (or minimum) constant or specific time-varying predicted control policy would often not be deployed in practice. The zero policy is chosen, however, due to the resulting mathematical simplicity (no forward integration required in the case of non-turning vehicles) and the popularity of minimum-norm controllers (e.g., [194, 195]) seeking the smallest admissible control effort. In the remainder of this chapter, only the methods introduced in Section 2.2.1 are considered.

The FF-CBF for collision avoidance, the intended effect of which is depicted in Figure 2.2, is now introduced:

$$h_{\hat{\tau},ij}(\boldsymbol{z}_i, \boldsymbol{z}_j) = D_{ij}^2(\hat{\boldsymbol{z}}_i(t+\hat{\tau}), \hat{\boldsymbol{z}}_j(t+\hat{\tau})) - (2R)^2, \tag{2.17}$$

where

$$\hat{\tau} = \hat{\tau}^* K_0(\hat{\tau}^*) + (\bar{\tau} - \hat{\tau}^*)K_{\bar{\tau}}(\hat{\tau}^*), \tag{2.18}$$

with $\bar{\tau} > 0$ representing the length of the look-ahead horizon, $K_\delta(s) = \frac{1}{2} + \frac{1}{2}\tanh\big(k(s-\delta)\big)$,

$k > 0$, and

$$\hat{\tau}^* = -\frac{\xi_x \nu_x + \xi_y \nu_y}{\nu_x^2 + \nu_y^2 + \varepsilon}, \tag{2.19}$$

where $0 < \varepsilon \ll 1$. Using (2.18) alleviates undesirable characteristics of (2.15), namely that τ^* may become unbounded. The inclusion of ε makes (2.19) well-defined, and $K_\delta(t)$ allows (2.18) to smoothly approximate $\hat{\tau}^*$ between 0 and $\bar{\tau}$.

It is worth mentioning that the FF-CBF is related to the backup CBFs used for safe control design in [196, 197] in the following sense: whereas past works have required a backup policy to actively intervene to preserve safety (e.g., by applying proportional braking, see [190]), this formulation encodes that present control actions prevent future unsafe scenarios that *would* occur if all vehicles employed a zero-control policy. Thus, the FF-CBF seeks to preserve the viability of the zero-control policy as a safe backup policy.

Theorem 2.1. *Consider two agents governed by the dynamics* (2.8) *whose states are* $\boldsymbol{z}_i$ *and* $\boldsymbol{z}_j$. *Suppose that* $h_{\hat{\tau},ij}$ *is defined by* (2.17)*, with* $\hat{\tau}$ *given by* (2.18)*. Then, the following hold for all bounded* $\boldsymbol{z}_i$*,* $\boldsymbol{z}_j$*:*

1. $h_{\hat{\tau},ij} \in \mathcal{C}^1$
2. $h_{\hat{\tau},ij} \leq h_{0,ij}$ *whenever* $\hat{\tau} \leq 2\hat{\tau}^*$

Proof. For the first part, it must be shown that the derivative of (2.17) is well-defined and continuous. Consider that from (2.14), (2.17), and (2.18)

$$\begin{aligned} \dot{h}_{\hat{\tau},ij}(\boldsymbol{z}) = {} & 2\xi_x \nu_x + 2\xi_y \nu_y + 2\dot{\hat{\tau}}(\xi_x \nu_x + \xi_y \nu_y) \\ & + 2\hat{\tau}(\nu_x^2 + \nu_y^2 + \xi_x \alpha_x + \xi_y \alpha_y) \\ & + 2\hat{\tau}\dot{\hat{\tau}}(\nu_x^2 + \nu_y^2) + 2\hat{\tau}^2(\nu_x \alpha_x + \nu_y \alpha_y). \end{aligned} \tag{2.20}$$

Since $\hat{\tau}$ is bounded by definition, it follows that $h_{\hat{\tau},ij} \in \mathcal{C}^1$ when $\hat{\tau} \in \mathcal{C}^1$. From (2.18), it holds that

$$\dot{\hat{\tau}} = \dot{\hat{\tau}}^* \left(K_0(\hat{\tau}^*) - K_{\bar{\tau}}(\hat{\tau}^*)\right) + \hat{\tau}^*(\dot{K}_0(\hat{\tau}^*) - \dot{K}_{\bar{\tau}}(\hat{\tau}^*)) + \bar{\tau}\dot{K}_{\bar{\tau}}(\hat{\tau}^*),$$

where

$$\dot{K}_\delta(\hat{\tau}^*) = \dot{\hat{\tau}}^* \frac{k}{2} \text{sech}^2\left(k(\hat{\tau}^* - \delta)\right)$$

and from (2.19)

$$\dot{\hat{\tau}}^* = -\frac{\alpha_x(2\nu_x \tau^* + \xi_x) + \alpha_y(2\nu_y \tau^* + \xi_y) + \nu_x^2 + \nu_y^2}{\nu_x^2 + \nu_y^2 + \varepsilon}$$

since $\dot{\hat{\tau}}^*$ and $\dot{K}_\delta(t)$ are bounded and continuous for bounded arguments, it is true that $\hat{\tau} \in \mathcal{C}^1$ for bounded $\boldsymbol{z}_i$, $\boldsymbol{z}_j$. Thus, $h_{\hat{\tau},ij} \in \mathcal{C}^1$.

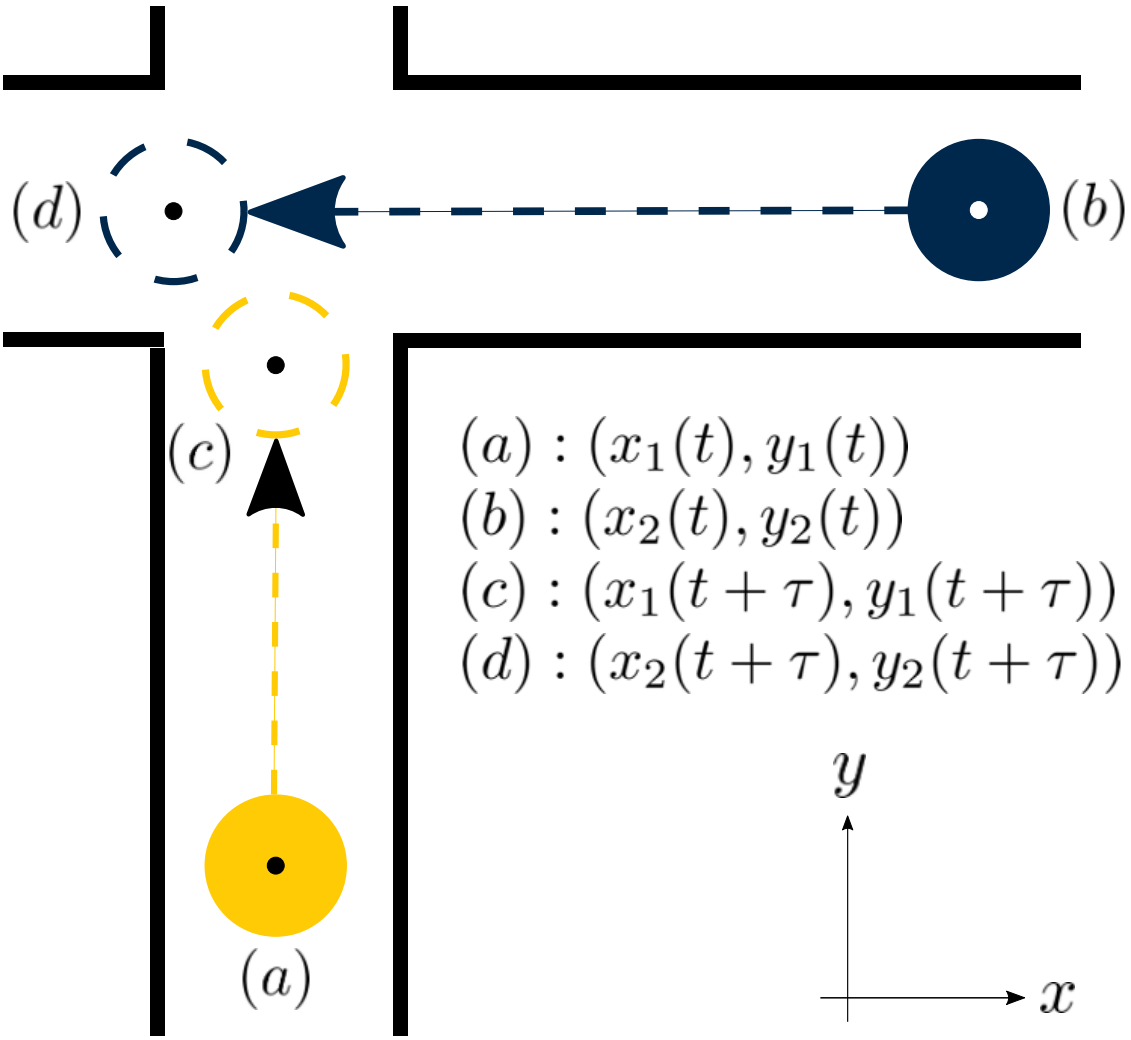

Figure 2.2: Visualization of the effect of the FF-CBF. Whereas $h_{0,12}$ is evaluated based on the locations of vehicles 1 and 2 at time t, i.e. (a) and (b), $h_{\tau,12}$ judges safety based on the predicted future locations of the vehicles at time $t+\tau$, i.e. (c) and (d), allowing the present control to take action to avoid predicted future danger.

For the second part, observe that $h_{\hat{\tau},ij}(\boldsymbol{z}) = h_{0,ij}(\boldsymbol{z}) + 2\hat{\tau}(\xi_x\nu_x + \xi_y\nu_y) + \hat{\tau}^2(\nu_x^2 + \nu_y^2)$, thus $h_{\hat{\tau},ij}(\boldsymbol{z}_i, \boldsymbol{z}_j) \leq h_{0,ij}(\boldsymbol{z}_i, \boldsymbol{z}_j)$ whenever

$$\hat{\tau} \leq -2\frac{\xi_x\nu_x + \xi_y\nu_y}{\nu_x^2 + \nu_y^2} = 2\tau^*. \tag{2.21}$$

With ε in the denominator of (2.19), it follows that $\hat{\tau}^* < \tau^*$ whenever $\tau^* > 0$ (and $\hat{\tau}^* = 0$ when $\tau^* = 0$), thus the inequality in (2.21) holds whenever $\hat{\tau} \leq 2\hat{\tau}^*$. It follows, then, that $h_{\hat{\tau},ij}(\boldsymbol{z}) \leq h_{0,ij}(\boldsymbol{z})$ whenever $\hat{\tau} \leq 2\hat{\tau}^*$. □

Remark 2.2. *The condition $\hat{\tau} \leq 2\hat{\tau}^*$ may be satisfied $\forall \hat{\tau}^* \geq 0$ for choices of $k \geq 1$ in $K_\delta(t)$. Since k is a shape parameter for the function K, higher values of k lead to smaller approximation error*

$e_\tau = |\hat{\tau} - \tau^*|$ *for* $\tau^* \in [0, T]$.

Since $h_{\hat{\tau},ij} \in \mathcal{C}^1$, it follows from Definition 2.3 that if there exists a function $\alpha \in \mathcal{K}_\infty$ such that (2.4) holds then $h_{\hat{\tau},ij}$ is a valid CBF. Under such conditions, the FF-CBF may be synthesized with any nominal control law using (2.5) for communicating agents or (2.7) for non-communicating agents. In contrast to when used with a generic CBF, the decentralized control law (2.7) guarantees collision avoidance under our FF-CBF $h_{\hat{\tau},ij}$ and dynamics (2.8) (as long as it is feasible) provided that all vehicles deploy (2.7) with $h_{\hat{\tau},ij}$ and are not turning, i.e. $\psi_i = \beta_i = 0$. This is because $L_f h_{\hat{\tau},ij} \to 0$ as[2] $\hat{\tau} \to \tau^*$, in which case (2.7c) becomes

$$L_{g_i} h_{\hat{\tau},ij} \boldsymbol{u}_i + \alpha_{ij}(h_{\hat{\tau},ij}) \geq 0, \quad \forall i \in \mathcal{A}, \tag{2.22}$$

which, for any given two agent pair i, j yields

$$\dot{h}_{\hat{\tau},ij} = L_{g_i} h_{\hat{\tau},ij} \boldsymbol{u}_i + L_{g_j} h_{\hat{\tau},ji} \boldsymbol{u}_j \geq -\alpha_{ij}(h_{\hat{\tau},ij}) - \alpha_{ji}(h_{\hat{\tau},ji})$$

where $h_{\hat{\tau},ij} = h_{\hat{\tau},ji}$, which satisfies (2.3) and thus prevents collisions. Intuitively, a zero CBF drift term i.e. $L_f h_{\hat{\tau},ij} = 0$ is explained by the fact that the FF-CBF $h_{\hat{\tau},ij}$ is already predicting the future minimum distance between vehicles i and j under zero-control policies, thus in the absence of an acceleration input the prediction is correct and the minimum distance between vehicles is reached at time $t + \hat{\tau}$.

2.2.4 Relaxed Future-Focused Control Barrier Functions

Note that the zero level set defined by candidate CBF $h_{\hat{\tau},ij}$ represents a *virtual* barrier. Specifically, $h_{\hat{\tau},ij}(\boldsymbol{z}_i, \boldsymbol{z}_j) < 0$ does not imply that a collision has occurred ($h_{0,ij}(\boldsymbol{z}_i, \boldsymbol{z}_j) < 0$), nor does it suggest that one is unavoidable; rather, $h_{\hat{\tau},ij}(\boldsymbol{z}_i, \boldsymbol{z}_j) < 0$ implies that a future collision will occur if the zero-control control policy, $\hat{\boldsymbol{u}}_k$, is applied uniformly by each vehicle $k \in \{i, j\}$. This motivates the notion of the RFF-CBF:

$$H_{ij}(\boldsymbol{z}_i, \boldsymbol{z}_j) = h_{\hat{\tau},ij}(\boldsymbol{z}_i, \boldsymbol{z}_j) + \alpha_0 \left(h_{0,ij}(\boldsymbol{z}_i, \boldsymbol{z}_j) \right), \tag{2.23}$$

where $\alpha_0 \in \mathcal{K}_\infty$. The zero super-level set of H_{ij} is then

$$\mathcal{S}_{H,ij} = \{(\boldsymbol{z}_i, \boldsymbol{z}_j) \in \mathbb{R}^{2n} \mid H_{ij}(\boldsymbol{z}_i, \boldsymbol{z}_j) \geq 0\}, \tag{2.24}$$

[2]In simulation, it has been observed that $L_f h_{\hat{\tau},ij}$ is on the order of the approximation error $e_\tau = |\hat{\tau} - \tau^*| \approx 10^{-9}$ for $\tau^* \in [0, \bar{\tau}]$, which may be accounted for by subtracting $\varepsilon \approx 10^{-9}$ from the left-hand side of (2.22).

which defines a *relaxed* virtual barrier that allows virtual constraint violations away from the physical barrier, and in that sense enlarges the admissible control space while preserving the collision avoidance guarantee. This is proved in the following result.

Theorem 2.2. *Consider two agents, each of whose dynamics are described by* (2.1)*. Suppose that* H_{ij} *is given by* (2.23)*, and that* $H_{ij} \geq 0$ *at* $t = 0$*. If there exist control inputs,* $\boldsymbol{u}_i$ *and* $\boldsymbol{u}_j$*, such that the following condition holds, for all* $t \geq 0$*,*

$$\sup_{\substack{\boldsymbol{u}_i \in \mathcal{U}_i \\ \boldsymbol{u}_j \in \mathcal{U}_j}} \left[L_{f_i} H_{ij} + L_{f_j} H_{ij} + L_{g_i} H_{ij} \boldsymbol{u}_i + L_{g_j} H_{ij} \boldsymbol{u}_j \right] \geq 0, \tag{2.25}$$

for all $\boldsymbol{z} \in \partial \mathcal{S}_{H,ij}$*, then, the physical safe set defined by* $\mathcal{S}_{0,ij}(t) = \{(\boldsymbol{z}_i, \boldsymbol{z}_j) \in \mathbb{R}^{2n} \mid h_{0,ij}(\boldsymbol{z}_i, \boldsymbol{z}_j) \geq 0\}$ *is forward invariant under* $\boldsymbol{u}_i$*,* $\boldsymbol{u}_j$*, i.e. there is no collision between agents* i *and* j*.*

Proof. In order to show that $\mathcal{S}_{0,ij}$ is rendered forward invariant by (2.25), it must be shown that (2.25) implies that $\dot{h}_{0,ij} \geq 0$ whenever $h_{0,ij} = 0$. This will be proved by contradiction.

Suppose that $H_{ij}, h_{0,ij} = 0$, and that (2.25) holds but $\dot{h}_{0,ij} < 0$. Note also that by Theorem 2.1 $h_{\hat{\tau},ij} \leq h_{0,ij}$. Then, it follows that $\dot{h}_{0,ij} = 2(\xi_x \nu_x + \xi_y \nu_y) < 0$, which by (2.18) implies that $\hat{\tau} > 0$. With $\hat{\tau} > 0$, it follows that $h_{\hat{\tau},ij} < h_{0,ij} = 0$. However, it was assumed that $H_{ij}, h_{0,ij} = 0$, which means by definition that $h_{\hat{\tau},ij} = 0$. Thus, a contradiction has been reached. It follows, then, that (2.25) implies that $\dot{h}_{0,ij} \geq 0$ whenever $h_{0,ij} = 0$. As such, $\mathcal{S}_{0,ij}$ is rendered forward invariant. □

As a result of Theorem 2.2, (2.23) may be used to encode safety in the context of a CBF-QP control scheme (2.5) or (2.7).

In the ensuing simulations section, a comparative study on the efficacy of the nominal (2.13), future-focused (2.17), and relaxed future-focused (2.23) CBFs is conducted using randomized trials of an automotive intersection crossing problem.

2.3 Case Studies

In this section, the use of FF-CBFs is demonstrated for collections of both communicating and non-communicating vehicles in the context of simulated and experimental trials of an unsignaled intersection scenario. Code and a selection of videos are provided on Github[3].

[3]Link to Github repository: github.com/6lackmitchell/ffcbf-control

2.3.1 Centralized Control: Simulated Trials

In an empirical study on a simulated 4-vehicle unsignaled intersection scenario, it is shown how using a RFF-CBF to control communicating vehicles in a centralized manner improves intersection throughput with promising empirical results on safety and QP feasibility. The successes of three different centralized controllers of the form (2.5) are investigated, namely

$$\boldsymbol{u}_i^* = [\omega_i^* \ a_i^*]^\top, \ \forall i = 1, \dots, A, \tag{2.26}$$

where the turning rate is

$$\omega_i^* = \min\left(\max(\omega_i^0, -\bar{\omega}), \bar{\omega}\right), \tag{2.27}$$

and the accelerations $a_1^*, \dots, a_p^*$ are computed via

$$[a_1^* \dots a_p^*]^\top = \underset{[a_1 \dots a_p]}{\arg\min} \frac{1}{2} \sum_{i=1}^{p} (a_i - a_i^0)^2 \tag{2.28a}$$

$$\text{s.t.} \quad \forall i, j = 1, \dots, p, \ j \neq i$$

$$\boldsymbol{A} a_i \leq \boldsymbol{b}, \tag{2.28b}$$

$$\phi_i + \boldsymbol{\gamma}_i a_i \geq 0, \tag{2.28c}$$

$$\phi_{ij} + \boldsymbol{\gamma}_{ij,[i]} a_i + \boldsymbol{\gamma}_{ij,[j]} a_j \geq 0, \tag{2.28d}$$

where ω_i^0 and a_i^0 denote the nominal inputs computed using LQR (see Appendix A for a detailed explanation), (2.28b) encodes input constraints of the form $-\bar{a} \leq a_i \leq \bar{a}$, (2.28c) enforces both the road speed limit and requires that vehicles do not reverse, and (2.28d) is the collision avoidance condition, where ϕ and γ are as in (2.6). Specifically, the controllers under examination are (2.26) with

1. 0-CBF: $h_{ij} = h_{0,ij}$ according to (2.13)
2. ff-CBF: $h_{ij} = h_{\hat{\tau},ij}$ from (2.17)
3. rff-CBF: $h_{ij} = H_{ij}$ via (2.23)

with $\alpha_0(h_{0,ij}) = k_0 h_{0,ij}$, where $k_0 = 0.1 \max(\hat{\tau} - 1, \varepsilon)$, $\varepsilon = 0.001$, the look-ahead horizon $\bar{\tau} = 5$s, and $\alpha_{ij}(h_{ij}) = 10 h_{ij}$, $\bar{\omega} = \pi/2$, and $\bar{a} = 9.81$ for all cases. Note that (2.26) is centralized in the sense that it is assumed that all states, $\boldsymbol{z}_i$, and nominal control inputs, $\boldsymbol{u}_i^0$, are known.

For each study, $N = 1000$ trials were performed simulating trajectories of 4 vehicles approaching the intersection from different lanes, all of whose dynamics are described by (2.8), using the control scheme described by (2.26) and a timestep of $\Delta t = 0.01$s. At the beginning of each trial,

Table 2.1: Controller Performance – All Proceed Straight

CBF	Success	Feas.	DLock	Unsafe	Avg. Time
$h_{ij} = h_{0,ij}$	0.653	1	0.347	0	5.67
$h_{ij} = h_{\hat{\tau},ij}$	1	1	0	0	3.45
$h_{ij} = H_{ij}$	1	1	0	0	3.21

the vehicles were assigned to a lane and their initial conditions were randomized via

$$d_i = d_0 + U(-\Delta_d, \Delta_d),$$
$$s_i = s_0 + U(-\Delta_s, \Delta_s),$$

where d_i denotes the initial distance of vehicle i from the intersection, s_i its initial speed, and $U(a, b)$ a sample from the uniform random distribution between a and b. The above parameters were chosen to be $d_0 = 12$m, $\Delta_d = 5$m, $s_0 = 6$m/s, and $\Delta_s = 3$m/s. Further, trials whose random initial conditions violated Assumption 2.1 were removed from the study. For the speed limit, $v_{max} = 10$m/s was used.

For performance evaluation, the following metrics were considered:

1. Success: $\frac{\text{Number of Successful Trials}}{\text{Number of Trials}}$,
2. Feas.: $\frac{\text{Number of Trials in which QP is Always Feasible}}{\text{Number of Trials}}$,
3. DLock: $\frac{\text{Number of Trials in which Vehicles become deadlocked}}{\text{Number of Trials}}$,
4. Unsafe: $\frac{\text{Number of Trials Vehicles in which } h_{0,ij}<0}{\text{Number of Trials}}$,

where a successful trial is characterized as one where all vehicles exit the intersection at their desired location, a deadlock is characterized as when all vehicles have stopped and remained stopped for 3 sec, and "Avg. Time" is defined as the average time in which the final vehicle reached the intersection exit over all successful trials.

The performance of each controller was examined under two circumstances: 1) each vehicle seeks to proceed straight through the intersection without turning, and 2) three vehicles seek to proceed straight without turning and one seeks to make a left turn. The results for the 3 different controllers are compiled in Tables 2.1 and 2.2 respectively. Although the 0-CBF in a centralized QP-based control law is known to guarantee safety and QP feasibility under certain conditions [190], such a controller has no predictive power and is therefore prone to deadlocks. Such a deadlock is illustrated in Figure 2.3a. The FF-CBF-based controller succeeded as long as it was feasible, offering a 39% reduction in average time over the 0-CBF in the straight scenario and an

Table 2.2: Controller Performance – One Left Turn

CBF	Success	Feas.	DLock	Unsafe	Avg. Time
$h_{ij} = h_{0,ij}$	0.689	1	0.311	0	7.75
$h_{ij} = h_{\hat{\tau},ij}$	0.963	0.963	0	0	5.33
$h_{ij} = H_{ij}$	1	1	0	0	4.91

31% time improvement in the turning scenario, but suffered from QP infeasibilities in the case of turning vehicles, one example of which is shown in Figure 2.3b. The RFF-CBF controller enjoyed both the same empirical feasibility and safety as the 0-CBF design and improved the average success time to a similar extent as the FF-CBF, specifically by 43% and 36% for the straight and turning scenarios respectively. In addition, the RFF-CBF control scheme achieved 100% feasibility even in the turning scenario, despite the constant velocity prediction model not taking a change of heading into account. Theoretical guarantees of feasibility, however, are left to future work. The control and RFF-CBF trajectories for a turning trial are illustrated in Figures 2.4a and 2.4b respectively, and the associated XY paths are shown in Figure 2.4c. It can be seen from Figure 2.4a that the control actions smoothly take action in advance of any dangerous scenario, and from Figure 2.4b that both H_{ij} and $h_{0,ij}$ remain non-negative for all i, j.

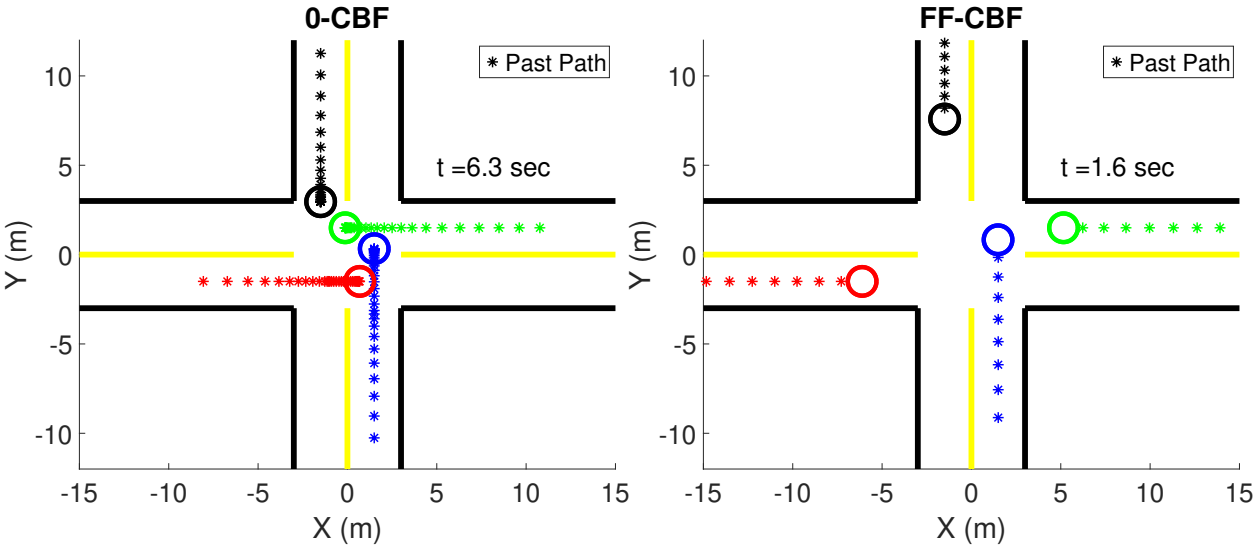

(a) 0-CBF (Straight Trial 582)

(b) FF-CBF (Turning Trial 137)

Figure 2.3: Selected XY trajectories for the intersection crossing problem using (a) 0-CBF and (b) FF-CBF. In (a), the centralized controller has no predictive power and the vehicles deadlock, whereas in (b) the FF-CBF-QP controller becomes infeasible for the blue vehicle despite a wide physical margin as the blue vehicle begins to turn left.

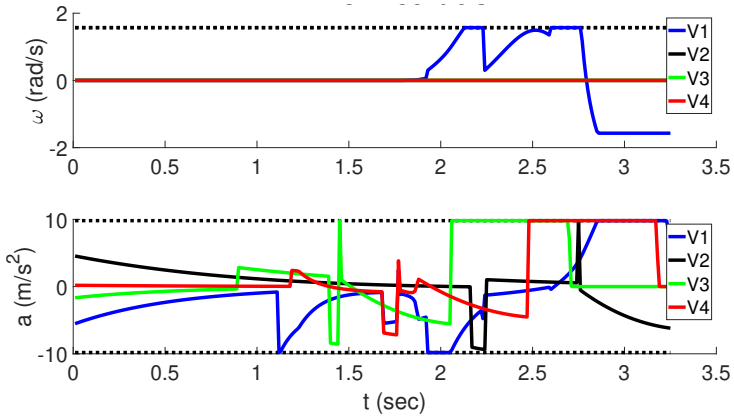

(a) RFF-CBF Controls

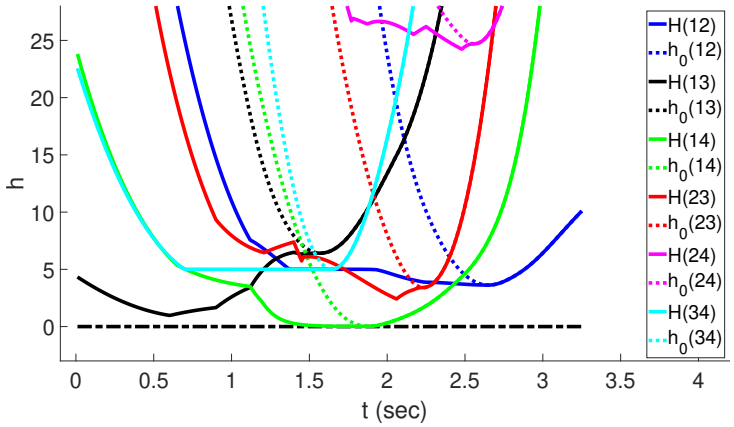

(b) RFF-CBF Values

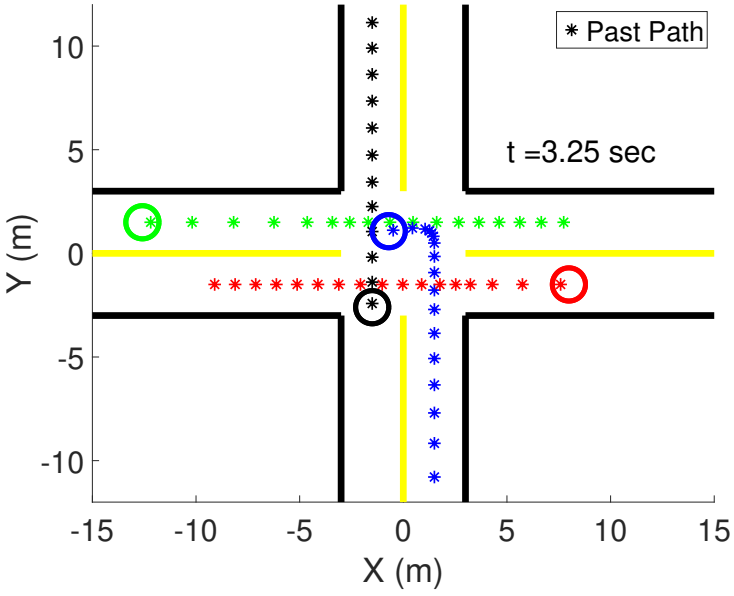

(c) RFF-CBF Paths

Figure 2.4: Trial 650 in the RFF-CBF controlled intersection study. (a) gives the control trajectories, (b) the RFF-CBF trajectories, and (c) the XY paths taken by the four vehicles. In (b), the notation (ij) denotes that the function is evaluated for vehicles i and j.

2.3.2 Decentralized Control: Rover Experiments

The success of the proposed decentralized RFF-CBF-QP controller was further demonstrated on a collection of AION R1 UGV rovers in an intersection scenario in the lab. Each of the 5 rovers was modeled as a bicycle according to (2.8) and was asked to proceed straight through the intersection while obeying a speed limit (encoded via (2.9)) and avoiding collisions with each other (using RFF-CBF (2.23)). A controller of the form (2.7) was used to compute acceleration a_i and angular rate ω_i inputs in order to send velocity $v_i(t_{k+1}) = v_i(t_k) + a_i \Delta t$ and ω_i commands to the rovers' customized on-board PID controllers. The full control loop ran at a frequency of 20 Hz, where the nominal input $\boldsymbol{u}_0$ was computed using the LQR law outlined in Appendix A, position feedback was obtained using a Vicon motion capture system, the extended Kalman filter output from the PX4 firmware running via the on-board Pixhawk was used for state estimation.

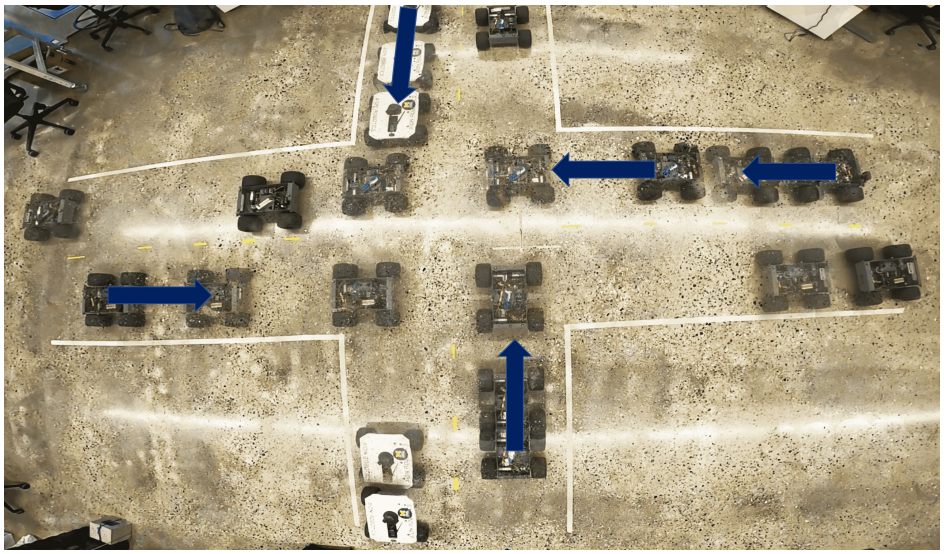

Figure 2.5: Five rovers safely traverse a four-way intersection in the laboratory environment using a decentralized rff-CBF-QP control law. The rovers at their initial positions are marked with arrows pointing in the direction of motion.

As shown in Figure 2.5, the RFF-CBF controller succeeds in driving the vehicles safely through the intersection without a deadlock. The video footage available at the provided GitHub link shows that, contrary to behavior expected using traditionally myopic, present-focused CBF-based control, some rovers accelerated into the intersection in order to avoid predicted future collisions whereas others braked to await their turn.

2.4 Conclusion

Improvements to traditionally myopic CBF-based safe control are introduced in the form of novel FF-CBFs and RFF-CBFs for collision avoidance. It is shown how the use of FF-CBFs for control design preserves safety of the system trajectories while simultaneously guaranteeing future predicted safety under an assumed zero-control policy over an arbitrarily large future time interval. With the FF-CBF defining a virtual barrier, the introduction of the RFF-CBF serves to permit relaxations thereof when away from the physical barrier between vehicles, and, in doing so, to afford the controller more time to deconflict predicted future collisions. An empirical study on an intersection crossing problem highlights the advantages of the proposed methods over existing CBF-based control, and the viability of the approach for real-time applications is demonstrated via a multi-rover experiment in the laboratory.

CHAPTER 3

Fixed-Time Parameter Identification for Safe Control Synthesis

In many dynamical systems, the presence of unknown or uncertain parameters in the system model (e.g., coefficients of drag for quadrotors) threatens the viability of model-based approaches to stabilizing and/or safe control design. While in some cases offline methods for learning the system model have been shown to mitigate this issue, online adaptation and control synthesis offers better robustness to environmental changes. With the above as motivation, this chapter studies the problem of online parameter identification for a class of nonlinear, control-affine systems subject to an additive, parameter-affine perturbation to the dynamics and its application to safe control design.

Whereas many works have investigated parameter identification with guarantees of asymptotic or exponential convergence, i.e., learning the true system parameters as time or the amount of data tends toward infinity, the notion of a Fixed-Time Stable (FxTS) equilibrium, i.e., one to which the system trajectories converge within a finite time bounded uniformly for any initial condition, has been shown to confer better disturbance rejection properties. In addition, system identification in the limit may be insufficient for control design when a system is subject to spatiotemporal constraints, e.g., if a vehicle must visit a target region within a specified time. As such, preliminaries are reviewed in Section 3.1, and then two FxTS parameter adaptation laws are proposed in Section 3.2 for learning the parametric model uncertainty under consideration within a fixed-time 1) under the assumption of system identifiability, and 2) when this assumption is removed. In the second case, conditions are presented under which the true disturbance to the system is learned even when the true parameters perturbing the system are not identified. In Section 3.3, time-varying bounds on the parameter estimation error are derived and used to propose a robust, adaptive Control Barrier Function (CBF) condition that renders a time-varying shrunken safe set forward invariant, thereby protecting against the worst-case instantaneous parameter estimation error while adapting to how the parameter estimates are changing with time. A Quadratic Program (QP)-based control law is then proposed for guaranteed safety throughout the model learning process. In Section 3.4 two case studies are conducted: in the first, the proposed methods are simulated against a sample of

similar methods from the literature on a safety- but also time-critical reach-avoid problem; whereas the second considers a quadrotor seeking to track a trajectory in a constant wind field.

The results in this chapter are based partly on [181] and [182]. The author wishes to acknowledge the contributions of Dr. Ehsan Arabi to the development of this work.

3.1 Preliminaries and Problem Statement

In this section, preliminaries are reviewed on fixed-time stability, set invariance, and parameter identification. Then, the problem under consideration is formally stated.

3.1.1 Fixed-Time Stability

Consider an autonomous, nonlinear dynamical system of the form

$$\dot{\boldsymbol{x}}(t) = f(\boldsymbol{x}(t)), \quad \boldsymbol{x}(t_0) = \boldsymbol{x}_0, \tag{3.1}$$

for which it is assumed that a unique solution exists, where $\boldsymbol{x} \in \mathbb{R}^n$, $f : \mathbb{R}^n \to \mathbb{R}^n$ is continuous, and $f(0) = 0$. The notion of fixed-time stability is essential to the proposed parameter adaptation laws in this chapter, and thus is reviewed for completeness. First, the notion of Lyapunov stability is required.

Definition 3.1 (Stability). *The origin of* (3.1) *is **stable** in the sense of Lyapunov if for every* $\epsilon > 0$ *there exists* $\delta(\epsilon) > 0$ *such that if* $\|\boldsymbol{x}_0\| < \delta$*, then* $\|\boldsymbol{x}(t)\| < \epsilon$ *for all* $t \geq 0$*.*

In contrast to various other notions of stability (e.g., asymptotic, exponential), the system trajectories converge to a fixed-time stable equilibrium within a finite time, independent of the initial condition.

Definition 3.2 (Fixed-Time Stability (FxTS)). *The origin of* (3.1) *is **fixed-time stable** if it is stable in the sense of Lyapunov and fixed-time convergent, i.e., any solution* $\boldsymbol{x}(t, \boldsymbol{x}_0)$ *of* (3.1) *reaches the origin in finite settling-time,* T*, independent of* $\boldsymbol{x}_0$*, i.e.,* $\boldsymbol{x}(t, \boldsymbol{x}_0) = 0$*,* $\forall t \geq T$*.*

In the following result introduced by [135], sufficient conditions are given for FxTS of the equilibrium of (3.1).

Theorem 3.1 (Lyapunov Conditions for FxTS). *Suppose there exists a continuously differentiable, positive definite, radially unbounded function* $V : \mathbb{R}^n \to \mathbb{R}$ *such that*

$$\dot{V}(x) \leq -aV(x)^p - bV(x)^q, \tag{3.2}$$

holds along the trajectories of (3.1) *with* $a, b > 0$, $0 < p < 1$ *and* $q > 1$. *Then, the origin of* (3.1) *is FxTS with settling time* $T(\boldsymbol{x}_0) \leq T_b$ *where*

$$T_b \leq \frac{1}{a(1-p)} + \frac{1}{b(q-1)}. \tag{3.3}$$

3.1.2 Set Invariance

For a given system, safety may be enforced by rendering some set of safe states forward invariant. The problem under consideration in this chapter concerns safe control design for the following class of nonlinear, control-affine systems subject to unknown, additive, parameter-affine uncertainty:

$$\begin{aligned} \dot{\boldsymbol{x}} &= f(\boldsymbol{x}(t)) + g(\boldsymbol{x}(t))\boldsymbol{u}(t) + \Delta(\boldsymbol{x}(t))\boldsymbol{\theta}^*, \\ \boldsymbol{x}(0) &= \boldsymbol{x}_0, \end{aligned} \tag{3.4}$$

where $\boldsymbol{x} \subset \mathbb{R}^n$ denotes the state, $\boldsymbol{u} \in \mathcal{U} \subset \mathbb{R}^m$ the control input, and $\boldsymbol{\theta}^* \in \Theta \subset \mathbb{R}^p$ a vector of unknown, static parameters. The availability of perfect state measurements is assumed in this chapter, and the state is assumed to be bounded. The sets $\mathcal{U}$ and Θ are the input constraint and admissible parameter sets respectively, where both are known and Θ is a polytope. It is assumed that the drift vector field $f : \mathbb{R}^n \to \mathbb{R}^n$, control matrix field $g : \mathbb{R}^n \to \mathbb{R}^{n\times m}$, and regressor $\Delta : \mathbb{R}^n \to \mathbb{R}^{n\times p}$ are known, continuous, and bounded for bounded inputs, such that for a continuous control input $\boldsymbol{u} : \mathbb{R} \to \mathcal{U}$ the system (3.4) admits a unique solution. The unknown term in the system, i.e., $d(\boldsymbol{x}) = \Delta(\boldsymbol{x})\boldsymbol{\theta}^*$, may describe disturbances or unmodelled phenomena that require estimation. In this chapter, it is assumed that the unknown parameters are static, i.e., that $\dot{\boldsymbol{\theta}}^* = \mathbf{0}_{p\times 1}$. As such, the estimated parameter vector is denoted $\hat{\boldsymbol{\theta}}$ so that the parameter estimation error vector is $\tilde{\boldsymbol{\theta}} = \boldsymbol{\theta}^* - \hat{\boldsymbol{\theta}}$ with dynamics given by

$$\dot{\tilde{\boldsymbol{\theta}}} = -\dot{\hat{\boldsymbol{\theta}}}. \tag{3.5}$$

Consider a continuously differentiable function $h : \mathbb{R}^n \to \mathbb{R}$ whose zero super-level set defines the set of safe states $\mathcal{S}$ for the system (3.4). The safe set is then given by

$$\mathcal{S} = \{\boldsymbol{x} \in \mathbb{R}^n : h(\boldsymbol{x}) \geq 0\}, \tag{3.6a}$$

$$\partial\mathcal{S} = \{\boldsymbol{x} \in \mathbb{R}^n : h(\boldsymbol{x}) = 0\}, \tag{3.6b}$$

$$\text{int}(\mathcal{S}) = \{\boldsymbol{x} \in \mathbb{R}^n : h(\boldsymbol{x}) > 0\}. \tag{3.6c}$$

Then, Nagumo's Theorem [188] provides a necessary and sufficient condition for the forward invariance of the set (3.6) under the system dynamics (3.4).

Lemma 3.1 (**Nagumo's Theorem**). *Suppose that $\boldsymbol{u} : \mathbb{R} \to \mathcal{U}$ is a continuous control input such that the closed-loop trajectories of* (3.4) *are uniquely determined in forward time. The set $\mathcal{S}$ is forward invariant for* (3.4) *if and only if the following holds, for all $\boldsymbol{x} \in \partial\mathcal{S}$:*

$$L_f h(\boldsymbol{x}) + L_g h(\boldsymbol{x})\boldsymbol{u} + L_\Delta h(\boldsymbol{x})\boldsymbol{\theta}^* \geq 0. \tag{3.7}$$

Note that (3.7) may be written alternatively as $L_F h(\boldsymbol{x}) + L_g h(\boldsymbol{x})\boldsymbol{u} \geq 0$, where $L_F h(\boldsymbol{x}) = L_f h(\boldsymbol{x}) + L_\Delta h(\boldsymbol{x})\boldsymbol{\theta}^*$. In this way, $L_F h(\boldsymbol{x})$ captures the complete drift dynamics of the function h over the trajectories of (3.4). One way to render a set $\mathcal{S}$ forward invariant is to use CBFs in the control design. The following definition is adapted from [3] to fit the class of systems (3.4) under consideration in this chapter.

Definition 3.3 (**Control Barrier Function (CBF)**). *Given a set $\mathcal{S} \subset \mathbb{R}^n$ defined by* (3.6) *for a continuously differentiable function $h : \mathbb{R}^n \to \mathbb{R}$, the function h is a **control barrier function** defined on a set $\mathcal{D}$, where $\mathcal{S} \subseteq \mathcal{D} \subset \mathbb{R}^n$, if there exists an extended class $\mathcal{K}_\infty$ function $\alpha : \mathbb{R} \to \mathbb{R}$ such that*

$$\sup_{\boldsymbol{u} \in \mathcal{U}} \left[L_F h(\boldsymbol{x}) + L_g h(\boldsymbol{x})\boldsymbol{u} \right] \geq -\alpha(h(\boldsymbol{x})),\ \forall \boldsymbol{x} \in \mathcal{D}. \tag{3.8}$$

The authors of [198] ensure that the closed-loop trajectories of (3.4) are safe with respect $\mathcal{S}$ by enforcing that a *shrunken* set, $\mathcal{S}_r$, is forward invariant. Before formally defining $\mathcal{S}_r$ the following assumption is required.

Assumption 3.1 (**Non-Increasing Parameter Estimation Error**). *The supremum norm of the parameter estimation error is non-increasing, i.e., $\frac{d}{dt}\|\tilde{\boldsymbol{\theta}}(t)\|_\infty \leq 0$, $\forall t \geq 0$.*

Since Θ is a polytope, it follows from Assumption 3.1 that if $\hat{\boldsymbol{\theta}}(0) \in \Theta$, then $\vartheta \triangleq \sup_{\boldsymbol{\theta}_1, \boldsymbol{\theta}_2 \in \Theta}(\|\boldsymbol{\theta}_1 - \boldsymbol{\theta}_2\|_\infty)$ such that $\|\tilde{\boldsymbol{\theta}}(t)\|_\infty \leq \vartheta$, for all $t \geq 0$. It is worth noting that Assumption 3.1 may be satisfied via the appropriate design of a parameter adaptation law, a trivial example of which is $\dot{\hat{\boldsymbol{\theta}}} = \mathbf{0}_{p\times 1}$. Now, let $\boldsymbol{\vartheta} = \vartheta \cdot \mathbf{1}_{p\times 1}$. The shrunken set $\mathcal{S}_r$ is then given by

$$\mathcal{S}_r = \left\{ \boldsymbol{x} \in \mathbb{R}^n : h(\boldsymbol{x}) \geq \frac{1}{2}\boldsymbol{\vartheta}^\top \boldsymbol{\Gamma}^{-1}\boldsymbol{\vartheta} \right\} \tag{3.9a}$$

$$\partial\mathcal{S}_r = \left\{ \boldsymbol{x} \in \mathbb{R}^n : h(\boldsymbol{x}) = \frac{1}{2}\boldsymbol{\vartheta}^\top \boldsymbol{\Gamma}^{-1}\boldsymbol{\vartheta} \right\} \tag{3.9b}$$

$$\text{int}(\mathcal{S}_r) = \left\{ \boldsymbol{x} \in \mathbb{R}^n : h(\boldsymbol{x}) > \frac{1}{2}\boldsymbol{\vartheta}^\top \boldsymbol{\Gamma}^{-1}\boldsymbol{\vartheta} \right\} \tag{3.9c}$$

where $\boldsymbol{\Gamma}$ is a constant, positive-definite matrix such that $h(\boldsymbol{x}_0) \geq \frac{1}{2}\boldsymbol{\vartheta}^\top \boldsymbol{\Gamma}^{-1}\boldsymbol{\vartheta}$. Then, define a new function

$$h_r(\boldsymbol{x}, \boldsymbol{\vartheta}) = h(\boldsymbol{x}) - \frac{1}{2}\boldsymbol{\vartheta}^\top \boldsymbol{\Gamma}^{-1}\boldsymbol{\vartheta}. \tag{3.10}$$

According to Definition 3.3, the function (3.10) is a CBF for $\mathcal{S}_r$ defined over $\mathcal{D}$ if

$$\sup_{\boldsymbol{u}\in\mathcal{U}} \left[L_F h(\boldsymbol{x}) + L_g h(\boldsymbol{x})\boldsymbol{u}\right] \geq -\alpha(h_r(\boldsymbol{x},\boldsymbol{\vartheta})) + \boldsymbol{\vartheta}^\top \boldsymbol{\Gamma}^{-1}\dot{\boldsymbol{\vartheta}}, \tag{3.11}$$

holds for all $\boldsymbol{x} \in \mathcal{D}$. Note that if $\dot{\boldsymbol{\vartheta}} = 0$ and $\boldsymbol{\vartheta} \neq 0$, then (3.11) becomes $\dot{h}_r \geq -\alpha(h) + \gamma$, where $\gamma > 0$, which is a Robust Control Barrier Function (R-CBF) condition [31]. This chapter, unlike what is to come in Chapter 6, does not address the viability of any form of CBF condition. Thus, it is assumed in the following that the function h_r is a valid CBF for the system (3.4) with respect to the set $\mathcal{S}_r$.

Assumption 3.2 (CBF Viability). *For all $\boldsymbol{x} \in \partial\mathcal{S}_r$, there exists a control input $\boldsymbol{u} \in \mathcal{U}$ such that the following condition holds:*

$$L_F h_r(\boldsymbol{x}) + L_g h_r(\boldsymbol{x})\boldsymbol{u} - \boldsymbol{\vartheta}^\top \boldsymbol{\Gamma}^{-1}\dot{\boldsymbol{\vartheta}} \geq 0. \tag{3.12}$$

Remark 3.1. *Since $\mathcal{S}_r \subseteq \mathcal{S}$, it follows that for all $\boldsymbol{x}_0 \in \mathcal{S}_r$, the satisfaction of* (3.11) *implies that $\boldsymbol{x}(t) \in \mathcal{S}$ for all $t \geq 0$.*

3.1.3 Parameter Identification

It is worth highlighting that up until this point no assumptions have been made concerning the rank of the regressor $\Delta(\boldsymbol{x})$. In other words, the unknown parameters $\boldsymbol{\theta}^*$ in the system (3.4) may or may not be *identifiable*. The notion of system identifiability is defined formally as follows according to [199, Def. 4.6].

Definition 3.4 (Identifiability). *The system* (3.4) *is **identifiable** at $(\boldsymbol{x}, \boldsymbol{u}, \boldsymbol{\theta}^*)$ if*

$$f(\boldsymbol{x}) + g(\boldsymbol{x})\boldsymbol{u} + \Delta(\boldsymbol{x})\boldsymbol{\theta} = f(\boldsymbol{x}) + g(\boldsymbol{x})\boldsymbol{u} + \Delta(\boldsymbol{x})\boldsymbol{\theta}^* \implies \boldsymbol{\theta} = \boldsymbol{\theta}^*.$$

The system (3.4) *is **unidentifiable** at $(\boldsymbol{x}, \boldsymbol{u}, \boldsymbol{\theta}^*)$ if it is not identifiable.*

Without identifiability of (3.4) there may be other vectors $\boldsymbol{\theta}$ that satisfy $\Delta(\boldsymbol{x})\boldsymbol{\theta} = \Delta(\boldsymbol{x})\boldsymbol{\theta}^*$, $\forall \boldsymbol{x} \in \mathbb{R}^n$. This motivates defining the following state- and parameter-dependent set, $\Omega(\boldsymbol{x}, \boldsymbol{\theta}^*)$, containing such vectors $\boldsymbol{\theta}$:

$$\Omega(\boldsymbol{x}, \boldsymbol{\theta}^*) = \{\boldsymbol{\theta} \in \Theta : \boldsymbol{\theta} = \boldsymbol{\theta}^* + \mathcal{N}(\Delta(\boldsymbol{x}))\}. \tag{3.13}$$

In the rest of this chapter, Ω is written in place of $\Omega(\boldsymbol{x}, \boldsymbol{\theta}^*)$ for conciseness. Intuitively, the set Ω contains the true parameter vector $\boldsymbol{\theta}^*$ as well as all parameter vectors $\boldsymbol{\theta}$ that may be expressed as

a sum of $\boldsymbol{\theta}^*$ and any other vector belonging to the null-space of $\Delta(\boldsymbol{x})$. It is worth noting that if $\tilde{\boldsymbol{\theta}} \in \mathcal{N}(\Delta(\boldsymbol{x}))$, then $\Delta(\boldsymbol{x})\boldsymbol{\theta}^* = \Delta(\boldsymbol{x})\hat{\boldsymbol{\theta}}$, which implies that $\hat{\boldsymbol{\theta}} \in \Omega$.

Related to identifiability is the notion of Persistence of Excitation (PE) [200, Def. 2.5.3], a prerequisite for many parameter estimation laws (see e.g., [117]).

Definition 3.5 (**Persistence of Excitation PE**). *A vector or matrix function, $\phi : [0, \infty) \to \mathbb{R}^{p\times q}$, is **persistently excited** (PE) if there exist $T > 0$, $\epsilon_1, \epsilon_2 > 0$, such that*

$$\epsilon_1 I \leq \int_t^{t+T} \phi(r)\phi^T(r)dr \leq \epsilon_2 I, \quad \forall t \geq 0.$$

Remark 3.2. *The PE condition is generally difficult to verify in practice for a given vector or matrix, especially a priori. For the system* (3.4)*, however, the regressor Δ cannot satisfy the PE condition if* (3.4) *is unidentifiable for all $(\boldsymbol{x}, \boldsymbol{u}, \boldsymbol{\theta})$ in $(\mathbb{R}^n, \mathcal{U}, \Theta)$ [201]. It is worth noting that if $\mathcal{N}(\Delta(\boldsymbol{x}))$ is nontrivial for all $\boldsymbol{x} \in \mathbb{R}^n$, i.e. $\Delta(\boldsymbol{x})$ is globally rank-deficient, then the system is globally unidentifiable.*

In what follows, an exponentially stable parameter estimation law from the literature [117] is reviewed for motivation. This requires the following assumption, analogous to system identifiability.

Assumption 3.3 (**System Identifiability**). *For all time $t \geq 0$ there is a known vector, $\boldsymbol{v}(t) \in \mathbb{R}^q$, and a known, full column rank matrix, $\boldsymbol{M}(t) \in \mathbb{R}^{q\times p}$, such that the parameter estimation error vector, $\tilde{\boldsymbol{\theta}}(t)$, is a solution to*

$$\boldsymbol{M}(t)\tilde{\boldsymbol{\theta}}(t) = \boldsymbol{v}(t). \tag{3.14}$$

This is a common assumption in the literature (see e.g., [116, 117, 115]), but is infrequently stated so explicitly; perhaps this is because it is natural to wonder why linear regression tools are not used to determine $\boldsymbol{\theta}^*$. Its utility is in enabling the design of adaptation laws that provide certain convergence guarantees when (3.14) is perturbed, i.e. when

$$\boldsymbol{M}(t)\tilde{\boldsymbol{\theta}}(t) = \boldsymbol{v}(t) - \boldsymbol{\delta}(t), \tag{3.15}$$

for some unknown $\boldsymbol{\delta} \in \mathbb{R}^q$. For example, in [115] the authors seek to design an adaptation law for a class of systems of the form (3.15), and assume that $\boldsymbol{M}(t)$ satisfies the property $\sigma_{min}(\boldsymbol{M}(t)) > \sigma > 0$ for all $t \geq 0$, which is equivalent to the identifiability condition and analogous to Assumption 3.3 in the disturbance-free case, i.e. when $\delta(t) \equiv 0$, which they treat explicitly. The authors of [117] further note that Assumption 3.3 can be satisfied when the regressor Δ of (3.4) satisfies the PE condition.

Now, the following result introduces the aforementioned exponentially stable parameter estimation law proposed in [117].

Theorem 3.2 (**Exponentially Stable Parameter Estimation**). *Consider a system* (3.4)*, for which it is known that Assumption 3.3 holds. Then, under the ensuing adaptation law,*

$$\dot{\hat{\boldsymbol{\theta}}} = \boldsymbol{\Gamma}\boldsymbol{v}, \tag{3.16}$$

where $\boldsymbol{\Gamma} > 0$ *is a constant, diagonal gain matrix, the parameter estimation error,* $\tilde{\boldsymbol{\theta}}$*, converges exponentially to the origin, i.e.* $\tilde{\boldsymbol{\theta}} \to 0$ *exponentially as* $t \to \infty$*.*

3.1.4 Problem Statement

Whereas exponential stability implies convergence to the origin as time tends toward infinity, fixed-time stability implies convergence to the origin within a uniformly bounded finite-time, i.e., within a finite time independent of the initial conditions. In addition, faster rates of convergence tend to imply better disturbance rejection properties, a desirable characteristic for the design of a parameter identification law. Such an adaptation law is of even greater utility, furthermore, when used in conjunction with a safe control law for the purpose of learning unmodelled phenomena in the system dynamics. As such, the main problem under consideration in this chapter is as follows.

Problem 3.1. *Consider a dynamical system of the form* (3.4)*. Design adaptation and control laws,* $\dot{\hat{\boldsymbol{\theta}}} = \tau(\boldsymbol{x}, \hat{\boldsymbol{\theta}})$ *and* $\boldsymbol{u} = k(\boldsymbol{x}, \hat{\boldsymbol{\theta}})$ *respectively, such that the following conditions are satisfied:*

1. *The estimated parameter vector,* $\hat{\boldsymbol{\theta}}$*, is rendered fixed-time stable to the set* Ω *given by* (3.13)*, i.e.,* $\hat{\boldsymbol{\theta}}(t) \to \Omega$ *as* $t \to T$ *and* $\hat{\boldsymbol{\theta}}(t) \in \Omega$ *for all* $t \geq T$*, independent of* $\hat{\boldsymbol{\theta}}(0)$*.*
2. *The system trajectories remain safe for all time, i.e.* $\boldsymbol{x}(t) \in \mathcal{S}$*,* $\forall t \geq 0$*.*

The first element of Problem 3.1 is addressed in Section 3.2 for cases both where the transpose of the system regressor matrix (i.e., $\Delta(\boldsymbol{x})^\top$) satisfies the PE condition, amd without this requirement. A solution to the second element of Problem 3.1 is introduced in Section 3.3.

3.2 FxTS System Identification

In this section, two FxTS parameter adaptation laws are proposed for learning the unknown, parameter-affine component of the dynamics of (3.4). The first law requires that the transpose of the system regressor be persistently excited, whereas the second law handles scenarios in which that requirement is relaxed.

3.2.1 Persistently Excited Regressor

The parameter adaptation law proposed in this section relies on a state filtering scheme that requires the following assumption on Δ.

Assumption 3.4 (**Persistent Excitation**). *The transpose of the regressor matrix in* (3.4)*,* $\Delta^\top(x)$*, satisfies the PE condition.*

Note that, as stated previously, the matrix $\Delta(\boldsymbol{x})^\top$ cannot satisfy the PE condition if the system (3.4) is globally unidentifiable.

Remark 3.3. *Positive-definiteness of* $\Delta^\top\Delta$ *is sufficient for* $\Delta^\top$ *to satisfy the PE condition.*

3.2.1.1 Filtering Scheme

The following filtering scheme forms the basis for the FxTS adaptation law and was inspired by [117], which used a similar strategy for finite-time parameter estimation for robotic applications. First, note that the system (3.4) may be rewritten as

$$\dot{\boldsymbol{x}}(t) = \varphi(\boldsymbol{x}, \boldsymbol{u}) + \Phi(\boldsymbol{x})\boldsymbol{\theta}^*, \tag{3.17}$$

where $\varphi(\boldsymbol{x}, \boldsymbol{u}) = f(\boldsymbol{x}) + g(\boldsymbol{x})\boldsymbol{u}$ and $\Phi(\boldsymbol{x}) = \Delta(\boldsymbol{x})$. Whereas the authors of [117] introduce $\boldsymbol{x}_f$, $\boldsymbol{\varphi}_f$, and $\boldsymbol{\Phi}_f$ as first-order filters to $\boldsymbol{x}$, $\boldsymbol{\varphi}$, and $\boldsymbol{\Phi}$, in this chapter the following second-order filters are used:

$$k_e^2\ddot{\boldsymbol{\xi}}_f + 2k_e\dot{\boldsymbol{\xi}}_f + \boldsymbol{\xi}_f = \boldsymbol{\xi}, \tag{3.18}$$

for $\boldsymbol{\xi} \in \{\boldsymbol{x}, \boldsymbol{\varphi}, \boldsymbol{\Phi}\}$, where $k > 0$ is a design parameter and all initial conditions are zero. This system is stable, strictly proper, minimum-phase, and critically damped with natural frequency $\omega_n = 1/k_e$. This is desirable, as critically damped systems exhibit the smallest settling time without oscillations [202]. By defining dynamics for an auxiliary and integrated regressor matrix $\boldsymbol{P}$ and vector $\boldsymbol{Q}$ as in [117], the following are obtained:

$$\dot{\boldsymbol{P}} = -\ell_e\boldsymbol{P} + {\boldsymbol{\Phi}_f}^\top\boldsymbol{\Phi}_f, \quad \boldsymbol{P}(0) = 0 \tag{3.19}$$

$$\dot{\boldsymbol{Q}} = -\ell_e\boldsymbol{Q} + {\boldsymbol{\Phi}_f}^\top(\dot{\boldsymbol{x}}_f - \boldsymbol{\varphi}_f), \quad \boldsymbol{Q}(0) = 0, \tag{3.20}$$

the solutions of which permit

$$\boldsymbol{W}(t) = \boldsymbol{P}(t)\hat{\boldsymbol{\theta}} - \boldsymbol{Q}(t) = -\boldsymbol{P}(t)\tilde{\boldsymbol{\theta}}, \tag{3.21}$$

where $\ell_e > 0$ is another design parameter.

In the following, the main result of this section is introduced: a parameter adaptation law which renders the trajectories $\tilde{\boldsymbol{\theta}}(t)$ of the parameter estimation error FxTS to the set $\Omega = \{\boldsymbol{\theta}^*\}$.

Theorem 3.3. *Consider a nonlinear, control-affine system with parametric uncertainty as in* (3.4)*. If* (3.18) *filters $\boldsymbol{x}$, $\boldsymbol{\varphi}$, and $\boldsymbol{\Phi}$, and the auxiliary matrix $\boldsymbol{P}$ and vectors $\boldsymbol{Q}$, $\boldsymbol{W}$ are defined by* (3.19)-(3.21)*, then, under the ensuing adaptation law*

$$\dot{\hat{\boldsymbol{\theta}}} = -\boldsymbol{\Gamma}\boldsymbol{W}\left(\boldsymbol{W}^\top \boldsymbol{P}^{-\top}\boldsymbol{W}\right)^{-1}\left(c_1\nu^{\gamma_1} + c_2\nu^{\gamma_2}\right), \tag{3.22}$$

the estimated parameters, $\hat{\boldsymbol{\theta}}(t)$, converge to the true parameters, $\boldsymbol{\theta}^*$, in fixed-time, T_θ, i.e., $\hat{\boldsymbol{\theta}}(t) \to \boldsymbol{\theta}^*$ as $t \to T_\theta$, where

$$T_\theta \leq T_b = \frac{1}{c_1(1-\gamma_1)} + \frac{1}{c_2(\gamma_2 - 1)}, \tag{3.23}$$

with $\nu = \frac{1}{2}\boldsymbol{W}^\top \boldsymbol{P}^{-\top}\boldsymbol{\Gamma}^{-1}\boldsymbol{P}^{-1}\boldsymbol{W}$, $c_1 > 0$, $c_2 > 0$, $0 < \gamma_1 < 1$, $\gamma_2 > 1$, and $\boldsymbol{\Gamma} \in \mathbb{R}^{p\times p}$ being a constant, positive-definite, gain matrix.

Proof. Consider the Lyapunov function candidate $V_{\tilde{\theta}} = \frac{1}{2}\tilde{\boldsymbol{\theta}}^\top \boldsymbol{\Gamma}^{-1}\tilde{\boldsymbol{\theta}}$ for the system of the parameter-error dynamics (4.3). Since $\dot{\boldsymbol{\theta}}^* = 0$, it follows that $\dot{V}_{\tilde{\theta}} = -\tilde{\boldsymbol{\theta}}^\top \boldsymbol{\Gamma}^{-1}\dot{\hat{\boldsymbol{\theta}}}$. Applying (3.22) yields $\dot{V}_{\tilde{\theta}} = \tilde{\boldsymbol{\theta}}^\top \boldsymbol{W}\left(\boldsymbol{W}^\top \boldsymbol{P}^{-\top}\boldsymbol{W}\right)^{-1}(c_1\nu^{\gamma_1} + c_2\nu^{\gamma_2})$. Then, by substituting (3.21), we obtain

$$\begin{aligned}\dot{V}_{\tilde{\theta}} &= -\tilde{\boldsymbol{\theta}}^\top P\tilde{\boldsymbol{\theta}}\big(\tilde{\boldsymbol{\theta}}^\top \boldsymbol{P}^\top \boldsymbol{P}^{-\top}\boldsymbol{P}\tilde{\boldsymbol{\theta}}\big)^{-1}\big(c_1(\tilde{\boldsymbol{\theta}}^\top \boldsymbol{\Gamma}^{-1}\tilde{\boldsymbol{\theta}})^{\gamma_1} + c_2(\tilde{\boldsymbol{\theta}}^\top \boldsymbol{\Gamma}^{-1}\tilde{\boldsymbol{\theta}})^{\gamma_2}\big), \\ &= -c_1 V_{\tilde{\theta}}^{\gamma_1} - c_2 V_{\tilde{\theta}}^{\gamma_2},\end{aligned} \tag{3.24}$$

i.e., the FxTS condition from Theorem 3.1. Hence, the origin of (4.3) is FxTS, and the trajectories $\tilde{\boldsymbol{\theta}}(t)$ reach the origin within time T_θ, given by (3.23). Consequently, the estimated parameter vector, $\hat{\boldsymbol{\theta}}(t)$, converges to the true parameter vector, $\boldsymbol{\theta}^*$, within a fixed time, T_θ, i.e., $\hat{\boldsymbol{\theta}}(T_\theta) = \boldsymbol{\theta}^*$. □

In theory, the time required to learn the unknown parameters may be made arbitrarily small by increasing the gains c_1, c_2; however, in practice the adaptation law (3.22) is implemented discretely and excessively high gains may destabilize the algorithm. The true system parameters are able to be learned due to the transpose of the regressor satisfying the PE condition. In what follows, this requirement is removed and a new adaptation law is proposed to handle this more general case.

3.2.2 Unidentifiable System

In this section, not only is the regressor not required to satisfy the PE condition but the system is permitted to be globally unidentifiable, i.e., nothing is assumed about the rank of the regressor. In what follows, the main result of this chapter will be presented: an adaptation law which guarantees

that the unknown term $\Delta(\boldsymbol{x})\boldsymbol{\theta}^*$ in the system (3.4) is learned within a fixed-time even if the true system parameters $\boldsymbol{\theta}^*$ cannot be determined.

Before introducing the result, a relaxed version of Assumption 3.3 is required.

Assumption 3.5. *For all $t \geq 0$ there is a known vector, $\boldsymbol{v}(t) \in \mathbb{R}^n$, and a known matrix, $\boldsymbol{M}(t) \in \mathbb{R}^{n\times p}$, that jointly satisfy the following properties:*

(i) ***Consistency****: the parameter estimation error, $\tilde{\boldsymbol{\theta}}(t)$, is one solution to* (3.14)

(ii) ***Boundedness****: $\boldsymbol{v}(t)$ and $\boldsymbol{M}(t)$ are bounded for bounded $\boldsymbol{x}(t)$*

(iii) ***Equivalence****: the nullspace of $\boldsymbol{M}(t)$ is equal to the nullspace of $\Delta(\boldsymbol{x}(t))$, i.e $\mathcal{N}(\Delta(\boldsymbol{x}(t))) = \mathcal{N}(\boldsymbol{M}(t))$.*

The first element of Assumption 3.5 specifies that the linear system of equations constructed using the parameter estimation error vector $\tilde{\boldsymbol{\theta}}$ is consistent in the sense that $\tilde{\boldsymbol{\theta}}$ is one solution. The second element is straightforward and requires boundedness of the vector $\boldsymbol{v}(t)$ and $\boldsymbol{M}(t)$ for bounded $\boldsymbol{x}(t)$. The third element, referred to here as equivalence, requires that the obtained matrix $\boldsymbol{M}(t)$ shares a null space with the regressor $\Delta(\boldsymbol{x}(t))$, which is self-evident if $\boldsymbol{M} = \Delta(\boldsymbol{x})$.

Remark 3.4. *In contrast to Assumption 3.3 required for the exponentially stable parameter adaptation law, it is not required by Assumption 3.5 that $\boldsymbol{M}$ be full column-rank. Instead, the condition is that $\mathcal{N}(\boldsymbol{M}) = \mathcal{N}(\boldsymbol{\Delta})$, which relaxes restrictions imposed by previous works [116, 117, 115].*

Since it is not immediately obvious whether Assumption 3.5 is reasonable for the class of systems under consideration, we now introduce two possible measurement schemes, the first for illustrative and the second for practical purposes, which lead to its satisfaction.

3.2.2.1 Rate Measurements

For the illustrative scheme, the following assumption is required:

Assumption 3.6. *The time derivative of the state, $\dot{\boldsymbol{x}}$, is bounded and perfectly measured.*

Under Assumption 3.6, we can rewrite the perturbed dynamics (3.4) to obtain a linear system of equations,

$$\underbrace{\Delta(\boldsymbol{x})}_{\boldsymbol{M}}\tilde{\boldsymbol{\theta}} = \underbrace{\dot{\boldsymbol{x}} - f(\boldsymbol{x}) - g(\boldsymbol{x})\boldsymbol{u} - \Delta(\boldsymbol{x})\hat{\boldsymbol{\theta}}}_{\boldsymbol{v}}, \tag{3.25}$$

all of whose terms are either known or measured except $\tilde{\boldsymbol{\theta}}$, and to which at least one solution (albeit not necessarily unique) exists by construction. It is also evident that the second facet of Assumption

3.5 is satisfied via assumptions on the components of (3.4), and that the third is satisfied due to $\boldsymbol{M} = \Delta(\boldsymbol{x})$. While exact measurements of $\dot{\boldsymbol{x}}$ may not be obtainable in practice, it may be approximated using state measurements and numerical differentiation. This may introduce some approximation error into (3.25) such that it takes the form (3.15). The effect of this disturbance, $\boldsymbol{\delta}(t)$, is addressed in Chapter 4.

3.2.2.2 State Predictor

A predictor-based technique adapted from [203] is now shown to also yield a linear system of equations that satisfies Assumption 3.5 under certain conditions. First, consider the following state predictor:

$$\begin{aligned} \dot{\boldsymbol{z}} &= f(\boldsymbol{x}) + g(\boldsymbol{x})\boldsymbol{u} + \Delta(\boldsymbol{x})\hat{\boldsymbol{\theta}} + k_e(\boldsymbol{x} - \boldsymbol{z}) + \boldsymbol{W}\dot{\hat{\boldsymbol{\theta}}} \\ \boldsymbol{z}(0) &= \boldsymbol{x}(0), \end{aligned} \tag{3.26}$$

where $\boldsymbol{z} \in \mathbb{R}^n$ is the predicted state, $\hat{\boldsymbol{\theta}} \in \mathbb{R}^p$ is the estimated parameter vector, $\dot{\hat{\boldsymbol{\theta}}}$ is its time derivative to be defined later, f, g, and Δ are as in (3.4), $k_e > 0$ is an error gain, and $\boldsymbol{W}$ is a matrix described by the following dynamics:

$$\dot{\boldsymbol{W}} = -k_e\boldsymbol{W} + \Delta(\boldsymbol{x}), \quad \boldsymbol{W}(0) = \boldsymbol{0}_{n\times p}. \tag{3.27}$$

Then, by defining the observation error as $\boldsymbol{e} = \boldsymbol{x} - \boldsymbol{z}$, the error dynamics are described by:

$$\dot{\boldsymbol{e}} = \Delta(\boldsymbol{x})\tilde{\boldsymbol{\theta}} - k_e\boldsymbol{e} - \boldsymbol{W}\dot{\hat{\boldsymbol{\theta}}}. \tag{3.28}$$

Next, define an auxiliary variable,

$$\boldsymbol{\xi} = \boldsymbol{e} - \boldsymbol{W}\tilde{\boldsymbol{\theta}}, \tag{3.29}$$

the dynamics of which become

$$\dot{\boldsymbol{\xi}} = \dot{\boldsymbol{e}} - \dot{\boldsymbol{W}}\tilde{\boldsymbol{\theta}} - \boldsymbol{W}\dot{\tilde{\boldsymbol{\theta}}}, \tag{3.30}$$

which, by substituting in (3.27) and (3.28), amounts to

$$\dot{\boldsymbol{\xi}} = -k_e\boldsymbol{e} + k_e\boldsymbol{W}\tilde{\boldsymbol{\theta}} = -k_e\boldsymbol{\xi}, \quad \boldsymbol{\xi}(0) = \boldsymbol{e}(0), \tag{3.31}$$

a linear system with an exponentially stable equilibrium point at the origin. Then, by using the initial conditions from (3.26) and (3.27), it follows that $\boldsymbol{\xi}(0) = \boldsymbol{0}$ and therefore $\dot{\boldsymbol{\xi}} = \boldsymbol{0}$ for all $t \geq 0$, i.e. $\boldsymbol{\xi}(t) = \boldsymbol{\xi}(0) = \boldsymbol{0}$. As such, (3.29) implies that

$$\boldsymbol{W}\tilde{\boldsymbol{\theta}} = \boldsymbol{e}, \tag{3.32}$$

which takes the form (3.14) and satisfies Assumption 3.5 in the following way: the first part is satisfied by construction; the second holds since, according to (3.27), $\boldsymbol{W}(t) = \int_0^t e^{-k_e(t-s)}\Delta(\boldsymbol{x}(s))ds$, and thus $\boldsymbol{W}$ is bounded for bounded $\Delta(\boldsymbol{x})$ (which is bounded for bounded $\boldsymbol{x}$); and the third part is satisfied if $\mathcal{N}(\Delta(\boldsymbol{x}))$ is constant, though this is a sufficient and not a necessary condition.

The following result, an adaptation law which renders $\hat{\boldsymbol{\theta}}$ FxTS to the set (3.13), is one of the main contributions of this chapter.

Theorem 3.4. *Consider a nonlinear, control-affine system of the form* (3.4) *and suppose that Assumption 3.5 holds. If the nullspace of the regressor $\Delta(\boldsymbol{x}(t))$ is constant over the interval $[0, T]$, i.e. $\mathcal{N}(\Delta(\boldsymbol{x}(t))) = \mathcal{N}(\Delta(\boldsymbol{x}(0)))$, $\forall t \in [0, T]$, where*

$$T = \frac{\mu\pi}{2k_V^2\sqrt{ab}}, \tag{3.33}$$

with $a, b > 0$, $\mu > 2$, and

$$k_V = \underline{\sigma}(\boldsymbol{M})\sqrt{2\lambda_{max}(\boldsymbol{\Gamma})}, \tag{3.34}$$

where $\boldsymbol{\Gamma} \in \mathbb{R}^{p\times p}$ is a constant, positive-definite, gain matrix and $\underline{\sigma}(\boldsymbol{M}) > 0$ denotes the smallest nonzero singular value of $\boldsymbol{M}$ over the time interval, then under the ensuing adaptation law,

$$\dot{\hat{\boldsymbol{\theta}}} = \boldsymbol{\Gamma}\boldsymbol{M}^\top \boldsymbol{v}\left(a\|\boldsymbol{v}\|^{\frac{2}{\mu}} + \frac{b}{\|\boldsymbol{v}\|^{\frac{2}{\mu}}}\right), \tag{3.35}$$

the estimated parameter vector, $\hat{\boldsymbol{\theta}}$, converges to Ω defined by (3.13) *within a fixed time T, i.e. $\hat{\boldsymbol{\theta}}(t) \to \Omega$ and $\tilde{\boldsymbol{\theta}}(t) \to \mathcal{N}(\Delta(\boldsymbol{x}(t))$ as $t \to T_c(\hat{\boldsymbol{\theta}}(0)) \leq T$, $\forall \hat{\boldsymbol{\theta}}(0) \in \mathbb{R}^p$.*

Proof. First, it will be shown that (3.35) is well-defined, and then proved that $\hat{\boldsymbol{\theta}}$ converges to the set Ω within fixed-time T.

It is obvious by boundedness of $\boldsymbol{v}$ and $\boldsymbol{M}$ that (3.35) is bounded whenever $0 < \|\boldsymbol{v}\| < \infty$, so the focus is on what happens when $\|\boldsymbol{v}\| \to 0$. Consider that (3.35) can be rewritten as $\dot{\hat{\boldsymbol{\theta}}} = G_1(\boldsymbol{M}, \boldsymbol{v}) + G_2(\boldsymbol{M}, \boldsymbol{v})$, where $G_1(\boldsymbol{M}, \boldsymbol{v}) = a\boldsymbol{\Gamma}\boldsymbol{M}^\top \boldsymbol{v}\|\boldsymbol{v}\|^{\frac{2}{\mu}}$ and $G_2(\boldsymbol{M}, \boldsymbol{v}) = b\boldsymbol{\Gamma}\boldsymbol{M}^\top \frac{\boldsymbol{v}}{\|\boldsymbol{v}\|^{\frac{2}{\mu}}}$. It is evident that $G_1(\boldsymbol{M}, \boldsymbol{v}) \to 0$ as $\|\boldsymbol{v}\| \to 0$, however, for $G_2(\boldsymbol{M}, \boldsymbol{v})$ it follows that

$$\|G_2(\boldsymbol{M}, \boldsymbol{v})\|^2 = \frac{b^2}{\|\boldsymbol{v}\|^{4/\mu}}\boldsymbol{v}^\top\left(\boldsymbol{M}\boldsymbol{\Gamma}^\top\boldsymbol{\Gamma}\boldsymbol{M}^\top\right)\boldsymbol{v}.$$

Then, defining $\boldsymbol{N} = \boldsymbol{M}\boldsymbol{\Gamma}^\top\boldsymbol{\Gamma}\boldsymbol{M}^\top$, it is obtained that

$$\frac{b^2\sigma_{min}(\boldsymbol{N})}{\|\boldsymbol{v}\|^{4/\mu}}\|\boldsymbol{v}\|^2 \leq \|G_2(\boldsymbol{M}, \boldsymbol{v})\|^2 \leq \frac{b^2\sigma_{max}(\boldsymbol{N})}{\|\boldsymbol{v}\|^{4/\mu}}\|\boldsymbol{v}\|^2.$$

Since $0 \leq \sigma_{min}(\boldsymbol{N}), \sigma_{max}(\boldsymbol{N}) < \infty$, it follows that if $\mu > 2$, then

$$\lim_{\|\boldsymbol{v}\| \to 0} \|G_2(\boldsymbol{M}, \boldsymbol{v})\| = 0.$$

Thus, it is required that $\mu > 2$, which results in $G_2(\boldsymbol{M}, \boldsymbol{v}) \to 0$ as $\|\boldsymbol{v}\| \to 0$ and therefore (3.35) is well-defined.

For the convergence of $\hat{\boldsymbol{\theta}}$ to the set Ω in fixed-time, begin by observing that $\tilde{\boldsymbol{\theta}}$, $\dot{\tilde{\boldsymbol{\theta}}}$, and $\dot{\hat{\boldsymbol{\theta}}}$ may always be expressed as the following linear combinations:

$$\tilde{\boldsymbol{\theta}} = \tilde{\boldsymbol{\theta}}_R + \tilde{\boldsymbol{\theta}}_N, \tag{3.36}$$

$$\dot{\tilde{\boldsymbol{\theta}}} = \dot{\tilde{\boldsymbol{\theta}}}_R + \dot{\tilde{\boldsymbol{\theta}}}_N, \tag{3.37}$$

$$\dot{\hat{\boldsymbol{\theta}}} = \dot{\hat{\boldsymbol{\theta}}}_R + \dot{\hat{\boldsymbol{\theta}}}_N \tag{3.38}$$

where $\tilde{\boldsymbol{\theta}}_R, \dot{\tilde{\boldsymbol{\theta}}}_R, \dot{\hat{\boldsymbol{\theta}}}_R \in \text{row}(\boldsymbol{M})$ and $\tilde{\boldsymbol{\theta}}_N, \dot{\tilde{\boldsymbol{\theta}}}_N, \dot{\hat{\boldsymbol{\theta}}}_N \in \mathcal{N}(\boldsymbol{M})$. By rank-nullity and the fact that $\text{row}(\boldsymbol{M})$ and $\mathcal{N}(\boldsymbol{M})$ are orthogonal complements, such a decomposition always exists [204]. Next, from (3.35) and Assumption 3.5 observe that

$$\begin{aligned}
\dot{\hat{\boldsymbol{\theta}}} &= \boldsymbol{\Gamma} \boldsymbol{M}^\top \boldsymbol{v} \left(a \|\boldsymbol{v}\|^{\frac{2}{\mu}} + \frac{b}{\|\boldsymbol{v}\|^{\frac{2}{\mu}}} \right), \\
&= \boldsymbol{\Gamma} \boldsymbol{M}^\top \boldsymbol{M} \tilde{\boldsymbol{\theta}} \left(a \|\boldsymbol{M}\tilde{\boldsymbol{\theta}}\|^{\frac{2}{\mu}} + \frac{b}{\|\boldsymbol{M}\tilde{\boldsymbol{\theta}}\|^{\frac{2}{\mu}}} \right).
\end{aligned}$$

Since $\boldsymbol{M}\tilde{\boldsymbol{\theta}} = \boldsymbol{M}(\tilde{\boldsymbol{\theta}}_R + \tilde{\boldsymbol{\theta}}_N) = \boldsymbol{M}\tilde{\boldsymbol{\theta}}_R$, it follows that

$$\begin{aligned}
\dot{\hat{\boldsymbol{\theta}}} &= \boldsymbol{\Gamma} \boldsymbol{M}^\top \boldsymbol{M} \tilde{\boldsymbol{\theta}}_R \left(a \|\boldsymbol{M}\tilde{\boldsymbol{\theta}}_R\|^{\frac{2}{\mu}} + \frac{b}{\|\boldsymbol{M}\tilde{\boldsymbol{\theta}}_R\|^{\frac{2}{\mu}}} \right), \\
&= \dot{\hat{\boldsymbol{\theta}}}_R.
\end{aligned}$$

Then, from (3.38) it is obtained that $\dot{\hat{\boldsymbol{\theta}}}_N = \boldsymbol{0}_{p\times 1}$ and by (4.3)

$$\dot{\tilde{\boldsymbol{\theta}}}_R = -\dot{\hat{\boldsymbol{\theta}}}_R, \quad \tilde{\boldsymbol{\theta}}_R(0) = \tilde{\boldsymbol{\theta}}_{R,0}, \tag{3.39}$$

$$\dot{\tilde{\boldsymbol{\theta}}}_N = \boldsymbol{0}_{p\times 1}, \quad \tilde{\boldsymbol{\theta}}_N(0) = \tilde{\boldsymbol{\theta}}_{N,0}. \tag{3.40}$$

By Assumption 3.5, it follows that $\tilde{\boldsymbol{\theta}}_N(0) \in \mathcal{N}(\Delta(\boldsymbol{x}(0)))$, and by $\mathcal{N}(\Delta(\boldsymbol{x}(t))) = \mathcal{N}(\Delta(\boldsymbol{x}(0)))$ for all $t \in [0, T]$ it then holds that $\hat{\boldsymbol{\theta}} \in \Omega$ whenever $\tilde{\boldsymbol{\theta}}_R = 0$. It is sufficient, therefore, to show that $\tilde{\boldsymbol{\theta}}_R(t) \to 0$ as $t \to T_c(\hat{\boldsymbol{\theta}}(0)) \leq T$.

Consider the Lyapunov function candidate $V = \frac{1}{2}\tilde{\boldsymbol{\theta}}_R^T \boldsymbol{\Gamma}^{-1} \tilde{\boldsymbol{\theta}}_R$. Its time derivative along the trajectories of (3.39) is

$$\begin{aligned}
\dot{V} &= -\tilde{\boldsymbol{\theta}}_R^T \boldsymbol{\Gamma}^{-1} \dot{\hat{\boldsymbol{\theta}}}_R \\
&= -\tilde{\boldsymbol{\theta}}_R^T \boldsymbol{M}^\top \boldsymbol{M} \tilde{\boldsymbol{\theta}}_R \left(a \|\boldsymbol{M}\tilde{\boldsymbol{\theta}}_R\|^{\frac{2}{\mu}} + \frac{b}{\|\boldsymbol{M}\tilde{\boldsymbol{\theta}}_R\|^{\frac{2}{\mu}}} \right) \\
&= -a\|\boldsymbol{M}\tilde{\boldsymbol{\theta}}_R\|^{2+\frac{2}{\mu}} - b\|\boldsymbol{M}\tilde{\boldsymbol{\theta}}_R\|^{2-\frac{2}{\mu}}
\end{aligned}$$

When $\tilde{\boldsymbol{\theta}}_R \neq 0$, it follows that $\|\boldsymbol{M}\tilde{\boldsymbol{\theta}}_R\| > 0$, and therefore

$$0 < \underline{\sigma}(\boldsymbol{M})\|\tilde{\boldsymbol{\theta}}_R\| \leq \|\boldsymbol{M}\tilde{\boldsymbol{\theta}}_R\| \leq \sigma_{max}(\boldsymbol{M})\|\tilde{\boldsymbol{\theta}}_R\|.$$

Then, since $\frac{1}{2}\lambda_{min}(\boldsymbol{\Gamma}^{-1})\tilde{\boldsymbol{\theta}}_R^T\tilde{\boldsymbol{\theta}}_R \leq V \leq \frac{1}{2}\lambda_{max}(\boldsymbol{\Gamma}^{-1})\tilde{\boldsymbol{\theta}}_R^T\tilde{\boldsymbol{\theta}}_R$ and $\lambda_{min}(\boldsymbol{\Gamma}^{-1}) = 1/\lambda_{max}(\boldsymbol{\Gamma})$, it follows then from the definition of V that $\|\tilde{\boldsymbol{\theta}}_R\| \leq \sqrt{2V\lambda_{max}(\boldsymbol{\Gamma})} = L(V)$. Using this, it is obtained that

$$\begin{aligned}
\dot{V} &\leq -a\Big(\underline{\sigma}(\boldsymbol{M})L(V)\Big)^{2+\frac{2}{\mu}} - b\Big(\underline{\sigma}(\boldsymbol{M})L(V)\Big)^{2-\frac{2}{\mu}} \\
&\leq -c_1 V^{1+\frac{1}{\mu}} - c_2 V^{1-\frac{1}{\mu}} \qquad (3.41)
\end{aligned}$$

which takes the form (3.2), where

$$c_1 = a k_V^{2+\frac{2}{\mu}} \qquad (3.42)$$

$$c_2 = b k_V^{2-\frac{2}{\mu}}, \qquad (3.43)$$

and k_V is given by (3.34). Thus, the requirements for FxTS provided in Theorem 3.1 are met insofar as $\tilde{\boldsymbol{\theta}}_R$ is concerned. Therefore, $\tilde{\boldsymbol{\theta}}_R \to 0$ in fixed-time, i.e. as $t \to T_c(\hat{\boldsymbol{\theta}}(0)) \leq T_b$ where T_b is given by (3.3) and $\gamma_1 = 1 + \frac{1}{\mu}$ and $\gamma_2 = 1 - \frac{1}{\mu}$. With γ_1, γ_2 in this form, it follows from [205, Lemma 2] that the settling time function T_c is bounded from above by T given by (3.33). Thus, we have that $\hat{\boldsymbol{\theta}} \to \Omega$ within time T, independent of the initial estimates, $\hat{\boldsymbol{\theta}}(0)$. This completes the proof. □

The adaptation law (3.35) is usable as long as there exists a way to satisfy Assumption 3.5. The measurement and prediction schemes outlined in Sections 3.2.2.1 and 3.2.2.2 are two avenues toward realizing this goal, though there may exist others. While it is not guaranteed that $\hat{\boldsymbol{\theta}} \to \boldsymbol{\theta}^*$ unless $\mathcal{N}(\Delta(\boldsymbol{x}(t))) = \{0\}$ for all $t \in [0, T]$, it is sufficient from a control-oriented perspective to learn some $\hat{\boldsymbol{\theta}}$ such that $\Delta(\boldsymbol{x})\hat{\boldsymbol{\theta}} = \Delta(\boldsymbol{x})\boldsymbol{\theta}^*$.

Remark 3.5. *The bound on settling time given by* (3.33) *requires knowledge of the minimum*

nonzero singular value of the matrix $\boldsymbol{M}$. While the exact value may not be known a priori, domain knowledge can be used to obtain a lower bound over the relevant region of the state space. If using the predictor-based measurement scheme, a warm-up time, T_w, may be required for $\underline{\sigma}(\boldsymbol{W})$ to eclipse such a lower bound. This warm-up time must be added to the convergence time derived in (3.33)*.*

3.3 Robust, Adaptive CBF-based Control

With knowledge of the parameter estimates converging to Ω in fixed-time (by means of either (3.22) or (3.35)), expressions are derived for the upper bound on the supremum norm of the parameter estimation error vector as an explicit function of time.

Corollary 3.1. *Suppose that the premises of Theorem 3.3 hold. If, in addition, the following conditions hold*

(i) The initial estimated parameter vector lies within the known admissible parameter set, Θ, i.e. $\hat{\boldsymbol{\theta}}(0) \in \Theta$,

(ii) The estimated parameter update law, $\dot{\hat{\boldsymbol{\theta}}}$, is given by (3.22)*, where $\boldsymbol{\Gamma}$ is constant, positive-definite, and also **diagonal**,*

(iii) $\gamma_1 = 1 - \frac{1}{\mu}$, $\gamma_2 = 1 + \frac{1}{\mu}$ for some $\mu > 1$,

then $\forall t \in [0, T_\theta]$, where T_θ is given by (3.23)*, the following expression constitutes a monotonically decreasing upper bound on $\|\tilde{\boldsymbol{\theta}}(t)\|_\infty$:*

$$\|\tilde{\boldsymbol{\theta}}(t)\|_\infty \leq \sqrt{2\lambda_{max}(\boldsymbol{\Gamma})\left(\sqrt{\frac{c_1}{c_2}}\tan\left(A(t)\right)\right)^{\mu}} \triangleq \eta(t), \tag{3.44}$$

where $c_1 > 0$ and $c_2 > 0$ are the design parameters in Theorem 3.3, and

$$A(t) = \max\left\{\Xi - \frac{\sqrt{c_1 c_2}}{\mu}t, 0\right\}, \tag{3.45}$$

$$\Xi = \tan^{-1}\left(\sqrt{\frac{c_2}{c_1}}\left(\frac{1}{2}\boldsymbol{\eta}(0)^T\Gamma^{-1}\boldsymbol{\eta}(0)\right)^{\frac{1}{\mu}}\right) \tag{3.46}$$

with $\boldsymbol{\eta}(t) = \eta(t) \cdot \mathbf{1}_{p\times 1}$, and $\|\tilde{\boldsymbol{\theta}}(t)\|_\infty = 0$, $\forall t > T_\theta$.

Proof. Consider the Lyapunov function candidate $V = V_{\tilde{\theta}} = \frac{1}{2}\tilde{\boldsymbol{\theta}}^T\boldsymbol{\Gamma}^{-1}\tilde{\boldsymbol{\theta}}$, the time-derivative of which is given by (3.24). Then, rearrange terms and use the change of variables $x = V^{\frac{1}{\mu}}$ and

$dx = \frac{1}{\mu} V^{\frac{1}{\mu}-1} dV$ to obtain

$$
\begin{aligned}
t &\leq \int_{V_0^{\frac{1}{\mu}}}^{V^{\frac{1}{\mu}}} \frac{\mu x^{\mu-1} dx}{-c_1 x^{\mu-1} - c_2 x^{\mu+1}} = \int_{V_0^{\frac{1}{\mu}}}^{V^{\frac{1}{\mu}}} \frac{\mu dx}{-c_1 - c_2 x^2} \\
&\leq -\frac{\mu}{\sqrt{c_1 c_2}} \left(\tan^{-1}\left(\sqrt{\frac{c_2}{c_1}} V^{\frac{1}{\mu}} \right) - \tan^{-1}\left(\sqrt{\frac{c_2}{c_1}} V_0^{\frac{1}{\mu}} \right) \right).
\end{aligned}
$$

By rearranging again, the following is obtained

$$
V(t) \leq \left(\sqrt{\frac{c_1}{c_2}} \tan\left(\tan^{-1}\left(\sqrt{\frac{c_2}{c_1}} V_0^{\frac{1}{\mu}} \right) - \frac{\sqrt{c_1 c_2}}{\mu} t \right) \right)^{\mu},
$$

where, by observing that $V_0 = \frac{1}{2}\tilde{\boldsymbol{\theta}}(0)^T \boldsymbol{\Gamma}^{-1} \tilde{\boldsymbol{\theta}}(0) \leq \frac{1}{2} \boldsymbol{\eta}(0)^T \boldsymbol{\Gamma}^{-1} \boldsymbol{\eta}(0)$, it follows that

$$
V(t) \leq \left(\sqrt{\frac{c_1}{c_2}} \tan\left(\Xi - \frac{\sqrt{c_1 c_2}}{\mu} t \right) \right)^{\mu}.
$$

Observe that in the limit $\Xi \to \frac{\pi}{2}$ as $\|\boldsymbol{\eta}(0)\| \to \infty$. With $\hat{\boldsymbol{\theta}}(0) \in \Theta$, however, it will not occur that $V_0 \to \infty$, and therefore, since the bound (3.23) holds for arbitrarily large V_0, it is possible that $\Xi - \frac{\sqrt{c_1 c_2}}{\mu} t < 0$ for some $t < T$. To account for this, $A(t)$ is defined by (3.45), which leads to

$$
V(t) \leq \left(\sqrt{\frac{c_1}{c_2}} \tan\left(A(t) \right) \right)^{\mu}. \tag{3.47}
$$

Now, since $\boldsymbol{\Gamma}$ diagonal it follows that $V = \frac{1}{2}(\boldsymbol{\Gamma}_{11}^{-1} \tilde{\theta}_1^2 + ... + \boldsymbol{\Gamma}_{pp}^{-1} \tilde{\theta}_p^2)$, and therefore that $V \geq \frac{1}{2} \lambda_{max}^{-1}(\boldsymbol{\Gamma}) \|\tilde{\boldsymbol{\theta}}\|^2 \geq \frac{1}{2} \lambda_{max}^{-1}(\boldsymbol{\Gamma}) \|\tilde{\boldsymbol{\theta}}\|_{\infty}^2$. Then, substitute (3.47) in this inequality and rearrange terms to recover (4.43). Then, for

$$
0 \leq t \leq \frac{\mu}{\sqrt{c_1 c_2}} \tan^{-1}\left(\sqrt{\frac{c_2}{c_1}} \left(\frac{1}{2} \boldsymbol{\eta}(0)^T \boldsymbol{\Gamma}^{-1} \boldsymbol{\eta}(0) \right)^{\frac{1}{\mu}} \right)
$$

we have that (4.43) decreases monotonically to zero. This completes the proof. □

For the case where the regressor may not satisfy the PE condition (and thus the system may be globally unidentifiable), the following introduces an analogous result for a bound on the component of the parameter estimation error vector belonging to the row-space of the regressor when using the parameter adaptation law (3.35).

Corollary 3.2. *Suppose that the premises of Theorem 3.4 hold. If, in addition, the following conditions hold*

(i) The initial estimated parameter vector lies within the known admissible parameter set, Θ, i.e. $\hat{\boldsymbol{\theta}}(0) \in \Theta$,

(ii) The estimated parameter update law, $\dot{\hat{\boldsymbol{\theta}}}$, is given by (3.35)*, where $\boldsymbol{\Gamma}$ is constant, positive-definite, and also **diagonal**,*

(iii) A lower bound on $\underline{\sigma}(\boldsymbol{M}(t)) > s > 0$, is known, $\forall t \leq T$, where T is given by (3.33)*,*

then, $\forall t \leq T$, the following expression constitutes a monotonically decreasing upper bound on $\|\tilde{\boldsymbol{\theta}}_R(t)\|_\infty$:

$$\|\tilde{\boldsymbol{\theta}}_R(t)\|_\infty \leq \sqrt{2\lambda_{max}(\boldsymbol{\Gamma})\left(\sqrt{\frac{c_1}{c_2}}\tan\left(A(t)\right)\right)^{\mu}} \triangleq \eta(t), \tag{3.48}$$

where c_1 and c_2 are defined by (3.42) *and* (3.43)*, and*

$$A(t) = \max\left\{\Xi - \frac{\sqrt{c_1 c_2}}{\mu}t, 0\right\}, \tag{3.49}$$

$$\Xi = \tan^{-1}\left(\sqrt{\frac{c_2}{c_1}}\left(\frac{1}{2}\boldsymbol{\eta}(0)^T\Gamma^{-1}\boldsymbol{\eta}(0)\right)^{\frac{1}{\mu}}\right) \tag{3.50}$$

with $\boldsymbol{\eta}(t) = \eta(t) \cdot \mathbf{1}_{p\times 1}$, and $\|\tilde{\boldsymbol{\theta}}_R(t)\|_\infty = 0$, $\forall t > T$.

Proof. The proof is identical to the proof of Corollary 3.1 with the exception of the following modifications: condition (iii) must hold, i.e., $\exists s > 0$ satisfying $\underline{\sigma}(\boldsymbol{M}(\boldsymbol{t})) > s$, $\forall t \leq T$, so that lower bounds on c_1 and c_2 may be determined, and $\tilde{\boldsymbol{\theta}}_R$ is substituted in place of $\tilde{\boldsymbol{\theta}}$. Note that condition (iii) of Corollary 3.1 is satisfied automatically by the form of (3.35). □

Remark 3.6. *Since it is assumed that $\boldsymbol{\theta}^* \in \Theta$ at $t = 0$, as a consequence of* (4.43) *the set of admissible parameters can be tightened at time t, i.e. it is known that $\boldsymbol{\theta}^* \in \Lambda(t) \subset \Theta$, where $\Lambda(t) = \{\boldsymbol{\lambda} \in \Theta : \|\boldsymbol{\lambda}_R - \hat{\boldsymbol{\theta}}_R\|_\infty \leq \eta(t)\}$, for all $t \in [0, T]$, where $\boldsymbol{\lambda} = \boldsymbol{\lambda}_R + \boldsymbol{\lambda}_N$, with $\boldsymbol{\lambda}_R, \hat{\boldsymbol{\theta}}_R \in$ row(Δ), $\boldsymbol{\lambda}_N, \hat{\boldsymbol{\theta}}_N \in \mathcal{N}(\Delta)$, and $\Lambda(t) = \{\hat{\boldsymbol{\theta}} + \mathcal{N}(\Delta)\}$ for all $t \in (T, \infty)$. As a special case, if Δ is full column rank, then $\Lambda(t) = \{\hat{\boldsymbol{\theta}}\}$ for all $t \in [T, \infty)$.*

Knowledge of the parameter estimation error bound as a function of time allows for the synthesis of a robust, adaptive CBF condition for guaranteed forward invariance of the shrunken set $\mathcal{S}_r$ given by (3.9), as proposed in the following result.

Theorem 3.5. *Consider a dynamical system belonging to the class of nonlinear, control-affine systems described by* (3.4)*, and a subset of the safe set, $\mathcal{S}_r \subseteq \mathcal{S}$, defined by* (3.9)*. If either of the following two conditions are met:*

(i) Both Assumption 3.4 and the premises of Corollary 3.1 hold, and the parameter estimates $\hat{\boldsymbol{\theta}}$ are adapted according to (3.22)*, with $\eta(t)$ given by* (3.44) *and $A(t)$ given by* (3.45)*, or*

(ii) Both Assumption 3.5 and the premises of Corollary 3.2 hold, and the parameter estimates $\hat{\boldsymbol{\theta}}$ are adapted according to (3.35)*, with $\eta(t)$ given by* (3.48) *and $A(t)$ given by* (3.49)*,*

then, the set $\mathcal{S}_r$ is rendered forward invariant if there exists a control input, $\boldsymbol{u}$, for which the following condition holds $\forall \boldsymbol{x} \in \mathcal{S}_r$, $\forall t \geq 0$:

$$\sup_{\boldsymbol{u} \in \mathcal{U}} \left[L_f h(\boldsymbol{x}) + L_g h(\boldsymbol{x}) \boldsymbol{u} \right] \geq -\alpha\big(h_r(\boldsymbol{x}, \boldsymbol{\eta})\big) + \boldsymbol{r}(t, \hat{\boldsymbol{\theta}}) \tag{3.51}$$

where $\boldsymbol{r}(t, \hat{\boldsymbol{\theta}}) = \mathrm{Tr}(\boldsymbol{\Gamma}^{-1}) \eta(t) \dot{\eta}(t) + \boldsymbol{\nu}(\hat{\boldsymbol{\theta}})$, and

$$\dot{\eta}(t) = -c_1 \sqrt{\frac{\lambda_{max}(\boldsymbol{\Gamma})}{2}} \left(\sqrt{\frac{c_1}{c_2}} \tan\left(A(t)\right) \right)^{\frac{\mu}{2}-1} \sec^2\left(A(t)\right) \tag{3.52}$$

$$\boldsymbol{\nu}(\hat{\boldsymbol{\theta}}) = \sum_{i=1}^{p} \min\left\{ C_i P_\Theta(\hat{\theta}_i - \eta), C_i P_\Theta(\hat{\theta}_i + \eta) \right\} \tag{3.53}$$

where C_i denotes the i^{th} column of $L_\Delta h(\boldsymbol{x})$ for $i \in \{1, \ldots, p\}$ and $P_\Theta : \mathbb{R}^p \to \Theta$ is the vector projection operator onto Θ, as defined in [206].

Proof. Recall that $\mathcal{S}_r$ is rendered forward invariant if (3.11) holds for all $\boldsymbol{x} \in \mathcal{S}_r$. Now, replace the constant ϑ from (3.10) with the time-varying $\boldsymbol{\eta}(t)$ (and henceforth omit the argument). With $\dot{h}_r = \frac{\partial h_r}{\partial \boldsymbol{x}} \dot{\boldsymbol{x}} + \frac{\partial h_r}{\partial \boldsymbol{\eta}} \dot{\boldsymbol{\eta}}$ from (3.10), it follows from $\frac{\partial h_r}{\partial \boldsymbol{x}} = \frac{\partial h}{\partial \boldsymbol{x}}$ and $\boldsymbol{\Gamma}$ being diagonal that

$$\frac{\partial h_r}{\partial \boldsymbol{x}} \dot{\boldsymbol{x}} = L_f h(\boldsymbol{x}) + L_g h(\boldsymbol{x}) \boldsymbol{u} + L_\Delta h(\boldsymbol{x}) \boldsymbol{\theta}^*, \tag{3.54}$$

$$\frac{\partial h_r}{\partial \boldsymbol{\eta}} \dot{\boldsymbol{\eta}} = -\boldsymbol{\eta}^\top \Gamma^{-1} \dot{\boldsymbol{\eta}} = -\mathrm{Tr}(\Gamma^{-1}) \eta \dot{\eta}, \tag{3.55}$$

where $\dot{\eta}$ is obtained via differentiation of η. Note that (3.54) includes the unknown term, $L_\Delta h(\boldsymbol{x}) \boldsymbol{\theta}^*$, and thus it must be proved that $\boldsymbol{\nu}$ given by (3.53) compensates for this unknown, and thus that (3.51) implies (3.11).

First, observe that $L_\Delta h(\boldsymbol{x}) \boldsymbol{\theta}^* = L_\Delta h(\boldsymbol{x}) \tilde{\boldsymbol{\theta}} + L_\Delta h(\boldsymbol{x}) \hat{\boldsymbol{\theta}} = L_\Delta h(\boldsymbol{x}) \tilde{\boldsymbol{\theta}}_R + L_\Delta h(\boldsymbol{x}) \hat{\boldsymbol{\theta}}$, where $\tilde{\boldsymbol{\theta}}_R$ is defined as in (3.36). Note that for a full column-rank regressor, $\tilde{\boldsymbol{\theta}}_R = \tilde{\boldsymbol{\theta}}$. Thus, it follows that (3.51) implies (3.11) if $L_\Delta h_r(\boldsymbol{x}) \boldsymbol{\theta}^* \geq L_\Delta h_r(\boldsymbol{x}) \tilde{\boldsymbol{\theta}}_R + L_\Delta h_r(\boldsymbol{x}) \hat{\boldsymbol{\theta}}$. Second, since $\|\tilde{\boldsymbol{\theta}}_R(t)\|_\infty = \eta(t)$, let the set of admissible unknown parameters at time t be denoted as $\Phi(t)$, where

$$\Phi(t) = \Theta \cap \{\boldsymbol{\theta} \in \mathbb{R}^p : \ \|\boldsymbol{\theta}_R - \hat{\boldsymbol{\theta}}_R(t)\|_\infty \leq \eta(t)\}, \tag{3.56}$$

where $\boldsymbol{\theta} = \boldsymbol{\theta}_R + \boldsymbol{\theta}_N$, with $\boldsymbol{\theta}_R \in \text{row}(\boldsymbol{M})$ and $\boldsymbol{\theta}_N \in \mathcal{N}(\boldsymbol{M})$. By definition, $\Phi(t)$ is compact and convex. As such, consider the following minimization problem:

$$J_{\boldsymbol{\phi}} = \min_{\boldsymbol{\phi} \in \Phi(t)} L_{\Delta} h(\boldsymbol{x}) \boldsymbol{\phi}, \tag{3.57}$$

which is a constrained linear program over a compact domain. It is well known that for this class of problems there exists a minimizer $\boldsymbol{\phi}^*$ corresponding to a minimum value, $J^*_{\phi} = L_{\Delta} h_r(\boldsymbol{x}) \boldsymbol{\phi}^*$.

Now, since $L_{\Delta} h(\boldsymbol{x}) \boldsymbol{\phi} = \sum_{i=1}^{p} C_i \phi_i$ with C_i as the ith column of $L_{\Delta} h(\boldsymbol{x})$, we have that $\bar{\phi}_1, \ \ldots \ , \bar{\phi}_p$ are the minimizers of the following p constrained linear programs:

$$\min_{\hat{\theta}_i - \eta \leq \phi_i \leq \hat{\theta}_i + \eta} C_i \phi_i, \quad \forall i \in \{1, \ldots, p\}.$$

Thus, for all $C_i \neq 0$ it follows that $\bar{\phi}_i = \hat{\theta}_i - \eta$ or $\bar{\phi}_i = \hat{\theta}_i + \eta$, and $\bar{\phi}_i$ can take any value for $C_i = 0$. Since it is possible that $\bar{\phi}_i \notin \Theta$, apply the projection operator to $\bar{\phi}_i$ and write that

$$\zeta^*_i = P_{\Theta} \bar{\phi}_i.$$

By linearity, it holds that

$$C_i \zeta^*_i = \min \Big\{ C_i P_{\Theta}(\hat{\theta}_i - \eta), C_i P_{\Theta}(\hat{\theta}_i + \eta) \Big\} \leq C_i \phi_i,$$

for all $\phi_i \in [\hat{\theta}_i - \eta, \hat{\theta}_i + \eta]$. As such, denote $\boldsymbol{\nu} = \sum_{i=1}^{p} C_i \zeta^*_i$, for which it holds that $\boldsymbol{\nu} \leq L_{\Delta} h(\boldsymbol{x}) \boldsymbol{\theta}^*$. Thus, it follows that (3.51) implies (3.11). Then, as long as there exists a control input, $\boldsymbol{u}$, which satisfies (3.51), the set $\mathcal{S}_r$ defined by (3.9) is forward invariant. This completes the proof. □

The use of the projection operator in Theorem 3.5 reduces the conservatism of the approach without compromising the robustness of the forward invariance condition.

Remark 3.7. *The condition* (3.51) *can easily be extended to CBFs of high relative degree with respect to the system dynamics by continuing to differentiate* h *and* η*.*

3.4 Case Studies

In this section, two numerical case studies are considered: the first is a comparative investigation on how the proposed robust, adaptive controller performs with respect to existing methods, namely the adaptive safety approach introduced in [32], the data-driven set-membership identification algorithm presented by [198], and the robust, adaptive QP controller proposed by [87]; the second

considers a 12 degree-of-freedom 3D quadrotor model with unknown drag coefficients in a wind field.

3.4.1 Comparative Study: Reach-Avoid with 2D Single-Integrator

As a basis for comparison, a 2D single-integrator system subject to parametric uncertainty is considered. The control objective is to safely reach the origin while avoiding static obstacles separated by a small gap, as shown in Figure 3.1. As such, this is referred to as the "Shoot the Gap" problem. Controllers using both adaptation laws proposed in Section 3.2 are simulated, with the former law (Proposed Method 1) using the state filtering scheme introduced in Section 3.2.1.1 and the latter (Proposed Method 2) using the rate measurement scheme outlined in Section 3.2.2.1. Table 3.1 provides the legend codes used to refer to the other considered works.

Table 3.1

Controllers from the Literature		
Authors	Citation	Legend Code
Black et al.	[189]	BLR
Lopez et al.	[198] (w/o SMID)	LOP
Lopez et al.	[198] (w/ SMID)	LSM
Taylor et al.	[32]	TAY
Zhao et al.	[87]	ZHA
Proposed Method 1		BLA
Proposed Method 2		PRO

Note: [198] presents RaCBF-based control formulations with and without SMID for parameter estimation. Both are considered here.

3.4.1.1 Dynamics

The system model is

$$\dot{\boldsymbol{z}} = \begin{bmatrix} \dot{x} \\ \dot{y} \end{bmatrix} = \begin{bmatrix} 1 & 0 \\ 0 & 1 \end{bmatrix} \begin{bmatrix} u_x \\ u_y \end{bmatrix} + \Delta(\boldsymbol{z}) \begin{bmatrix} \theta_1 \\ \theta_2 \end{bmatrix}, \tag{3.58}$$

where $\boldsymbol{z} = [x \ y]^\top$ is the state vector comprised of x and y, the lateral and longitudinal position coordinates with respect to an inertial frame, θ_1, θ_2 are constant parameters that are unknown within some bounds, and Δ is the regressor.

Two instantiations of this problem are investigated: in the first, the regressor is full-rank at all times; in the second, the regressor is rank-deficient at all times. In the full-rank regressor scenario,

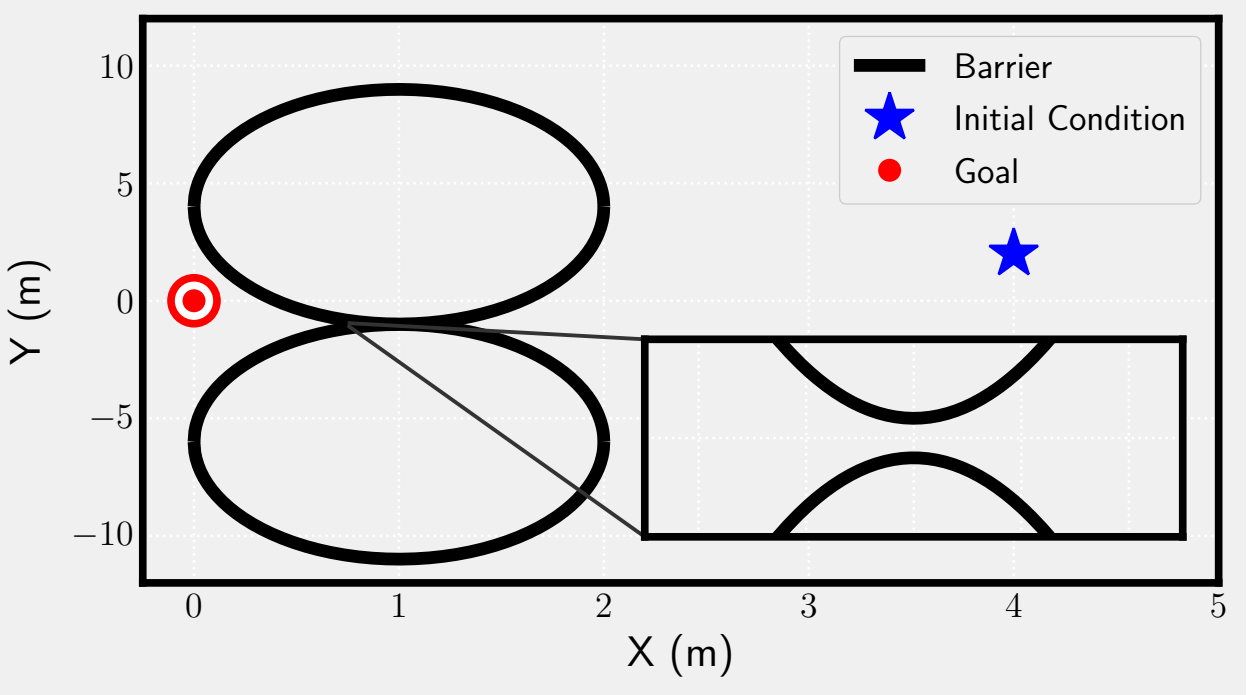

Figure 3.1: Problem Setup for the Shoot the Gap scenario.

$\Delta = \Delta_F$, where

$$\Delta_F(\boldsymbol{z}) = K_\Delta \begin{bmatrix} 1 + \sin^2(2\pi f_1 x) & 0 \\ 0 & 1 + \cos^2(2\pi f_2 y) \end{bmatrix},$$

with $K_\Delta, f_1, f_2 > 0$. In the rank-deficient regressor scenario, $\Delta = \Delta_D$, where

$$\Delta_D(\boldsymbol{z}) = \begin{bmatrix} -ax & -2ax \\ -\frac{a}{2}x & -ax \end{bmatrix},$$

and $a = 1/2$.

3.4.1.2 Controller

To encode the goal-convergence criterion the Control Lyapunov Function (CLF)

$$V(\boldsymbol{z}) = K_V(x^2 + y^2),$$

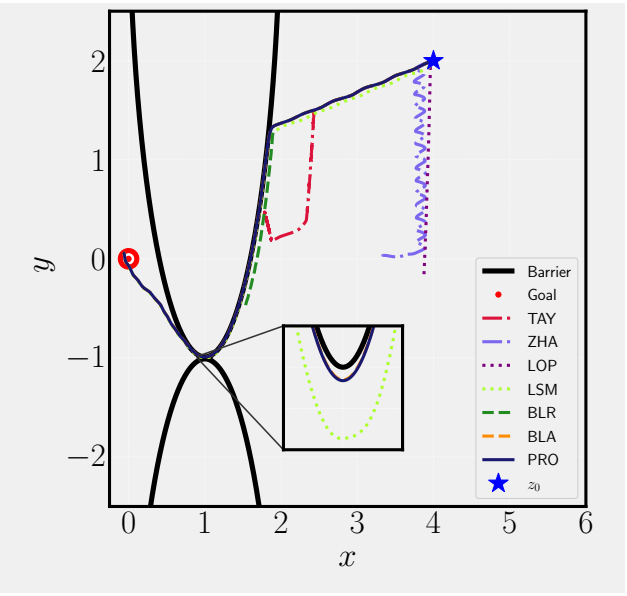

(a) States

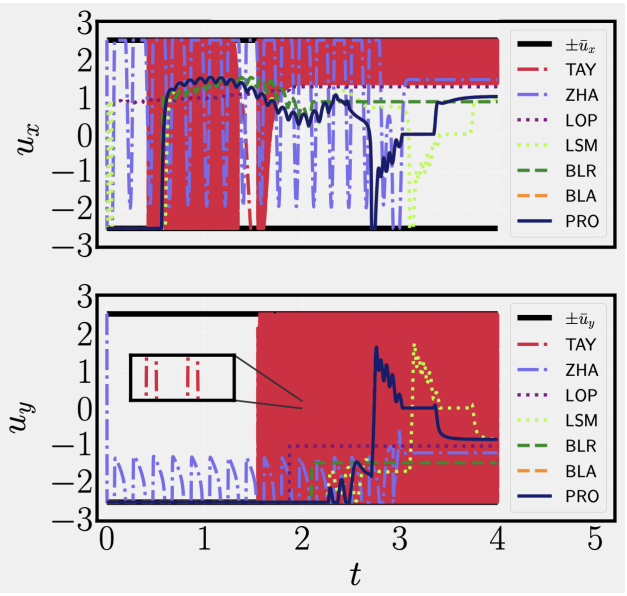

(b) Control Inputs

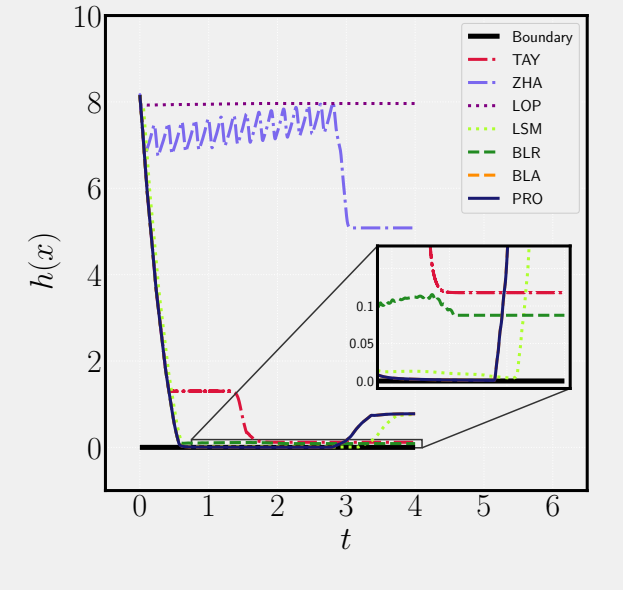

(c) Minimum CBF Values

Figure 3.2: Evolutions of the states, control inputs, and control barrier functions for the full-rank regressor "Shoot the Gap" example.

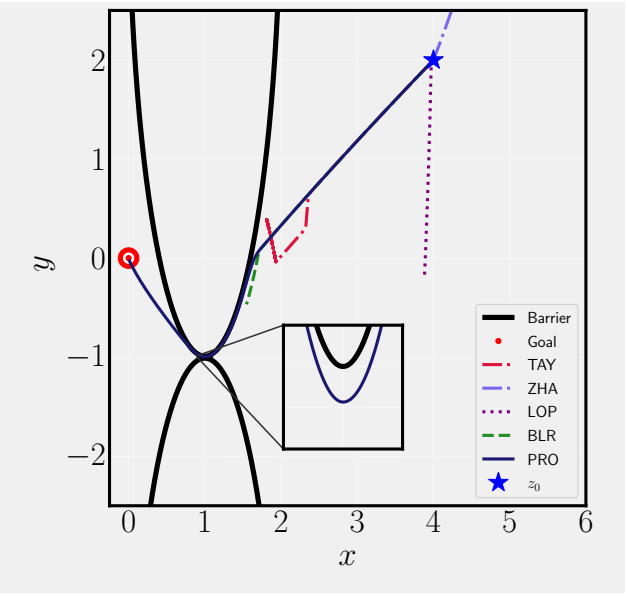

(a) States

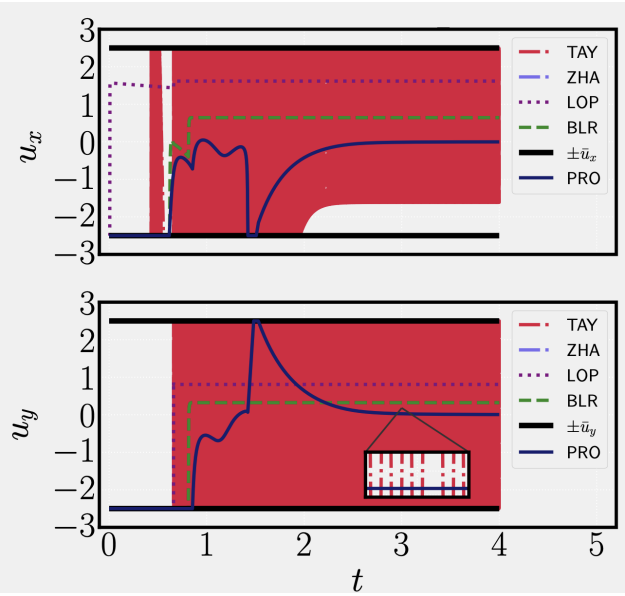

(b) Control Inputs

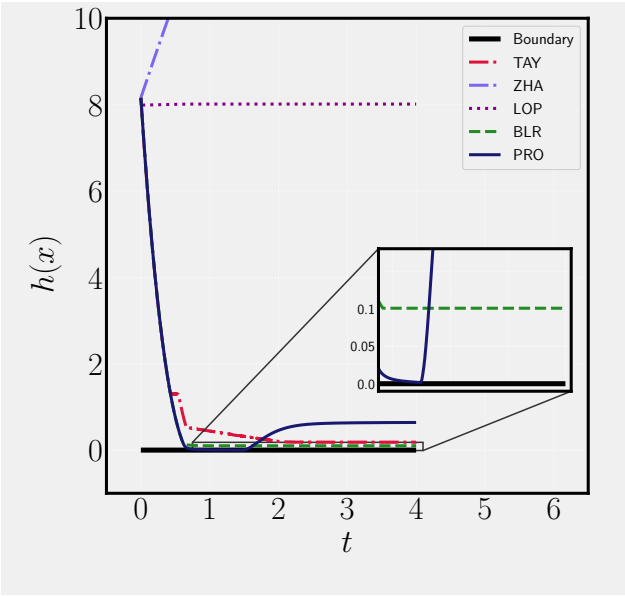

(c) Minimum CBF Values

Figure 3.3: Evolutions of the states, control inputs, and control barrier functions for the rank-deficient regressor "Shoot the Gap" example.

is defined, where $K_V = 1$. The safe states are those residing outside of the two ellipses shown in Figure 3.1, which results in the following CBFs:

$$h_i(\boldsymbol{z}) = \frac{(x - x_i)^2}{a_1^2} + \frac{(y - y_i)^2}{a_2^2} - 1, \tag{3.59}$$

for $i \in \{1, 2\}$, where x_1, x_2, y_1, y_2, a_1, and a_2 are parameters that define the location, size, and shape of the ellipses.

The CLF-CBF-QP framework is [65, 3, 189] is selected for control design. To more fairly compare the proposed approaches with the controllers from the literature, the FxT-CLF condition was used in all controllers in addition to their individual approaches to stabilization. Because no meaningful differences between the native and FxT-CLF implementations were found in their abilities to "shoot the gap", results for the latter cases are presented. The control framework is then:

$$\min_{\boldsymbol{u}, \delta_0, \delta_1, \ldots, \delta_q} \frac{1}{2}\boldsymbol{u}^T Q \boldsymbol{u} + q_0 \delta_0^2 + \sum_{i=1}^{q} p_i \delta_i^2 \tag{3.60a}$$

s.t.

$$-\bar{u}_j \leq u_j \leq \bar{u}_j \tag{3.60b}$$

$$1 \leq \delta_i \tag{3.60c}$$

$$L_f V + L_g V \boldsymbol{u} + \phi_V \leq \delta_0 - c_1 V^{\gamma_1} - c_2 V^{\gamma_2} \tag{3.60d}$$

$$L_f h_i + L_g h_i \boldsymbol{u} + \phi_h \geq -\delta_i h_i, \tag{3.60e}$$

$\forall i \in \{1, \ldots, q\}$ and $\forall j \in \{1, \ldots, m\}$, where the arguments of V and h_i have been omitted for conciseness. For this problem $u_1 = u_x$ and $u_2 = u_y$, δ_0 is a relaxation parameter (penalized by $q_0 > 0$) on the performance objective whose inclusion aids the feasibility of the QP, δ_i allows for larger negative values of $\dot{h}_i$ away from the boundary of the safe set, and $p_i > 0$ penalizes values of δ_i. The terms $\phi_V = \phi_V(\boldsymbol{x}, \Delta(\boldsymbol{x}), \hat{\boldsymbol{\theta}}, \eta)$ and $\phi_h = \phi_h(\boldsymbol{x}, \Delta(\boldsymbol{x}), \hat{\boldsymbol{\theta}}, \eta)$ are left intentionally vague and are used as placeholders that represent the specific way in which each work from the literature treats the parametric uncertainty in the system dynamics. To summarize, (3.60b) enforces input constraints, (3.60c) imposes a lower bound on the relaxation coefficients δ_i, (3.60d) encodes FxT convergence to the goal, and safety is guaranteed by (3.60e).

3.4.1.3 Results

The simulated state, control, and CBF trajectories for the case of the full-rank regressor, $\Delta = \Delta_F$, are shown in Figure 3.2. It is worth noting from Figure 3.2a that the only controllers that suc-

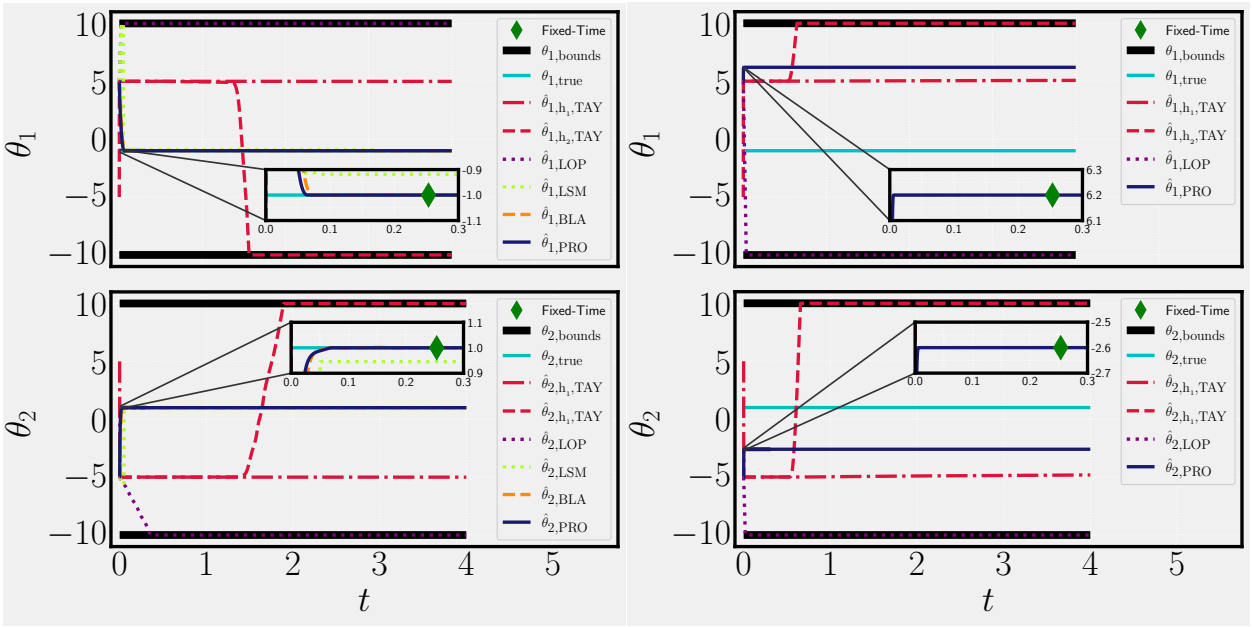

(a) Full-Rank Regressor

(b) Rank-Deficient Regressor

Figure 3.4: True unknown parameters and their estimates for the Shoot the Gap example with (a) full-rank regressor and (b) rank-deficient regressor matrix.

cessfully reach the goal while maintaining safety at all times are those that closely estimate the unknown parameters in the system dynamics, i.e. the BLA, LSM, and PRO approaches. In fact, it is observed from Figure 3.4a that, in accordance with the proven FxTS properties of the proposed adaptation laws, the parameter estimates, $\hat{\boldsymbol{\theta}}$, converge to their true values within fixed-time T (resp. T_θ) given by (3.33) (resp. (3.23)). Figure 3.2c further highlights that the proposed technique accomplishes safe goal-reaching while avoiding the undesirable chattering control behavior exhibited by the TAY approach [32], as shown in Figure 3.2b.

When a rank-deficient regressor appears in (3.58), i.e. $\Delta = \Delta_D$, however, both the BLA and LSM methods that succeed under a full-rank regressor fail; each requires the inversion of a non-invertible matrix. As illustrated by Figure 3.3, the proposed controller with adaptation given by (3.35) succeeds in safely reaching the goal by learning a parameter vector, $\hat{\boldsymbol{\theta}}$, within a fixed time that satisfies $\Delta_D(\boldsymbol{x})\hat{\boldsymbol{\theta}} = \Delta_D(\boldsymbol{x})\boldsymbol{\theta}^*$, as supported by Figure 3.4b. Under these dynamics, the proposed approach is the only controller that successfully reaches the goal.

In the case of the full-rank regressor, it is evident that the ability of the adaptation law (3.35) to learn the system uncertainty in fixed-time allowed the controller to succeed in driving the state to the goal where others did not. Doing so despite a rank-deficient regressor further demonstrates that it adds value to controllers for the class of systems under consideration, especially when none of the considered approaches from the literature were capable of succeeding under such conditions.

3.4.2 Quadrotor Trajectory Tracking

The second study examines a simulated quadrotor in a wind field. Consider a quadrotor whose objective is to track a Gerono lemniscate (i.e., figure-eight) trajectory while obeying attitude and altitude constraints despite wind perturbing the nominal system dynamics.

3.4.2.1 Dynamics

For the nominal system model, consider the 6 degree-of-freedom rigid-body dynamic model of the quadrotor as described in [207]. Denote $\boldsymbol{\chi} = [x\ y\ z\ u\ v\ w\ \phi\ \theta\ \psi\ p\ q\ r]^\top$ as the state, where x, y, and z are the position coordinates (in m) with respect to an inertial frame, u, v, and w are the translational velocities (in m/s) with respect to the body-fixed frame, ϕ, θ, and ψ (in rad) are the roll, pitch, and yaw Euler angles defining a ZYX rotation from the inertial frame to the body-fixed frame, and p, q, and r are the roll, pitch, and yaw rates (in rad/s) defined with respect to the body-fixed frame.

Much attention has been given to the effect of wind on the nominal dynamics of a quadrotor system [208, 209, 210]. Specifically, the phenomena of blade flapping, induced velocity, and aerodynamic drag have been studied extensively. In this example, the effects of blade flapping and induced velocity are neglected, with the focus instead on aerodynamic drag. It is assumed that a constant, known wind field perturbs the quadrotor, whose drag coefficient vector $\boldsymbol{C}_d = [C_x\ C_y\ C_z]^\top$ is unknown, where C_x, C_y, and C_z are the components in the principal body-fixed directions.

The system is then described by:

$$
\begin{aligned}
\begin{pmatrix}\dot{x}\\ \dot{y}\\ \dot{z}\end{pmatrix} &= \begin{pmatrix} c\theta c\psi & s\phi s\theta c\psi - c\phi s\psi & c\phi s\theta c\psi + s\phi s\psi \\ c\theta s\psi & s\phi s\theta s\psi + c\phi c\psi & c\phi s\theta s\psi - s\phi c\psi \\ s\theta & -s\phi c\theta & -c\phi c\theta \end{pmatrix} \begin{pmatrix} u \\ v \\ w \end{pmatrix} \\
\begin{pmatrix}\dot{u}\\ \dot{v}\\ \dot{w}\end{pmatrix} &= \begin{pmatrix} rv - qw \\ pw - ru \\ qu - pw \end{pmatrix} + \begin{pmatrix} -gs\theta \\ gc\theta s\phi \\ gc\theta c\phi \end{pmatrix} + \frac{1}{M}\begin{pmatrix} 0 \\ 0 \\ -F \end{pmatrix} + \Delta_a(\boldsymbol{\chi})\boldsymbol{C}_d \\
\begin{pmatrix}\dot{\phi}\\ \dot{\theta}\\ \dot{\psi}\end{pmatrix} &= \begin{pmatrix} 1 & s\phi t\theta & c\phi t\theta \\ 0 & c\phi & -s\phi \\ 0 & \frac{s\phi}{c\theta} & \frac{c\phi}{c\theta} \end{pmatrix} \begin{pmatrix} p \\ q \\ r \end{pmatrix} \\
\begin{pmatrix}\dot{p}\\ \dot{q}\\ \dot{r}\end{pmatrix} &= \begin{pmatrix} \frac{J_y - J_z}{J_x} qr \\ \frac{J_z - J_x}{J_y} pr \\ \frac{J_x - J_y}{J_z} pq \end{pmatrix} + \begin{pmatrix} \frac{1}{J_x}\tau_\phi \\ \frac{1}{J_y}\tau_\theta \\ \frac{1}{J_z}\tau_\psi \end{pmatrix}
\end{aligned}
\tag{3.61}
$$

where g is the acceleration due to gravity (in m/sec^2), the functions $\sin$, $\cos$, and $\tan$ are denoted s, c, and t for brevity, M is the mass of the quadrotor (in kg), J_x, J_y, and J_z are the principal

moments of inertia (in kg·m^2), F is the thrust of the rotors (in N), and τ_ϕ, τ_θ, and τ_ψ are rolling, pitching, and yawing torques (in N·m) respectively due to the rotors. Since (3.61) is affine in both the control, $\boldsymbol{u} = [F\ \tau_\phi\ \tau_\theta\ \tau_\psi]^\top$, and unknown parameters, $\boldsymbol{C}_d$, it can be written as

$$\dot{\boldsymbol{\chi}} = f(\boldsymbol{\chi}) + g(\boldsymbol{\chi})\boldsymbol{u} + \Delta(\boldsymbol{\chi})\boldsymbol{C}_d,$$

where $\Delta(\boldsymbol{\chi}) = [\boldsymbol{0}_{3\times3}\ \Delta_a(\boldsymbol{\chi})\ \boldsymbol{0}_{6\times3}]^\top$, with

$$\Delta_a(\boldsymbol{\chi}) = K_\Delta \frac{\|\boldsymbol{v}_r\|}{M} \begin{bmatrix} v_{r,1} & 0 & 0 \\ 0 & v_{r,2} & 0 \\ 0 & 0 & v_{r,3} \end{bmatrix}$$

where $K_\Delta > 0$, $\boldsymbol{v}_r = \boldsymbol{R}\boldsymbol{v}_w - \boldsymbol{v}_q$ is the relative wind-velocity vector in the body-fixed frame, with $\boldsymbol{v}_q = [u\ v\ w]^T$ the quadrotor velocity vector in the body-fixed frame, $\boldsymbol{v}_w$ being the wind velocity vector in the inertial frame, and $\boldsymbol{R}$ being the rotation matrix from the inertial to the body-fixed frame. Additionally, $v_{r,1}$, $v_{r,2}$, and $v_{r,3}$ are the principal components of $\boldsymbol{v}_r$ such that the term $\Delta(\boldsymbol{\chi})\boldsymbol{C}_d$ models the effect of aerodynamic drag acting on the center of mass of the quadrotor.

3.4.2.2 Controller

Define $\boldsymbol{v} = [\boldsymbol{u}\ \delta_1\ \delta_2]^\top \in \mathbb{R}^6$ and use the following CBF-QP-based controller [211, 212, 189]:

$$\boldsymbol{v}^* = \arg\min_{\boldsymbol{v}} \frac{1}{2}\|\boldsymbol{u} - \boldsymbol{u}_{nom}\|^2 + p_1\delta_1^2 + p_2\delta_2^2 \tag{3.62a}$$

s.t.

$$A\boldsymbol{v} \leq \boldsymbol{b} \tag{3.62b}$$

$$L_f h_1(\boldsymbol{\chi}) + L_g h_1(\boldsymbol{\chi})\boldsymbol{u} \geq -\delta_1 h_1(\boldsymbol{\chi}) - \boldsymbol{r}(t, \hat{\boldsymbol{C}}_d) \tag{3.62c}$$

$$L_f h_2(\boldsymbol{\chi}) + L_g h_2(\boldsymbol{\chi})\boldsymbol{u} \geq -\delta_2 h_2(\boldsymbol{\chi}) - \boldsymbol{r}(t, \hat{\boldsymbol{C}}_d) \tag{3.62d}$$

where $p_1, p_2 > 0$. The cost function (3.62a) seeks to minimize the deviation of $\boldsymbol{u}^*$ from some nominal control $\boldsymbol{u}_{nom}$, and to minimize the slack variables δ_1^*, δ_2^* penalized by $p_1, p_2 > 0$; (3.62b) encodes input constraints on $\boldsymbol{u}^*$ and enforces that $\delta_1^*, \delta_2^* \geq \underline{\delta} > 0$; and (3.62c) and (3.62d) enforce safety according to the following CBFs,

$$h_1(\boldsymbol{\chi}) = 1 - \left(\frac{z - c_z}{p_z}\right)^{n_z} \tag{3.63}$$

$$h_2(\boldsymbol{\chi}) = \cos(\phi)\cos(\theta) - \cos(\alpha), \tag{3.64}$$

where $c_z = 2.5$, $p_z = 2.5$, and $n_z = 2$ are parameters such that h_1 defines the safe altitude range, i.e. between 0 and 5 meters, and h_2 restricts the thrust vectoring angle of the quadrotor to be within α rad of the vertical. In this case, $\alpha = \frac{\pi}{2}$ so that the quadrotor could not flip upside-down. The tracking controller developed for quadrotors by [213] and used for safe quadrotor control in [214] was selected as a nominal input $\boldsymbol{u}_{nom}$. The adaptation law was (3.35) using the state predictor scheme from Section 3.2.2.2 (results denoted SP-CW), which is defined here as

$$\dot{\hat{\boldsymbol{C}}}_d = \boldsymbol{\Gamma} \boldsymbol{W}^T \boldsymbol{e} \left(a \|\boldsymbol{e}\|^{\frac{2}{\mu}} + \frac{b}{\|\boldsymbol{e}\|^{\frac{2}{\mu}}} \right),$$

where $\boldsymbol{e} = \boldsymbol{\chi} - \boldsymbol{z}$, with

$$\begin{aligned} \dot{\boldsymbol{z}} &= f(\boldsymbol{\chi}) + g(\boldsymbol{\chi})\boldsymbol{u} + \Delta(\boldsymbol{\chi})\hat{\boldsymbol{C}}_d + k_e \boldsymbol{e} + \boldsymbol{W}\dot{\hat{\boldsymbol{C}}}_d, \\ \boldsymbol{z}(0) &= \boldsymbol{\chi}(0), \end{aligned}$$

and

$$\dot{\boldsymbol{W}} = -k_e \boldsymbol{W} + \Delta(\boldsymbol{\chi}), \quad \boldsymbol{W}(0) = \boldsymbol{0}_{n \times p},$$

where $a, b, \mu = 5$ and $k_e = 10$. For comparison, we additionally studied the case where $\dot{\hat{\boldsymbol{C}}}_d = \boldsymbol{0}_{3\times 1}$ (results denoted 0-CW). The wind-velocity vector $\boldsymbol{v}_w$ was held constant at $\boldsymbol{v}_r = [10,\ -8,\ -5]^T$, which resulted in the regressor being full-rank for all $t \geq 0$. To account for the warm-up time required in the state prediction scheme, we set $T_w = 0.1$ sec and added it to the theoretical bound given by (3.33). It is possible that a longer warm-up time could result in a decrease in the minimum non-zero singular value of the regressor, thereby reducing the upper bound on convergence time, but this is problem-dependent and can be viewed as a tuning parameter.

3.4.2.3 Results

It may be seen from Figure 3.5 that the estimates of the coefficients of drag converged to their true values within the fixed-time bound. Figures 3.6 and 3.7 highlight that the controller is able to safely track the reference trajectory using the adaptation law (3.35) with the state prediction scheme, whereas poor tracking, albeit safe, is achieved without parameter adaptation. Control trajectories are provided in Figure 3.8. Note that the quadrotor under the effect of unknown wind gusts (denoted by SP-WG in the figures) will be considered using new theory presented in Chapter 4.

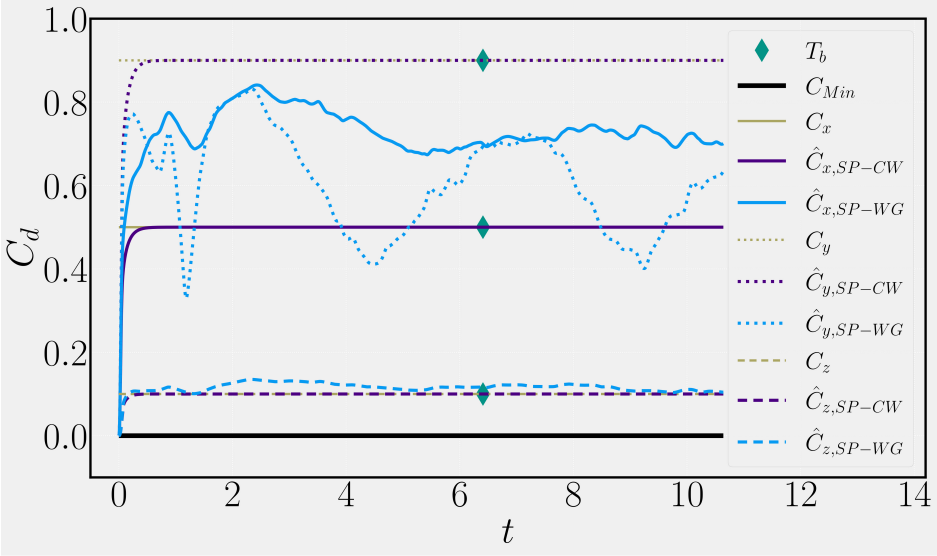

Figure 3.5: Principal coefficient of drag estimates for the quadrotor in a 1) constant (CW) and 2) gusty (WG) wind field under the proposed controller with the state prediction (SP) scheme.

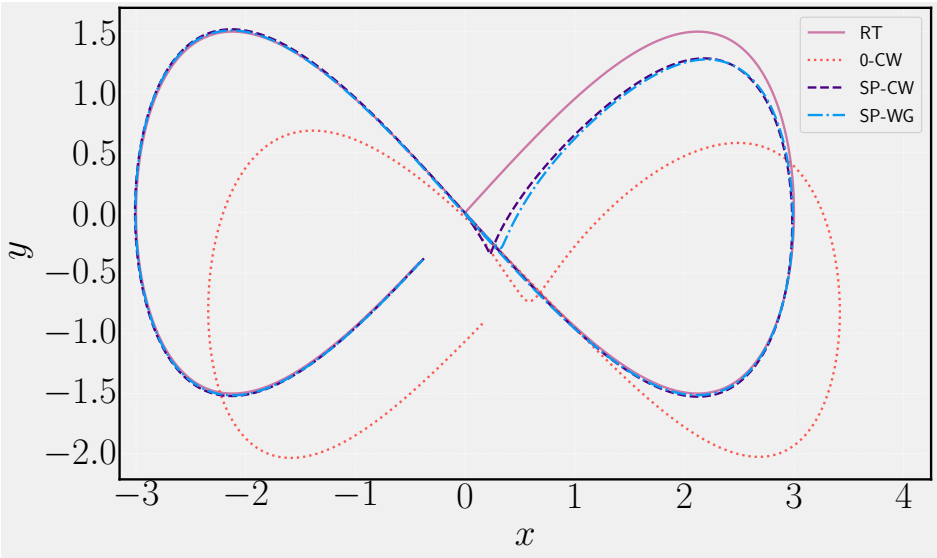

Figure 3.6: Quadrotor XY trajectories as the controller seeks to track the reference trajectory (RT) in a wind field.

3.5 Conclusion

In this chapter, two fixed-time stable parameter adaptation laws were introduced for learning the effect of an additive, parameter-affine perturbation on a class of nonlinear, control-affine dynamical systems. Under a common persistence of excitation condition, the first law was shown to learn the true system parameters within a fixed-time independent of the initial parameter estimates,

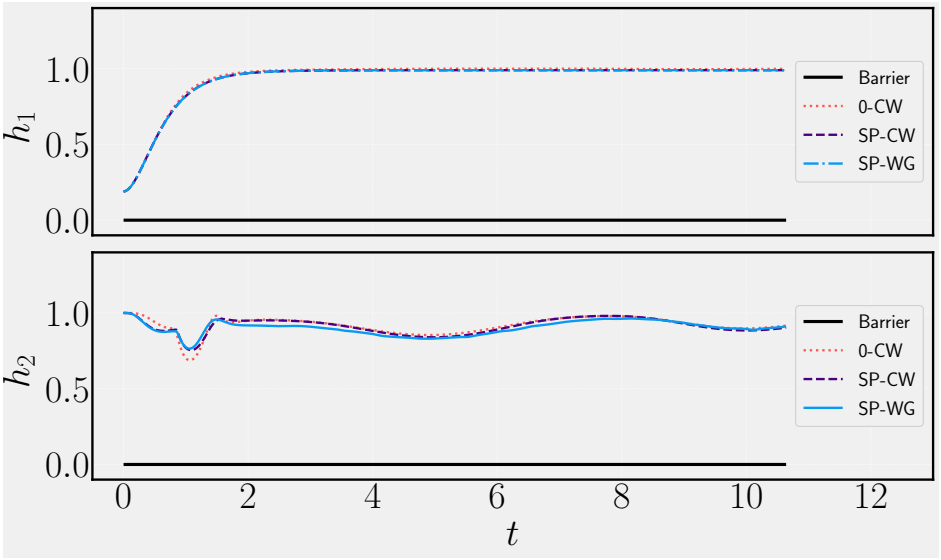

Figure 3.7: CBF trajectories for the quadrotor numerical study.

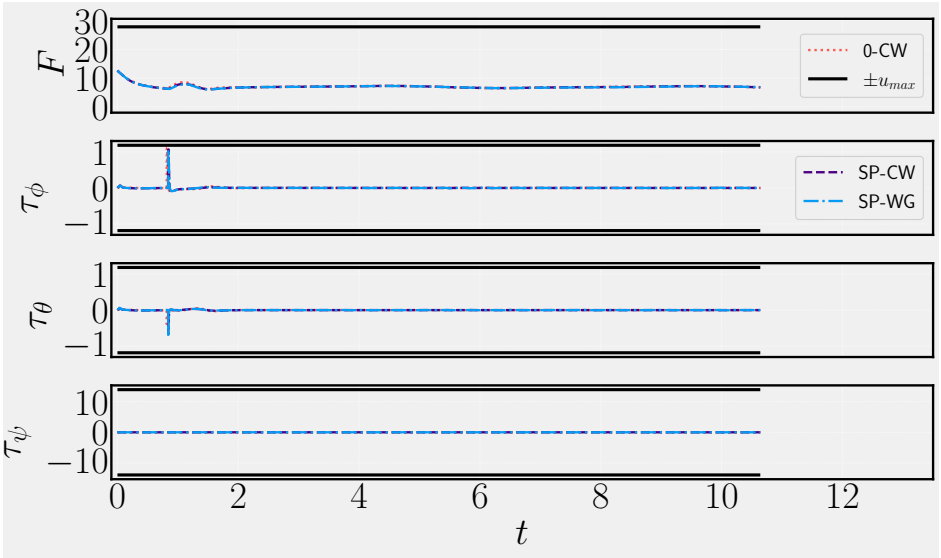

Figure 3.8: Control inputs for the quadrotor numerical study.

whereas the second law was shown to learn the true system disturbance within a fixed-time even under global system unidentifiability. In both cases, error bounds were derived on the estimated disturbance error as functions of time, which allowed for the synthesis of a robust, adaptive control barrier function condition for preserving safety throughout the model identification process.

CHAPTER 4

Fixed-Time Identification for Safe Control of Unknown, Nonlinear Systems

Whereas Chapter 3 treated the problem of fixed-time system identification for safe control design of a class of nonlinear, control- and parameter-affine systems in the idealized sense, i.e., with the availability of perfect measurements, the conditions required for the application of such results are often violated in practical scenarios. For many dynamical systems of practical relevance, system models are perturbed by unmodelled dynamics, measurement error, or exogenous disturbances. As such, this chapter explores the problem of fixed-time system identification for safe control design under such phenomena.

Specifically, Section 4.1 investigates robustness properties of the latter of the parameter adaptation laws proposed in Chapter 3 to a class of bounded disturbance that model, e.g., measurement noise or exogenous perturbations. Under such conditions, it is shown that the proposed parameter adaptation law converges to a neighborhood of the goal set within a fixed-time. Several technical lemmas are introduced both to prove this result and to characterize the associated neighborhood and its domain of attraction. In Section 4.2, the class of systems under consideration is further generalized to consider an unknown, additive, nonlinear, yet bounded perturbation to the nominal system model. Leveraging recent advancements in the field of Koopman operator theory (KOT), by which a nonlinear system may be modelled via an analogous linear, but notably infinite-dimensional, system, the parameter adaptation law from Chapter 3 is used to recursively learn a finite-dimensional matrix representation of the Koopman generator within a fixed-time. To the best of the author's knowledge, this marks the first use of KOT for recursive system identification in fixed-time. Under certain assumptions, it is shown that this provides exact reconstruction of the unknown, nonlinear system disturbance. In Section 4.3, robust- and robust, adaptive- Control Barrier Function (CBF) conditions are proposed for safe control synthesis under the proposed Koopman-based adaptation law. Simulations are conducted in Section 4.4 first on the 12 dimensional, 6 degree-of-freedom quadrotor model under an unknown wind gust and then on a double integrator example inspired by the quadrotor problem.

The results in this chapter are based partly on [182] and [183].

4.1 Robust Parameter Identification

This section represents a continuation of the work of Chapter 3 in that it investigates the robustness of the parameter adaptation law (3.35) under additional, bounded perturbations to the system (3.4).

4.1.1 System Model

Consider the following nonlinear, control-, and parameter-affine system subject also to an additive, bounded disturbance:

$$\dot{\boldsymbol{x}} = f(\boldsymbol{x}(t)) + g(\boldsymbol{x}(t))\boldsymbol{u}(t) + \Delta(\boldsymbol{x}(t))\boldsymbol{\theta}^* + d(\boldsymbol{x}(t), t), \tag{4.1}$$

where $\boldsymbol{x} \subset \mathbb{R}^n$ denotes the state, $\boldsymbol{u} \in \mathcal{U} \subset \mathbb{R}^m$ the control input, $\boldsymbol{\theta}^* \in \Theta \subset \mathbb{R}^p$ a vector of unknown, static parameters, and $d : \mathbb{R}^n \times \mathbb{R} \to \mathcal{D}$ where it is known that $\|\boldsymbol{d}\|_\infty \leq C < \infty$, for all $\boldsymbol{d} \in \mathcal{D}$. It is again assumed that the drift vector field $f : \mathbb{R}^n \to \mathbb{R}^n$, control matrix field $g : \mathbb{R}^n \to \mathbb{R}^{n\times m}$, and regressor $\Delta : \mathbb{R}^n \to \mathbb{R}^{n\times p}$ are known, continuous, and bounded for bounded inputs, such that for a continuous control input $\boldsymbol{u} : \mathbb{R} \to \mathcal{U}$ the system (4.1) admits a unique solution, and that the unknown parameters are static, i.e., that $\dot{\boldsymbol{\theta}}^* = \mathbf{0}_{p\times 1}$. It is worth noting, however, that the above system (4.1) could also model a system with time-varying parameters $\boldsymbol{\phi}^* : \mathbb{R} \to \Phi \subset \mathbb{R}^p$, i.e., if

$$d(\boldsymbol{x}, t) = \Delta(\boldsymbol{x})\boldsymbol{\phi}^*(t) - \Delta(\boldsymbol{x})\boldsymbol{\theta}^*, \tag{4.2}$$

for some compact set Φ. As such, the estimated parameter vector is again denoted $\hat{\boldsymbol{\theta}}$ so that the parameter estimation error vector is $\tilde{\boldsymbol{\theta}} = \boldsymbol{\theta}^* - \hat{\boldsymbol{\theta}}$ with dynamics given by

$$\dot{\tilde{\boldsymbol{\theta}}} = -\dot{\hat{\boldsymbol{\theta}}}. \tag{4.3}$$

In Chapter 3 two methods were proposed for the satisfaction of Assumption 3.5, a main component of which was consistency, i.e., that the parameter estimation error vector $\tilde{\boldsymbol{\theta}}$ is one solution to a system of equations of the form $\boldsymbol{M}(t)\tilde{\boldsymbol{\theta}}(t) = \boldsymbol{v}(t)$ for $\boldsymbol{M} : \mathbb{R} \to \mathbb{R}^{n\times p}$ and $\boldsymbol{v} : \mathbb{R} \to \mathbb{R}^n$. For the system (4.1) neither the rate measurement scheme from Section 3.2.2.1 nor the state predictor scheme from Section 3.2.2.2 satisfy Assumption 3.5. Specifically, for rate measurements it follows that

$$\underbrace{\dot{\boldsymbol{x}} - f(\boldsymbol{x}) - g(\boldsymbol{x})\boldsymbol{u} - \Delta(\boldsymbol{x})\hat{\boldsymbol{\theta}}}_{\boldsymbol{v}} = \underbrace{\Delta(\boldsymbol{x})}_{\boldsymbol{M}}\tilde{\boldsymbol{\theta}} + \underbrace{d(\boldsymbol{x}, t)}_{\boldsymbol{\delta}}, \tag{4.4}$$

and for the state predictor scheme,

$$\dot{\boldsymbol{\xi}} = -k\boldsymbol{\xi} + d(t, \boldsymbol{x}), \quad \boldsymbol{\xi}(0) = \boldsymbol{e}(0), \tag{4.5}$$

which implies that $\boldsymbol{e} = \boldsymbol{W}\tilde{\boldsymbol{\theta}} + \boldsymbol{\alpha}$ for all $t > 0$, where $\boldsymbol{\alpha} \in \mathbb{R}^n$ is unknown. Observe, however, that these new relations may be expressed in the form (3.15), provided here for completeness:

$$\boldsymbol{M}(t)\tilde{\boldsymbol{\theta}}(t) = \boldsymbol{v}(t) - \boldsymbol{\delta}(t), \tag{4.6}$$

for $\boldsymbol{\delta} : \mathbb{R} \to \mathbb{R}^n$. As such, the following modified version of Assumption 3.5 is introduced.

Assumption 4.1. *For all $t \geq 0$ there is a known vector, $\boldsymbol{v}(t) \in \mathbb{R}^n$, a known matrix, $\boldsymbol{M}(t) \in \mathbb{R}^{n\times p}$, and an unknown vector, $\boldsymbol{\delta}(t)$ that jointly satisfy the following properties:*

(i) ***Consistency****: the parameter error, $\tilde{\boldsymbol{\theta}}(t)$, is one solution to* (4.6)*,*

(ii) ***Bounded Perturbation****: for $\boldsymbol{\delta}(t)$ in* (4.6) *there exists a known $\Upsilon > 0$ such that*

$$\sup_{t\in\mathbb{R}} \|\boldsymbol{\delta}(t)\| \leq \Upsilon,$$

(iii) ***Boundedness*** *and* ***Equivalence*** *of Assumption 3.5 hold, i.e., items (ii) and (iii) of Assumption 3.5.*

Part (ii) of Assumption 4.1 is reasonable given that it is assumed that the disturbance d in (4.1) is bounded. Note again that by expressing the parameter estimation error as $\tilde{\boldsymbol{\theta}} = \tilde{\boldsymbol{\theta}}_R + \tilde{\boldsymbol{\theta}}_N$, for $\tilde{\boldsymbol{\theta}}_R \in \text{row}(\boldsymbol{M})$ and $\tilde{\boldsymbol{\theta}}_N \in \mathcal{N}(\boldsymbol{M})$, it may be determined that

$$\dot{\tilde{\boldsymbol{\theta}}} = \dot{\tilde{\boldsymbol{\theta}}}_R + \dot{\tilde{\boldsymbol{\theta}}}_N, \tag{4.7}$$

$$\dot{\hat{\boldsymbol{\theta}}} = \dot{\hat{\boldsymbol{\theta}}}_R + \dot{\hat{\boldsymbol{\theta}}}_N \tag{4.8}$$

where $\dot{\tilde{\boldsymbol{\theta}}}_R, \dot{\hat{\boldsymbol{\theta}}}_R \in \text{row}(\boldsymbol{M})$ and $\dot{\tilde{\boldsymbol{\theta}}}_N, \dot{\hat{\boldsymbol{\theta}}}_N \in \mathcal{N}(\boldsymbol{M})$. By rank-nullity and the fact that $\text{row}(\boldsymbol{M})$ and $\mathcal{N}(\boldsymbol{M})$ are orthogonal complements, such a decomposition always exists [204].

4.1.2 Technical Lemmas

The following technical Lemmas are requirements for the proof of the main result in this section.

Lemma 4.1. *Suppose that $c_1, c_2 > 0$, $c_3 \in \mathbb{R}$, $\gamma_1 = 1 + \frac{1}{\mu}$, $\gamma_2 = 1 - \frac{1}{\mu}$, $\mu > 1$, $0 < k < 1$, and that $\bar{V} = 1$ and $V_0 > 1$. Consider the following integral,*

$$I \triangleq \int_{V_0}^{\bar{V}} \frac{dV}{-c_1 V^{\gamma_1} - c_2 V^{\gamma_2} + c_3 V}. \tag{4.9}$$

Then, the following holds:

(i) if $c_3 < 2\sqrt{c_1 c_2}$, then for all $V_0 > 1$

$$I \leq \frac{\mu}{c_1 k_1} \left(\frac{\pi}{2} - \tan^{-1} k_2 \right), \tag{4.10}$$

where

$$k_1 = \sqrt{\frac{4c_1 c_2 - c_3^2}{4c_1^2}} \tag{4.11}$$

$$k_2 = \frac{2c_1 - c_3}{\sqrt{4c_1 c_2 - c_3^2}}. \tag{4.12}$$

(ii) if $c_3 \geq 2\sqrt{c_1 c_2}$, and $1 \leq V_0^{\frac{1}{\mu}} \leq k^{\frac{c_3 - \sqrt{c_3^2 - 4c_1 c_2}}{2c_1}}$, then

$$I \leq \frac{\mu k}{(1-k)\sqrt{c_1 c_2}}. \tag{4.13}$$

Proof. Follows directly by changing the upper integration bound from $\bar{V} = 0$ in [215, Lemma 2] to $\bar{V} = 1$ here. □

Lemma 4.2. *Suppose that $\boldsymbol{x}, \boldsymbol{y} \in \mathbb{R}^n$, and define*

$$P(\boldsymbol{x}, \boldsymbol{y}) \triangleq \boldsymbol{x}^T \boldsymbol{y} \left(a \|\boldsymbol{x} + \boldsymbol{y}\|^{\frac{2}{m}} + \frac{b}{\|\boldsymbol{x} + \boldsymbol{y}\|^{\frac{2}{m}}} \right). \tag{4.14}$$

If $a, b > 0$, $m > 2$, and there exists $B_y > 0$ such that $\|\boldsymbol{y}\| \leq B_y$ and $\|\boldsymbol{x}\| > 2B_y$, then it holds that

$$P(\boldsymbol{x}, \boldsymbol{y}) \geq -B_y \left(a \|\boldsymbol{x}\|^{1 + \frac{2}{m}} + 2^{\frac{2}{m}} b \|\boldsymbol{x}\|^{1 - \frac{2}{m}} \right). \tag{4.15}$$

Proof. Provided in Appendix B. □

4.1.3 Robust FxTS Parameter Adaptation

The following result derives a robustness property for the Fixed-Time Stable (FxTS) adaptation law proposed in (3.35), namely that the parameter error converges to a neighborhood of the goal set within a fixed-time.

Theorem 4.1 (**Robust FxTS Parameter Adaptation**). *Consider a perturbed dynamical system of the form* (4.1)*. Suppose that Assumption 4.1 holds, and that* $\mathcal{N}(\Delta(\boldsymbol{x}(t))) = \mathcal{N}(\Delta(\boldsymbol{x}(0)))$, $\forall t \in [0, T]$*. Then, under the adaptation law* (3.35)*, with* $\lambda_{min}(\boldsymbol{\Gamma}) \geq 2(\frac{\Upsilon}{\underline{\sigma}(\boldsymbol{M})})^2$*, there exist neighborhoods* D_0 *and* D *of* Ω *such that for all* $\hat{\boldsymbol{\theta}}(0) \in D_0$*, the trajectories of* (3.39) *satisfy* $\tilde{\boldsymbol{\theta}}_R(t) \in D_0$ *for all* $t \geq 0$*, and reach* D *within a fixed time* T*, where* $D = \{\tilde{\boldsymbol{\theta}}_R \mid V(\tilde{\boldsymbol{\theta}}_R) \leq 1\}$*, and*

$$D_0 = \begin{cases} \mathbb{R}^p; & \Upsilon < Y, \\ \left\{ \tilde{\boldsymbol{\theta}}_R \mid V(\tilde{\boldsymbol{\theta}}_R) \leq \left(k \frac{\alpha_3 - \sqrt{\alpha_3^2 - 4\alpha_1\alpha_2}}{2\alpha_1} \right)^{\mu} \right\}; & \Upsilon \geq Y, \end{cases} \tag{4.16}$$

$$T \leq \begin{cases} \frac{\mu}{\alpha_1 k_1} \left(\frac{\pi}{2} - \tan^{-1} k_2 \right); & \Upsilon < Y, \\ \frac{\mu k}{(1-k)\sqrt{\alpha_1\alpha_2}}; & \Upsilon \geq Y, \end{cases} \tag{4.17}$$

where $\mu > 2$*,* $0 < k < 1$*,* k_1 *and* k_2 *are given by* (4.11) *and* (4.12) *respectively, and*

$$\alpha_1 = 2^{\frac{-2}{\mu}} a k_V^{2+\frac{2}{\mu}}, \tag{4.18}$$

$$\alpha_2 = 2^{\frac{2}{\mu}} b k_V^{2-\frac{2}{\mu}}, \tag{4.19}$$

$$\alpha_3 = a\Upsilon k_V^{1+\frac{2}{\mu}} + 2^{\frac{2}{\mu}} b \Upsilon k_V^{1-\frac{2}{\mu}}, \tag{4.20}$$

with k_V *defined as in* (3.34)*, and*

$$Y = 2\frac{k_V^2\sqrt{ab}}{a k_V^{1+\frac{2}{\mu}} + 2^{\frac{2}{\mu}} b k_V^{1-\frac{2}{\mu}}}. \tag{4.21}$$

Proof. Consider the Lyapunov function candidate $V = \frac{1}{2}\tilde{\boldsymbol{\theta}}_R^T \boldsymbol{\Gamma}^{-1} \tilde{\boldsymbol{\theta}}_R$. Let $\boldsymbol{q} = \boldsymbol{M}\tilde{\boldsymbol{\theta}}_R$. Under the adaptation law (3.35), it follows that

$$\dot{V} = -\boldsymbol{q}^T (\boldsymbol{q} + \boldsymbol{\delta}) \left(a\|\boldsymbol{q} + \boldsymbol{\delta}\|^{\frac{2}{\mu}} + \frac{b}{\|\boldsymbol{q} + \boldsymbol{\delta}\|^{\frac{2}{\mu}}} \right),$$

where $a, b > 0$ and $\mu > 2$. By definition of the vector inner product, it follows that $\boldsymbol{q}^T\boldsymbol{q} > |\boldsymbol{q}^T\boldsymbol{\delta}|$ as long as $\|\boldsymbol{q}\| > \|\boldsymbol{\delta}\|$. Thus, when $\|\boldsymbol{q}\| > \|\boldsymbol{\delta}\|$ it holds that $\boldsymbol{q}^T(\boldsymbol{q} + \boldsymbol{\delta}) > 0$ and therefore that $\dot{V} < 0$. By Assumption 4.1 and the vector triangle inequality, $\|\boldsymbol{q} + \boldsymbol{\delta}\| > \Upsilon$ whenever $\|\boldsymbol{q}\| > 2\Upsilon$. As such,

$\|\boldsymbol{q}+\boldsymbol{\delta}\| > \frac{1}{2}\|\boldsymbol{q}\|$ for all $\|\boldsymbol{q}\| > 2\Upsilon$. Thus, from Theorem 3.4 it is true that whenever $\|\boldsymbol{q}\| > 2\Upsilon$ the following holds:

$$\begin{aligned}\dot{V} \leq & -\boldsymbol{q}^T\boldsymbol{q}\left(a\left(\frac{\|\boldsymbol{q}\|}{2}\right)^{\frac{2}{\mu}} + b\left(\frac{2}{\|\boldsymbol{q}\|}\right)^{\frac{2}{\mu}}\right) - F(\boldsymbol{q},\boldsymbol{\delta}) \\ \leq & -\alpha_1 V^{1+\frac{1}{\mu}} - \alpha_2 V^{1-\frac{1}{\mu}} - F(\boldsymbol{q},\boldsymbol{\delta}) < 0,\end{aligned}$$

where α_1 and α_2 are given by (4.18) and (4.19), and $F(\boldsymbol{q},\boldsymbol{\delta}) = \boldsymbol{q}^T\boldsymbol{\delta}\left(a\|\boldsymbol{q}+\boldsymbol{\delta}\|^{\frac{2}{\mu}} + b\|\boldsymbol{q}+\boldsymbol{\delta}\|^{-\frac{2}{\mu}}\right)$. Then, using Lemma 4.2 it follows that

$$F(\boldsymbol{q},\boldsymbol{\delta}) \geq -\Upsilon\left(a\|\boldsymbol{q}\|^{1+\frac{2}{\mu}} + 2^{\frac{2}{\mu}}b\|\boldsymbol{q}\|^{1-\frac{2}{\mu}}\right),$$

and therefore that

$$\begin{aligned}\dot{V} &\leq -\alpha_1 V^{1+\frac{1}{\mu}} - \alpha_2 V^{1-\frac{1}{\mu}} + a\Upsilon\|\boldsymbol{q}\|^{1+\frac{2}{\mu}} + 2^{\frac{2}{\mu}}b\Upsilon\|\boldsymbol{q}\|^{1-\frac{2}{\mu}}, \\ &\leq -\alpha_1 V^{1+\frac{1}{\mu}} - \alpha_2 V^{1-\frac{1}{\mu}} + \beta_1 V^{\frac{1}{2}+\frac{1}{\mu}} + \beta_2 V^{\frac{1}{2}-\frac{1}{\mu}},\end{aligned}$$

where $\beta_1 = a\Upsilon k_V^{1+\frac{2}{\mu}}$ and $\beta_2 = 2^{\frac{2}{\mu}}b\Upsilon k_V^{1-\frac{2}{\mu}}$, and which, for all $V \geq 1$, obeys

$$\dot{V} \leq -\alpha_1 V^{1+\frac{1}{\mu}} - \alpha_2 V^{1-\frac{1}{\mu}} + \alpha_3 V, \tag{4.22}$$

where $\alpha_3 = \beta_1 + \beta_2$. Now, observe that $\frac{1}{2}\lambda_{max}^{-1}(\boldsymbol{\Gamma})\|\tilde{\boldsymbol{\theta}}\|^2 \leq V \leq \frac{1}{2}\lambda_{min}^{-1}(\boldsymbol{\Gamma})\|\tilde{\boldsymbol{\theta}}\|^2$, and $\underline{\sigma}^2(\boldsymbol{M})\|\tilde{\boldsymbol{\theta}}\|^2 \leq \|\boldsymbol{q}\|^2 \leq \sigma_{max}^2(\boldsymbol{M})\|\tilde{\boldsymbol{\theta}}\|^2$, and thus

$$V_{min}(\tilde{\boldsymbol{\theta}}_R) = \frac{1}{2}g_1\|\boldsymbol{q}\|^2 \leq V(\tilde{\boldsymbol{\theta}}_R) \leq \frac{1}{2}g_2\|\boldsymbol{q}\|^2 = V_{max}(\tilde{\boldsymbol{\theta}}_R),$$

where $g_1 = (\lambda_{max}(\boldsymbol{\Gamma})\sigma_{max}^2(\boldsymbol{M}))^{-1}$ and $g_2 = (\lambda_{min}(\boldsymbol{\Gamma})\underline{\sigma}^2(\boldsymbol{M}))^{-1}$. Then, since (4.22) holds for all $V \geq 1$ and $\dot{V} < 0$ for all $\|\boldsymbol{q}\| > 2\Upsilon$, it follows that $\dot{V} < 0$ for all $V > 1$ if $V_{max}(\tilde{\boldsymbol{\theta}}_R) \leq 1$ when $\|\boldsymbol{q}\| = 2\Upsilon$. To satisfy this condition, it must hold that $\lambda_{min}(\boldsymbol{\Gamma}) \geq 2(\frac{\Upsilon}{\underline{\sigma}(\boldsymbol{M})})^2$.

It is now established that for all $\|\boldsymbol{q}\| > 2\Upsilon$, both $\dot{V} < 0$ and (4.22) hold. Thus, it follows from using Lemma 4.1 in combination with [215, Theorem 1] that for all $\tilde{\boldsymbol{\theta}}_R(0) \in D_0$, the trajectories of (3.39) satisfy $\tilde{\boldsymbol{\theta}}_R(t) \in D_0$ for all $t \geq 0$, and reach the set D within a fixed time T, where the terms $\alpha_1, \alpha_2, \alpha_3$ have been rearranged to rewrite the conditions $r < 1, r \geq 1$ from [215, Theorem 1] as $\Upsilon < Y, \Upsilon \geq Y$, where Y is given by (4.21). This completes the proof. □

4.2 Koopman-based Fixed-Time System Identification for Safe Control Design

In this section, an adaptation law of the form (3.35) is proposed for learning an additive, bounded, nonlinear disturbance to class of nonlinear, control-affine dynamical systems. The underlying machinery for using linear parameter adaptation techniques to learn a generic, nonlinear disturbance is a branch of mathematics known as Koopman operator theory, the preliminaries of which are now reviewed.

4.2.1 Koopman Operator Theory

Consider a nonlinear, autonomous system of the form

$$\dot{\boldsymbol{x}} = F(\boldsymbol{x}), \quad \boldsymbol{x}(0) = \boldsymbol{x}_0, \tag{4.23}$$

where $F : \mathbb{R}^n \to \mathbb{R}^n$ is continuous such that (4.23) admits a unique solution for all $\boldsymbol{x}_0 \in \mathbb{R}^n$, the value of which at time t is denoted $\boldsymbol{\varphi}_t(\boldsymbol{x}_0)$, and where $F(0) = 0$.

Koopman operator theory dictates that a nonlinear system of the form (4.23) has an analogous and notably linear representation in an infinite-dimensional Hilbert space $\mathcal{Q}$ consisting of continuous, real-valued functions $q : \mathbb{R}^n \to \mathbb{R}$ referred to as *observables*. The continuous-time Koopman dynamical system analogous to (4.23) is then described by

$$\dot{q} = \mathcal{L}q, \quad q \in \mathcal{Q}, \tag{4.24}$$

where $\mathcal{L}$ denotes the infinitesimal generator of the linear semigroup of Koopman operators $\mathcal{U}^t : \mathcal{Q} \to \mathcal{Q}$, i.e.

$$\mathcal{L}q = \lim_{t \to 0} \frac{\mathcal{U}^t q - q}{t} = F \cdot \nabla q.$$

For tractability, however, many works (e.g. [119, 123], among others) derive matrix representations $\boldsymbol{U} \in \mathbb{R}^{N \times N}$ and $\boldsymbol{L} \in \mathbb{R}^{N \times N}$ of the respective finite-rank operators $\mathcal{U}_N^t = \Pi_N \mathcal{U}^t|_{\mathcal{Q}_N}$ and $\mathcal{L}_N = \Pi_N \mathcal{L}|_{\mathcal{Q}_N}$, where $\Pi_N : \mathcal{Q} \to \mathcal{Q}_N$ is a projection operator onto the subspace $\mathcal{Q}_N \subset \mathcal{Q}$ (spanned by $N > n$ linearly independent basis functions $\{\psi_i : \mathbb{R}^n \to \mathbb{R}\}_{i=1}^N$) and $\mathcal{O}|_{\mathcal{Q}_N}$ denotes the restriction of the operator $\mathcal{O}$ to $\mathcal{Q}_N$. For additional details on the technical details of Koopman operator theory, see [131]. In practice $\boldsymbol{U}$ and $\boldsymbol{L}$ are taken to be the respective solutions to

$$\boldsymbol{\psi}^T(\boldsymbol{x})\boldsymbol{U} = (\boldsymbol{\psi}(\boldsymbol{\varphi}_t(\boldsymbol{x})))^T, \tag{4.25}$$

$$\boldsymbol{L}^T\boldsymbol{\psi}(\boldsymbol{x}) = \frac{\partial \boldsymbol{\psi}(\boldsymbol{x})}{\partial \boldsymbol{x}} F(\boldsymbol{x}), \tag{4.26}$$

where $\boldsymbol{\psi}(\boldsymbol{x}) = [\psi_1(\boldsymbol{x}) \dots \psi_N(\boldsymbol{x})]^T \in \mathbb{R}^N$ and $\frac{\partial \boldsymbol{\psi}(\boldsymbol{x})}{\partial \boldsymbol{x}} \in \mathbb{R}^{N \times n}$.

If $\boldsymbol{L}$ can be identified directly (as in e.g. [122]), the vector field F may be reconstructed by solving (4.26) for $F(\boldsymbol{x})$. When this is not possible, identification of $\boldsymbol{U}$ may be used to reconstruct F after computing $\boldsymbol{L}$ via

$$\boldsymbol{L} = \frac{1}{T_s} \log \boldsymbol{U}, \tag{4.27}$$

in the case of sampled data, where $\log$ denotes the principal matrix logarithm and $T_s > 0$ is the sampling interval. Observe that both (4.25) and (4.26) describe linear systems of equations of the form $\boldsymbol{a}^T \boldsymbol{X} = \boldsymbol{b}$, and thus $\boldsymbol{X}$ (in this case $\boldsymbol{U}$ or $\boldsymbol{L}$) can be identified using linear identification techniques such as the parameter identification law (3.35).

4.2.2 Problem Statement

In the remainder of this section, consider the following class of perturbed nonlinear, control-affine systems

$$\dot{\boldsymbol{x}} = f(\boldsymbol{x}(t)) + g(\boldsymbol{x}(t))\boldsymbol{u}(t) + d(\boldsymbol{x}(t)), \quad \boldsymbol{x}(0) = \boldsymbol{x}_0, \tag{4.28}$$

where $\boldsymbol{x} \in \mathbb{R}^n$ and $\boldsymbol{u} \in \mathcal{U} \subseteq \mathbb{R}^m$ denote the state and control input vectors, the drift vector field $f : \mathbb{R}^n \to \mathbb{R}^n$ and control matrix field $g : \mathbb{R}^n \to \mathbb{R}^{n \times m}$ are known and continuous, and $d : \mathbb{R}^n \to \mathbb{R}^n$ is an unknown disturbance known to be continuous and to obey $\|d(\boldsymbol{x})\|_\infty \leq C < \infty$ for all $\boldsymbol{x} \in \mathbb{R}^n$. Consider also for completeness the following set of safe states,

$$\mathcal{S} = \{\boldsymbol{x} \in \mathbb{R}^n \mid h(\boldsymbol{x}) \geq 0\}, \tag{4.29a}$$

$$\partial\mathcal{S} = \{\boldsymbol{x} \in \mathbb{R}^n \mid h(\boldsymbol{x}) = 0\}, \tag{4.29b}$$

$$\mathrm{Int}(\mathcal{S}) = \{\boldsymbol{x} \in \mathbb{R}^n \mid h(\boldsymbol{x}) > 0\}, \tag{4.29c}$$

for a continuously differentiable function $h : \mathbb{R}^n \to \mathbb{R}$. Having established already in this dissertation that the set $\mathcal{S}$ is forward invariant (and thus the trajectories of (4.28) safe) if the function h is a CBF, consider now that for the system (4.28) the CBF condition is

$$\sup_{\boldsymbol{u} \in \mathcal{U}} \left[L_f h(\boldsymbol{x}) + L_g h(\boldsymbol{x}) \boldsymbol{u} + L_d h(\boldsymbol{x}) \right] \geq -\alpha(h(\boldsymbol{x})),$$

where, without identification of $d(\boldsymbol{x})$, the precise value of $L_d h(\boldsymbol{x})$ is unknown. By $\|d(\boldsymbol{x})\|_\infty \leq C$, however, it is known that

$$-b_c \leq L_d h(\boldsymbol{x}) \leq b_c,$$

where $b_c = C \left| \frac{\partial h(\boldsymbol{x})}{\partial \boldsymbol{x}} \right| \mathbf{1}_{n \times 1}$. Under such circumstances, a Robust Control Barrier Function (R-CBF) [216] may be used for safe control design.

Definition 4.1 (**Robust Control Barrier Function**). *Given a set $\mathcal{S} \subseteq \mathcal{X} \subset \mathbb{R}^n$ defined by* (4.29) *for a continuously differentiable function $h : \mathbb{R}^n \to \mathbb{R}$, the function h is a **robust control barrier function** for the system* (4.28) *defined on the set $\mathcal{X}$ if there exists a Lipschitz continuous class $\mathcal{K}_\infty$ function $\alpha : \mathbb{R} \to \mathbb{R}$ such that*

$$\sup_{\boldsymbol{u} \in \mathcal{U}} \left[L_f h(\boldsymbol{x}) + L_g h(\boldsymbol{x}) \boldsymbol{u} - b_c \right] \geq -\alpha(h(\boldsymbol{x})), \tag{4.30}$$

for all $\boldsymbol{x} \in \mathcal{X}$.

Designing a controller to protect against the worst possible disturbance in perpetuity, however, may lead to prohibitively conservative behavior, especially if C is large. This may be mitigated by using an estimate of the unknown disturbance $\hat{d}(\boldsymbol{x})$. Thus, define the vector field estimation error $\tilde{d}(\boldsymbol{x})$ as

$$\tilde{d}(\boldsymbol{x}) \triangleq d(\boldsymbol{x}) - \hat{d}(\boldsymbol{x}).$$

Now, suppose that an estimate of the Koopman generator matrix $\hat{\boldsymbol{L}}$ for the system (4.28) is available, and let the estimated unknown vector field $\hat{d}(\boldsymbol{x})$ then via (4.26) be the solution to

$$\hat{\boldsymbol{L}}^T \boldsymbol{\psi}(\boldsymbol{x}) = \frac{\partial \boldsymbol{\psi}(\boldsymbol{x})}{\partial \boldsymbol{x}} \big(f(\boldsymbol{x}) + g(\boldsymbol{x}) \boldsymbol{u} + \hat{d}(\boldsymbol{x}) \big).$$

Note that even an arbitrary estimate is sufficient, i.e., $\hat{\boldsymbol{L}} = \boldsymbol{0}_{N \times N}$. It is assumed that $\frac{\partial \boldsymbol{\psi}(\boldsymbol{x})}{\partial \boldsymbol{x}}$ is full column rank, which may be satisfied by design (e.g. sinusoidal basis functions), and thus $\hat{d}(\boldsymbol{x}) \to d(\boldsymbol{x})$ as $\hat{\boldsymbol{L}} \to \boldsymbol{L}$ (which can also be satisfied if $\hat{\boldsymbol{U}} \to \boldsymbol{U}$). Define the vectorized Koopman matrix and generator ($\boldsymbol{\mu}^*$ and $\boldsymbol{\lambda}^*$), and their estimates ($\hat{\boldsymbol{\mu}}$ and $\hat{\boldsymbol{\lambda}}$), as

$$\boldsymbol{\mu}^* \triangleq [\mathrm{col}_1^T(\boldsymbol{U}) \dots \mathrm{col}_N^T(\boldsymbol{U})]^T, \tag{4.31}$$

$$\boldsymbol{\lambda}^* \triangleq [\mathrm{col}_1^T(\boldsymbol{L}) \dots \mathrm{col}_N^T(\boldsymbol{L})]^T, \tag{4.32}$$

$$\hat{\boldsymbol{\mu}} \triangleq [\mathrm{col}_1^T(\hat{\boldsymbol{U}}) \dots \mathrm{col}_N^T(\hat{\boldsymbol{U}})]^T, \tag{4.33}$$

$$\hat{\boldsymbol{\lambda}} \triangleq [\mathrm{col}_1^T(\hat{\boldsymbol{L}}) \dots \mathrm{col}_N^T(\hat{\boldsymbol{L}})]^T, \tag{4.34}$$

and observe that for the system (4.28) the relations (4.25) and (4.26) are equivalent to

$$\boldsymbol{\Psi}(\boldsymbol{x}) \boldsymbol{\mu}^* = (\boldsymbol{\psi}(\boldsymbol{\varphi}_t(\boldsymbol{x})))^T, \tag{4.35}$$

and

$$\boldsymbol{\Psi}(\boldsymbol{x}) \boldsymbol{\lambda}^* = \frac{\partial \boldsymbol{\psi}(\boldsymbol{x})}{\partial \boldsymbol{x}} \big(f(\boldsymbol{x}) + g(\boldsymbol{x}) \boldsymbol{u} + d(\boldsymbol{x}) \big), \tag{4.36}$$

respectively, where

$$\boldsymbol{\Psi}(\boldsymbol{x}) \triangleq \begin{bmatrix} \boldsymbol{\psi}^T(\boldsymbol{x}) & 0 & \dots & 0 \\ 0 & \boldsymbol{\psi}^T(\boldsymbol{x}) & \dots & 0 \\ \vdots & & \ddots & \vdots \\ 0 & \dots & 0 & \boldsymbol{\psi}^T(\boldsymbol{x}) \end{bmatrix} \in \mathbb{R}^{N \times N^2}. \tag{4.37}$$

Let the Koopman matrix and Koopman generator estimation errors respectively be denoted

$$\tilde{\boldsymbol{\mu}} = \boldsymbol{\mu}^* - \hat{\boldsymbol{\mu}},$$
$$\tilde{\boldsymbol{\lambda}} = \boldsymbol{\lambda}^* - \hat{\boldsymbol{\lambda}},$$

and observe that $\boldsymbol{\Psi}(\boldsymbol{x})\hat{\boldsymbol{\lambda}} = \boldsymbol{\Psi}(\boldsymbol{x})\boldsymbol{\lambda}^*$ for all $\tilde{\boldsymbol{\lambda}} \in \mathcal{N}(\boldsymbol{\Psi}(\boldsymbol{x}))$.

Problem 4.1. *Consider a dynamical system of the form* (4.28)*. Design adaptation and control laws,* $\dot{\hat{\boldsymbol{\lambda}}} = \eta(\boldsymbol{x}, \boldsymbol{u}, \hat{\boldsymbol{\lambda}})$ *and* $\boldsymbol{u} = \kappa(\boldsymbol{x}, \hat{\boldsymbol{\lambda}})$ *respectively, such that*

1. *the Koopman generator error vector,* $\tilde{\boldsymbol{\lambda}}$*, is rendered fixed-time stable to the nullspace of* $\boldsymbol{\Psi}(\boldsymbol{x})$*, i.e.* $\tilde{\boldsymbol{\lambda}}(t) \to \mathcal{N}(\boldsymbol{\Psi}(\boldsymbol{x}))$ *as* $t \to T$ *and* $\tilde{\boldsymbol{\lambda}}(t) \in \mathcal{N}(\boldsymbol{\Psi}(\boldsymbol{x}))$ *for all* $t \geq T$*, independent of* $\hat{\boldsymbol{\lambda}}(0)$*, and*
2. *the system trajectories remain safe for all time, i.e.* $\boldsymbol{x}(t) \in \mathcal{S}$*,* $\forall t \geq 0$*.*

4.2.3 Fixed-Time System Identification

This section introduces the proposed adaptation law $\dot{\hat{\boldsymbol{\lambda}}} = \eta(\boldsymbol{x}, \boldsymbol{u}, \hat{\boldsymbol{\lambda}})$ for the fixed-time identification of the Koopman generator vector $\boldsymbol{\lambda}$, which allows for the identification of the unknown vector field $d(\boldsymbol{x})$ in (4.28) within a fixed-time. Before introducing the main result, the following assumptions are required.

Assumption 4.2. *The projection of the infinite-dimensional Koopman operator* $\mathcal{U}^t$ *onto the finite-rank subspace* $\mathcal{Q}_N$ *exactly describes the evolution of observables* $q \in \mathcal{Q}$*, i.e.* $\mathcal{U}_N^t q = (\Pi_N \mathcal{U}^t)q$*, for all* $q \in \mathcal{Q}$*.*

Assumption 4.3. *There exist scalars* $s > 0$*,* $T > 0$ *such that* $\sigma_N(\boldsymbol{\Psi}(\boldsymbol{x}(t))) \geq s$ *for all* $0 \leq t \leq T$*, where* $\boldsymbol{\Psi}(\boldsymbol{x}(t))$ *is given by* (4.37)*.*

The satisfaction of Assumption 4.2 depends on the set of basis functions $\boldsymbol{\psi}$ and its cardinality N, and while generally this is an open problem, recent work has studied the existence of Koopman invariant subspaces (see e.g. [217]), i.e. subspaces $\mathcal{Q}_N \subset \mathcal{Q}$ over which Assumption 4.2 holds.

The satisfaction of Assumption 4.3, which is needed for the proposed adaptation law and bounds the minimum non-zero singular value of $\boldsymbol{\Psi}$, evidently also depends on the choice of basis functions. Note, however, that $\boldsymbol{\Psi}(\boldsymbol{x}(t))$ is guaranteed to be full row-rank (which implies that $\sigma_N(\boldsymbol{\Psi}(\boldsymbol{x}(t))) > 0$) provided that $\exists i \in [N]$ such that $\psi_i(\boldsymbol{x}(t)) \neq 0$. This can be guaranteed with an appropriate choice of bases, e.g. $\psi_1(\boldsymbol{x}(t)) = 1$.

The following is the main result of this section.

Theorem 4.2. *Suppose that Assumptions 4.2 and 4.3 hold, where*

$$T = \frac{w\pi}{4s\lambda_{max}(\boldsymbol{\Gamma})\sqrt{ab}}, \tag{4.38}$$

with $a, b > 0$, $w > 2$, and $\boldsymbol{\Gamma} \in \mathbb{R}^{N^2 \times N^2}$ a constant, positive-definite gain matrix. Then, under the ensuing adaptation law

$$\dot{\hat{\boldsymbol{\lambda}}} = \boldsymbol{\Gamma}\boldsymbol{\Psi}^T(\boldsymbol{x})\boldsymbol{\nu}(\boldsymbol{x}, \hat{\boldsymbol{\lambda}}) \left(a\|\boldsymbol{\nu}(\boldsymbol{x}, \hat{\boldsymbol{\lambda}})\|^{2/w} + \frac{b}{\|\boldsymbol{\nu}(\boldsymbol{x}, \hat{\boldsymbol{\lambda}})\|^{2/w}} \right), \tag{4.39}$$

the Koopman generator error vector $\tilde{\boldsymbol{\lambda}}$ is rendered FxTS to the nullspace of $\boldsymbol{\Psi}(\boldsymbol{x})$, i.e. $\tilde{\boldsymbol{\lambda}}(t) \to \mathcal{N}(\boldsymbol{\Psi}(\boldsymbol{x}(t)))$ as $t \to T$ and $\tilde{\boldsymbol{\lambda}}(t) \in \mathcal{N}(\boldsymbol{\Psi}(\boldsymbol{x}))$ for all $t \geq T$, independent of $\hat{\boldsymbol{\lambda}}(0)$, where

$$\boldsymbol{\nu}(\boldsymbol{x}, \hat{\boldsymbol{\lambda}}) = \frac{\partial \boldsymbol{\psi}(\boldsymbol{x})}{\partial \boldsymbol{x}}\dot{\boldsymbol{x}} - \boldsymbol{\Psi}(\boldsymbol{x})\hat{\boldsymbol{\lambda}}. \tag{4.40}$$

Proof. It is first shown that there exists a time-invariant Koopman generator vector $\boldsymbol{\lambda}(t) = \boldsymbol{\lambda}^*$, $\forall t \geq 0$, and then proved that under (4.39) the associated Koopman generator error vector $\tilde{\boldsymbol{\lambda}}$ is rendered FxTS to $\mathcal{N}(\boldsymbol{\Psi}(\boldsymbol{x}))$.

First, under Assumption 4.2 it follows that there exists a finite-rank operator $\mathcal{L}_N : \mathcal{Q}_N \to \mathcal{Q}_N$ such that the nonlinear dynamics of (4.28) may be represented by the following linear system in the space of observables:

$$\dot{q} = \mathcal{L}_N q, \quad q \in \mathcal{Q}.$$

Then, there exists a finite-dimensional matrix representation $\boldsymbol{L} \in \mathbb{R}^{N \times N}$ in a basis $\{\psi_i : \mathcal{X} \to \mathbb{R}\}_{i=1}^N$ corresponding to the operator $\mathcal{L}_N$ such that the relation (4.26) holds over the trajectories of (4.28). Thus, the Koopman generator matrix $\boldsymbol{L}$ admits the (time-invariant) Koopman generator vector $\boldsymbol{\lambda}^*$ defined by (4.32).

Next, observe that (4.36) over the trajectories of (4.28) may be modified to obtain

$$\begin{aligned}\boldsymbol{\Psi}(\boldsymbol{x})\boldsymbol{\lambda}^* - \boldsymbol{\Psi}(\boldsymbol{x})\hat{\boldsymbol{\lambda}} &= \frac{\partial \boldsymbol{\psi}(\boldsymbol{x})}{\partial \boldsymbol{x}}\dot{\boldsymbol{x}} - \boldsymbol{\Psi}(\boldsymbol{x})\hat{\boldsymbol{\lambda}},\\ \boldsymbol{\Psi}(\boldsymbol{x})\tilde{\boldsymbol{\lambda}} &= \boldsymbol{\nu}(\boldsymbol{x}, \hat{\boldsymbol{\lambda}}),\end{aligned}$$

where $\boldsymbol{\nu}(\boldsymbol{x}, \hat{\boldsymbol{\lambda}})$ is given by (4.40). Thus, the premises of Theorem 3.4 are satisfied with $\boldsymbol{M} = \boldsymbol{\Psi}$ and $\boldsymbol{v} = \boldsymbol{\nu}$ and the adaptation law (4.39) takes the form of (3.35). Then, with Assumption 4.3 it follows directly from Theorem 3.35 that $\tilde{\boldsymbol{\lambda}}$ is rendered FxTS to $\mathcal{N}(\boldsymbol{\Psi}(\boldsymbol{x}))$ with settling time given by (4.38). This completes the proof. □

While the above result requires perfect measurements, it is predicated on Theorem 3.35, which was shown to be robust to bounded perturbations in Section 4.1. In what follows, it is shown how the parameter adaptation law (4.39) results in learning the exact disturbance $d(\boldsymbol{x})$ to the system dynamics (4.28) within fixed-time.

Corollary 4.1. *Consider the system* (4.28)*. Suppose that the premises of Theorem 4.2 hold, and that the estimated Koopman vector* $\hat{\boldsymbol{\lambda}}$ *is adapted according to* (4.39)*. If the estimated disturbance* $\hat{d}(\boldsymbol{x})$ *is taken to be*

$$\hat{d}(\boldsymbol{x}(t)) = \frac{\partial \boldsymbol{\psi}(\boldsymbol{x}(t))}{\partial \boldsymbol{x}}^{\dagger} \boldsymbol{\Psi}(\boldsymbol{x}(t))\hat{\boldsymbol{\lambda}}(t) - a(\boldsymbol{x}(t), \boldsymbol{u}(t)), \tag{4.41}$$

where $a(\boldsymbol{x}(t), \boldsymbol{u}(t)) = f(\boldsymbol{x}(t)) + g(\boldsymbol{x}(t))\boldsymbol{u}(t)$*, then, the vector field estimation error* $\tilde{d}(\boldsymbol{x}(t))$ *is rendered FxTS to the origin and the estimated disturbance* $\hat{d}(\boldsymbol{x}(t))$ *converges to the true disturbance* $d(\boldsymbol{x}(t))$ *within a fixed-time* T *given by* (4.38)*, i.e.* $\tilde{d}(\boldsymbol{x}(t)) \to 0$ *and* $\hat{d}(\boldsymbol{x}(t)) \to d(\boldsymbol{x}(t))$ *as* $t \to T$ *independent of* $\hat{d}(\boldsymbol{x}(0))$*.*

Proof. First, observe from (4.36) that the disturbance $d(\boldsymbol{x}(t))$ is the solution to

$$\frac{\partial \boldsymbol{\psi}(\boldsymbol{x}(t))}{\partial \boldsymbol{x}} d(\boldsymbol{x}(t)) = \boldsymbol{\Psi}(\boldsymbol{x}(t))\boldsymbol{\lambda}^* - \frac{\partial \boldsymbol{\psi}(\boldsymbol{x}(t))}{\partial \boldsymbol{x}} a(\boldsymbol{x}(t), \boldsymbol{u}(t)). \tag{4.42}$$

Next, it follows from Theorem 4.2 that under (4.39) $\hat{\boldsymbol{\lambda}}(t) \to \boldsymbol{\lambda}^*$ as $t \to T$. Then, $\boldsymbol{\Psi}(\boldsymbol{x}(t))\hat{\boldsymbol{\lambda}}(t) \to \boldsymbol{\Psi}(\boldsymbol{x}(t))\boldsymbol{\lambda}^*$ and thus $\frac{\partial \boldsymbol{\psi}(\boldsymbol{x}(t))}{\partial \boldsymbol{x}} \hat{d}(\boldsymbol{x}(t)) \to \frac{\partial \boldsymbol{\psi}(\boldsymbol{x}(t))}{\partial \boldsymbol{x}} d(\boldsymbol{x}(t))$ as $t \to T$ when $\hat{d}(\boldsymbol{x}(t))$ is taken to be the solution to (4.42). Finally, with $\frac{\partial \boldsymbol{\psi}(\boldsymbol{x}(t))}{\partial \boldsymbol{x}}$ full column rank, the use of its pseudoinverse $\frac{\partial \boldsymbol{\psi}(\boldsymbol{x}(t))}{\partial \boldsymbol{x}}^{\dagger}$ recovers (4.41) and thus it is true that $\hat{d}(\boldsymbol{x}(t)) \to d(\boldsymbol{x}(t))$ as $t \to T$. □

For the purpose of control design it is important to know how the estimation error signals behave during the transient period $t \leq T$ before the unknown vector field $d(\boldsymbol{x})$ has been learned. In contrast to least-squares and related regression based approaches to learning the Koopman matrix

$\boldsymbol{U}$ and/or generator matrix $\boldsymbol{L}$, the FxTS parameter adaptation law allows for the derivation of explicit estimation error bounds as a function of time.

Corollary 4.2. *Suppose that the premises of Corollary 4.1 hold. If, in addition, the initial estimated Koopman generator vector is set to zero, i.e.* $\hat{\boldsymbol{\lambda}}(0) = \mathbf{0}_{N^2\times 1}$*, and* $\boldsymbol{\Gamma}$ *in* (4.39) *is constant, positive-definite, and also diagonal, then* $\forall t \in [0, T]$*, where* T *is given by* (4.38)*, the following expression constitutes a monotonically decreasing upper bound on* $\|\tilde{d}(\boldsymbol{x}(t))\|_\infty$*:*

$$\|\tilde{d}(\boldsymbol{x}(t))\|_\infty \leq \Lambda \sigma_{max}(\boldsymbol{W}(t)) \tan^{\frac{w}{2}}(A(t)) \triangleq \xi(t), \tag{4.43}$$

where

$$\Lambda = \sqrt{2\lambda_{max}(\boldsymbol{\Gamma})} \left(\frac{a}{b}\right)^{w/4}, \tag{4.44}$$

and

$$\boldsymbol{W}(t) = \frac{\partial \boldsymbol{\psi}(\boldsymbol{x}(t))}{\partial \boldsymbol{x}}^{\dagger} \boldsymbol{\Psi}(\boldsymbol{x}), \tag{4.45}$$

$$A(t) = \max\left\{\Xi - \frac{\sqrt{ab}}{w} t, 0\right\}, \tag{4.46}$$

$$\Xi = \tan^{-1}\left(\sqrt{\frac{b}{a}} \left(\frac{1}{2}\boldsymbol{l}^T \Gamma^{-1} \boldsymbol{l}\right)^{\frac{1}{w}}\right), \tag{4.47}$$

where $\boldsymbol{l} = \frac{2C}{\sigma_{min}(\boldsymbol{W}(0))} \cdot \mathbf{1}_{N^2\times 1}$*, and* $\|\tilde{d}(\boldsymbol{x}(t))\|_\infty = 0$*,* $\forall t > T$*.*

Proof. Follows from Corollary 3.2, though provided here for completeness.

Using (4.41) and (4.45) the disturbance vector field error may be expressed as

$$\begin{aligned}\tilde{d}(\boldsymbol{x}(t)) &= d(\boldsymbol{x}(t)) - \hat{d}(\boldsymbol{x}(t)),\\ &= \boldsymbol{W}(t)\tilde{\boldsymbol{\lambda}}(t),\end{aligned}$$

and thus $\|d(\boldsymbol{x}(t))\|_\infty = \|\boldsymbol{W}(t)\tilde{\boldsymbol{\lambda}}(t)\|_\infty \leq \sigma_{max}(\boldsymbol{W}(t))\|\tilde{\boldsymbol{\lambda}}(t)\|_\infty$. Then, from Corollary 3.2, it follows that $\|\tilde{\boldsymbol{\lambda}}(t)\|_\infty \leq \Lambda \tan^{\frac{w}{2}}(A(t))$ for all $t \leq T$, where Λ, $A(t)$, and T are given by (4.44), (4.46), (4.38) respectively, and $\|\tilde{\boldsymbol{\lambda}}(t)\|_\infty = 0$ for all $t > T$.

Then, to obtain Ξ in (4.47), observe that with $\hat{\boldsymbol{\lambda}}(0) = \mathbf{0}_{N^2\times 1}$ and the assumption that $\|d(\boldsymbol{x})\|_\infty \leq C$, $\forall \boldsymbol{x} \in \mathcal{X}$, it follows that at $t = 0$

$$\sigma_{min}(\boldsymbol{W})\|\tilde{\boldsymbol{\lambda}}\|_\infty \leq \|\boldsymbol{W}\tilde{\boldsymbol{\lambda}}\|_\infty = \|\tilde{d}(\boldsymbol{x})\|_\infty \leq 2C,$$

from which we obtain that

$$\|\tilde{\boldsymbol{\lambda}}(0)\|_\infty \leq \frac{2C}{\sigma_{min}\left(\boldsymbol{W}(0)\right)}.$$

Thus we obtain $\boldsymbol{l} = \frac{2C}{\sigma_{min}(\boldsymbol{W}(0))} \cdot \mathbf{1}_{N^2\times 1}$, and this completes the proof. □

Knowledge of the upper bound on the disturbance estimation error bound (4.43) permits the use of the robust, adaptive model-based control techniques developed in Chapter 3.

4.3 Robust, Adaptive Control Design

In this section, two approaches are proposed for synthesizing the Koopman-based parameter adaptation law with a CBF-based control law for safe control under model uncertainty.

4.3.1 Robust-CBF Approach

In the first approach, R-CBF principles are applied to design a safe controller $\boldsymbol{u} = \kappa(\boldsymbol{x}, \hat{\boldsymbol{\lambda}})$ when using the Koopman-based adaptation scheme (4.39).

Theorem 4.3. *Consider a system of the form* (4.28)*, a safe set $\mathcal{S}$ defined by* (4.29) *for a continuously differentiable function $h : \mathbb{R}^n \to \mathbb{R}$, and suppose that the premises of Corollary 4.2 hold. Then, any control input $\boldsymbol{u}$ satisfying*

$$\sup_{\boldsymbol{u}\in\mathcal{U}} \left[L_f h(\boldsymbol{x}) + L_g h(\boldsymbol{x})\boldsymbol{u} + L_{\hat{d}} h(\boldsymbol{x}) - b_c(t)\right] \geq -\alpha(h(\boldsymbol{x})) \tag{4.48}$$

renders the trajectories of (4.28) *safe, where*

$$b_c(t) = \left|\frac{\partial h}{\partial \boldsymbol{x}}\right| \xi(t) \cdot \mathbf{1}_{n\times 1}, \tag{4.49}$$

and $\xi(t)$ is given by (4.43)*.*

Proof. Observe that over the trajectories of (4.28)

$$\begin{aligned}
\dot{h} &= L_f h(\boldsymbol{x}) + L_g h(\boldsymbol{x})\boldsymbol{u} + L_d h(\boldsymbol{x}) \\
&= L_f h(\boldsymbol{x}) + L_g h(\boldsymbol{x})\boldsymbol{u} + \frac{\partial h}{\partial \boldsymbol{x}}\hat{d}(\boldsymbol{x}) + \frac{\partial h}{\partial \boldsymbol{x}}\tilde{d}(\boldsymbol{x}) \\
&\geq L_f h(\boldsymbol{x}) + L_g h(\boldsymbol{x})\boldsymbol{u} + \frac{\partial h}{\partial \boldsymbol{x}}\hat{d}(\boldsymbol{x}) - \left|\frac{\partial h}{\partial \boldsymbol{x}}\right| \xi(t) \cdot \mathbf{1}_{n\times 1}.
\end{aligned}$$

By Corollary 4.2 it follows that $\|\tilde{d}(\boldsymbol{x}(t))\|_\infty \leq \xi(t)$ for all $t \geq 0$. Therefore, $\dot{h} \geq -\alpha(h(\boldsymbol{x}))$ whenever (4.48) holds, and thus $\mathcal{S}$ is rendered forward invariant by any control input satisfying (4.48). □

It is worth noting that as the estimated disturbance $\hat{d}(\boldsymbol{x})$ converges to the true disturbance $d(\boldsymbol{x})$ the robustness term $b_c(t)$ will go to zero. So while initially the condition (4.48) may demand large control inputs to guarantee safety in the face of a the unknown disturbance, as $t \to T$ the term $b_c(t) \to 0$ and the standard CBF condition is recovered.

4.3.2 Robust-Adaptive CBF Approach

This approach is analogous to the robust, adaptive CBF approach proposed in (3.51), and is provided here for completeness. First, define the following robust-adaptive safe set

$$\mathcal{S}_r = \{\boldsymbol{x} \in \mathbb{R}^n : h_r(\boldsymbol{x}, \boldsymbol{\xi}) \geq 0\} \tag{4.50}$$

for the continuously differentiable function

$$h_r(\boldsymbol{x}, \boldsymbol{\xi}) = h(\boldsymbol{x}) - \frac{1}{2}\boldsymbol{\xi}^T \boldsymbol{\Omega}^{-1} \boldsymbol{\xi},$$

for $\boldsymbol{\xi}(t) = \xi(t) \cdot \mathbf{1}_{n\times 1}$ with $\xi(t)$ given by (4.43), and a constant, positive-definite matrix $\boldsymbol{\Omega} \in \mathbb{R}^{n\times n}$. The set $\mathcal{S}_r$ defined by (4.50) is a subset of the safe set $\mathcal{S}$ defined by (4.29), i.e. $\mathcal{S}_r \subseteq \mathcal{S}$. In the following, the robust-adaptive CBF condition that renders the trajectories of (4.28) safe is formalized.

Theorem 4.4. *Consider a system of the form* (4.28)*, a set $\mathcal{S}_r$ defined by* (4.50) *for a continuously differentiable function $h_r : \mathbb{R}^n \to \mathbb{R}$, and suppose that the premises of Corollary 4.2 hold. Then, any control input $\boldsymbol{u}$ satisfying*

$$\sup_{\boldsymbol{u}\in\mathcal{U}} \Big[L_f h_r(\boldsymbol{x}) + L_g h_r(\boldsymbol{x})\boldsymbol{u} - r\big(\hat{d}(\boldsymbol{x}), \xi\big) \Big] \geq -\alpha(h_r(\boldsymbol{x})) \tag{4.51}$$

renders the trajectories of (4.28) *safe, where*

$$r\big(\hat{d}(\boldsymbol{x}), \xi\big) = \mathrm{Tr}(\boldsymbol{\Omega}^{-1})\xi(t)\dot{\xi}(t) + b_c(t),$$

where $\xi(t)$ is given by (4.43)*, $b_c(t)$ is given by* (4.49)*, and*

$$\begin{aligned}\dot{\xi}(t) = &\Lambda\dot{\sigma}_{max}(\boldsymbol{W}(t))\tan^{\frac{w}{2}}(A(t)) \\ &- \frac{1}{2}\Lambda\sigma_{max}(\boldsymbol{W}(t))\sqrt{ab}\tan^{\frac{w}{2}-1}(A(t))\sec^2(A(t))\end{aligned} \tag{4.52}$$

Follows directly from Theorem 3.5 by replacing $\tilde{\boldsymbol{\theta}}$ with $\tilde{d}(\boldsymbol{x})$.

Remark 4.1. *The robust-adaptive CBF condition* (4.51) *requires the time-derivative of the maximum singular value of the matrix $\boldsymbol{W}(t)$ given by* (4.45)*, i.e. $\dot{\sigma}_{max}(\boldsymbol{W}(t))$. While this may not be available in closed-form, it may be approximated in practice using finite-difference methods.*

Since both the robust (4.48) and robust-adaptive (4.51) CBF conditions ensure safety of the trajectories of (4.28), either condition may be included as an affine constraint in a Quadratic Program (QP)-based control law (eg. [3]):

$$\boldsymbol{u}^* = \underset{\boldsymbol{u}\in\mathcal{U}}{\arg\min}\frac{1}{2}\|\boldsymbol{u}-\boldsymbol{u}^0\|^2 \tag{4.53a}$$

s.t.

$$\text{Either (4.48) or (4.51)}, \tag{4.53b}$$

the objective (4.53a) of which seeks to find a minimally deviating solution $\boldsymbol{u}^*$ from a nominal, potentially unsafe input $\boldsymbol{u}^0$ subject to the specified CBF constraint (4.53b).

4.4 Simulations

4.4.1 Quadrotor Trajectory Tracking: 12D Dynamics Model

In this section, an extension of the quadrotor case study undertaken in Chapter 3 is considered. Specifically, unknown wind gusts are assumed to perturb the system dynamics.

The 6 degree-of-freedom rigid-body dynamic model of the quadrotor as described in [207] is provided again here for completeness. Denote $\boldsymbol{\chi} = [x\ y\ z\ u\ v\ w\ \phi\ \theta\ \psi\ p\ q\ r]^\top$ as the state, where x, y, and z are the position coordinates (in m) with respect to an inertial frame, u, v, and w are the translational velocities (in m/s) with respect to the body-fixed frame, ϕ, θ, and ψ (in rad) are the roll, pitch, and yaw Euler angles defining a ZYX rotation from the inertial frame to the body-fixed frame, and p, q, and r are the roll, pitch, and yaw rates (in rad/s) defined with respect to the body-fixed frame.

The effect of aerodynamic drag on the center of mass of the quadrotor due to wind gusts appears

in the dynamics as an unknown, additive disturbance

$$\boldsymbol{d}_a(t,\boldsymbol{\chi}) = \left(\frac{\|\boldsymbol{v}_r^*\|}{M} \begin{bmatrix} v_{r,1}^* & 0 & 0 \\ 0 & v_{r,2}^* & 0 \\ 0 & 0 & v_{r,3}^* \end{bmatrix} - \Delta_a(\boldsymbol{\chi}) \right) \begin{bmatrix} C_x \\ C_y \\ C_z \end{bmatrix},$$

where $\boldsymbol{v}_r^* = \boldsymbol{R}(\boldsymbol{v}_w + \boldsymbol{v}_G) - \boldsymbol{v}_q$ is the relative-wind velocity vector considering both a constant, known wind velocity $\boldsymbol{v}_w$ and unknown gust velocity $\boldsymbol{v}_G$ generated using the model from [218], with principal components $v_{r,1}^*$, $v_{r,2}^*$, and $v_{r,3}^*$, $\boldsymbol{v}_q = [u\ v\ w]^T$ is the quadrotor velocity vector in the body-fixed frame, and $\boldsymbol{R}$ is the rotation matrix from the inertial to the body-fixed frame. M is the mass of the quadrotor (in kg), C_x, C_y, and C_z are the coefficients of drag in the principal body-fixed directions such that the unknown drag coefficient vector is $\boldsymbol{C}_d = [C_x\ C_y\ C_z]^\top$, and

$$\Delta_a(\boldsymbol{\chi}) = \frac{\|\boldsymbol{v}_{rc}\|}{M} \begin{bmatrix} v_{rc,1} & 0 & 0 \\ 0 & v_{rc,2} & 0 \\ 0 & 0 & v_{rc,3} \end{bmatrix},$$

where $\boldsymbol{v}_{rc} = \boldsymbol{R}\boldsymbol{v}_w - \boldsymbol{v}_q$. Thus, $\Delta_a(\boldsymbol{\chi})$ represents the effect on the dynamics by a constant wind. The quadrotor dynamical system is then described by:

$$\begin{aligned}
\begin{pmatrix} \dot{x} \\ \dot{y} \\ \dot{z} \end{pmatrix} &= \begin{pmatrix} c\theta c\psi & s\phi s\theta c\psi - c\phi s\psi & c\phi s\theta c\psi + s\phi s\psi \\ c\theta s\psi & s\phi s\theta s\psi + c\phi c\psi & c\phi s\theta s\psi - s\phi c\psi \\ s\theta & -s\phi c\theta & -c\phi c\theta \end{pmatrix} \begin{pmatrix} u \\ v \\ w \end{pmatrix} \\
\begin{pmatrix} \dot{u} \\ \dot{v} \\ \dot{w} \end{pmatrix} &= \begin{pmatrix} rv - qw \\ pw - ru \\ qu - pw \end{pmatrix} + \begin{pmatrix} -gs\theta \\ gc\theta s\phi \\ gc\theta c\phi \end{pmatrix} + \frac{1}{M} \begin{pmatrix} 0 \\ 0 \\ -F \end{pmatrix} + \Delta_a(\boldsymbol{\chi})\boldsymbol{C}_d + \boldsymbol{d}_a(t,\boldsymbol{\chi}) \\
\begin{pmatrix} \dot{\phi} \\ \dot{\theta} \\ \dot{\psi} \end{pmatrix} &= \begin{pmatrix} 1 & s\phi t\theta & c\phi t\theta \\ 0 & c\phi & -s\phi \\ 0 & \frac{s\phi}{c\theta} & \frac{c\phi}{c\theta} \end{pmatrix} \begin{pmatrix} p \\ q \\ r \end{pmatrix} \\
\begin{pmatrix} \dot{p} \\ \dot{q} \\ \dot{r} \end{pmatrix} &= \begin{pmatrix} \frac{J_y - J_z}{J_x} qr \\ \frac{J_z - J_x}{J_y} pr \\ \frac{J_x - J_y}{J_z} pq \end{pmatrix} + \begin{pmatrix} \frac{1}{J_x}\tau_\phi \\ \frac{1}{J_y}\tau_\theta \\ \frac{1}{J_z}\tau_\psi \end{pmatrix}
\end{aligned} \tag{4.54}$$

i.e., a system of the form (4.1) where g is the acceleration due to gravity (in m/sec^2), the functions $\sin$, $\cos$, and $\tan$ are denoted s, c, and t for brevity, M is the mass of the quadrotor (in kg), J_x, J_y, and J_z are the principal moments of inertia (in kg·m^2), F is the thrust of the rotors (in N), and τ_ϕ, τ_θ, and τ_ψ are rolling, pitching, and yawing torques (in N·m) respectively due to the rotors.

The quadrotor dynamical model (4.54) is simulated using the controller (3.62) and state predictor scheme (3.26) in the unknown wind field (denoted SP-WG). In the presence of an unknown disturbance $\boldsymbol{d}(t, \boldsymbol{\chi})$, it is not guaranteed that the estimates of the drag coefficients $\hat{\boldsymbol{C}}_d$ converge to the set Ω but rather to a neighborhood of this set as specified in Theorem 4.1. Values of $Y = 3.65$ for (4.21) and $\Upsilon = 0.69$ were computed from the wind gust model. Thus, $\Upsilon < Y$, $D_0 = \mathbb{R}^p$, and the fixed-time bound T is given by (4.17) plus the warm-up time $T_w = 0.1$ sec. In addition, the choice of $\lambda_{min}(\boldsymbol{\Gamma}) = 63.16$ satisfies the requirement that $\lambda_{min}(\boldsymbol{\Gamma}) > 2(\frac{\Upsilon}{\underline{\sigma}(\boldsymbol{M})})^2 = 26.36$, where $\underline{\sigma}(\boldsymbol{M}(t)) \geq 0.19$ for all $t \geq T_w$. From Figures 3.6 and 3.7, it is seen that the controller achieves safe, accurate tracking despite the parameter estimates not converging to the true values. It is believed that this is because the parameter estimates are capturing the effect of the unknown perturbation in the system dynamics in addition to the parameter-affine disturbance, i.e. $\Delta_a(\boldsymbol{\chi})\hat{\boldsymbol{C}}_d \approx \Delta_a(\boldsymbol{\chi})\boldsymbol{C}_d + d(t, \boldsymbol{\chi})$.

4.4.2 Quadrotor Trajectory Tracking: Double-Integrator Model

In this section, the Koopman-based robust- (4.48) and robust, adaptive CBF (4.51) controllers are simulated on a quadrotor-inspired trajectory tracking problem.

Let $\mathcal{F}$ be an inertial frame with a point s_0 denoting its origin. Consider, again, a quadrotor seeking to track a Gerono lemnisicate (i.e. figure-eight) trajectory, this time amidst circular obstacles in the 2D plane. Quadrotor dynamics are known to be differentially flat, thus as shown to be feasible in [219] the model is taken to be the following 2D double-integrator subject to an unknown, wind disturbance:

$$\begin{bmatrix} \dot{x} \\ \dot{y} \\ \dot{v}_x \\ \dot{v}_y \end{bmatrix} = \begin{bmatrix} v_x \\ v_y \\ a_x \\ a_y \end{bmatrix} + \begin{bmatrix} 0 \\ 0 \\ d_x(\boldsymbol{z}) \\ d_y(\boldsymbol{z}) \end{bmatrix}, \tag{4.55}$$

where x and y denote the position coordinates (in m), v_x and v_y are the velocities (in m/s), and a_x and a_y are the accelerations (in m/s^2). The full state and control input vectors are $\boldsymbol{z} = [x \;\; y \;\; v_x \;\; v_y]^T \in \mathbb{R}^4$ and $\boldsymbol{u} = [a_x \;\; a_y]^T \in \mathbb{R}^2$ respectively, and $d_x : \mathbb{R}^4 \to \mathbb{R}$ and $d_y : \mathbb{R}^4 \to \mathbb{R}$ are unknown wind-gust accelerations satisfying the requirements of d in (4.28). Again, the wind-gust model from [218] is used to obtain spatially varying wind velocities $w_i(\boldsymbol{z})$ and set $d_i(\boldsymbol{z}) = C_d(w_i(\boldsymbol{z}) - v_i)$ for $i \in \{x, y\}$, where C_d is a drag coefficient, such that $\|d_x(\boldsymbol{z})\|_\infty, \|d_y(\boldsymbol{z})\|_\infty \leq C = 10$.

Two circular obstacles are considered, each of which occludes the desired quadrotor path. As such, the safe set is defined as

$$\mathcal{S} = \{\boldsymbol{z} \in \mathbb{R}^4 : h_1(\boldsymbol{z}) \geq 0\} \cap \{\boldsymbol{z} \in \mathbb{R}^4 : h_2(\boldsymbol{z}) \geq 0\},$$

where $h_i(\boldsymbol{z}) = (x - c_{x,i})^2 + (y - c_{y,i})^2 - R^2$ for $i \in \{1, 2\}$, $(c_{x,i}, c_{y,i})$ denotes the center of the ith obstacle, and R is its radius. Since h_1, h_2 are relative-degree two with respect to (4.55), forms of the Future-Focused Control Barrier Function (FF-CBF) developed in Chapter 2 are used for a form of safe, predictive control.

The control laws are the CBF-QP[1] (4.53) corresponding to both the robust (4.48) and robust-adaptive (4.51) CBF conditions, whose results are compared against the following naive (i.e. assuming exact identification, $\hat{d} = d$) Koopman-based controllers from the literature: 1) a CBF controller equipped with the data-driven Koopman-based identification scheme proposed in [119] (denoted DD-KM) 2) the same control law with the data-driven identification scheme proposed by [122] (denoted DD-KG). In each case, the last 500 measurements were used for computing the Koopman matrix (or generator). For the robust and robust-adaptive simulations, additive Gaussian measurement noise was injected into both $\boldsymbol{x}$ and $\dot{\boldsymbol{x}}$ in order to stress-test the proposed algorithm under non-ideal conditions. The nominal control law was that introduced for quadrotors in [213] and modified for the double-integrator dynamics, where the reference trajectory is the Gerono lemniscate defined by

$$
\begin{aligned}
x^*(t) &= 4\sin(0.2\pi t) \\
y^*(t) &= 4\sin(0.2\pi t)\cos(0.2\pi t),
\end{aligned}
$$

which specifies that one figure-eight pattern be completed every 10s. The circular obstacles were centered on $(-2.5, 0)$ and $(2, -1)$ respectively, each with a radius of $R = 1.5$m. For all controllers, the class $\mathcal{K}_\infty$ functions were $\alpha(h) = h$. For the Koopman basis functions, sinusoids of the form $\psi_i = \sqrt{2}\cos(n\pi z)$, $\psi_{i+1} = \sqrt{2}\sin(n\pi z)$, for $n \in \{1, 2\}$ and $z \in \{x, y, v_x, v_y\}$ were selected. The sampling time was $\Delta t = 0.001$s.

The resulting paths taken by the simulated CBF-controlled vehicles (Koopman-based naive, robust, and robust-adaptive), as well as the path taken for the nominally controlled vehicle without disturbance estimation are displayed in Figure 4.1. Here, only the robust and robust-adaptive CBF controllers that use the proposed fixed-time identification approach preserve safety (as seen in Figure 4.2). As the data-driven Koopman matrix ([119]) and generator ([122]) approaches are non-recursive and unable to quantify the identification error, they are neither sufficiently responsive nor accurate enough to guarantee safety in this example. Figure 4.3 highlights that the disturbance estimates converge to a neighborhood of the true values within the fixed-time $T = 0.12$ sec, computed using (4.38), despite measurement noise and the control inputs are shown in Figure 4.4. Even when measurement noise is injected into the system, the adaptation-based approach succeeds

[1]All simulation code and data are available online at https://github.com/6lackmitchell/nonlinear-fxt-adaptation-control

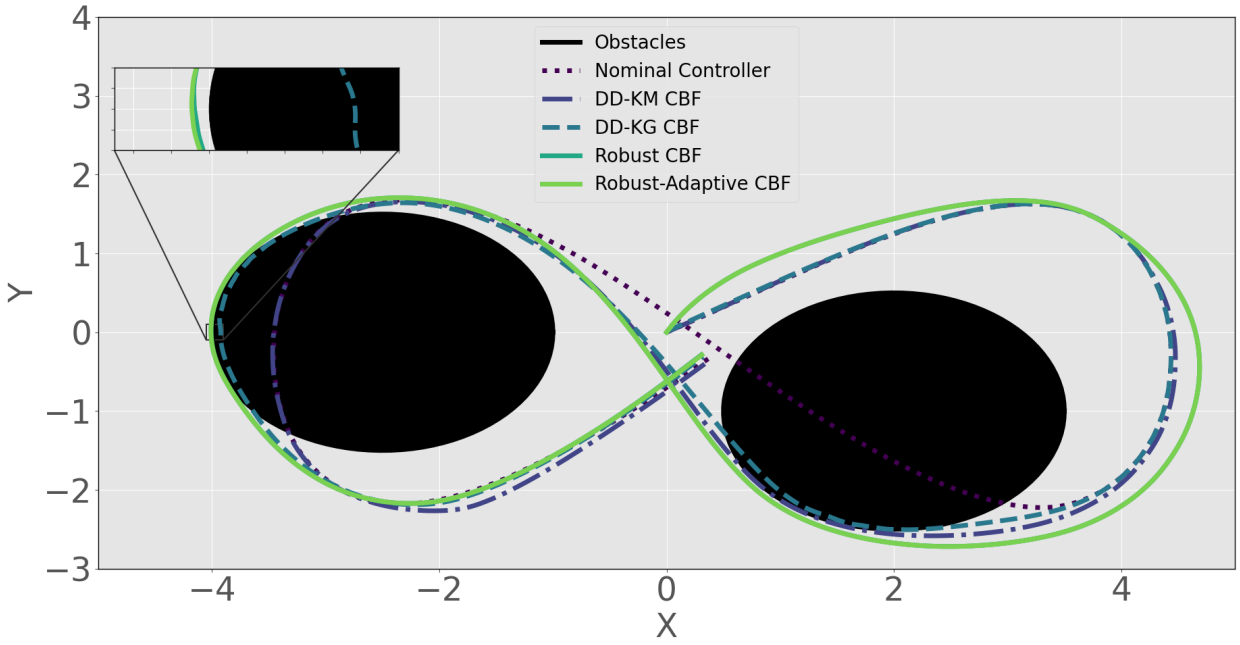

Figure 4.1: XY paths under the various CBF-QP control laws in the double-integrator example. Only the controllers using the proposed Koopman-based fixed-time identification scheme succeed in preserving safety.

in both reconstructing the unknown disturbance to within a small error and preserving safety. Any quantification of the error associated with representing the infinite-dimensional Koopman operator in a finite-dimensional subspace is left to future work.

4.5 Conclusion

A new FxTS condition is derived to analyze the robustness properties of a parameter adaptation law from Chapter 3 to measurement noise and/or time-varying parameters. It is shown that the estimated parameters converge to a neighborhood of the goal set within a fixed-time, and this neighborhood and its domain of attraction are characterized. Then, a related parameter adaptation law is proposed using Koopman operator theory for linear identification of an unknown, nonlinear disturbance to a class of nonlinear, control-affine dynamical systems. Under certain conditions, the Koopman generator is learned within a fixed-time and thus the system disturbance is recovered. Robust- and robust, adaptive- CBF conditions are proposed for safe control synthesis under parameter adaptation, and a safety-critical quadrotor case study are undertaken to demonstrate the success of the method in situations where existing Koopman-based identification and control strategies fail.

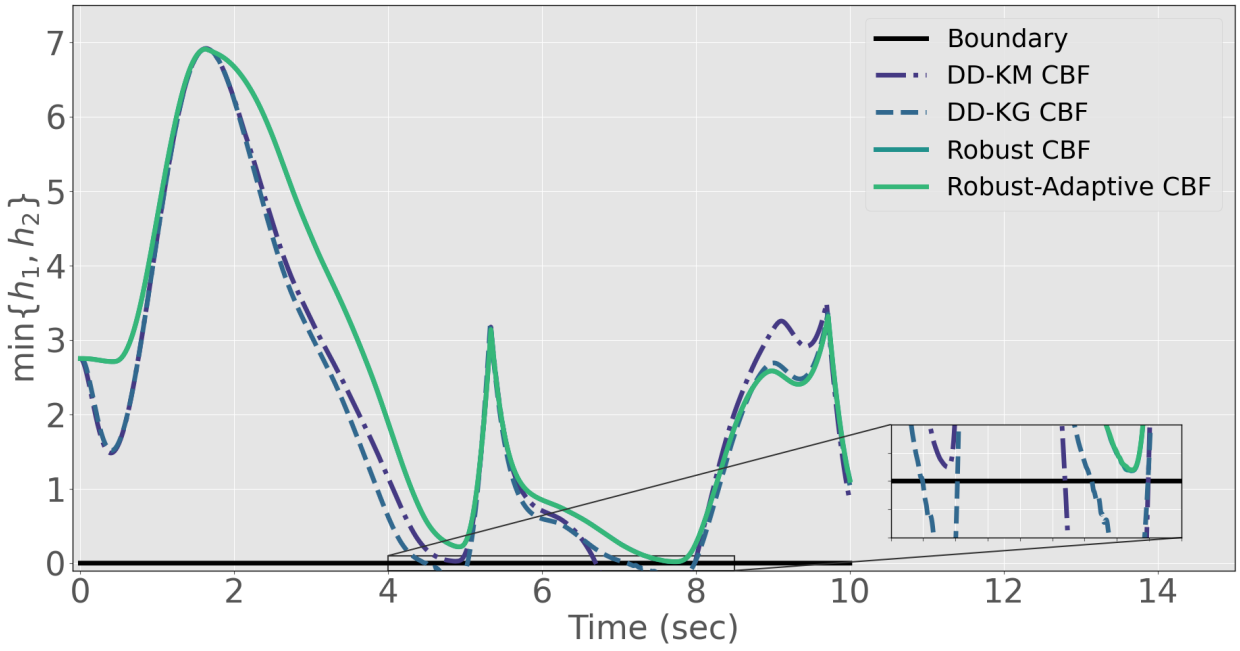

Figure 4.2: Evolutions of h_1 and h_2 for the various controllers considered in the double-integrator example.

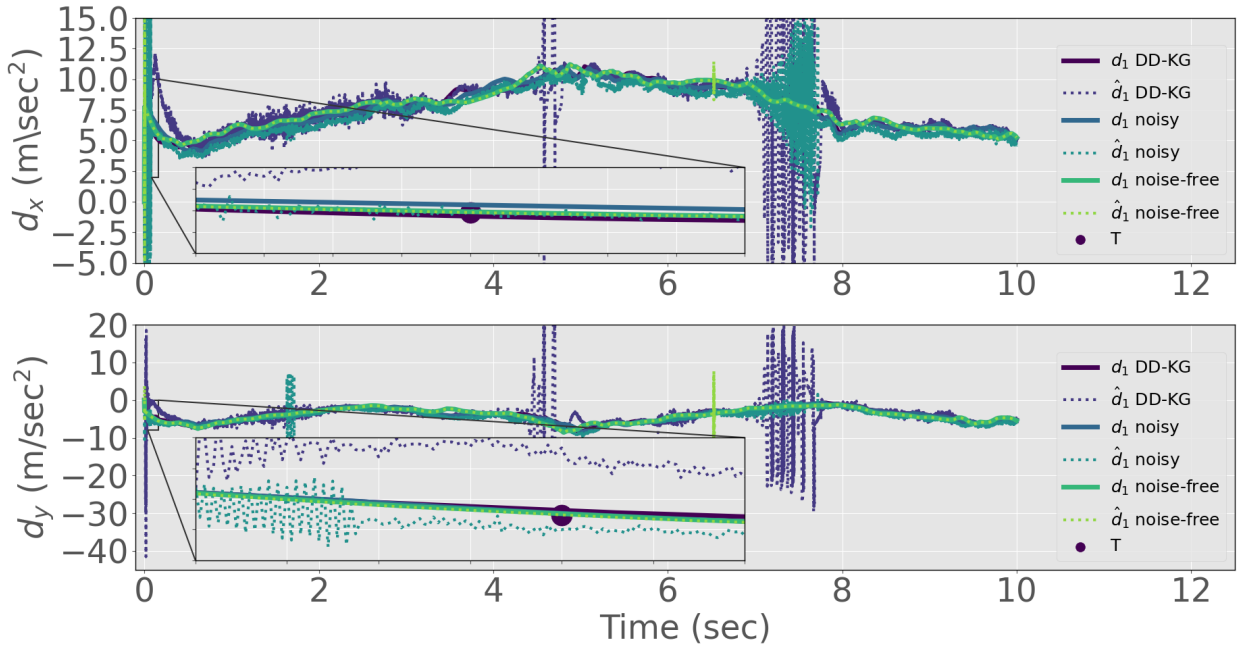

Figure 4.3: The ground truths d_x, d_y and estimates $\hat{d}_x$, $\hat{d}_y$ of the unknown wind gusts. In our scheme, the estimates converge to the true values within the fixed-time T without noise, and converge to a close approximation in the presence of measurement noise.

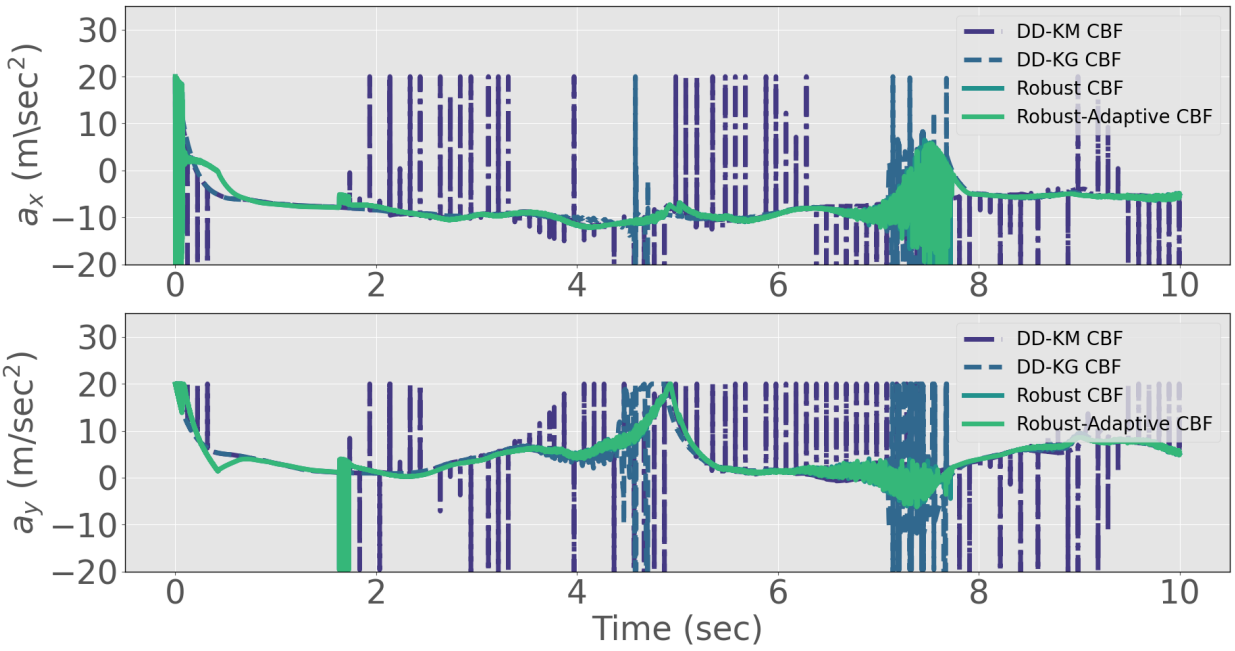

Figure 4.4: Control inputs for the double-integrator example.

CHAPTER 5

Risk-Aware Control Barrier Functions

In contrast to the classes of unknown but notably deterministic systems studied in Chapters 3 and 4, systems modelled according to classes of Stochastic Differential Equations (SDEs) account for the effect of randomness on the evolution of the system trajectories. Specifically, the class of SDEs under consideration in this chapter may be modelled as a difference equation, the right-hand side of which consists of the sum of a drift term (how the system would evolve in the deterministic regime) and a diffusion term containing a Brownian motion process that injects randomness. In practical applications, random phenomena may perturb the system dynamics in the form of, e.g., measurement noise (via imperfect sensors) or exogenous disturbances (via e.g., wind gusts, uncontrolled agents, etc.), and must be taken into consideration when encoding stability or safety (in the stochastic sense) via model-based control design. For stochastic safety-critical systems, however, the notion of safety via set invariance underpinning the results from previous chapters must be adapted to account for the (non-zero) risk of random events leading to unsafe outcomes. As demonstrated via an illustrative example in Section 5.1, existing approaches to probabilistically safe control design for this class of systems may lead to extreme conservatism.

Thus, in Section 5.2, a novel form of Risk-Aware Control Barrier Functions (RA-CBFs) is introduced for bounding via control design the probability that a class of stochastic, nonlinear, control-affine systems becomes unsafe within a given (finite) time interval. The proposed formulation leverages an existing result from the stochastic level-crossing literature [220] to derive an (infinitesimal) generator[1] condition, the satisfaction of which via control design results in a user-specified risk bound on the system becoming unsafe over a time interval. It is then shown how to further decrease conservatism by tightening the risk bound, which requires recursive application of the RA-CBF to subsets of the safe set and the use of Bayes' rule to obtain the total probability of becoming unsafe. For classes of systems with a control-affine drift term, the RA-CBF condition is likewise control-affine and is thus amenable to inclusion in a RA-CBF-Quadratic Program (QP) control law. Under certain conditions related to the magnitude of the diffusion term, it is derived

[1]The (infinitesimal) generator of a stochastic process is analogous to the Lie derivative for deterministic systems.

that this RA-CBF-QP controller leads to less conservative outcomes than the state-of-the-art, a fact that is supported by an empirical study consisting of 400,000 total trials presented in Section 5.3. Application of the proposed approach to a highway merging problem amongst dense traffic demonstrates the efficacy of RA-CBF-based control in a more realistic scenario.

The results of this chapter are based on [221]. The author wishes to acknowledge the many contributions of his co-authors Dr. Georgios Fainekos, Dr. Bardh Hoxha, and Dr. Danil Prokhorov to the development of this research.

5.1 Mathematical Preliminaries

In this section, an overview of the stochastic system model under consideration and some preliminaries related to control for probabilistic set invariance is presented. But first, some additional notation is reviewed. A bold $\boldsymbol{x}_t$ denotes a vector stochastic process at time t. The Gauss error function is $\text{erf}(z) = \frac{2}{\sqrt{\pi}} \int_0^z e^{-t^2} dt$, and $\text{erf}^{-1}(\cdot)$ is its inverse.

5.1.1 Stochastic System Model

We consider the following class of nonlinear, control-affine, SDEs,

$$d\boldsymbol{x}_t = \big(f(\boldsymbol{x}_t) + g(\boldsymbol{x}_t)\boldsymbol{u}_t\big)dt + \sigma(\boldsymbol{x}_t)d\boldsymbol{w}_t, \quad \boldsymbol{x}_0 \in \mathcal{X}_0, \tag{5.1}$$

where $\boldsymbol{x} \in \mathcal{X} \subset \mathbb{R}^n$ denotes the state, $\boldsymbol{u} \in \mathcal{U} \subseteq \mathbb{R}^m$ the control input, and $\boldsymbol{w} \in \mathbb{R}^q$ a standard q-dimensional Wiener process (i.e., Brownian motion) defined over the complete probability space $(\Omega, \mathcal{F}, P)$ for sample space Ω, σ-algebra $\mathcal{F}$ over Ω, and probability measure $P : \mathcal{F} \to [0, 1]$. In this chapter, a class of memoryless, state-feedback controllers is considered such that the control signal is $\boldsymbol{u}_t = k(\boldsymbol{x}_t)$, with $f : \mathcal{X} \to \mathbb{R}^n$, $g : \mathcal{X} \to \mathbb{R}^{n\times m}$, $k : \mathcal{X} \to \mathcal{U}$, and $\sigma : \mathbb{R}^n \to \mathbb{R}^{n\times q}$ known, locally Lipschitz, and bounded on $\mathcal{X}$, which is assumed to be bounded[2]. With the above regularity conditions, we thus assume that for all $\boldsymbol{x}_0 \in \mathcal{X}_0 \subseteq \mathcal{X}$ the process $\{\boldsymbol{x}_t : t \in [0, \infty)\}$ is a strong solution to (5.1) (see [222, Ch. 5, Def. 2.1]).

For strong solutions to an SDE of the form (5.1), the (infinitesimal) generator is defined as follows.

Definition 5.1. *[223, Def. 7.3.1] The (infinitesimal) generator $\mathcal{A}$ of the stochastic process $\boldsymbol{x}_t$ is*

[2]Note that in the more general case it is required for existence and uniqueness of a strong solution to (5.1) that f, g, k, and σ satisfy the linear growth condition on $\mathcal{X}$. With $\mathcal{X}$ assumed to be bounded, however, this may be replaced by boundedness of $f(\boldsymbol{x})$, $g(\boldsymbol{x})$, $k(\boldsymbol{x})$, and $\sigma(\boldsymbol{x})$.

defined by

$$\mathcal{A}\phi(\boldsymbol{y}) = \lim_{t \downarrow 0} \frac{\mathbb{E}\left[\phi(\boldsymbol{x}_t) \mid \boldsymbol{x}_0 = \boldsymbol{y}\right] - \phi(\boldsymbol{y})}{t}, \tag{5.2}$$

where $\phi : \mathbb{R}^n \to \mathbb{R}$ belongs to $\mathcal{D}_{\mathcal{A}}$, the set of all functions such that the limit exists for all $\boldsymbol{x} \in \mathbb{R}^n$.

The generator is the stochastic analog to the Lie derivative for deterministic systems in that it characterizes the derivative of ϕ over the trajectories of (5.1) in expectation. By [223, Thm. 7.3.3], for a twice continuously differentiable function ϕ with compact support, i.e., $\phi \in \mathcal{C}_0^2(\mathbb{R}^n) \subset \mathcal{D}_{\mathcal{A}}$, the generator $\mathcal{A}$ of $\boldsymbol{x}_t$ is described by

$$\mathcal{A}\phi(\boldsymbol{x}) = L_f\phi(\boldsymbol{x}) + L_g\phi(\boldsymbol{x})k(\boldsymbol{x}) + \frac{1}{2}\mathrm{Tr}\left(\sigma(\boldsymbol{x})^\top \frac{\partial^2 \phi}{\partial \boldsymbol{x}^2}\sigma(\boldsymbol{x})\right). \tag{5.3}$$

For notational convenience, in the remainder we use $\Gamma_\phi(\boldsymbol{x}, \boldsymbol{u}) \triangleq \mathcal{A}\phi(\boldsymbol{x})$ by substituting in $\boldsymbol{u} = k(\boldsymbol{x})$ to (5.3).

5.1.2 Controlled Probabilistic Set Invariance

Consider a set of states $\mathcal{S} \subset \mathcal{X}$ defined by a twice continuously differentiable, positive semi-definite function $B : \mathbb{R}^n \to \mathbb{R}$:

$$\mathcal{S} = \{\boldsymbol{x} \in \mathcal{X} : \ 0 \leq B(\boldsymbol{x}) < 1\}, \tag{5.4}$$

and assume that for some known $\gamma \in [0, 1]$,

$$B(\boldsymbol{x}) \leq \gamma, \ \forall \boldsymbol{x} \in \mathcal{X}_0, \tag{5.5}$$

which amounts to a worst-case bound on the initial condition. As in previous chapters, it is assumed here that the set $\mathcal{S}$ represents a set of *safe* states, and thus it is desirable to render $\mathcal{S}$ *forward invariant*. For completeness, recall that in the deterministic setting the set $\mathcal{S}$ is said to be forward invariant if $\boldsymbol{x}_0 \in \mathcal{S} \implies \boldsymbol{x}_t \in \mathcal{S}, \forall t \geq 0$. In the stochastic setting, however, there may be failure cases in which $\boldsymbol{x}_t$ exits $\mathcal{S}$, i.e., the system becomes unsafe. We therefore consider the stopped process, $\tilde{\boldsymbol{x}}_t$, and the notion of probabilistic forward invariance, adapted from [224].

Definition 5.2 (**Stopped Process**, [225])**.** *Suppose that $\tau > 0$ is the first time of exit of $\boldsymbol{x}_t$ from the open set $\mathcal{S}$. The stopped process $\tilde{\boldsymbol{x}}_t$ is*

$$\tilde{\boldsymbol{x}}_t = \begin{cases} \boldsymbol{x}_t; & t < \tau, \\ \boldsymbol{x}_\tau; & t \geq \tau. \end{cases}$$

Definition 5.3 (**Probabilistic Forward-Invariant Set**). *Let* $0 < p \leq 1$*, and consider the stopped process over a time interval of length* $T > 0$*, i.e.,* $\{\tilde{\boldsymbol{x}}_t : t \in [0, T]\}$*, with respect to the set* $\mathcal{S}$ *defined by* (5.4)*. The set* $\mathcal{S} \subset \mathcal{X} \subset \mathbb{R}^n$ *is a* ***probabilistic forward-invariant set with probability p*** *for system* (5.1) *over the interval* $[0, T]$ *if* $P\left(\tilde{\boldsymbol{x}}_t \in S, \forall t \in [0, T]\right) \geq p$*.*

Thus, the trajectories of (5.1) are **safe** with probability p over the time interval $[0, T]$ if $\mathcal{S}$ is a probabilistic forward-invariant set with probability p over $[0, T]$. Alternatively, the probability of the system becoming unsafe over the specified time interval, i.e., $\rho \triangleq P(\exists t \in [0, T] : \tilde{\boldsymbol{x}}_t \notin \mathcal{S})$, is bounded according to $\rho \leq 1 - p$. In the remainder, ρ is referred to as the "system risk".

One approach to bounding the system risk of (5.1) is to use Stochastic Control Barrier Functions (S-CBFs) in the control design [154, 155].

Definition 5.4 (**Stochastic Control Barrier Function (S-CBF)**). *Consider a set* $\mathcal{S} \subset \mathcal{X} \subset \mathbb{R}^n$ *defined by* (5.4) *for a twice continuously differentiable, positive semi-definite function* B *satisfying* (5.5)*. The function* B *is a* ***stochastic control barrier function*** *defined on the set* $\mathcal{S}$ *if there exist* $\alpha, \beta \geq 0$ *such that for the system* (5.1) *the generator* $\Gamma_B(\boldsymbol{x}, \boldsymbol{u})$ *satisfies the following condition, for all* $\boldsymbol{x} \in \mathcal{S}$*,*

$$\inf_{\boldsymbol{u} \in \mathcal{U}} \Gamma_B(\boldsymbol{x}, \boldsymbol{u}) \leq -\alpha B(\boldsymbol{x}) + \beta. \tag{5.6}$$

A valid S-CBF guarantees that the system risk is bounded from above, as shown in the following [154, Prop. 1].

Theorem 5.1 (**Bounded System Risk with S-CBFs**). *Consider a stochastic system of the form* (5.1)*, a set of safe states* $\mathcal{S}$ *implicitly defined by a twice continuously differentiable, positive semi-definite function* B *as in* (5.4)*, and the time interval* $[0, T]$ *for* $T > 0$*. Let the probability that the stopped process* $\{\tilde{\boldsymbol{x}}_t : t \in [0, T]\}$ *exits* $\mathcal{S}$ *be denoted* $\rho_{S\text{-}CBF} \triangleq P(\exists t \in [0, T] : \tilde{\boldsymbol{x}}_t \notin \mathcal{S} \mid \tilde{\boldsymbol{x}}(0) \in \mathcal{X}_0)$*. If* B *is a S-CBF for* (5.1) *over the set* $\mathcal{S}$*, then*

$$\rho_{S\text{-}CBF} \leq \begin{cases} 1 - (1 - \gamma)\, e^{-\beta T}; & \alpha > 0 \text{ and } \alpha \leq \beta, \\ \left(\gamma + (e^{\beta T} - 1)\frac{\beta}{\alpha}\right) e^{-\beta T}; & \alpha > 0 \text{ and } \alpha > \beta, \\ \gamma + \beta T; & \alpha = 0. \end{cases} \tag{5.7}$$

Remark 5.1. *A S-CBF controller can certify that at best a fraction of* $1 - \gamma$ *of the trajectories will be safe over a time interval for any choice of* $\alpha, \beta, T \geq 0$*. Note that, due to the martingale origins of S-CBFs, the strength of the process noise (*$\sigma(\boldsymbol{x})$*) in* (5.1) *does not appear in* (5.7)*. It was initially hypothesized that this may be a source of conservatism in S-CBF-based control design, and thus serves to motivate the problem formalized in Section 5.1.3.*

With the generator $\Gamma_B(\boldsymbol{x}, \boldsymbol{u})$ being affine in the control $\boldsymbol{u}$, S-CBFs are suitable for use in a version of the following Control Barrier Function (CBF)-QP control law:

$$\boldsymbol{u}^* = \underset{\boldsymbol{u}\in\mathcal{U}}{\arg\min} \frac{1}{2}\|\boldsymbol{u} - \boldsymbol{u}_0\|^2 \tag{5.8a}$$

s.t.

$$A\boldsymbol{u} + b \leq 0, \tag{5.8b}$$

where $\boldsymbol{u}_0$ is the desired input, and (5.8b) in this case represents the S-CBF condition (5.6), with $b \in \mathbb{R}$, $A \in \mathbb{R}^{1\times m}$. In the remainder, (5.8) is used to compare emergent behaviors of systems under S-CBF constraints versus those using our proposed risk-aware CBF.

5.1.3 Problem Formulation

Based on Remark 5.1, it was hypothesized that S-CBFs may introduce unnecessary conservatism into risk-aware control design. An illustrative example is used to show that this is indeed true, and thereby motivates the problem.

Example 5.1 (**Mobile Robot Reach-Avoid**). *Consider a mobile robot seeking to achieve the following objective: visit a circular region of radius $R_g > 0$ centered on $s_g = (x_g, y_g)$, defined with respect to the origin $s_0 = (0, 0)$ of an inertial frame $\mathcal{I}$, while avoiding an unsafe region defined as the area outside a circle of radius R_c centered on s_0. The goal specification may be thought of as visiting a point of interest, while the constraint may model, e.g., limited communication range. The following parameters are used: $s_g = (2, 2)$, $R_c = 1$, and $R_g = 0.25$, such that the goal and safe sets do not intersect (see Figure 5.1). Assume that the robot may be modeled as a 2D stochastic single-integrator,*

$$d\boldsymbol{z}_t = \begin{bmatrix} 1 & 0 \\ 0 & 1 \end{bmatrix} \begin{bmatrix} v_x \\ v_y \end{bmatrix} dt + \begin{bmatrix} \sigma_x & 0 \\ 0 & \sigma_y \end{bmatrix} d\boldsymbol{w}_t, \tag{5.9}$$

where $\boldsymbol{z} = [x\ y]^\top$ denotes the robot's position (in m) with respect to s_0, the control $\boldsymbol{u} = [v_x\ v_y]^\top$ consists of velocities along x and y axes (in m/s), and $\sigma_x, \sigma_y \in \mathbb{R}$ dictate the strength of noise introduced by the Wiener process $\boldsymbol{w} \in \mathbb{R}^2$.

As seen from Figure 5.1, completing the reach task is impossible to accomplish safely. It remains to be seen, however, the degree to which the S-CBF-based controller approaches the boundary of the safe set in pursuit of reaching the goal. As such, the controller (5.8) is simulated with a nominal input of $\boldsymbol{u}_0 = -k[(x - x_g)\ (y - y_g)]^\top$ with $k = 2$. The input constraints were taken to

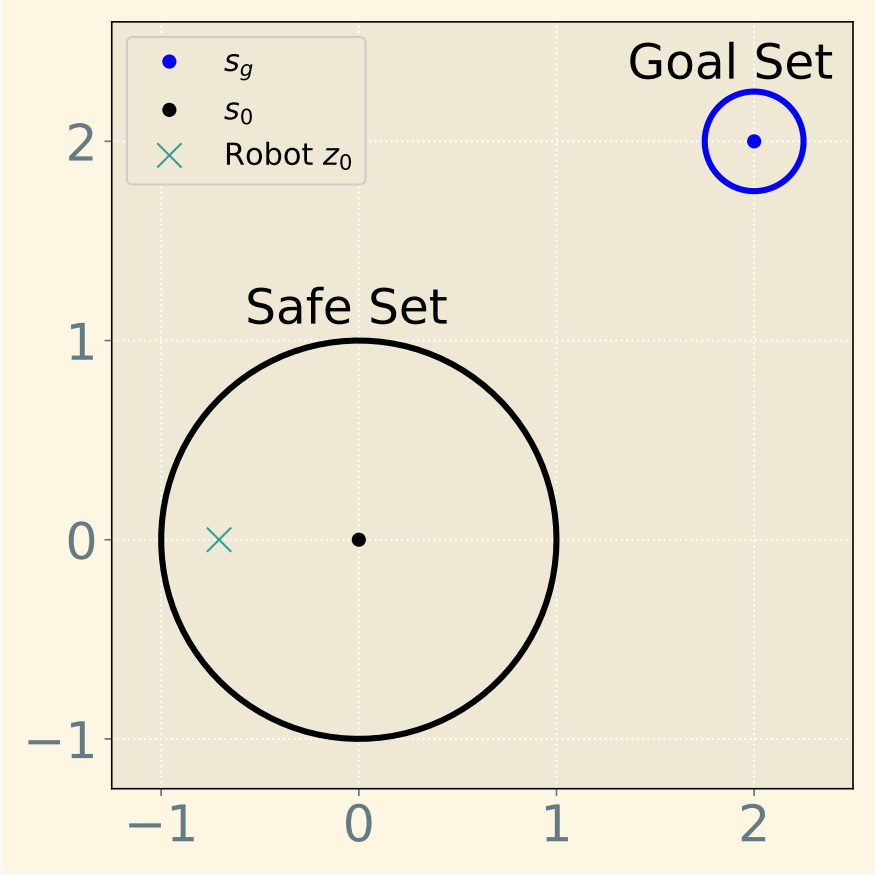

Figure 5.1: Problem setup for the mobile robot goal-seeking problem subject to limited radio communication.

be $|v_x, v_y| \leq v_{max} = 10$, and (5.8b) is the S-CBF condition (5.6), with

$$B(\boldsymbol{z}) = \frac{x^2 + y^2}{R_c^2}.$$

The initial state $\boldsymbol{z}_0 = [1/\sqrt{2},\ 0]^\top$ was fixed such that $B(\boldsymbol{z}_0) = 0.5 = \gamma$, and a time horizon of $T = 1$ sec was used at a time-step of $\Delta t = 0.001$ sec. A numerical study consisting of $N = 100,000$ individual trials of Example 5.1 was conducted with $\sigma_x, \sigma_y = 0.3 v_{max} \cdot \Delta t$, i.e., a strength of 30% of the maximum control input. Different values of $\alpha, \beta \geq 0$ were selected in order to achieve system risk bounds of 0.505 and 0.990 as computed by (5.7) (and shown in Table 5.1).

The results (also shown in Table 5.1) confirmed the stated hypothesis: the theory supporting the derivation of the S-CBF constraint may yield a theoretical system risk bound that significantly overestimates the actual fraction of unsafe outcomes. Despite bounded failure rates of 0.505 and 0.990, the S-CBF-QP controller (5.8) preserved safety in 100% of the $200,000$ total trials (0 failures) over both cases during the $T = 1$ sec intervals. It is clear from this example that the S-CBF

system risk bounds may not, and certainly here do not, provide any meaningful guidelines.

Table 5.1: Stochastic CBF Trials $N = 100,000$

Theoretical ρ	Measured ρ	α	β	γ	T
0.505	0	0.1	0.01	0.50	1.0
0.990	0	10.0	4.0	0.50	1.0

As such, the design of a stochastic control framework is addressed to bound the system risk over a finite time interval while bridging the gap between results derived in theory and those observed in practice.

Problem 5.1. *Consider the stochastic dynamical system of the form* (5.1) *and an associated safe set $\mathcal{S}$ defined by a twice continuously differentiable, positive semi-definite function B satisfying* (5.5)*. Design a feedback controller $\boldsymbol{u}_t = k(\boldsymbol{x}_t)$ such that under certain conditions $\rho \triangleq P(\exists t \in [0,T] : \tilde{\boldsymbol{x}}_t \notin S) < \rho_{S\text{-}CBF}$, where $\rho_{S\text{-}CBF}$ is given by* (5.7)*. Further, identify the conditions under which this relation holds.*

5.2 Risk-Aware Control Barrier Functions

In this section, a novel class of RA-CBFs is proposed as a solution to Problem 5.1. First, the following Lemma, a main ingredient in the derivation of the RA-CBF, is required.

Lemma 5.1 (Level Crossing for Wiener Process). *Suppose that $w : \mathbb{R}_{\geq 0} \to \mathbb{R}$ is a standard Wiener process, and $T > 0$ and $a > 0$ are constants. Then, the probability that $w_t < a$, for all $t \in [0,T]$ is given by*

$$P\left(\sup_{0\leq t\leq T} w(t) < a\right) = \operatorname{erf}\left(\frac{a}{\sqrt{2T}}\right). \tag{5.10}$$

Proof. The proof follows directly from [220, Section 3]. □

In what follows, the integral of the drift term of (5.1) is denoted by

$$I_L(t) \triangleq \int_0^t \big(L_f B(\tilde{\boldsymbol{x}}_s) + L_g B(\tilde{\boldsymbol{x}}_s)\boldsymbol{u}_s\big) ds, \tag{5.11}$$

which may be included as an integrator state in an augmented system of dimension $n+1$. Now, the formal definition of a RA-CBF is introduced.

Definition 5.5 (**Risk-Aware Control Barrier Function (RA-CBF)**). *Consider a set $\mathcal{S} \subset \mathcal{X} \subset \mathbb{R}^n$ defined by* (5.4) *for a twice continuously differentiable, positive semi-definite function B satisfying* (5.5). *The function B is a **risk-aware control barrier function** on the set $\mathcal{S}$ if there exists a Lipschitz continuous function $\alpha \in \mathcal{K}_\infty$ such that for the system* (5.1) *the following holds for all $\boldsymbol{x} \in \mathcal{S}$,*

$$\inf_{\boldsymbol{u} \in \mathcal{U}} \left[L_f B(\boldsymbol{x}) + L_g B(\boldsymbol{x}) \boldsymbol{u} \right] \leq \alpha\big(h(I_L(t))\big), \tag{5.12}$$

where

$$h(I_L(t)) = 1 - \gamma - (\sqrt{2}\eta T)\operatorname{erf}^{-1}(1 - \rho_d) - I_L(t), \tag{5.13}$$

with $I_L(t)$ given by (5.11)*, $\rho_d \in \left[1 - \operatorname{erf}\left(\frac{1-\gamma}{\sqrt{2}\eta T}\right), 1\right]$ a design parameter, and*

$$\eta = \sup_{\boldsymbol{x} \in \mathcal{S}} \|L_\sigma B(\boldsymbol{x})\|. \tag{5.14}$$

In the following theorem, it is proved that RA-CBFs bound the risk that a system of the form (5.1) becomes unsafe over a finite time interval.

Theorem 5.2 (**Bounded System Risk with RA-CBFs**). *Let $T > 0$, and denote the system risk as $\rho \triangleq P\left(\exists t \in [0, T] : \tilde{\boldsymbol{x}}_t \notin \mathcal{S} \mid \tilde{\boldsymbol{x}}_0 \in \mathcal{X}_0\right)$. If B is a RA-CBF on the set $\mathcal{S}$, then,*

$$\rho \leq \rho_d, \tag{5.15}$$

where $\rho_d \in \left[1 - \operatorname{erf}\left(\frac{1-\gamma}{\sqrt{2}\eta T}\right), 1\right]$ is a design parameter with η given by (5.14).

Proof. Let $\tau > 0$ be the first time of exit of $\boldsymbol{x}_t$ from the open set $\mathcal{S}$. With $\{\boldsymbol{x}_t : t \in [0, \infty)\}$ a strong solution to (5.1), it follows from Itô's Formula [223, Theorem 4.2.1] that $\forall t < \tau$,

$$dB(\tilde{\boldsymbol{x}}_t) = \big(L_f B(\tilde{\boldsymbol{x}}_t) + L_g B(\tilde{\boldsymbol{x}}_t)\boldsymbol{u}\big)dt + L_\sigma B(\tilde{\boldsymbol{x}}_t) d\boldsymbol{w}_t,$$

which leads to the integral equation $B(\tilde{\boldsymbol{x}}_t) = B(\tilde{\boldsymbol{x}}_0) + I_L(t) + I_S(t)$, where $I_L(t)$ is a Lebesgue integral defined by (5.11) and $I_S(t)$ is a stochastic integral defined by

$$I_S(t) = \int_0^t L_\sigma B(\tilde{\boldsymbol{x}}_s) d\boldsymbol{w}_s. \tag{5.16}$$

While (5.11) can be evaluated deterministically, the stochastic integral (5.16) is an Itô integral [223, Def. 3.1.6] and thus induces a distribution on $B(\tilde{\boldsymbol{x}}_t)$ based on

$$I_S(t) \sim \mathcal{N}\left(0,\ \mathbb{E}\left[\left(\int_0^t L_\sigma B(\tilde{\boldsymbol{x}}_s) d\boldsymbol{w}_s\right)^2\right]\right).$$

With $\boldsymbol{w} \in \mathbb{R}^q$ a standard Wiener process, it follows from the q-dimensional version of the Itô isometry [226, Lemma 18] (an extension of the 1-dimensional Itô isometry [223, Lemma 3.1.5]) that

$$\mathbb{E}\left[\left(\int_0^t L_\sigma B(\tilde{\boldsymbol{x}}_s) d\boldsymbol{w}_s\right)^2\right] = \int_0^t \left\|L_\sigma B(\tilde{\boldsymbol{x}}_s)\right\|^2 ds,$$

and thus that $B(\tilde{\boldsymbol{x}}_t) \sim \mathcal{N}(\mu_B(t), \sigma_B^2(t))$, where $\mu_B(t) = B(\tilde{\boldsymbol{x}}_0) + I_L(t)$ and $\sigma_B^2(t) = \int_0^t \left\|L_\sigma B(\tilde{\boldsymbol{x}}_s)\right\|^2 ds$. As such, the probability that $\exists t \in [0, T]$ such that $\tilde{\boldsymbol{x}}_t \notin \mathcal{S}$, i.e., the system risk ρ, may be expressed as

$$\rho = 1 - P\left(\sup_{0 \le t \le T} B(\tilde{\boldsymbol{x}}_t) < 1 \mid B(\tilde{\boldsymbol{x}}_0) \le \gamma\right).$$

Now, define $\bar{B}(\tilde{\boldsymbol{x}}_t) = B(\tilde{\boldsymbol{x}}_0) + I_L(t) + \bar{I}_S(t)$ for $\bar{I}_S(t) \sim \mathcal{N}(0, \int_0^t \eta^2 ds)$ such that $\bar{B}(\tilde{\boldsymbol{x}}_t) \sim \mathcal{N}(B(\tilde{\boldsymbol{x}}_0) + I_L(t), \int_0^t \eta^2 ds)$. Since by (5.14) it holds that $\int_0^t \eta^2 ds \ge \sigma_B^2(t)$, for all $t \ge 0$, it then follows that

$$\rho \le \bar{\rho} \triangleq 1 - P\left(\sup_{0 \le t \le T} \bar{B}(\tilde{\boldsymbol{x}}_t) < 1 \mid B(\tilde{\boldsymbol{x}}_0) \le \gamma\right). \tag{5.17}$$

However, we observe that $\int_0^t \eta^2 ds = \eta^2 t$, and thus by Gaussian linearity $\bar{I}_S(t) = \eta\sqrt{t} w(t)$, where $w(t)$ is the 1-dimensional standard Wiener process, which implies that $\bar{B}(\boldsymbol{x}_t) = B_0 + I_L(t) + \eta\sqrt{t} w(t)$. Therefore,

$$\begin{aligned}
\bar{\rho} &= 1 - P\left(\sup_{0 \le t \le T} w(t) < \frac{1 - \gamma - I_L(t)}{\eta\sqrt{t}} \mid B_0 \le \gamma\right), \\
&\le 1 - P\left(\sup_{0 \le t \le T} w(t) < \frac{1 - \gamma - \bar{I}_L}{\eta\sqrt{T}} \mid B_0 \le \gamma\right),
\end{aligned} \tag{5.18}$$

where $\bar{I}_L = \sup_{0 \le t \le T} I_L(t)$. Thus, from (5.17), (5.18), and Lemma 5.1 we have

$$\rho \le \bar{\rho} \le 1 - \operatorname{erf}\left(\frac{1 - \gamma - \bar{I}_L}{\sqrt{2}\eta T}\right). \tag{5.19}$$

Now, in order for (5.19) to be true it must hold that $\bar{I}_L \le 1 - \gamma - (\sqrt{2}\eta T)\operatorname{erf}^{-1}(1 - \bar{\rho})$, a sufficient condition for which is that $I_L(t) \le 1 - \gamma - (\sqrt{2}\eta T)\operatorname{erf}^{-1}(1 - \bar{\rho}), \quad \forall t \in [0, T]$. Then, define a set $\mathcal{S}_I = \{I_L \in \mathbb{R} \mid h(I_L) \ge 0\}$, where $h(I_L) = 1 - \gamma - (\sqrt{2}\eta T)\operatorname{erf}^{-1}(1 - \bar{\rho}) - I_L$, and observe that if h is a valid CBF for the set $\mathcal{S}_I$, i.e., if there exists $\alpha \in \mathcal{K}_\infty$ such that, $\forall I_L \in \mathcal{S}_I$ and $\forall t \in [0, T]$, (5.12) holds then the set $\mathcal{S}$ is probabilistically forward invariant with probability $p = 1 - \rho \ge 1 - \bar{\rho}$. Thus, from (5.19) it follows that since $I_L(0) = 0$ by definition, $\bar{\rho}_0 \le 1 - \operatorname{erf}\left(\frac{1-\gamma}{\sqrt{2}\eta T}\right)$ where $\bar{\rho}_0$ is $\bar{\rho}$ at $t = 0$. Therefore, for $h(I_L) \ge 0$ it must hold that $\rho_d \in [\bar{\rho}_0, 1]$. This completes the proof. □

Remark 5.2. *Under an RA-CBF controller, the upper bound ρ on the system risk is a function only of the initial condition γ, the length of the time interval T, and the maximum effect of the stochastic noise on B over the set $\mathcal{S}$, i.e., η. The function h measures how closely the controller has taken the system to the tolerable risk threshold ρ via actions integrated to form $I_L(t)$.*

Conditions are now introduced under which the bound on the system risk guaranteed by Theorem 5.2 is strictly less than the bound guaranteed under the S-CBF control framework.

Theorem 5.3 (Conditions for Tighter System Risk Bounds)**.** *Let the premises of Theorem 5.1 hold, and let ρ_d be as defined in Theorem 5.2. If B is a risk-aware control barrier function, then*

$$\min_{\rho_d \in \mathcal{R}} \rho_d < \rho_{S\text{-}CBF} \tag{5.20}$$

whenever

$$\eta < \frac{1-\gamma}{\sqrt{2}T\text{erf}^{-1}(1-\gamma)}, \tag{5.21}$$

where η is given by (5.14) *and* $\mathcal{R} = [1 - \text{erf}\left(\frac{1-\gamma}{\sqrt{2}\eta T}\right), 1]$.

Proof. The proof follows immediately from the property observed in Remark 5.1, i.e., that $\rho_{S\text{-}CBF} \geq \gamma$, $\forall \alpha, \beta, T \geq 0$. Then, from Theorem 5.2, $\min_{\rho_d \in \mathcal{R}} \rho_d < \rho_{S\text{-}CBF}$ whenever $1 - \text{erf}\left(\frac{1-\gamma}{\sqrt{2}\eta T}\right) < \gamma$. By rearranging terms, we recover (5.21). □

This result provides guidelines as to when a RA-CBF-based controller would predict lower levels of risk than a S-CBF-based controller, or vice versa. In the robot motion problem from Section 5.1.3, with dynamics (5.9) and barrier function $B(\boldsymbol{z}) = \frac{x^2+y^2}{R_c^2}$ we have $\eta \approx 0.009$. As such, $\min \rho_d \geq \rho_{S\text{-}CBF}$ over the $T = 1$ sec time interval would have required either $\gamma < 1e\text{-}15$ given σ_x, σ_y or $\sigma_x, \sigma_y \approx 50 v_{max} \cdot \Delta t$ given $\gamma = 0.5$, both of which are unrealistic for the problem.

When η given by (5.14) is large, however, the allowable risk specifications using a RA-CBF controller (based on $\min \rho_d$) may not be acceptable. In this case, it may be more useful to design the controller to remain inside a smaller sub-level set $S_\mu = \{\boldsymbol{x} \in \mathbb{R}^n : \ 0 \leq B(\boldsymbol{x}) < \mu \leq 1\}$, or to derive a total risk of the system becoming unsafe by cascading sets $S_{\mu_1}, \ldots, S_{\mu_k}$, as shown in the following result.

Theorem 5.4. *Suppose that the premises of Theorem 5.2 hold. Consider an increasing sequence $\mu_0, \ldots, \mu_k$ such that $\gamma = \mu_0 < \mu_1 < \ldots < \mu_k = 1$ with sub-level sets $\mathcal{S}_{\mu_i} = \{\boldsymbol{x} \in \mathbb{R}^n : \ 0 \leq B(\boldsymbol{x}) < \mu_i\} \subseteq \mathcal{S}$, $\forall i \in \{1, \ldots, k\}$, each of which has η_i defined by* (5.14) *over $\mathcal{S}_{\mu_i}$. If B is a RA-CBF on each set $\mathcal{S}_{\mu_i}$, then $\rho \leq \rho_d$, where ρ_d is a design parameter bounded by*

$$\prod_{i=1}^{k} \left(1 - \text{erf}\left(\frac{\mu_i - \mu_{i-1}}{\sqrt{2}T\eta_i}\right)\right) \leq \rho_d \leq 1. \tag{5.22}$$

Proof. First, observe that by Definition 5.5 the function B is a RA-CBF on the set $\mathcal{S}_{\mu_i}$ if (5.12) holds for all $\boldsymbol{x} \in \mathcal{S}_{\mu_i}$, where the $1-\gamma$ term in (5.13) is replaced by $\mu_i - \gamma$. Let $\rho_{\mu_i} \triangleq P\left(\exists t \in [0,T] : \tilde{\boldsymbol{x}}_t \notin \mathcal{S}_{\mu_i} \mid \tilde{\boldsymbol{x}}_0 \in \mathcal{S}_{\mu_i} \setminus \mathcal{S}_{\mu_{i-1}}\right)$. Then, with B a RA-CBF on $\mathcal{S}_{\mu_i}$, it follows from Theorem 5.2 that

$$\rho_{\mu_i} \leq 1 - \operatorname{erf}\left(\frac{\mu_i - \mu_{i-1}}{\sqrt{2}T\eta_i}\right), \tag{5.23}$$

where η_{μ_i} is defined by (5.14) over the set $\mathcal{S}_{\mu_i}$. By (5.5) and Bayes' rule, we then obtain that $\rho \leq \prod_{i=1}^{k} \rho_{\mu_i}$ and thus by (5.23) we recover (5.22). □

The bound in (5.23) is particularly useful when $\eta_1 < \ldots < \eta_k$, as this is the best reduction in the conservatism in using η over all $\mathcal{S}$. The number of partitions k is a design choice, and should be adjusted according to the desired system risk and each η_i. For control design, the RA-CBF condition (5.12) must be satisfied on each $\mathcal{S}_{\mu_i}$ with a choice of $\rho_{d_i} \geq \rho_{\mu_i}$.

5.3 Numerical Case Studies

In this section, we the efficacy of the proposed RA-CBF controller is highlighted in solving two illustrative examples: the robot problem from Section 5.1.3, and a highway merging problem.

5.3.1 Single-Integrator Robot

The problem setup is identical to that in Example 5.1, with the robot's dynamics given by (5.9) and its controller of the form (5.8) with RA-CBF condition (5.12) substituted for (5.8b) The results were a striking departure from the S-CBF based controller. When an upper bound on system risk was set to 0.505 to match the S-CBF trial, a fraction of 0.458 of the trials violated the safety condition, as shown in Table 5.2. When the RA-CBF controller was used at a maximum system risk

Table 5.2: Risk-Aware CBF Trials $N = 100,000$

Predicted ρ	Measured ρ	γ	η
0.010	10^{-4}	0.50	0.006
0.505	0.458	0.50	0.006

of $\rho = 0.01$, however, not only did the measured ρ satisfy this bound ($1e$-4), but the system trajectories took more aggressive actions toward the boundary of the safe set than the S-CBF controller even when its risk level was set to $\rho_{S\text{-}CBF} = 0.505$, as shown in Figure 5.2.

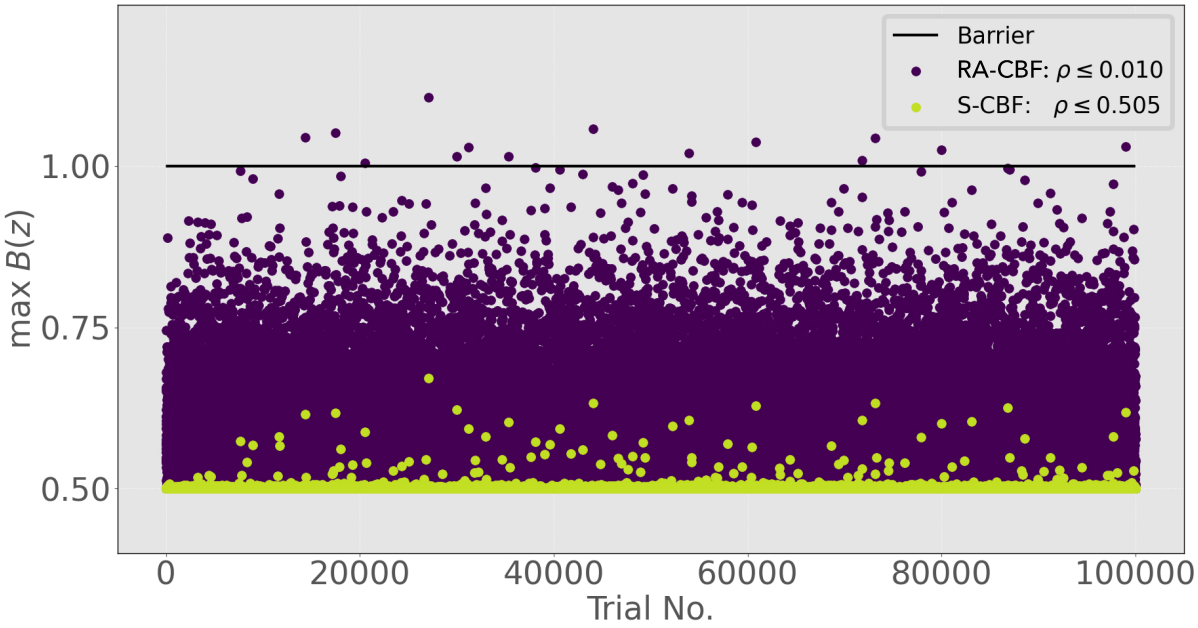

Figure 5.2: Maximum barrier function values ($\max_{0\leq t\leq T} B(\boldsymbol{z}_t)$) over each trial for RA-CBF (resp. S-CBF) with system risk bounded by $\rho \leq 0.01$ (resp. $\rho_{S\text{-}CBF} \leq 0.505$).

5.3.2 Highway Merging

Let $\mathcal{I}$ be an inertial frame with an origin point s_0. Consider a collection of automobiles $\mathcal{A}$, a subset of which travel on a two-lane highway near an on-ramp (i.e., $\mathcal{A}_H \subset \mathcal{A}$), and the remainder of which seek to merge onto the highway via the on-ramp (i.e., $\mathcal{A}_M \subset \mathcal{A}$). Suppose that the dynamics of vehicle $i \in \mathcal{A}$ obey a stochastic bicycle model of the form (5.1) whose drift component is described by [191, Ch. 2] and used to model cars in [180]. The system model for the ith vehicle is provided for completeness:

$$d\boldsymbol{z}_t^i = \big(f(\boldsymbol{z}_t^i) + g(\boldsymbol{z}_t^i)\boldsymbol{u}_t^i\big)dt + \sigma(\boldsymbol{z}_t^i)d\boldsymbol{w}^i, \tag{5.24}$$

for which the state vector is $\boldsymbol{z}^i = [x^i \; y^i \; \psi^i \; \beta^i \; v^i]^\top$ and where

$$f(\boldsymbol{z}_t^i) = \begin{bmatrix} v^i\big(\cos(\psi^i) - \sin(\psi^i)\tan(\beta^i)\big) \\ v^i\big(\sin(\psi^i) + \cos(\psi^i)\tan(\beta^i)\big) \\ \frac{v^i}{l_r}\tan(\beta^i) \\ 0 \\ 0 \end{bmatrix},$$

and

$$g(\boldsymbol{z}_t^i) = \begin{bmatrix} \mathbf{0}_{3\times 2} & \mathbf{0}_{3\times 3} \\ \mathbf{0}_{2\times 3} & \mathbf{I}_{2\times 2} \end{bmatrix},$$

where (omitting the vehicle identifier) x and y denote the position (in m) of the center of gravity (c.g.) of the vehicle with respect to s_0, ψ is the orientation (in rad) of its body-fixed frame, $\mathcal{B}$, with respect to $\mathcal{I}$, β is the slip angle[3] (in rad) of the c.g. of the vehicle relative to $\mathcal{B}$ (with $|\beta| < \frac{\pi}{2}$), and v is the velocity of the rear wheel with respect to $\mathcal{I}$. The control input is $\boldsymbol{u} = [\omega \ a]^\top$, where ω is the angular velocity (in rad/s) of β and a is the acceleration of the rear wheel (in m/s^2). The front and rear wheelbases are l_f and l_r. See Figure 2.1 for a model diagram. The stochastic term is $\sigma(\boldsymbol{z}_t^i) = \boldsymbol{\sigma}^\top \mathbf{I}_{5\times 5}$ with $\boldsymbol{\sigma} = [0 \ 0 \ 0 \ \sigma_a \ \sigma_\omega]^\top$. The vector $\boldsymbol{w} \in \mathbb{R}^5$ is the 5D standard Wiener process.

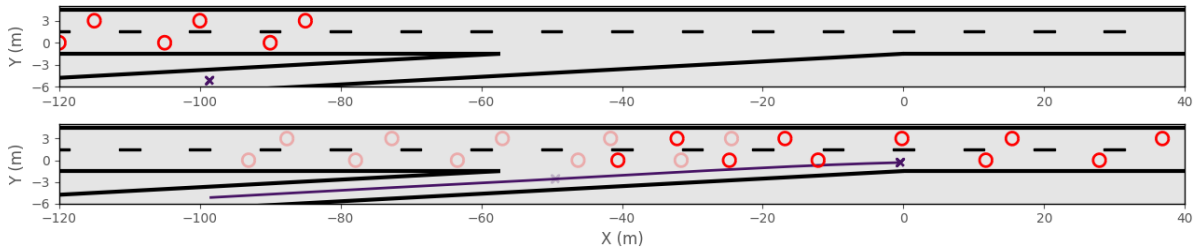

Figure 5.3: Snapshots at $t = 0.0$s (a) and $t = 4.0$s (with $t = 2.0s$ translucent) (b) of one trial from the empirical study on the RA-CBF-QP controller in the highway merging scenario. Traffic flows left to right, the ego vehicle is a blue X, and highway vehicles are red circles.

A set of 1000 trials of a $T = 4$s highway merging scenario was simulated with 11 vehicles, where $\mathcal{A}_M = \{0\}$ was the ego vehicle and $\mathcal{A}_H = \{1, \ldots, 10\}$. Highway vehicles $i \in \mathcal{A}_H$ were initialized 15m apart in the x direction, and distributed evenly between lanes 1 ($y = 0$) and 2 ($y = 3$). Their initial velocities were distributed according to $v_{i,0} \sim U[29, 31]$. The ego vehicle was initialized 98.75m down the on-ramp with an initial velocity $v_{e,0} \sim U[24, 26]$ such that (deterministically) under its nominal acceleration policy it would collide directly with vehicle 2. The noise components were $\sigma_a = A_{drag}\Delta t$ and $\sigma_\omega = \sigma_a \frac{\bar{\omega}}{\bar{a}}$, where $\bar{\omega} = \frac{\pi}{16}$ (rad/s) and $\bar{a} = 2.0$ (m/s^2) define the input constraints $a^i \in [-\bar{a}, \bar{a}]$ and $\omega^i \in [-\bar{\omega}, \bar{\omega}]$, and $A_{drag} = 0.1 + 5\bar{v} + 0.25\bar{v}^2$, with $\bar{v} = 35$ (m/s), such that the noise at one standard deviation represents the acceleration due to aerodynamic drag [227] traveling at 35m/s. The ego vehicle was controlled using (5.8) with 11 RA-CBF constraints corresponding to the occupied sub-level set $\mathcal{S}_{\mu_i}$, where it was chosen that $\mu_i = i/5$ for $i \in \{1, \ldots, 5\}$. The 10 ego collision avoidance constraints were encoded via $B_{ei}(\boldsymbol{z}^e, \boldsymbol{z}^i) = e^{-h_{ei}(\boldsymbol{z}^e, \boldsymbol{z}^i)}$, where $h_{ei}(\boldsymbol{z}^e, \boldsymbol{z}^i)$ is the relaxed future-focused CBF (rff-CBF) (introduced for collision avoidance in Chapter 2) with $\gamma(h_0) = 0.1h_0$. The road constraints were en-

[3] β is related to the steering angle δ via $\tan\beta = \frac{l_r}{l_r + l_f}\tan\delta$, where $l_f + l_r$ is the wheelbase with l_f (resp. l_r) the distance from the c.g. to the center of the front (resp. rear) wheel.

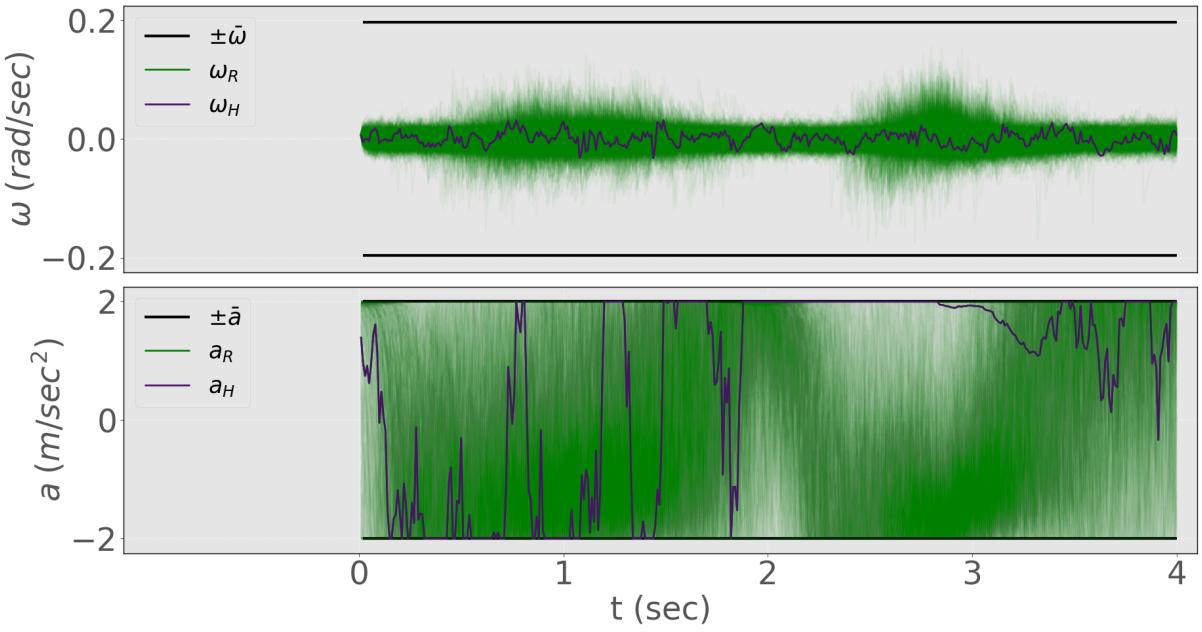

Figure 5.4: Ego vehicle control inputs from both the highlighted trial in Figure 5.3 (subscript H) and remaining trials (subscript R).

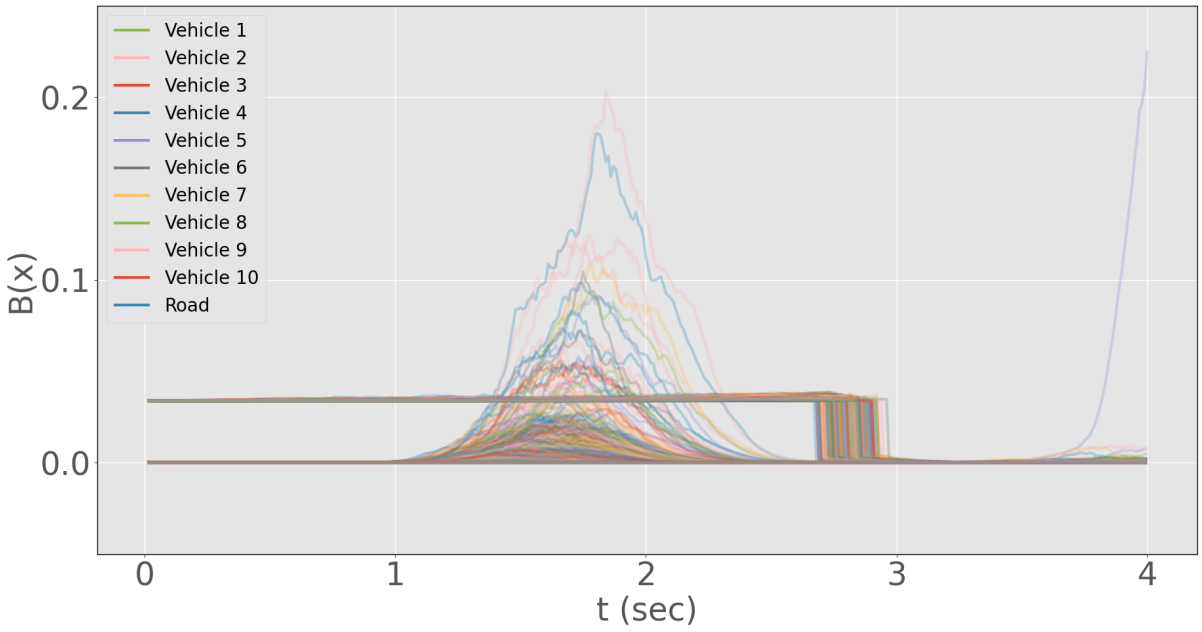

Figure 5.5: RA-CBF trajectories over 1000 highway merging trials.

coded with a rff-CBF of the form $B_r(\boldsymbol{z}^e) = e^{-h_r(\boldsymbol{z}^e)}$ for $h_r(\boldsymbol{z}^e) = h_{r,0}(\boldsymbol{z}^e, 0) + h_{r,0}(\boldsymbol{z}^e, 1)$, where

$$h_{r,0}(\boldsymbol{z}^e, \tau) = -\left(x^e \tan(\theta) + \frac{w_l}{2\cos(\theta)} - (y^e + \dot{y}^e \tau - y_l)\right)^2$$

with θ the road angle with respect to the x-axis, w_l the width of a lane, and y_l the lane center. For all RA-CBFs, the corresponding η_i values were determined numerically by simulating 1000 trials and taking $\eta_i = \max_{\boldsymbol{x} \in S_{\mu_i}} \|L_\sigma B(\boldsymbol{x})\|$ over all trials and all time. The resulting η_i values are provided in Table 5.3. For the on-ramp, the angle of attack was $\theta = 3^\circ$ ($\theta = 0^\circ$ for highway lanes). The ego nominal control $\boldsymbol{u}_0$ was the LQR law detailed in Appendix A based on the desired lane and velocity ($v_d = 30$m/s). For naturalistic driving behavior, the intelligent driver model (IDM)[228] was used

Table 5.3: η_i values derived empirically

CBF	η_1	η_2	η_3	η_4	η_5
Road	0.012	0.025	0.035	0.046	0.067
Collision	0.018	0.031	0.049	0.063	0.076

to compute acceleration inputs a^i of the highway vehicles $i \in \mathcal{A}_H$. For varying driver aggression, we randomized the vehicles' desired time gaps in the IDM according to $\tau \sim U[0.25, 0.75]$. Their steering inputs ω^i were computed using LQR based on the desired heading ($\psi_d = 0$).

Based on η_i from Table 5.3, a simulation length of $T = 4$ sec, known γ for all $B(\boldsymbol{z}_0)$, the minimum specifiable risks associated with leaving each sub-level set $\mathcal{S}_{\mu_i}$ for road safety and collision avoidance are provided in Table 5.4. The $\rho_{d,i}$ values provided in Table 5.5 were selected such that

Table 5.4: ρ_i values for sub-level sets $\mathcal{S}_{\mu_i}$

CBF	ρ_1	ρ_2	ρ_3	ρ_4	ρ_5
Road	8.58e-4	0.046	0.153	0.277	0.456
Collision	0.026	0.107	0.308	0.427	0.511

the probability of remaining safe with respect to the road is 0.99999, the probability of remaining safe with respect to all 10 highway vehicles combined is 0.991, and thus the total probability of safety is $p \geq 0.99$, which yields $\rho \leq 0.01$.

Table 5.5: Specified risk bounds $\rho_{d,i}$ for sub-level sets $\mathcal{S}_{\mu_i}$

CBF	$\rho_{d,1}$	$\rho_{d,2}$	$\rho_{d,3}$	$\rho_{d,4}$	$\rho_{d,5}$
Road	0.001	0.1	0.25	0.5	0.6
Collision	0.05	0.15	0.4	0.5	0.6

Over 1000 simulated trials, the RA-CBF based controller safely merged 1000 times, satisfying the risk bound of $\rho \leq 0.01$. Figure 5.3 highlights one of these safe merges in which the ego vehicle merges behind vehicle 2, where the applied control inputs are shown in Figure 5.4. In this study, it was observed that in all 1000 trials the ego vehicle merged behind vehicle 2. In another study, in which a risk of $\rho \leq 0.12$ was specified, it was observed that the ego vehicle safely merged in 914 of the 1000 trials ($p = 0.914$). Interestingly, of these 914 safe trials, the ego vehicle merged behind vehicle 2 at a rate of 0.749 and merged ahead of it the remaining 0.251 fraction of safe trials, an indicator of the willingness of the ego vehicle in the second study to take on additional risk.

5.4 Conclusion

In this chapter, a new class of risk-aware control barrier functions was proposed for probabilistically safe control design of stochastic, nonlinear, control-affine systems over a finite time interval. A motivating example showed the extreme conservatism exhibited by an existing state-of-the-art approach, and, as such, conditions were derived under which RA-CBF-based control design confers a tighter bound on the probability of incurring safety violations. An empirical study of over 400,000 trials validated these theoretical novelties in simulation. Then, an algorithm for further decreasing conservatism was proposed in the form of a recursive application of the RA-CBF to subsets of the safe set, and its efficacy was demonstrated on an autonomous vehicle highway merging problem required to satisfy a safety specification of 99.1%.

CHAPTER 6

Consolidated Control Barrier Functions: Synthesis and Online Verification via Adaptation

In the preceding chapters, the advancements to the theory of Control Barrier Function (CBF)-based safe control design have all required a foundational (and often strong) assumption, namely that the CBF *candidate* (or candidates) is, in fact, *valid*. Proving that this assumption holds in practice is challenging, particularly so for systems facing multiple spatiotemporal and input constraints, a problem that is especially relevant in practical applications, for example involving autonomous vehicles and mobile robots. The prevailing intuition behind the results presented in this chapter is the following: given a set of arbitrarily many spatiotemporal constraint functions, their relative weightings (i.e., how strongly each function affects the space of admissible control inputs) ought to vary as the system moves through the state space, and ought to vary, specifically, in a way that permits simultaneous spatiotemporal and input constraint satisfaction in perpetuity. In this chapter, therefore, the problem of valid CBF synthesis is undertaken *online* via parameter adaptation for a class of control-affine, nonlinear systems subject to multiple spatiotemporal and input constraints.

In pursuit of this objective, after reviewing preliminaries in Section 6.1, the notion of a Consolidated Control Barrier Function (C-CBF) candidate is formalized in Section 6.2. It is shown that the C-CBF candidate admits a zero super-level set that under-approximates the intersection of all spatiotemporal constraint sets (i.e., the complete constraint set) and, consequently, that the system trajectories evolve within the complete constraint set if the C-CBF is proven to be valid. For verification of validity, two parameter adaptation laws are introduced respectively for the cases of unbounded and limited control authority: the first is taken to be the solution to a Quadratic Program (QP) enforcing that the C-CBF dynamics are always controllable, i.e. that the C-CBF singularity is avoided; the second evolves according to new dynamical system, the state of which tracks the solution to a time-varying optimization problem via a predictor-corrector interior point method. The C-CBF is rendered valid whenever a solution to the adaptation-based optimization problems exist, and as such is synthesized in a C-CBF-QP control law, the viability of which is discussed in Section 6.3. Demonstrations of the proposed adaptive C-CBF-QP control law are

conducted in Section 6.4 for both single- and multi-agent scenarios, with which it is shown that the method is capable of satisfying constraint functions of arbitrary relative degree.

The results of this chapter are based partly on [185] and [186].

6.1 Preliminaries and Problem Formulation

In this section, preliminaries on time-varying convex optimization and constrained control using CBFs are reviewed, and then the problem under consideration is introduced.

Before proceeding, the following supplementary notation is required. Given a positive-definite matrix $\boldsymbol{M} \in \mathbb{R}^{n\times n}$ and scalar $a > 0$, the relation $\boldsymbol{M} \succeq a\boldsymbol{I}$ implies that all eigenvalues of $\boldsymbol{M}$ are greater than or equal to a, where $\boldsymbol{I}$ denotes the identity matrix of appropriate dimension. A function $\phi : \mathbb{R}\times\mathbb{R} \to \mathbb{R}$ belongs to class-$\mathcal{LL}$ (i.e., $\phi \in \mathcal{LL}$) if for each fixed r (resp. s), the function $\phi(r, s)$ is decreasing with respect to s (resp. r) and is such that $\phi(r, s) \to 0$ for $s \to \infty$ (resp. $r \to \infty$). Given a multivariate function $V : \mathbb{R}\times\mathbb{R}^n$ denoted by $V(t, \boldsymbol{x})$, let $\nabla_t V(t, \boldsymbol{x})$ denote the derivative of V with respect to $t \in \mathbb{R}$, $\nabla_{tt} V(t, \boldsymbol{x})$ its second derivative, $\nabla_{\boldsymbol{x}} V(t, \boldsymbol{x})$ the row vector of derivatives (i.e., gradient) of V with respect to $\boldsymbol{x} \in \mathbb{R}^n$, and $\nabla_{\boldsymbol{xx}} V(t, \boldsymbol{x})$ its Hessian matrix.

6.1.1 Predictor-Corrector Interior Point Method

Consider a time-varying, possibly non-convex optimization problem, a local solution trajectory to which takes the form

$$\boldsymbol{y}^*(t) = \underset{\boldsymbol{y}\in\mathbb{R}^p}{\arg\min}\ J(t, \boldsymbol{y}), \quad \text{s.t. } c_i(t, \boldsymbol{y}) \le 0,\ \forall i \in [q], \tag{6.1}$$

where $J : \mathbb{R}\times\mathbb{R}^p \to \mathbb{R}$ is a (uniformly strongly convex) objective function, the collection of $q \ge 0$ (not necessarily convex) inequality constraints is $c_i : \mathbb{R}\times\mathbb{R}^p \to \mathbb{R}$ for $i \in [q]$, and where all of J and c_i are twice continuously differentiable in $\boldsymbol{y}$ and piecewise continuously differentiable in t. Denote the feasible region of (6.1) as $\mathcal{Y}(t) = \{\boldsymbol{y} \in \mathbb{R}^p : c_i(t, \boldsymbol{y}) \le 0, \forall i \in [q]\}$, and further assume that the feasible region has an interior point at all times, i.e., that $\mathrm{Int}(\mathcal{Y}(t)) \neq \emptyset$, $\forall t \ge 0$. Though J is assumed to be uniformly strongly convex, without convexity of the inequality constraints it is not guaranteed that (6.1) is the global solution trajectory; nevertheless, barrier function methods may be employed to approximate a local solution (6.1) (see e.g., [229, Sec. 9.4]). Consider such an approximate solution $\hat{\boldsymbol{y}}^*(t)$, constructed using Frisch's logarithmic barrier functions:

$$\hat{\boldsymbol{y}}^*(t) = \underset{\boldsymbol{y}\in\mathbb{R}^p}{\arg\min}\ \Psi(t, \boldsymbol{y}) \triangleq J(t, \boldsymbol{y}) - \frac{1}{s}\sum_{i=1}^{q} \log(-c_i(t, \boldsymbol{y})), \tag{6.2}$$

where $s > 0$ is a barrier design parameter. In the limit, as $s \to \infty$, the function $-\frac{1}{s}\log(-c_i(t,\boldsymbol{y})) \to \mathbb{I}_-(c_i(t,\boldsymbol{y}))$, where $\mathbb{I}_- : \mathbb{R} \to \{0,\infty\}$ is defined such that $\mathbb{I}_-(u) = 0$ for $u \leq 0$ and $\mathbb{I}_-(u) = \infty$ for $u > 0$. In addition to facilitating this non-smooth function approximation, the barrier parameter may also convexify the augmented objective function Ψ. Though $\log(-c_i)$ may be non-convex, it is assumed (similar to e.g., [230]) that for sufficiently large s the function Ψ is strongly, uniformly convex, stated formally as follows.

Assumption 6.1 (**Convexity**). *For all $\boldsymbol{y} \in \mathrm{Int}(\mathcal{Y}(t))$, $\forall t \geq 0$, there exist $s, a > 0$ such that*

$$\nabla_{\boldsymbol{yy}}\Psi(t,\boldsymbol{y}) \triangleq \nabla_{\boldsymbol{yy}}J(t,\boldsymbol{y}) - \frac{1}{s}\sum_{i=1}^{q}\nabla_{\boldsymbol{yy}}\log(-c_i(t,\boldsymbol{y})) \succeq a\boldsymbol{I}.$$

In practice, for strongly uniformly convex J the above may be satisfied by using sufficiently large s, which may be determined either online or iteratively offline. It follows then that $\nabla_{\boldsymbol{yy}}\Psi$ exists and is bounded, which permits the review of a version of [231, Lemma 2] relating the approximate (locally) optimal trajectory $\hat{\boldsymbol{y}}^*(t)$ given by (6.2) to the solution of a continuous-time dynamical system.

Lemma 6.1 (**Strictly Feasible Convergence to Approximate Solution**). *Let $\hat{\boldsymbol{y}}^*(t)$ be defined by* (6.2) *and $\boldsymbol{z}(t)$ be the solution to the following ordinary differential equation,*

$$\begin{aligned} \dot{\boldsymbol{z}} &= -\nabla_{\boldsymbol{zz}}^{-1}\Psi(t,\boldsymbol{z})\big[\boldsymbol{P}\nabla_{\boldsymbol{z}}\Psi(t,\boldsymbol{z}) + \nabla_{\boldsymbol{z}t}\Psi(\boldsymbol{z},t)\big], \\ \boldsymbol{z}(0) &= \boldsymbol{z}_0 \in \mathcal{Y}(0), \end{aligned} \tag{6.3}$$

where $\boldsymbol{P} \in \mathbb{R}^{p\times p}$ is a positive-definite gain matrix satisfying $\boldsymbol{P} \succeq b\boldsymbol{I}$ for some $b > 0$, and $\Psi : \mathbb{R}\times\mathbb{R}^p$ is defined as in (6.2) *and known to satisfy Assumption 6.1. Then, $\boldsymbol{z}(t) \in \mathcal{Y}(t)$ for all $t \geq 0$ and*

$$\|\boldsymbol{z}(t) - \hat{\boldsymbol{y}}^*(t)\| \leq Ce^{-bt},$$

where $0 \leq C \triangleq \frac{1}{a}\|\nabla_{\boldsymbol{z}}\Psi(\boldsymbol{z}(0),0)\| < \infty$.

The above result implies that the solution $\boldsymbol{z}(t)$ to (6.3) approaches the approximate optimal trajectory $\hat{\boldsymbol{y}}^*(t)$ asymptotically while remaining in the feasible region $\mathcal{Y}(t)$ at all times. Intuitively, the dynamics of (6.3) consist of a prediction term

$$\dot{\boldsymbol{z}}_p = -\nabla_{\boldsymbol{zz}}^{-1}\Psi(t,\boldsymbol{z})\nabla_{\boldsymbol{z}t}\Psi(\boldsymbol{z},t),$$

and a Newton-like correction term

$$\dot{\boldsymbol{z}}_c = -\nabla_{\boldsymbol{zz}}^{-1}\Psi(t,\boldsymbol{z})\boldsymbol{P}\nabla_{\boldsymbol{z}}\Psi(t,\boldsymbol{z}),$$

which together ensure that $\boldsymbol{z}(t) \in \mathrm{Int}(\mathcal{Y}(t))$ at all times (hence predictor-corrector interior point method). The findings of Lemma 6.1 are required in the proof of one of the main results on parameter adaptation for constrained control design presented in Section 6.2, the premises of which will now be reviewed.

6.1.2 Constrained Control Design

The remainder of this chapter considers a class of nonlinear, control-affine dynamical systems of the form

$$\dot{\boldsymbol{x}} = f(\boldsymbol{x}(t)) + g(\boldsymbol{x}(t))\boldsymbol{u}(t), \quad \boldsymbol{x}(0) = \boldsymbol{x}_0 \tag{6.4}$$

where $t \in \mathcal{T} = [t_0, \infty)$ represents time, $\boldsymbol{x} \in \mathbb{R}^n$ and $\boldsymbol{u} \in \mathcal{U} \subset \mathbb{R}^m$ are the state and control input vectors, with $\mathcal{U}$ the input constraint set, and where $f : \mathbb{R}^n \to \mathbb{R}^n$ and $g : \mathbb{R}^n \to \mathbb{R}^{n\times m}$ are known and locally Lipschitz. It is assumed that the control input $\boldsymbol{u} : \mathcal{T} \to \mathcal{U}$ yields a unique solution to (6.4) for all $t \in \mathcal{T}$.

Consider one of $c \geq 1$ (possibly time-varying) twice continuously differentiable constraint functions $h_i : \mathcal{T} \times \mathbb{R}^n \to \mathbb{R}$, which may encode a safety, performance, and/or specification based constraint, and let the set of states over which this particular constraint is satisfied at a given time be

$$\mathcal{S}_i(t) = \{\boldsymbol{x} \in \mathbb{R}^n \mid h_i(t, \boldsymbol{x}) \geq 0\}. \tag{6.5}$$

The set of all constraint functions is denoted as

$$\mathcal{H} = \{h_1, \cdots, h_c\}, \tag{6.6}$$

such that the focus of this chapter is synthesizing a control law that confines the state within the intersection of all individual constraint sets, hereafter referred to as the complete constraint set:

$$\mathcal{S}(t) = \bigcap_{i=1}^{c} \mathcal{S}_i(t). \tag{6.7}$$

It is assumed that the complete constraint set possesses an interior point, i.e., $\mathrm{Int}(\mathcal{S}(t)) \neq \emptyset$, $\forall t \in \mathcal{T}$, and thus the goal is to design a controller that renders a subset $\mathcal{D}(t) \subseteq \mathcal{S}(t)$ *forward invariant* with respect to the system (6.4), i.e., to ensure that $\boldsymbol{x}(0) \in \mathcal{D}(0) \subseteq \mathcal{S}(0) \implies \boldsymbol{x}(t) \in \mathcal{D}(t) \subseteq \mathcal{S}(t)$, $\forall t \in \mathcal{T}$. Of note is that the functions h_i are required to be twice continuously differentiable, a stricter (though often reasonable) condition than the more typical continuous differentiability requirement, for reasons pertaining to the proposed parameter adaptation law in Section 6.2.

For the remainder of this section, preliminaries specific to the case of one constraint function

($c = 1$) will be reviewed. Under such circumstances, one approach to controlled set invariance is to use CBFs in the control design. In what follows, the notion of a time-varying CBF inspired by [232, 173] is presented, and it is then shown to enforce forward invariance via control design.

Definition 6.1. *Given a time-varying set $\mathcal{S}_i(t)$, $t \in \mathcal{T}$, defined by* (6.5) *for a twice continuously differentiable function $h_i : \mathcal{T} \times \mathbb{R}^n \to \mathbb{R}$, the function h_i is a* ***control barrier function*** *(CBF) for the system* (6.4) *with respect to $\mathcal{S}_i(t)$ if there exists a locally Lipschitz continuous extended class-$\mathcal{K}_\infty$ function α such that, for all $\boldsymbol{x} \in \mathcal{S}_i(t)$, $t \in \mathcal{T}$,*

$$\sup_{\boldsymbol{u} \in \mathcal{U}} \dot{h}_i(t, \boldsymbol{x}, \boldsymbol{u}) \geq -\alpha\big(h_i(t, \boldsymbol{x})\big). \tag{6.8}$$

Equation (6.8) is referred to as the CBF condition. Note that if the function h_i has relative-degree[1] $r > 1$ with respect to the system (6.4) then the control input $\boldsymbol{u}$ has no effect on (6.8). In many cases this deficiency can be resolved by deriving high-order CBFs (see e.g., [168, 233] for details), though this may require careful parameter design [40]. One of the methods proposed in Section 6.2, however, requires no assumptions about the relative-degree of the constraint functions under consideration, a fact that is highlighted in a numerical case study in Section 6.4. For a particular constraint function h_i, the set of control actions satisfying its CBF condition (6.8) is referred to as its CBF control set, and is denoted by

$$\begin{aligned} \mathcal{U}_{h_i}(t, \alpha) = \big\{ &\boldsymbol{u} \in \mathcal{U} : \\ &\dot{h}_i(t, \boldsymbol{x}(t), \boldsymbol{u}) + \alpha\big(h_i(t, \boldsymbol{x}(t))\big) \geq 0 \big\}, \end{aligned} \tag{6.9}$$

noting that $\mathcal{U}_{h_i}$ is parameterized by the set of functions $\alpha \in \mathcal{K}_\infty$. In the following result inspired by [173], it is shown that controls belonging to the CBF control set $\mathcal{U}_{h_i}$ render the constraint set $\mathcal{S}_i(t)$ forward invariant.

Theorem 6.1. *If h_i is a control barrier function for the system* (6.4) *with respect to the set $\mathcal{S}_i(t)$ defined by* (6.5)*, then $\boldsymbol{x}(0) \in \mathcal{S}_i(0) \implies \boldsymbol{x}(t) \in \mathcal{S}_i(t)$ for all $t \in \mathcal{T}$, i.e., $\mathcal{S}_i(t)$ is forward invariant.*

Proof. Consider an absolutely continuous function $\eta : \mathcal{T} \to \mathbb{R}$ and locally Lipschitz function $\gamma \in \mathcal{K}_\infty$. By [171, Lem. 2] it is true that if $\dot{\eta}(t) \geq -\gamma(\eta(t))$ for every $t \in \mathcal{T}$ and $\eta(0) \geq 0$, then $\eta(t) \geq 0$ for all $t \in \mathcal{T}$. With assumed unique solutions to (6.4) and taking $\eta(t) = h_i(t, \boldsymbol{x}(t))$ and $\gamma = \alpha$, it follows that $h_i(t, \boldsymbol{x}(t)) \geq 0$ for all $t \in \mathcal{T}$ and thus $\mathcal{S}_i(t)$ is forward invariant. □

[1] A function $p : \mathbb{R}_+ \times \mathbb{R}^n \to \mathbb{R}$ is said to be of relative-degree r with respect to the dynamics (6.4) if r is the number of times p must be differentiated before one of the control inputs u appear explicitly.

Note that h_i being a CBF implies that there exists $\alpha \in \mathcal{K}_\infty$ such that the CBF control set is non-empty for all time, i.e., $\mathcal{U}_{h_i}(t,\alpha) \neq \emptyset$, $\forall t \in \mathcal{T}$. Under such circumstances, for the class of control-affine systems described by (6.4) the CBF condition (6.8) may be included as a linear constraint in the following QP-based control law (see e.g., [180, 3]):

$$\boldsymbol{u}^*(t) = \arg\min_{\boldsymbol{u}\in\mathcal{U}} \frac{1}{2}\|\boldsymbol{u} - \boldsymbol{u}_0(t,\boldsymbol{x})\|^2 \tag{6.10a}$$

$$\text{s.t.}$$

$$\frac{\partial h_i}{\partial t} + \frac{\partial h_i}{\partial \boldsymbol{x}} f(\boldsymbol{x}) + \frac{\partial h_i}{\partial \boldsymbol{x}} g(\boldsymbol{x})\boldsymbol{u} \geq -\alpha\big(h_i(t,\boldsymbol{x})\big), \tag{6.10b}$$

where (6.10a) seeks to produce a control solution $\boldsymbol{u}^* \in \mathcal{U}$ that deviates minimally from some desired input $\boldsymbol{u}_0 : \mathcal{T} \times \mathbb{R}^n \to \mathbb{R}^m$, and (6.10b) encodes the CBF condition (6.8). For systems without input constraints (i.e., $\mathcal{U} = \mathbb{R}^m$), other works (e.g., [234]) highlight that the constraint function h_i is a CBF if there exists a function $\alpha \in \mathcal{K}_\infty$ satisfying

$$\begin{aligned} \frac{\partial h_i}{\partial \boldsymbol{x}} g(\boldsymbol{x}) = \boldsymbol{0} \implies \\ \frac{\partial h_i}{\partial t} + \frac{\partial h_i}{\partial \boldsymbol{x}} f(\boldsymbol{x}) + \alpha(h_i(t,\boldsymbol{x})) > 0 \end{aligned} \tag{6.11}$$

for all $\boldsymbol{x}(t) \in \mathcal{S}_i(t)$, $t \in \mathcal{T}$. For systems with bounded inputs (i.e., $\mathcal{U} \neq \mathbb{R}^m$), the analogous requirement is that

$$\begin{aligned} \sup_{\boldsymbol{u}\in\mathcal{U}} \frac{\partial h_i}{\partial \boldsymbol{x}} g(\boldsymbol{x})\boldsymbol{u} = \delta \implies \\ \frac{\partial h_i}{\partial t} + \frac{\partial h_i}{\partial \boldsymbol{x}} f(\boldsymbol{x}) + \alpha(h_i(t,\boldsymbol{x})) > -\delta \end{aligned} \tag{6.12}$$

for all $\boldsymbol{x}(t) \in \mathcal{S}_i(t)$, $t \in \mathcal{T}$, $\delta \geq 0$. Here, δ serves to define the strongest drift to the CBF dynamics which the controller can overcome to satisfy the CBF condition (6.8). It is worth highlighting that both cases (6.11) and (6.12) are equivalent to the condition that the CBF control set $\mathcal{U}_{h_i}$ is never empty. While for systems with unlimited control authority it may be straightforward for certain constraints to show that $\mathcal{U}_{h_i} \neq \emptyset$ (see e.g., the collision avoidance constraint between two vehicles in [190]), this is generally much more difficult under multiple constraints. Verifying that (6.12) is true a priori for a given constraint function, moreover, is challenging even under a single constraint. Unless (6.11) or (6.12) are proven to hold for their respective systems, the constraint function h_i is only a *candidate* CBF for (6.4) with respect to $\mathcal{S}_i(t)$, and thus may or may not render $\mathcal{S}_i(t)$ forward invariant. Recent works have addressed the problem of synthesizing a *valid* CBF via offline analysis [176], by construction [168], inclusion of additional constraints in the

QP controller [46], or through online adaptation [169]. The scopes of these solutions, however, are limited to only one time-invariant constraint function ($c = 1$) and therefore do not extend to situations in which the state must remain within a complete constraint set of the form (6.7) comprised of multiple, time-varying constituent constraint functions.

6.1.3 Problem Statements

The main open problem in constrained control design under multiple state constraints is in certifying that all constraints will satisfied *jointly* in perpetuity. This chapter bridges this gap by 1) synthesizing one C-CBF candidate from the collection of constraint functions and then 2) certifying the C-CBF candidate as *valid* via online parameter adaptation.

Problem 6.1. *Consider a collection of $c \geq 1$ twice continuously differentiable constraint functions $h_i : \mathcal{T} \times \mathbb{R}^n \to \mathbb{R}$ corresponding to constraint sets $\mathcal{S}_i(t)$ given by* (6.5)*. Design a new constraint function $H : \mathcal{T} \times \mathbb{R}^c_+ \times \mathbb{R}^n \to \mathbb{R}$ with constituent constraint function weights $\boldsymbol{w} = (w_1, \cdots, w_c) \in \mathbb{R}^c_+$ such that the set*

$$\mathcal{D}(t, \boldsymbol{w}) = \{\boldsymbol{x} \in \mathbb{R}^n \mid H(t, \boldsymbol{w}, \boldsymbol{x}) \geq 0\} \tag{6.13}$$

satisfies $\mathcal{D}(t, \boldsymbol{w}) \subseteq \mathcal{S}(t)$ for the complete constraint set given by (6.7)*, $\forall t \in \mathcal{T}$.*

This new constraint function H is referred to as a C-CBF candidate, the zero super-level set $\mathcal{D}(t, \boldsymbol{w})$ of which is to be rendered forward invariant. Consolidating many separate constraint functions h_i into one function H means that each weight w_i affects the relative importance of h_i in H (and by extension the set $\mathcal{D}$). It also permits, however, the use of existing CBF results for certifiable constrained control design. Notably, the class of QP-based controllers (6.10) may be used with the new function H to render $\mathcal{D}$ forward invariant and thus to ensure that the state remains within the complete constraint set $\mathcal{S}$. Proving that H is a valid C-CBF, however, may be difficult when using static constituent function weights $\boldsymbol{w}$, i.e., weights chosen a priori with $\dot{\boldsymbol{w}} \equiv \boldsymbol{0}_{c\times 1}$. Thus, the design of a weight adaptation law $\dot{\boldsymbol{w}} = \omega(t, \boldsymbol{w}, \boldsymbol{x}, \boldsymbol{u})$ for $\omega : \mathcal{T} \times \mathbb{R}^c_+ \times \mathbb{R}^n \times \mathcal{U} \to \mathbb{R}^c$ is investigated to vary the weights $\boldsymbol{w}$ online and, in doing so, render the C-CBF candidate H valid. With $\boldsymbol{w}$ then dependent on time t, in the remainder the dependence of $\mathcal{D}$ on the weights $\boldsymbol{w}$ is omitted for conciseness. To render the C-CBF candidate H valid is to ensure that

$$\sup_{\boldsymbol{u}\in\mathcal{U}} \dot{H}(t, \boldsymbol{w}, \dot{\boldsymbol{w}}, \boldsymbol{x}, \boldsymbol{u}) \geq -\alpha\big(H(t, \boldsymbol{w}, \boldsymbol{x})\big), \tag{6.14}$$

holds for all $\boldsymbol{x}(t) \in \mathcal{D}(t)$, $\forall t \in \mathcal{T}$. Notice that the above is to the C-CBF candidate H as (6.8) is to a CBF candidate h_i. Thus, (6.14) is referred to as the C-CBF condition. While it has been established that the CBF condition (6.8) is affine in the control input $\boldsymbol{u}$ for the class of systems

described by (6.4), the C-CBF condition (6.14) is only affine in $\boldsymbol{u}$ if the adaptation law $\dot{\boldsymbol{w}}$ is affine in (or independent of) $\boldsymbol{u}$, i.e., if $\dot{\boldsymbol{w}}$ takes the form

$$\dot{\boldsymbol{w}} = \omega(t, \boldsymbol{w}, \boldsymbol{x}, \boldsymbol{u}) \triangleq \mu(t, \boldsymbol{w}, \boldsymbol{x}) + \nu(t, \boldsymbol{w}, \boldsymbol{x})\boldsymbol{u}, \tag{6.15}$$

for some functions $\mu : \mathcal{T} \times \mathbb{R}^c_+ \times \mathbb{R}^n \to \mathbb{R}^c$ and $\nu : \mathcal{T} \times \mathbb{R}^c_+ \times \mathbb{R}^n \to \mathbb{R}^{c \times m}$. With $\dot{\boldsymbol{w}}$ taking this form, the C-CBF condition (6.14) may be included directly as a linear constraint in a QP-based control law of the form (6.10). As such, the second problem under consideration is formally introduced.

Problem 6.2. *Given a function $\alpha \in \mathcal{K}_\infty$, a C-CBF candidate H, and its corresponding CBF control set*

$$\begin{aligned} \mathcal{U}_H(t, \alpha) = \big\{ &\boldsymbol{u} \in \mathcal{U} : \\ &\dot{H}(t, \boldsymbol{w}, \dot{\boldsymbol{w}}, \boldsymbol{x}, \boldsymbol{u}) + \alpha\big(H(t, \boldsymbol{w}, \boldsymbol{x})\big) \geq 0 \big\}, \end{aligned} \tag{6.16}$$

design a control-affine weight adaptation law of the form (6.15) *such that $\mathcal{U}_H(t, \alpha) \neq \emptyset$ for all $t \in \mathcal{T}$, i.e., such that*

$$\begin{aligned} \sup_{\boldsymbol{u} \in \mathcal{U}} \left(\frac{\partial H}{\partial \boldsymbol{x}} g(\boldsymbol{x}) + \frac{\partial H}{\partial \boldsymbol{w}} \nu(t, \boldsymbol{w}, \boldsymbol{x}) \right) \boldsymbol{u} = \delta \implies \\ \frac{\partial H}{\partial t} + \frac{\partial H}{\partial \boldsymbol{x}} f(\boldsymbol{x}) + \frac{\partial H}{\partial \boldsymbol{w}} \mu(t, \boldsymbol{w}, \boldsymbol{x}) + \alpha\big(H(t, \boldsymbol{w}, \boldsymbol{x})\big) > -\delta, \end{aligned} \tag{6.17}$$

for all $\boldsymbol{x}(t) \in \mathcal{D}(t)$, $\forall t \in \mathcal{T}$, $\delta \geq 0$.

Notice that (6.17) constitutes a sufficient condition for the satisfaction of the C-CBF condition (6.14), and therefore ensures that the CBF control set $\mathcal{U}_H(t, \alpha)$ is never empty.

6.2 Consolidated Control Barrier Functions

In this section, a solution is introduced to Problem 6.1 in the form of a C-CBF candidate that smoothly synthesizes multiple constraint functions into one whose zero super-level set under-approximates the complete constraint set. Then, two solutions to Problem 6.2 are proposed in the form of parameter adaptation laws for adapting the weights of the C-CBF's constituent functions such that the C-CBF is rendered valid, i.e., so that the condition (6.14) is viable in perpetuity, for 1) the class of systems described by (6.4) with unbounded control authority, and 2) the same class of systems subject to input constraints.

6.2.1 Consolidated CBFs

Given the set of constraint functions $\mathcal{H}$ (6.6) with cardinality $c \geq 1$, the form of the C-CBF candidate $H : \mathcal{T} \times \mathbb{R}_+^c \times \mathbb{R}^n \to \mathbb{R}$ is

$$H(t, \boldsymbol{w}, \boldsymbol{x}) = 1 - \sum_{i=1}^{c} \phi\Big(h_i(t, \boldsymbol{x}), w_i\Big), \tag{6.18}$$

where $\phi : \mathbb{R}_+ \times \mathbb{R}_+ \to \mathbb{R}_+$ belongs to class-$\mathcal{LL}$, is twice continuously differentiable, and satisfies $\phi(r, 0) = \phi(0, s) = \phi(0, 0) = 1$. Note that the specified domain considers only positive values for w_i and h_i, a reasonable choice since it encodes that $\boldsymbol{x}(t) \notin \mathcal{D}(t)$ if some $h_i(t, \boldsymbol{x}(t)) \leq 0$ with $w_i \geq 0$ or if some $w_i \leq 0$ with $h_i(t, \boldsymbol{x}(t)) \geq 0$. Both the decaying exponential function $\phi(r, s) = e^{-rs}$ and the class of reciprocal functions of the form $\phi(r, s) = v/(rs + v)$, $v > 0$, for example, satisfy the above requirements over the admissible domain. It is straightforward to see, therefore, that the function ϕ encodes that the zero super-level set of H is a subset of the complete constraint set $\mathcal{S}(t)$, i.e.,

$$\mathcal{D}(t) = \{\boldsymbol{x} \in \mathbb{R}^n \mid H(t, \boldsymbol{w}(t), \boldsymbol{x}) \geq 0\} \subset \mathcal{S}(t), \ \forall t \in \mathcal{T},$$

provided that $\boldsymbol{w} \in \mathbb{R}_+^c$. Note that the weights behave as a shape parameter for the function ϕ, and are neither used to construct a weighted average nor required to sum to any specific amount. Instead, observe that larger weights $\boldsymbol{w}$ allow $\mathcal{D}(t)$ to more closely approach $\mathcal{S}(t)$, as for a given state it follows that $\phi(h_i(t, \boldsymbol{x}), w_i^l) < \phi(h_i(t, \boldsymbol{x}), w_i^s)$ for $w_i^l > w_i^s > 0$. This means that a higher weight w_i confers smaller relative importance of its associated constraint function h_i to the C-CBF candidate H. For example, in Figure 6.1 the effect of two different weights on the level sets of two obstacle avoidance constraint functions is depicted. In this case, obstacle two has smaller relative importance (i.e., $w_2 > w_1$) and thus the system takes actions toward obstacle two until it reaches a region where the level set values decrease very quickly to zero, at which point it makes an evasive maneuver. Thus, the system effectively ignores obstacle two until it must take action to avoid it.

Thus, H defined by (6.18) solves Problem 6.1 and is referred to as a C-CBF *candidate*. Given an arbitrary weight vector $\boldsymbol{w}$, however, it may not be true that H is a *valid* CBF for (6.4) with respect to the set $\mathcal{D}(t)$. Without adapting the weights as the system moves through the state space the C-CBF condition (6.17) may be violated.

In the next two sections, solutions to Problem 6.2 are proposed for the system (6.4) first under unbounded control authority and then when subject to input constraints.

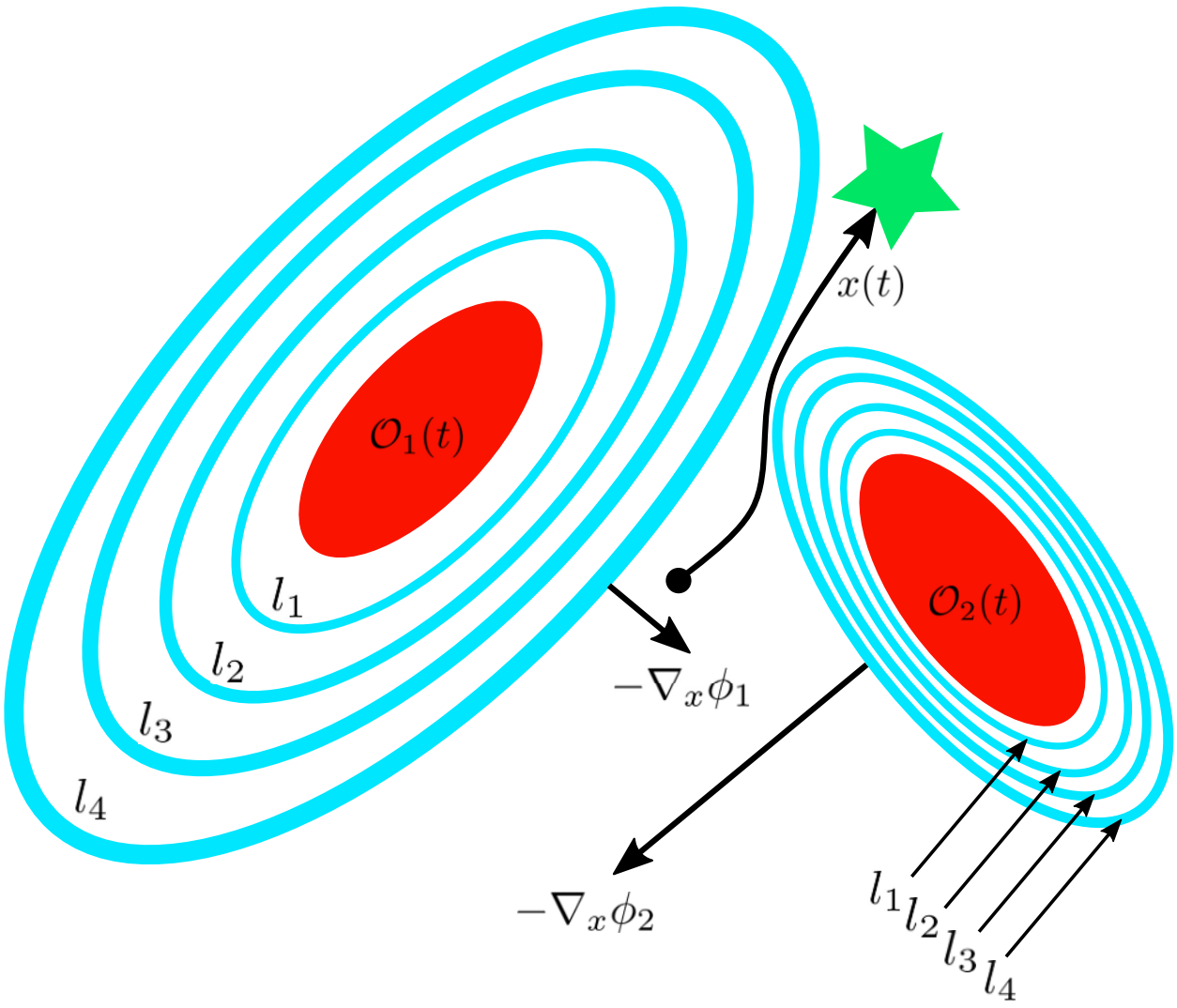

Figure 6.1: A contrived example of a system seeking to reach a target location (green star) while adapting weights $\boldsymbol{w}$ in the presence of two elliptical obstacles of identical size and shape whose constraint functions h_1 and h_2 define exclusion sets $\mathcal{O}_1(t) = \mathbb{R}^n \setminus \mathcal{S}_1(t)$ and $\mathcal{O}_2(t) = \mathbb{R}^n \setminus \mathcal{S}_2(t)$. Here, the system gives greater relative importance to obstacle one (i.e., $w_1 < w_2$) and therefore the function H views obstacle one as having a shallow level curve topography (depicted as level curves $l_1 < l_2 < l_3 < l_4$ spaced further apart with smaller gradient magnitude $\nabla_x \phi_1$), whereas it sees obstacle two as having steep gradients (level curves close together, with larger $\nabla_x \phi_2$) near the obstacle. This allows the state to more closely approach obstacle two before deciding to take evasive action.

6.2.2 Validation under Unbounded Control Authority

In this subsection, it is assumed that the input constraint set is unbounded, i.e. that $\mathcal{U} = \mathbb{R}^m$. In this case, it follows that a sufficient condition for the viability of the C-CBF condition (6.14) is that

$$\frac{\partial H}{\partial \boldsymbol{x}} g(\boldsymbol{x}(t)) \neq \mathbf{0}, \ \forall \boldsymbol{x}(t) \in \mathcal{D}(t) \subset \mathcal{S}(t), \ \forall t \in \mathcal{T}. \tag{6.19}$$

Thus, the weight adaptation law in this subsection seeks to ensure that the above condition holds. For this to be possible, some component of the C-CBF dynamics must be controllable, i.e., at least one constraint function must have relative-degree $r = 1$ with respect to the system (6.4).

Assumption 6.2 (**Controllability**). *The matrix of controlled candidate CBF dynamics is not all zero, i.e.*

$$\boldsymbol{L}_g \triangleq \begin{bmatrix} L_g h_1 \\ \vdots \\ L_g h_c \end{bmatrix} \neq \boldsymbol{0}_{c\times m}. \tag{6.20}$$

Now, the main result of this subsection, an adaptation law that solves Problem 6.2 for the case of $\mathcal{U} = \mathbb{R}^m$ and thus renders H a valid C-CBF for the set $\mathcal{D}(t)$, for all $t \in \mathcal{T}$, may be presented.

Theorem 6.2. *Consider $c \geq 1$ twice continuously differentiable constraint functions h_i defining sets $\mathcal{S}_i(t)$ as in* (6.5)*, $\forall i \in [c]$, and the associated C-CBF candidate given by* (6.18) *with constituent weights $\boldsymbol{w}$. Suppose that Assumption 6.2 holds, that the input constraint set for the system* (6.4) *is $\mathcal{U} = \mathbb{R}^m$, and that there exists a feasible solution to the following problem for all time,*

$$\boldsymbol{v}^*(t,\boldsymbol{w},\boldsymbol{x}) = \underset{\boldsymbol{v}\in\mathbb{R}^c}{\arg\min}\ \frac{1}{2}(\boldsymbol{v}-\boldsymbol{v}_0(t,\boldsymbol{w},\boldsymbol{x}))^\top \boldsymbol{P}(\boldsymbol{v}-\boldsymbol{v}_0(t,\boldsymbol{w},\boldsymbol{x})), \tag{6.21a}$$

$$\text{s.t.}$$

$$v_i + \alpha_w(w_i - w_{min}) \geq 0,\ \forall i \in [c], \tag{6.21b}$$

$$v_i + \alpha_w(w_{max} - w_i) \geq 0,\ \forall i \in [c], \tag{6.21c}$$

$$\boldsymbol{p}^T\boldsymbol{Q}\dot{\boldsymbol{p}} + \boldsymbol{p}^T\dot{\boldsymbol{Q}}\boldsymbol{p} + \alpha_p(h_p) \geq 0, \tag{6.21d}$$

where $\boldsymbol{P} \in \mathbb{R}^{c\times c}$ is a positive-definite gain matrix, $\alpha_w, \alpha_p \in \mathcal{K}_\infty$, $\boldsymbol{v}_0 : \mathcal{T}\times\mathbb{R}^c_+\times\mathbb{R}^n$ is the desired adaptation $\dot{\boldsymbol{w}}$, $w_{min} > 0$ is the lower bound on any element of $\boldsymbol{w}$, and

$$\boldsymbol{p} = \begin{bmatrix} \dfrac{\partial\phi}{\partial h_1} & \cdots & \dfrac{\partial\phi}{\partial h_c} \end{bmatrix}^T, \tag{6.22}$$

$$\boldsymbol{Q} = \boldsymbol{I} - (\boldsymbol{N}\boldsymbol{N}^T)^T - \boldsymbol{N}\boldsymbol{N}^T - (\boldsymbol{N}\boldsymbol{N}^T)^T\boldsymbol{N}\boldsymbol{N}^T \tag{6.23}$$

with $h_p = \frac{1}{2}\boldsymbol{p}^T\boldsymbol{Q}\boldsymbol{p} - \varepsilon$, $\varepsilon > 0$, and

$$\boldsymbol{N} = [\boldsymbol{n}_1\ \cdots\ \boldsymbol{n}_r], \tag{6.24}$$

such that $\{\boldsymbol{n}_1,\ldots,\boldsymbol{n}_r\}$ constitutes a basis for the null space of $\boldsymbol{L}_g^T$, i.e. $\mathcal{N}(\boldsymbol{L}_g^T) = \text{span}\{\boldsymbol{n}_1,\ldots,\boldsymbol{n}_r\}$, where $\boldsymbol{L}_g$ is given by (6.20)*. If $\boldsymbol{w}(0)$ is such that $\frac{\partial H}{\partial \boldsymbol{x}}g(\boldsymbol{x}) \neq \boldsymbol{0}_{1\times m}$ at $t = 0$,*

then, under the ensuing adaptation law,

$$\omega(t, \boldsymbol{w}, \boldsymbol{x}) = \boldsymbol{v}^*(t, \boldsymbol{w}, \boldsymbol{x}), \tag{6.25}$$

the C-CBF candidate H given by (6.18) *is rendered valid for the system* (6.4) *with respect to the set $\mathcal{D}(t)$, i.e., the condition* (6.17) *is viable for all $\boldsymbol{x}(t) \in \mathcal{D}(t)$ and $\delta \geq 0$, for all $t \geq 0$.*

Proof. First, given (6.18), we have that

$$\begin{aligned}
\dot{H} &= -\sum_{i=1}^{c} \left(\frac{\partial \phi}{\partial h_i} \dot{h}_i + \frac{\partial \phi}{\partial w_i} \dot{w}_i \right) \\
&= -\left(\boldsymbol{p}^T \dot{\boldsymbol{h}} + \boldsymbol{q}^T \dot{\boldsymbol{w}} \right) \\
&= -\left(\boldsymbol{p}^T (\boldsymbol{L}_t + \boldsymbol{L}_f + \boldsymbol{L}_g \boldsymbol{u}) + \boldsymbol{q}^T \dot{\boldsymbol{w}} \right)
\end{aligned}$$

where $\boldsymbol{p}$ is given by (6.22), $\boldsymbol{L}_g$ by (6.20), $\boldsymbol{L}_t = [\frac{\partial h_1}{\partial t} \ \dots \ \frac{\partial h_c}{\partial t}]^\top$, $\boldsymbol{L}_f = [L_f h_1 \ \dots \ L_f h_c]^\top$, and $\boldsymbol{q} = [\frac{\partial \phi}{\partial w_1} \ \dots \ \frac{\partial \phi}{\partial w_c}]^\top$. With $\mathcal{U} = \mathbb{R}^M$, it follows that as long as (6.19) holds it is possible to choose $\boldsymbol{u}$ such that (6.14) holds. It will now be shown that $\dot{\boldsymbol{w}} = \omega(t, \boldsymbol{w}, \boldsymbol{x})$ given by (6.25) guarantees that (6.19) is true and thus that H is a valid C-CBF for $\mathcal{D}(t)$, for all $t \in \mathcal{T}$.

Since $\frac{\partial H}{\partial \boldsymbol{x}} g(\boldsymbol{x}) = -\boldsymbol{p}^T \boldsymbol{L}_g$, the problem of showing that (6.19) holds is equivalent to proving that $\boldsymbol{p} \notin \mathcal{N}(\boldsymbol{L}_g{}^\top) = \text{span}\{\boldsymbol{n}_1, \dots, \boldsymbol{n}_r\}$. Since the vector $\boldsymbol{p}$ can be expressed as a sum of vectors perpendicular to and parallel to $\mathcal{N}(\boldsymbol{L}_g^T)$ (respectively $\boldsymbol{p}^\perp$ and $\boldsymbol{p}^\parallel$), it follows that $\boldsymbol{p} \notin \mathcal{N}(\boldsymbol{L}_g^T)$ as long as $\|\boldsymbol{p}^\perp\| > 0$, where $\boldsymbol{p}^\perp = \left(\boldsymbol{I} - \boldsymbol{N}\boldsymbol{N}^T\right)\boldsymbol{p}$ by vector projection, and $\boldsymbol{N}$ is given by (6.24). Thus, a sufficient condition for $\boldsymbol{p} \notin \mathcal{N}(\boldsymbol{L}_g^T)$ is that

$$\frac{1}{2}\|(\boldsymbol{I} - \boldsymbol{N}\boldsymbol{N}^T)\boldsymbol{p}\|^2 = \frac{1}{2}\boldsymbol{p}^T \boldsymbol{Q} \boldsymbol{p} > \varepsilon \tag{6.26}$$

for some $\varepsilon > 0$, where $\boldsymbol{Q}$ is given by (6.23). Then, by defining a function $h_p = \frac{1}{2}\boldsymbol{p}^T \boldsymbol{Q} \boldsymbol{p} - \varepsilon$, it follows from (6.8) that when (6.26) is true at $t = 0$, it is true $\forall t \geq 0$ as long as (6.21d) holds. The conditions (6.21b) and (6.21c) ensure that $\boldsymbol{w} \in \mathbb{R}^c_+$ and that $\boldsymbol{w}$ is bounded respectively.

Therefore, gains $\boldsymbol{w}$ adapted according to the law (6.25) are guaranteed to result in $\frac{\partial H}{\partial \boldsymbol{x}} g(\boldsymbol{x}) \neq \boldsymbol{0}_{1\times m}$. Thus, H is a valid C-CBF for the set $\mathcal{D}(t)$, for all $t \in \mathcal{T}$. This completes the proof. □

Remark 6.1. *With $\boldsymbol{Q}$ depending on basis vectors spanning $\mathcal{N}(\boldsymbol{L}_g^T)$, it is not immediately obvious under what conditions $\dot{\boldsymbol{Q}}$ is continuous (or even well-defined). Prior results show that if the rank of $\mathcal{N}(\boldsymbol{L}_g^T)$ is constant then $\dot{\boldsymbol{Q}}$ varies continuously, $\forall \boldsymbol{x} \in B_\epsilon(\boldsymbol{x})$ [235], but analytical derivations of $\dot{\boldsymbol{Q}}$ are not available. For the simulations and experiments presented in this chapter using this method, it was observed that the rank of $\mathcal{N}(\boldsymbol{L}_g^T)$ was indeed constant, and thus $\dot{\boldsymbol{Q}}$ was approximated numerically using finite-difference methods.*

6.2.3 Validation under Limited Control Authority

In this subsection, it is assumed that the input constraint set is of the form

$$\mathcal{U} = \{\boldsymbol{u} \in \mathbb{R}^m \mid -\boldsymbol{u}_{max} \leq \boldsymbol{u} \leq \boldsymbol{u}_{max}\}, \tag{6.27}$$

where the inequalities are interpreted element-wise and $\boldsymbol{u}_{max} = (\bar{u}_1, \cdots, \bar{u}_m)$ with $0 < \bar{u}_j < \infty$ for $j \in [m]$. Thus, the set $\mathcal{U}$ is a polytope symmetric about the origin.

Consider that in addition to the C-CBF weights $\boldsymbol{w}$ being used to enforce the condition (6.14), it may be desirable to choose weights that are optimal with respect to some objective function $J : \mathcal{T} \times \mathbb{R}^c \times \mathbb{R}^n \to \mathbb{R}$. As such, a predictor-corrector interior point method is proposed for weight adaptation to track the following optimal solution trajectory:

$$\boldsymbol{w}^*(t) = \underset{\boldsymbol{w} \in \mathbb{R}^c}{\arg\min}\ J(t, \boldsymbol{w}, \boldsymbol{x}), \quad \text{s.t. } \boldsymbol{w} \in \mathcal{W}(t), \tag{6.28}$$

where J is strongly uniformly convex with respect to $\boldsymbol{w}$, twice continuously differentiable in both $\boldsymbol{w}$ and $\boldsymbol{x}$, and piecewise continuously differentiable in t. The feasible region is defined by

$$\mathcal{W}(t) = \{\boldsymbol{w} \in \mathbb{R}^c \mid b_j(t, \boldsymbol{w}, \boldsymbol{x}) \leq 0, \forall j \in [2c+1]\}, \tag{6.29}$$

where the first c constraint functions $b_j : \mathcal{T} \times \mathbb{R}^c \times \mathbb{R}^n \to \mathbb{R}$ enforce that each w_j remains above the user-specified minimum threshold $w_{min} > 0$ to ensure that $\boldsymbol{w}(t) \in \mathbb{R}^c_+, \forall t \in \mathcal{T}$, i.e.,

$$b_j(t, \boldsymbol{w}, \boldsymbol{x}) = w_{min} - w_j,\ \forall j \in [c], \tag{6.30}$$

the second c constraint functions $b_j : \mathcal{T} \times \mathbb{R}^c \times \mathbb{R}^n \to \mathbb{R}$ enforce that each w_j remains below a user-specified maximum threshold $w_{max} < \infty$ to ensure that $\boldsymbol{w}(t)$ is well-defined, i.e.,

$$b_{j+c}(t, \boldsymbol{w}, \boldsymbol{x}) = w_j - w_{max},\ \forall j \in [c], \tag{6.31}$$

and the final constraint function $b_{2c+1} : \mathcal{T} \times \mathbb{R}^c \times \mathbb{R}^n \to \mathbb{R}$ enforces that the C-CBF condition (6.17) is satisfied, i.e., namely that

$$\begin{aligned} \beta(t, \boldsymbol{w}, \boldsymbol{x}) \triangleq &- \frac{\partial H}{\partial t} - \frac{\partial H}{\partial \boldsymbol{x}} f(\boldsymbol{x}) - \frac{\partial H}{\partial \boldsymbol{w}} \dot{\boldsymbol{w}} \\ &- \alpha(H(t, \boldsymbol{w}, \boldsymbol{x})) - \sup_{\boldsymbol{u} \in \mathcal{U}} \left[\frac{\partial H}{\partial \boldsymbol{x}} g(\boldsymbol{x}) \boldsymbol{u} \right] \leq 0. \end{aligned} \tag{6.32}$$

For the moment, consider that $b_{2c+1} = \beta$. Note that the optimal solution trajectory (6.28) is of the

form (6.1), and thus consider the approximate optimal solution trajectory

$$\hat{\boldsymbol{w}}^*(t) = \underset{\boldsymbol{w}\in\mathbb{R}^c}{\arg\min}\ \Phi(t, \boldsymbol{w}, \boldsymbol{x}), \tag{6.33}$$

where Φ is analogous to Ψ in (6.2) and is defined by

$$\Phi(t, \boldsymbol{w}, \boldsymbol{x}) \triangleq J(t, \boldsymbol{w}, \boldsymbol{x}) - \frac{1}{s}\sum_{j=1}^{2c+1} \log\big(-b_j(t, \boldsymbol{w}, \boldsymbol{x})\big), \tag{6.34}$$

for barrier parameter $s > 0$. It is taken that Assumption 6.1 holds for Φ i.e., that there exists $s > 0$ rendering Φ strongly uniformly convex with respect to $\boldsymbol{w}$. As stated previously, this is reasonable in practice given a sufficiently large choice of s. It is therefore proposed to adapt the weights $\boldsymbol{w}$ according to a control-affine dynamical system of the form (6.3):

$$\dot{\boldsymbol{w}} = \mu(t, \boldsymbol{w}, \boldsymbol{x}) + \nu(t, \boldsymbol{w}, \boldsymbol{x})\boldsymbol{u}, \tag{6.35}$$

where $\mu : \mathcal{T} \times \mathbb{R}^c \times \mathbb{R}^n \to \mathbb{R}^c$ and $\nu : \mathcal{T} \times \mathbb{R}^c \times \mathbb{R}^n \to \mathbb{R}^{c\times m}$ are defined by

$$\mu(t, \boldsymbol{w}, \boldsymbol{x}) = -\nabla_{\boldsymbol{ww}}^{-1}\Phi\big(\boldsymbol{P}\nabla_{\boldsymbol{w}}\Phi + \nabla_{\boldsymbol{wx}}\Phi f(\boldsymbol{x}) + \nabla_{\boldsymbol{w}t}\Phi\big), \tag{6.36}$$

$$\nu(t, \boldsymbol{w}, \boldsymbol{x}) = -\nabla_{\boldsymbol{ww}}^{-1}\Phi\nabla_{\boldsymbol{wx}}\Phi g(\boldsymbol{x}), \tag{6.37}$$

for which $\boldsymbol{P} \in \mathbb{R}^{c\times c}$ is a positive-definite gain matrix. Note that $\dot{\boldsymbol{w}}$ given by (6.35) is affine in $\boldsymbol{u}$ as required in the statement of Problem 6.2, but, however, that because $\dot{\boldsymbol{w}}$ appears explicitly in (6.32) (and therefore in (6.34)) the adaptation law given by (6.35) with $b_{2c+1} = \beta$ requires solving a partial differential equation (PDE). Rather than attempt to solve this (possibly intractable) PDE, the algebraic loop is broken by introducing $\boldsymbol{\mu}^f(t)$ and $\boldsymbol{\nu}^f(t)$ as filtered versions of $\boldsymbol{\mu}(t) \triangleq \mu(t, \boldsymbol{w}(t), \boldsymbol{x}(t))$ and $\boldsymbol{\nu}(t) \triangleq \nu(t, \boldsymbol{w}(t), \boldsymbol{x}(t))$. It is assumed that these filtered variables track their unfiltered counterparts sufficiently closely, as stated in the following.

Assumption 6.3 (Quality Filtering). *There exist bounded, positive constants η_μ and η_ν, i.e., $0 < \eta_\mu, \eta_\nu < \infty$, such that the following relations hold:*

$$\min_{t\in\mathcal{T}}\left[\frac{\partial H}{\partial \boldsymbol{w}}\left(\boldsymbol{\mu}^f(t) - \boldsymbol{\mu}(t)\right)\right] \geq -\eta_\mu, \tag{6.38}$$

which implies that the deviation between the effect of the filtered signal $\boldsymbol{\mu}^f$ and true signal $\boldsymbol{\mu}$ on

the C-CBF dynamics is bounded by η_μ, and

$$\min_{t\in\mathcal{T}}\left[\sup_{\boldsymbol{u}\in\mathcal{U}}\left(\frac{\partial H}{\partial \boldsymbol{x}}g(\boldsymbol{x}(t))+\frac{\partial H}{\partial \boldsymbol{w}}\boldsymbol{\nu}^f(t)\right)\boldsymbol{u}\right. \\ \left.-\sup_{\boldsymbol{u}\in\mathcal{U}}\left(\frac{\partial H}{\partial \boldsymbol{x}}g(\boldsymbol{x}(t))+\frac{\partial H}{\partial \boldsymbol{w}}\boldsymbol{\nu}(t)\right)\boldsymbol{u}\right]\geq -\eta_\nu, \tag{6.39}$$

which similarly implies that the deviation (considering the worst possible control input) between the effect of the filtered signal $\boldsymbol{\nu}^f$ and true signal $\boldsymbol{\nu}$ on the C-CBF dynamics is bounded by η_ν.

The above implicitly define worst-case error bounds η_μ and η_ν on how the filtered signals $\boldsymbol{\mu}^f$ and $\boldsymbol{\nu}^f$ affect $\dot{H}$ versus the true signals $\boldsymbol{\mu}$ and $\boldsymbol{\nu}$, and thus the inequality in (6.32) may be satisfied by using $\boldsymbol{\mu}^f$, $\boldsymbol{\nu}^f$, η_μ, and η_ν instead of $\boldsymbol{\mu}$ and $\boldsymbol{\nu}$. In practice, (6.38) and (6.39) may be satisfied via appropriate filter design. The final constraint function is thus defined as

$$b_{2c+1}(t,\boldsymbol{w},\boldsymbol{x})=\delta(t,\boldsymbol{w},\boldsymbol{x})-\left|q(t,\boldsymbol{w},\boldsymbol{x})\right|^\top \boldsymbol{u}_{max}, \tag{6.40}$$

which is directly (6.32) with the filter variables (and error bounds), specifically

$$\delta(t,\boldsymbol{w},\boldsymbol{x})=\eta_\mu+\eta_\nu-\frac{\partial H}{\partial t}-\frac{\partial H}{\partial \boldsymbol{x}}f(\boldsymbol{x}) \\ -\frac{\partial H}{\partial \boldsymbol{w}}\boldsymbol{\mu}^f(t)-\alpha(H), \tag{6.41}$$

and

$$q(t,\boldsymbol{w},\boldsymbol{x})\triangleq \boldsymbol{L}_g^T p_h(\boldsymbol{w},\boldsymbol{x})+\boldsymbol{\nu}^f(t)^T p_w(\boldsymbol{w},\boldsymbol{x}), \tag{6.42}$$

with the C-CBF control matrix $\boldsymbol{L}_g$ (omitting the dependence on $\boldsymbol{x}$) defined by

$$\boldsymbol{L}_g=\left[\frac{\partial h_1}{\partial \boldsymbol{x}}\cdots\frac{\partial h_c}{\partial \boldsymbol{x}}\right]^T g(\boldsymbol{x})\in\mathbb{R}^{c\times m}, \tag{6.43}$$

and the functions $p_h:\mathbb{R}^c\times\mathbb{R}^n\to\mathbb{R}^c$ and $p_w:\mathbb{R}^c\times\mathbb{R}^n\to\mathbb{R}^c$ given by

$$p_h(\boldsymbol{w},\boldsymbol{x})=\left[\frac{\partial\phi(w_1,\boldsymbol{x})}{\partial h_1}\ \cdots\ \frac{\partial\phi(w_c,\boldsymbol{x})}{\partial h_c}\right]^\top, \tag{6.44}$$

$$p_w(\boldsymbol{w},\boldsymbol{x})=\left[\frac{\partial\phi(w_1,\boldsymbol{x})}{\partial w_1}\ \cdots\ \frac{\partial\phi(w_c,\boldsymbol{x})}{\partial w_c}\right]^\top. \tag{6.45}$$

These modifications allow for the inclusion of b_{2c+1} directly as a function constraining the optimal solution trajectory given by (6.28) without needing to solve a complicated PDE.

Now, the main result of this subsection.

Theorem 6.3. *Consider $c \geq 1$ twice continuously differentiable constraint functions h_i defining sets $\mathcal{S}_i(t)$ as in* (6.5)*, $\forall i \in [c]$, and the associated C-CBF candidate given by* (6.18) *with constituent weights $\boldsymbol{w}$. Suppose that Assumption 6.3 holds, and that $\mathrm{Int}(\mathcal{W}(t)) \neq \emptyset$ for all $t \geq 0$ with $\boldsymbol{w}(0) \in \mathrm{Int}(\mathcal{W}(0))$. Then, under the adaptation law* (6.35)*, the C-CBF candidate H given by* (6.18) *is rendered valid, i.e., the condition* (6.17) *is satisfied for all $\boldsymbol{x}(t) \in \mathcal{D}(t)$ and $\delta \geq 0$, for all $t \geq 0$.*

Proof. First, an expression for $\dot{H}$ will be derived, and then it will be shown that when $\dot{\boldsymbol{w}}$ is given by (6.35) there always exists a control input $\boldsymbol{u} \in \mathcal{U}$ such that $\sup_{\boldsymbol{u}\in\mathcal{U}} \dot{H}(t, \boldsymbol{w}, \dot{\boldsymbol{w}}, \boldsymbol{x}, \boldsymbol{u}) \geq -\alpha(H)$.

First, observe that according to (6.18) the C-CBF candidate time-derivative $\dot{H}$ takes the following form:

$$\begin{aligned}
\dot{H} &= -\sum_{i=1}^{c} \left(\frac{\partial \phi}{\partial h_i} \dot{h}_i + \frac{\partial \phi}{\partial w_i} \dot{w}_i \right) \\
&= -\left(p_h^T \dot{\boldsymbol{h}} + p_w^T \dot{\boldsymbol{w}} \right) \\
&= -\left(p_h^T \left(\boldsymbol{L}_t + \boldsymbol{L}_f + \boldsymbol{L}_g \boldsymbol{u} \right) + p_w^T (\boldsymbol{\mu} + \boldsymbol{\nu} \boldsymbol{u}) \right),
\end{aligned}$$

where $\boldsymbol{\mu} = \mu(t, \boldsymbol{w}, \boldsymbol{x})$ and $\boldsymbol{\nu} = \nu(t, \boldsymbol{w}, \boldsymbol{x})$ are given by (6.36) and (6.37) respectively, $\boldsymbol{L}_g$ by (6.43), p_h and p_w by (6.44) and (6.45), and where (omitting the dependence on $\boldsymbol{x}$ and $\boldsymbol{w}$)

$$\begin{aligned}
\boldsymbol{L}_t &= \left[\frac{\partial h_1}{\partial t} \cdots \frac{\partial h_c}{\partial t} \right]^T \in \mathbb{R}^c, \\
\boldsymbol{L}_f &= \left[\frac{\partial h_1}{\partial \boldsymbol{x}} \cdots \frac{\partial h_1}{\partial \boldsymbol{x}} \right]^T f(\boldsymbol{x}) \in \mathbb{R}^c .
\end{aligned}$$

Given $\alpha \in \mathcal{K}_\infty$, it follows that $\dot{H} + \alpha(H) = a + \boldsymbol{b}^T \boldsymbol{u}$, with $a = \alpha(H) - p_h^T(\boldsymbol{L}_t + \boldsymbol{L}_f) - p_w^T \boldsymbol{\mu}$ and $\boldsymbol{b} = -(\boldsymbol{L}_g^T p_h + \boldsymbol{\nu}^T p_w)$. Observe that given (6.4), the adaptation law (6.35) may be expressed as

$$\dot{\boldsymbol{w}} = -\nabla_{\boldsymbol{w}\boldsymbol{w}}^{-1} \Phi \left(\boldsymbol{P} \nabla_{\boldsymbol{w}} \Phi + \nabla_{\boldsymbol{w}\boldsymbol{x}} \Phi \dot{\boldsymbol{x}} + \nabla_{\boldsymbol{w}t} \Phi \right),$$

which, for Φ defined by (6.34) defines a dynamical system of the form (6.3). With Φ strongly, uniformly convex, $\mathrm{Int}(\mathcal{W}(t)) \neq \emptyset$ for all $t \geq 0$, and $\boldsymbol{w}(0) \in \mathrm{Int}(\mathcal{W}(0))$, it follows from Lemma 6.1 that the solution remains within the feasible set for all time, i.e., $\boldsymbol{w}(t) \in \mathcal{W}(t)$, $\forall t \geq 0$, which implies that $b_j(t, \boldsymbol{w}(t), \boldsymbol{x}(t)) \leq 0$ for all $j \in [2c+1]$, $t \geq 0$. While constraints $j \in [c]$ encode that each $w_j > w_{min} > 0$ and constraints $j + c$ for $j \in [c]$ encode that each $w_j < w_{max} < \infty$, it may be seen by substituting (6.41) and (6.42) into (6.40) that the final constraint function b_{2c+1} encodes

that

$$\frac{\partial H}{\partial t} + \frac{\partial H}{\partial \boldsymbol{x}} f(\boldsymbol{x}) + \frac{\partial H}{\partial \boldsymbol{w}} \boldsymbol{\mu}^f - \eta_\mu + \alpha(H) + \left| \frac{\partial H}{\partial \boldsymbol{x}} g(\boldsymbol{x}) + \frac{\partial H}{\partial \boldsymbol{w}} \boldsymbol{\nu}^f \right| \boldsymbol{u}_{max} - \eta_\nu \geq 0.$$

Then, by observing from the input constraint set (6.27) that

$$\left| \frac{\partial H}{\partial \boldsymbol{x}} g(\boldsymbol{x}) + \frac{\partial H}{\partial \boldsymbol{w}} \boldsymbol{\nu}^f \right| \boldsymbol{u}_{max} = \sup_{\boldsymbol{u} \in \mathcal{U}} \left(\frac{\partial H}{\partial \boldsymbol{x}} g(\boldsymbol{x}) + \frac{\partial H}{\partial \boldsymbol{w}} \boldsymbol{\nu}^f \right) \boldsymbol{u}$$

and taking by (6.38) and (6.39) from Assumption 6.3, it follows that that $b_{2c+1} \leq 0$ implies that

$$\begin{aligned} \dot{H} &= \frac{\partial H}{\partial t} + \frac{\partial H}{\partial \boldsymbol{x}} f(\boldsymbol{x}) + \frac{\partial H}{\partial \boldsymbol{w}} \mu(t, \boldsymbol{w}, \boldsymbol{x}) + \alpha(H) + \sup_{\boldsymbol{u} \in \mathcal{U}} \left[\left(\frac{\partial H}{\partial \boldsymbol{x}} g(\boldsymbol{x}) + \frac{\partial H}{\partial \boldsymbol{w}} \nu(t, \boldsymbol{w}, \boldsymbol{x}) \right) \boldsymbol{u} \right], \\ &= \frac{\partial H}{\partial t} + \frac{\partial H}{\partial \boldsymbol{x}} f(\boldsymbol{x}) + \frac{\partial H}{\partial \boldsymbol{w}} \dot{\boldsymbol{w}} + \sup_{\boldsymbol{u} \in \mathcal{U}} \frac{\partial H}{\partial \boldsymbol{x}} g(\boldsymbol{x}) \boldsymbol{u} \geq -\alpha(H), \end{aligned}$$

and therefore there always exists a control input $\boldsymbol{u} \in \mathcal{U}$ such that the C-CBF condition (6.14) is viable. Thus, the adaptation law (6.35) renders the C-CBF candidate valid. This completes the proof. □

Remark 6.2. *The above result is predicated on the following assumptions holding. First, the convexity condition imposed on Φ as outlined in Assumption 6.1: this may require monitoring the eigenvalues of $\nabla_{\boldsymbol{ww}} \Phi$ online and increasing s if necessary, but in the numerical experiments conducted this has been unproblematic. Second, and most challenging, the filter design for $\boldsymbol{\mu}(t)$ and $\boldsymbol{\nu}(t)$ must be sufficiently accurate as detailed in Assumption 6.3. The robustness margins η_μ and η_ν may be difficult to determine a priori without knowledge of how the system will evolve over time. In the numerical experiments, a trial and error process with first-order low-pass filters was used to determined that $\eta_\mu, \eta_\nu \leq 0.05$ typically worked well for the case studies undertaken. The third and final set of assumptions involves the feasible region $\mathcal{W}$, namely that $\mathrm{Int}(\mathcal{W}(t)) \neq \emptyset$ and that $\boldsymbol{w}(0) \in \mathcal{W}(0)$. Ensuring that the initial weights belong to the feasible set is fairly straightforward: choose a set of weights and, if they do not belong to the feasible set, adapt them using only the correction term of the adaptation law $\dot{\boldsymbol{w}}_0 = -\nabla_{\boldsymbol{ww}}^{-1} \Phi \boldsymbol{P} \nabla_{\boldsymbol{w}} \Phi$ until $\boldsymbol{w}_0 \in \mathrm{Int}(\mathcal{W}(0))$. Ensuring that $\mathrm{Int}(\mathcal{W}(t)) \neq \emptyset$ for all $t \in \mathcal{T}$ is currently an open problem, and thus must be assumed to be true. What the result in Theorem 6.3 does imply, however, is that if the feasible region has an interior point then the adaptation law* (6.35) *will find it. If no interior feasible point exists, then use various relaxation strategies on the constraint functions b_j, $j \in [2c]$ (which excludes the constraint function encoding the C-CBF condition) may be used in order to consider an enlarged feasible region and ensure that the adaptation law is well-defined. The discussion in [231, Section III.C] contains more details on this strategy.*

Remark 6.3. *Notably absent from the set of requisite assumptions is any condition on the relative-degree of the state constraint functions h_i. For the proposed method it is actually acceptable for the C-CBF control matrix $\boldsymbol{L}_g$ to consist only of zeros because the parameter adaptation law $\dot{\boldsymbol{w}}$ contributes to the viability of the C-CBF condition* (6.14) *via the term $\frac{\partial H}{\partial \boldsymbol{w}}\nu(t, \boldsymbol{w}, \boldsymbol{x})\boldsymbol{u}$. In this case, the adaptation of the weights would be fully responsible for ensuring that* (6.14) *holds. This does not come without tradeoffs, however, since it may be more difficult to satisfy the assumption on the initial condition that $\boldsymbol{w}(0) \in \mathcal{W}(0)$ (which may restrict the set of allowable initial states) or to ensure that $\mathrm{Int}(\mathcal{W}(t)) \neq \emptyset$.*

6.3 Control Synthesis with C-CBFs

In this section, a controller based on the proposed consolidated control barrier function is proposed and its present limitations are discussed.

6.3.1 C-CBF-QP Control Design

Previously, the CBF-QP control law given by (6.10) was reviewed and it was suggested that the C-CBF could be directly inserted into such a framework for certified constrained control design. The C-CBF-QP controller can be described by

$$\boldsymbol{u}^*(t) = \underset{\boldsymbol{u}\in\mathbb{R}^m}{\arg\min}\ J_u(t, \boldsymbol{x}, \boldsymbol{u}), \quad \text{s.t. } \boldsymbol{u} \in \mathcal{U}_H(t, \alpha), \tag{6.46}$$

where the objective function $J_u : \mathcal{T} \times \mathbb{R}^n \times \mathbb{R}^m \to \mathbb{R}$ is given by

$$J_u(t, \boldsymbol{x}, \boldsymbol{u}) = \frac{1}{2}\|\boldsymbol{u} - \boldsymbol{u}_0(t, \boldsymbol{x})\|^2,$$

and the feasible region $\mathcal{U}_H$ is the C-CBF control set given by (6.16), defined more concisely here as

$$\mathcal{U}_H(t, \alpha) = \{\boldsymbol{u} \in \mathbb{R}^m \mid d_k(t, \boldsymbol{w}, \boldsymbol{x}, \boldsymbol{u}) \leq 0, \forall k \in [2m + 1]\}$$

for input constraint functions

$$d_k(t, \boldsymbol{w}, \boldsymbol{x}, \boldsymbol{u}) = \bar{u}_k - u_k,\ \forall k \in [m], \tag{6.47}$$

$$d_{k+m}(t, \boldsymbol{w}, \boldsymbol{x}, \boldsymbol{u}) = u_k - \bar{u}_k,\ \forall k \in [m], \tag{6.48}$$

and the C-CBF constraint function

$$d_{2m+1}(t, \boldsymbol{w}, \boldsymbol{x}, \boldsymbol{u}) = -\alpha(H) - \frac{\partial H}{\partial t} - \frac{\partial H}{\partial \boldsymbol{x}} f(\boldsymbol{x}) - \frac{\partial H}{\partial \boldsymbol{w}} \dot{\boldsymbol{w}} - \frac{\partial H}{\partial \boldsymbol{x}} g(\boldsymbol{x}) \boldsymbol{u}.$$

The following results highlights how this proposed controller results in complete satisfaction of all constraint functions belonging to $\mathcal{H}$ when $\dot{\boldsymbol{w}}$ is given by (6.35).

Theorem 6.4. *Consider the set of $c \geq 1$ constraint functions $\mathcal{H}$ given by* (6.6) *and the complete constraint set $\mathcal{S}(t)$ given by* (6.7)*. Assume that either*

(i) the premises of Theorem 6.2 hold, and $\dot{\boldsymbol{w}}$ is given by (6.25)*, or*

(ii) the premises of Theorem 6.3 hold, and $\dot{\boldsymbol{w}}$ is given by (6.35)*.*

Then, under the control law (6.46) *the state remains inside the complete constraint set and thus all constraints encoded via functions $h \in \mathcal{H}$ are satisfied for all time, i.e., $\boldsymbol{x}(t) \in \mathcal{S}(t)$, $\forall t \in \mathcal{T}$ under control policy $\boldsymbol{u}^*(t)$ given by* (6.46)*.*

Proof. First, under the premises of Theorem 6.2 the input constraint set is $\mathcal{U} = \mathbb{R}^m$. It was shown that when the adaptation law is given by (6.25), the controllable component of the C-CBF dynamics is never zero, i.e., $\frac{\partial H}{\partial \boldsymbol{x}} g(\boldsymbol{x}) \neq \boldsymbol{0}_{1\times m}$, and therefore that the C-CBF constraint set is never empty, i.e. $\mathcal{U}_H(t, \alpha) \neq \emptyset, \forall t \in \mathcal{T}$.

Alternatively, from Theorem 6.3 and its requisite assumptions it follows that when $\dot{\boldsymbol{w}}$ is given by (6.35) then the C-CBF control set is non-empty at all times, i.e., $\mathcal{U}_H(t, \alpha) \neq \emptyset, \forall t \in \mathcal{T}$.

Thus, both cases imply that the optimization problem (6.46) is feasible at all times, from which it follows that $\boldsymbol{u}^*(t) \in \mathcal{U}_H(t, \alpha), \forall t \in \mathcal{T}$. Thus, the function H is a valid CBF with respect to the set $\mathcal{D}(t)$ for the system (6.4). It then follows from Theorem 6.1 that $\boldsymbol{x}(t) \in \mathcal{D}(t), \forall t \in \mathcal{T}$. Since the set $\mathcal{D}(t)$ is a subset of the complete constraint set $\mathcal{S}(t)$ at all times, i.e., $\mathcal{D}(t) \subset \mathcal{S}(t), \forall t \in \mathcal{T}$, then $\boldsymbol{x}(t) \in \mathcal{S}(t)$ and therefore $h(t, \boldsymbol{x}(t)) \geq 0, \forall h \in \mathcal{H}$, for all $t \in \mathcal{T}$. □

6.3.2 Discussion

From the above result, it is evident that the motivation behind the parameter adaptation laws introduced in Section 6.2 is to enable the feasibility of the QP controller described by (6.46). In this sense, the feasibility problem has been transferred from one optimization problem (the control law (6.46)) to another ((6.28), the basis for the adaptation law (6.35)) without providing any formal feasibility guarantees. There is some precedent for this type of approach, e.g., in [46] the authors augment the QP-control law with an additional constraint encoding feasibility under input constraints and (at some point) assume feasibility of this new problem.

Considering henceforth only the predictor-corrector interior point adaptation law (6.35), it is assumed that the foundational optimization problem for the adaptation satisfies Slater's condition, i.e., that the feasible region contains an interior point. Without this assumption, analyzing the stability properties of the interconnected dynamical system

$$\dot{\boldsymbol{\xi}} = \begin{bmatrix} \dot{\boldsymbol{x}} \\ \dot{\boldsymbol{w}} \end{bmatrix} = \begin{bmatrix} f(\boldsymbol{x}) \\ \mu(t, \boldsymbol{w}, \boldsymbol{x}) \end{bmatrix} + \begin{bmatrix} g(\boldsymbol{x}) \\ \nu(t, \boldsymbol{w}, \boldsymbol{x}) \end{bmatrix} \boldsymbol{u}^*,$$

is a difficult task. This is a limitation to the proposed method, although there is potential in this line of research in that interior point methods similar to that used to derive the adaptation law (6.35) from optimization problem (6.28) may be used to introduce a new dynamical system $\dot{\boldsymbol{u}} = \upsilon(t, \boldsymbol{w}, \boldsymbol{x}, \boldsymbol{u})$ for the input $\boldsymbol{u}$ to systems (6.4) and (6.35), as outlined in what follows.

Given that the objective function J_u for (6.46) is twice continuously differentiable and strongly, uniformly convex in $\boldsymbol{u}$ and that the constraint functions d_k, $k \in [2m+1]$ are convex (because they are affine) in $\boldsymbol{u}$, log-barriers may again be used to introduce the approximate optimal control trajectory as

$$\hat{\boldsymbol{u}}^*(t) = \underset{\boldsymbol{u} \in \mathbb{R}^m}{\arg\min}\ \Omega(t, \boldsymbol{w}, \boldsymbol{x}, \boldsymbol{u}), \tag{6.49}$$

where

$$\Omega(t, \boldsymbol{w}, \boldsymbol{x}, \boldsymbol{u}) \triangleq J_u(t, \boldsymbol{x}, \boldsymbol{u}) - \frac{1}{s} \sum_{k=1}^{2m+1} \log\big(-d_k(t, \boldsymbol{w}, \boldsymbol{x}, \boldsymbol{u})\big), \tag{6.50}$$

for barrier parameter $s > 0$. Assume (as for Ψ in (6.2), Φ in (6.33)) that Assumption 6.1 holds for Ω, i.e., that there exists $s > 0$ that renders Ω strongly, uniformly convex in $\boldsymbol{u}$, and consider the following dynamical system

$$\begin{aligned} &\dot{\boldsymbol{u}} = \upsilon(t, \boldsymbol{w}, \boldsymbol{x}, \boldsymbol{u}) \triangleq -\nabla_{\boldsymbol{uu}}^{-1}\Omega\Big(\boldsymbol{B}\nabla_{\boldsymbol{u}}\Omega + \nabla_{\boldsymbol{uw}}\Omega\dot{\boldsymbol{w}} + \nabla_{\boldsymbol{ux}}\Omega\dot{\boldsymbol{x}} + \nabla_{\boldsymbol{ut}}\Omega\Big), \\ &\boldsymbol{u}(0) \in \mathcal{U}_H(0, \alpha), \end{aligned} \tag{6.51}$$

with $\boldsymbol{B} \in \mathbb{R}^{m \times m}$ a positive-definite gain matrix affecting the strength of the correction term, $\dot{\boldsymbol{w}}$ the adaptation law given by (6.35), and $\dot{\boldsymbol{x}}$ the state dynamics given by (6.4). In this case, the control law could then be given as the solution $\boldsymbol{u}(t)$ to the system (6.51), i.e.,

$$\boldsymbol{u}(t) = \varphi_t(\boldsymbol{u}(0)), \tag{6.52}$$

where φ^t is the flow map of (6.51) such that $t \mapsto \varphi^t(\boldsymbol{u}(0))$ solves (6.51) for initial condition $\boldsymbol{u}(0)$. The motivation for using interior point methods to introduce the dynamical system (6.51) is that it enables the expression of the state $\boldsymbol{x}$, weight $\boldsymbol{w}$, and control $\boldsymbol{u}$ dynamics as one interconnected

dynamical system with no external inputs:

$$\dot{\boldsymbol{\chi}} = F(t, \boldsymbol{\chi}) = \begin{bmatrix} \dot{\boldsymbol{x}} \\ \dot{\boldsymbol{w}} \\ \dot{\boldsymbol{u}} \end{bmatrix} = \begin{bmatrix} f(\boldsymbol{x}) + g(\boldsymbol{x})\boldsymbol{u} \\ \mu(t, \boldsymbol{w}, \boldsymbol{x}) + \nu(t, \boldsymbol{w}, \boldsymbol{x})\boldsymbol{u} \\ \upsilon(t, \boldsymbol{w}, \boldsymbol{x}, \boldsymbol{u}) \end{bmatrix} \tag{6.53}$$

where $\boldsymbol{\chi} = (\boldsymbol{x}, \boldsymbol{w}, \boldsymbol{u}) \in \mathbb{R}^{n+c+m}$ is the state, and for which a block diagram is provided in Figure 6.2. Though this is not the first time that a continuous-time interior point method has been used in place of a CBF-QP control law (see e.g., [236]), any work which uses such an approach for joint adaptation and control laws for constrained control design is unknown to the author. This permits the use of available tools like Barbalat's lemma [237, Lem. 8.2] for stability analysis of time-varying systems, and the hope is to investigate the properties of this system in the future.

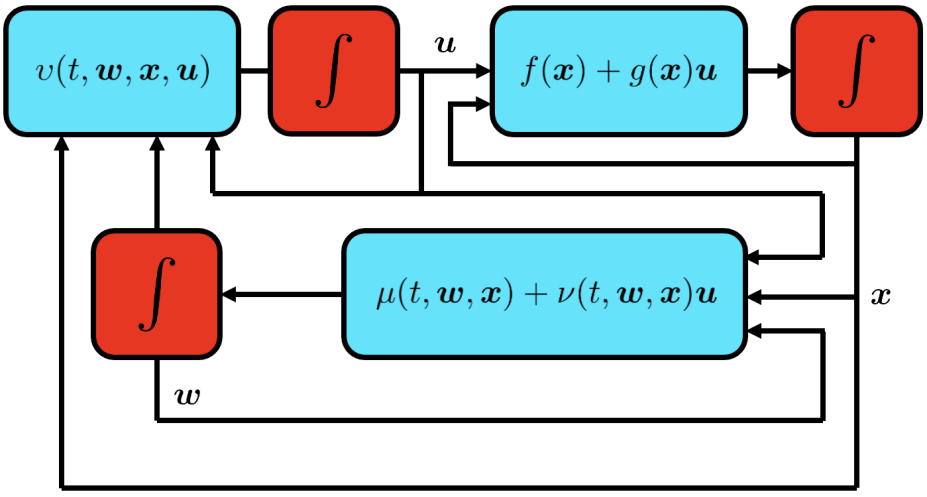

Figure 6.2: Block diagram for the $\dot{\boldsymbol{\chi}}$ dynamics described by (6.53).

6.4 Case Studies

For code and simulation videos, visit the linked Github repository[2].

6.4.1 Single-Agent Studies

In this section, two examples are considered to highlight the use of the C-CBF-QP controller introduced by (6.46) with the adaptation law (6.35): an illustrative one-dimensional problem, and

[2]Github repo: https://github.com/6lackmitchell/CCBF-Control

a reach-avoid scenario inspired by mobile robots by which the method is compared to several baseline controllers.

6.4.1.1 One-Dimensional Nonlinear System

Consider the following nonlinear, control-affine dynamical system:

$$\dot{x} = x(e^{kx^2} - 1) + (4 - x^2)u, \quad x(0) = 0, \tag{6.54}$$

where $x \in \mathbb{R}$ denotes the state, $u \in \mathcal{U} \subset \mathbb{R}$ the control input, and where $k = \ln(2)/p^2$ with $p = 1.5616$. It may be seen that the uncontrolled system has a unique (unstable) equilibrium at $x = 0$, and that there are two distinct control singularities at $x = 2$ and $x = -2$ respectively in the sense that the control u has no effect on the dynamics at these points. The control objective is to track a known trajectory

$$x^*(t) = 4\sin(2\pi\frac{t}{5} + \theta),$$

where considered separately are the cases $\theta = 0$ and $\theta = \pi$ (i.e., the sinusoid evolving in both positive and negative directions) subject to the state constraints $x \leq 2$ and $x \geq -2$, which may be encoded via constraint functions

$$h_1(x) = 2 - x,$$
$$h_2(x) = x + 2.$$

It is evident that perfect tracking of the desired state would result in violations of both of the above constraint functions as the signal $x^*(t)$ oscillates. The input constraint set is $\mathcal{U} = [-1, 1]$, which creates two infinite potential wells in the following sense: if it occurs that $2 > x > p_1 = p$ (resp. $-2 < x < p_2 = -p$) then x will escape to ∞ (resp. $-\infty$) and violate h_1 (resp. h_2) in doing so. In short, though the state constraints are $x \leq 2$ and $x \geq -2$, due to the input constraint set $\mathcal{U}$ these constraints are guaranteed to be violated if either $x > p$ or $x < -p$ regardless of the control applied thereafter. The proposed C-CBF controller has the ability to protect against these types of potential wells via online parameter adaptation, and it is now shown how it manages to continuously satisfy both constraints h_1 and h_2 simultaneously despite seeking to track an unsafe nominal trajectory.

The tracking problem was simulated using three different iterations of the C-CBF-QP controller (6.46) with a proportional control law tracking the desired trajectory $x^*(t)$ as a nominal input. The controllers differed in their tracking aggressiveness as encoded via the following class-$\mathcal{K}$ functions appearing in the C-CBF condition: $\alpha(H) = \gamma \cdot H^3$ with $\gamma = 0.01, 0.1, 1.0$. This made for a total of six trials: three controllers tested each on two separate desired trajectories. In all six scenarios the initial weights were $\boldsymbol{w}(0) = (2.38, 2.38)$. For the C-CBF H (6.18) was used with decaying

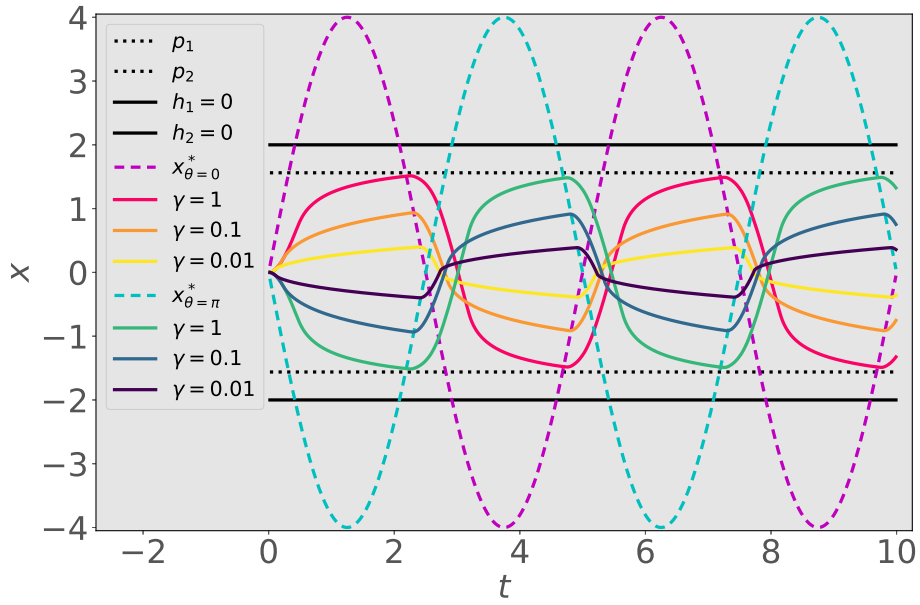

(a) State x

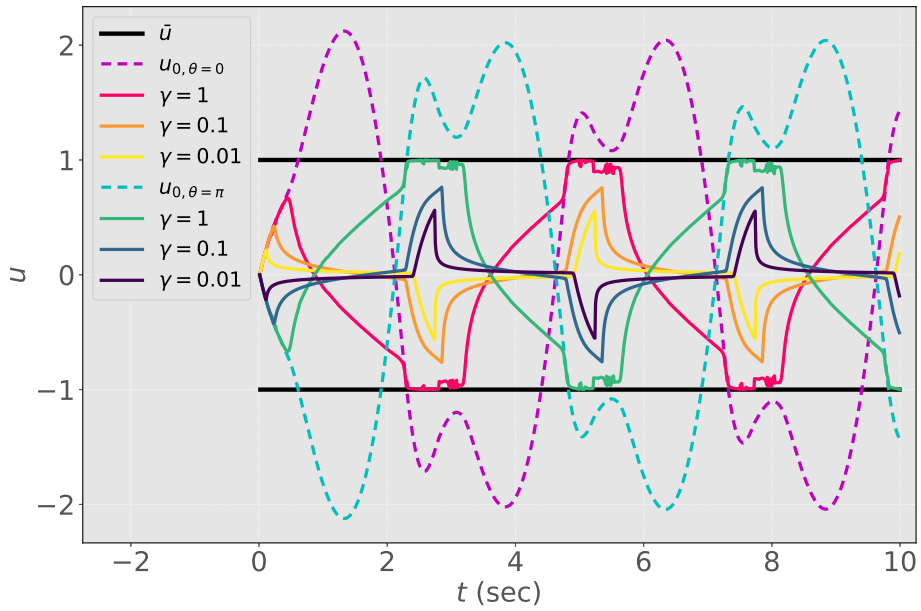

(b) Control u

Figure 6.3: Evolution of the (a) state x and (b) control u for the 1-D trajectory tracking problem using the C-CBF controller with 3 different class $\mathcal{K}_\infty$ functions of the form $\alpha(H) = \gamma \cdot H^3$ for the given γ values.

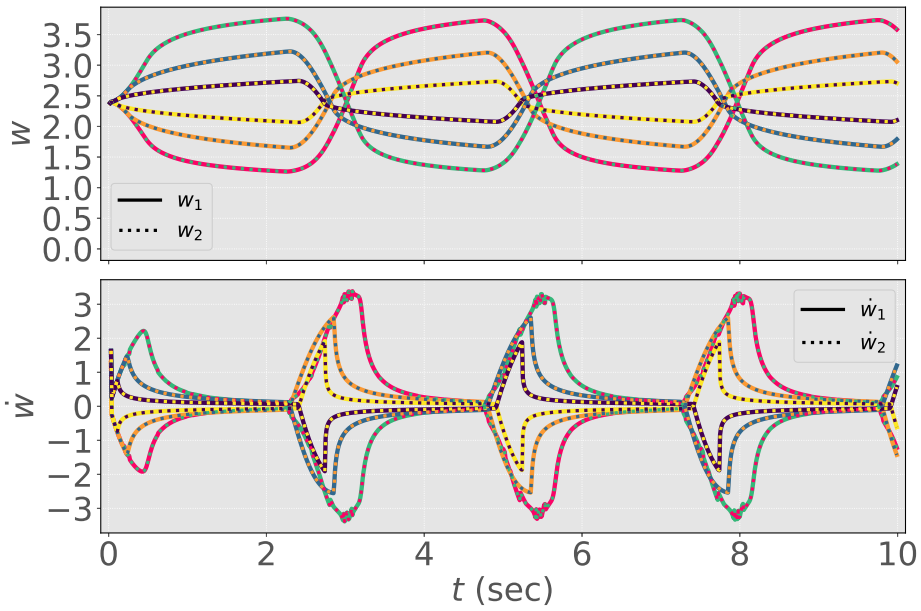

(a) Weights $\boldsymbol{w}$

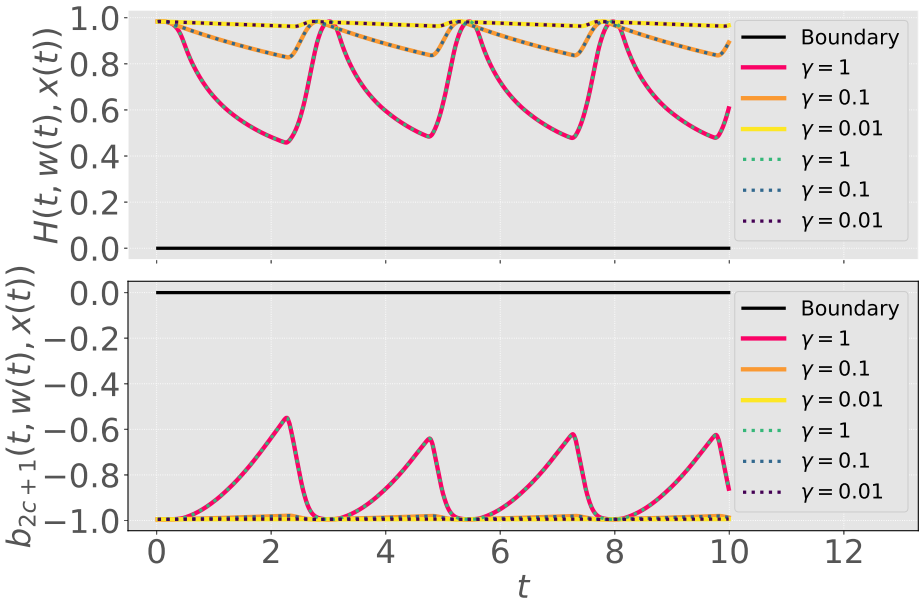

(b) C-CBFs

Figure 6.4: Constraint function (a) weights $\boldsymbol{w}$ and (b) values h_i, $i \in \{1, 2\}$, H, and b_{2c+1} for the 6 trials of the 1-D trajectory tracking problem.

exponentials, i.e., $\phi(r, s) = e^{-rs}$. For the adaptation law (6.35), $w_{min} = 0.01$, $w_{max} = 50.0$, and $\boldsymbol{P} = 100\boldsymbol{I}$ were used.

The evolution of the state in each trial is shown in Figure 6.3a, from which it may be seen that not only are the position constraints satisfied at all times despite the unsafe reference path but also every iteration of the C-CBF controller succeeds in preventing the system from entering one of the infinite potential wells. As can reasonably be expected, the controllers equipped with more aggressive parameters γ approached the boundary of the potential wells more closely. It is evident from Figure 6.3b that the proposed controller modifies the nominally unsafe inputs in advance of any danger. Note that while no guarantees of Lipschitz continuous control inputs or weights are provided, the approach produced both inputs and weights that varied smoothly, as seen also in Figure 6.4a. It is worth highlighting the symmetry of the adaptation for identical controllers tracking an inverted reference trajectory, which makes sense given the symmetry of the dynamics about the equilibrium point and the identical initial conditions. Figure 6.4b verifies that the C-CBF H remained non-negative at all times and that the C-CBF condition remained viable at all times under the input constraints thanks to the proposed adaptation law (6.35).

6.4.1.2 Mobile Robot Reach-Avoid Scenario

In the second numerical case study, under consideration is a (car-like) mobile robot with bicycle dynamics seeking to reach a target location within a prescribed time in the presence of static obstacles, a speed limit, and steering constraints.

Let s_0 be a local origin in an inertial frame $\mathcal{I}$, and suppose that the robot dynamics may be described by the following dynamic extension of the non-holonomic bicycle model studied in Chapter 2 and described by [191, Ch. 2], provided here for completeness:

$$\dot{x} = v\left(\cos\psi - \sin\psi\tan\beta\right), \tag{6.55a}$$

$$\dot{y} = v\left(\sin\psi + \cos\psi\tan\beta\right), \tag{6.55b}$$

$$\dot{\psi} = \frac{v}{l_r}\tan\beta, \tag{6.55c}$$

$$\dot{\beta} = \omega, \tag{6.55d}$$

$$\dot{v} = a, \tag{6.55e}$$

where x and y denote the position (in m) of the center of gravity (c.g.) of the robot with respect to s_0, ψ is the orientation (in rad) of its body-fixed frame, $\mathcal{B}$, with respect to $\mathcal{I}$, β is the slip angle[3] (in rad) of the c.g. of the vehicle relative to $\mathcal{B}$ (with $|\beta| < \frac{\pi}{2}$), and v is the velocity of the rear wheel

[3] β is related to the steering angle δ via $\tan\beta = \frac{l_r}{l_r+l_f}\tan\delta$, where $l_f + l_r$ is the wheelbase with l_f (resp. l_r) the distance from the c.g. to the center of the front (resp. rear) wheel.

with respect to $\mathcal{I}$. The state is denoted $\boldsymbol{z} = [x\ y\ \psi\ \beta\ v]^T$, and the control input is $\boldsymbol{u} = [\omega\ a]^T$, where ω is the angular velocity (in rad/s) of β and a is the acceleration of the rear wheel (in m/s^2). The objective of the robot is to reach a neighborhood of the goal location $(x_g, y_g) = (2, 2)$ from initial condition $\boldsymbol{z}_0 = [0,\ 0,\ \arctan\big((y_g - y)/(x_g - x)\big)\ 0.5,\ 0.0]^T$ while obeying the following 8 constraints: avoid five circular obstacles, obey the speed limit of $S = 2$m/s, obey the slip angle limit $B = \pi/3$, and reach the goal set within $T = 5$sec. The constraint functions encoding avoidance of the ith circular obstacle are given by

$$h_i(t, \boldsymbol{z}) = (x - c_{x,i})^2 + (y - c_{y,i})^2 - R_i^2,\ \forall i \in [5],$$

for radius $R_i > 0$ and center point $(c_{x,i}, c_{y,i})$. The speed and slip angle constraints are

$$h_6(t, \boldsymbol{z}) = S^2 - v^2,$$
$$h_7(t, \boldsymbol{z}) = B^2 - \beta^2,$$

and the time-specification is defined by

$$h_8(t, \boldsymbol{z}) = R_g^2 + R_i^2 \left(1 - \frac{t}{T}\right)^2 - (x - x_g)^2 - (y - y_g)^2,$$

for the goal set centered at (x_g, y_g) with radius $R_g = 0.1$m and shrinking radius $R_i = 4$m. Note that with the exception of constraint functions h_6 and h_7, all other constraint functions have relative-degree two with respect to the dynamics (6.55), which means that the C-CBF control matrix $\boldsymbol{L}_g$ has six rows consisting only of zeros. If these functions were used as CBF candidates directly, their control terms would be zero at all times, i.e., $L_g h_i = \mathbf{0}$ for $i \in \{1, 2, 3, 4, 5, 8\}$, $\forall t \geq 0$. The C-CBF is then of the form (6.18), where again use exponentials $\phi(r, s) = e^{-rs}$ with initial weights $\boldsymbol{w}(0) = 1.0 \cdot \mathbf{1}_{8\times 1}$. We use the function $\alpha(H) = H$.

For comparison against existing works, the following were simulated: a HO-CBF-QP controller (with guaranteed input constraint satisfaction for a single CBF) proposed by [168], and an exponential (E-) CBF-QP controller (a subset of the class of HO-CBF controllers from [238]) introduced in [40], both of which require reformulating constraint functions h_i for $i \in \{1, 2, 3, 4, 5, 8\}$ as high-order CBFs. Each class of controller was simulated over a time interval of $\mathcal{T} = [0, 5]$ sec at a timestep of $\Delta t = 0.01$ sec and under four different class-$\mathcal{K}_\infty$ functions with varying levels of conservatism, from most (e.g., HO-CBF-1) to least conservative (e.g., HO-CBF-4). The resulting paths and controls applied by the simulated bicycle robots are shown in Figures 6.5 and 6.6 respectively. Although the HO-CBF-QP controller proposed by [168] guarantees constraint adherence under input constraints for one constraint function, under multiple constraint functions the

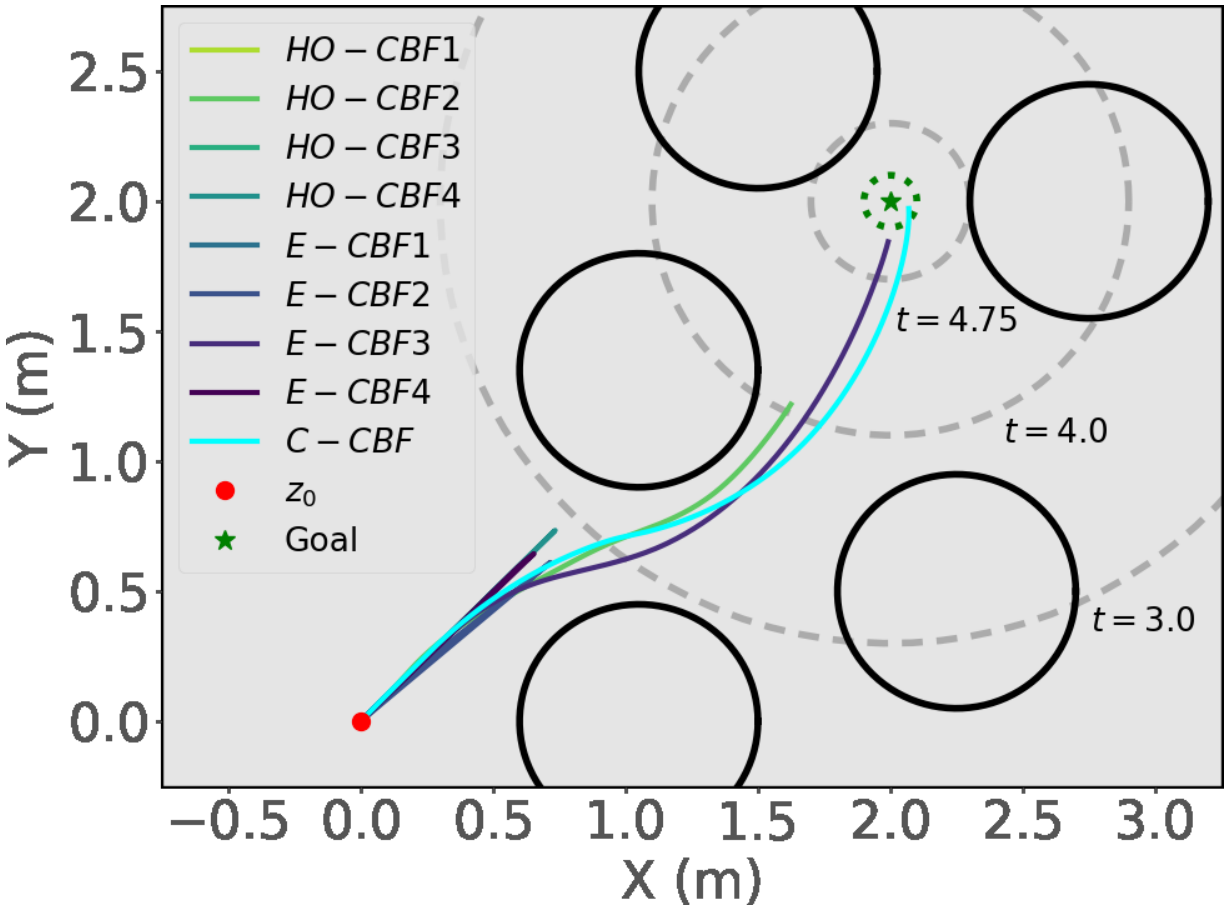

Figure 6.5: XY paths for bicycle robots seeking to reach the goal set (dotted green circle) within a prescribed time in the presence of static obstacles (black circles), a speed limit, and a slip angle constraint. Gray dashed lines indicate the reach constraint set at various times. All 6 HO- and E-CBF QP controllers become infeasible (though one E-CBF comes very close to the goal), while our adaptive C-CBF controller guarantees sufficient control authority for the feasibility of (6.46) under input constraints and thus reaches the goal.

QP controller becomes infeasible in all four simulated trials (doing so, in fact, almost immediately for the most conservative HO-CBF-1 case) and therefore does not reach the goal. The E-CBF-QP controller has no guaranteed input constraint satisfaction and consequently takes more aggressive control actions. Notice, however, that the performance is highly sensitive to the choice of E-CBF gains: too conservative (E-CBF-1) and the QP quickly becomes infeasible; too aggressive (E-CBF-4) and the QP becomes infeasible when it no longer has sufficient control authority to avoid a collision with the first obstacle. It is clear that for this example both trial and error and expert knowledge are required to tune the E-CBF-QP controller to solve the problem.

For the C-CBF controller, however, the assumption that the feasible region $\mathcal{W}(t)$ has an interior point at all times holds, and thus the proposed adaptation law finds a weighting of the constraint

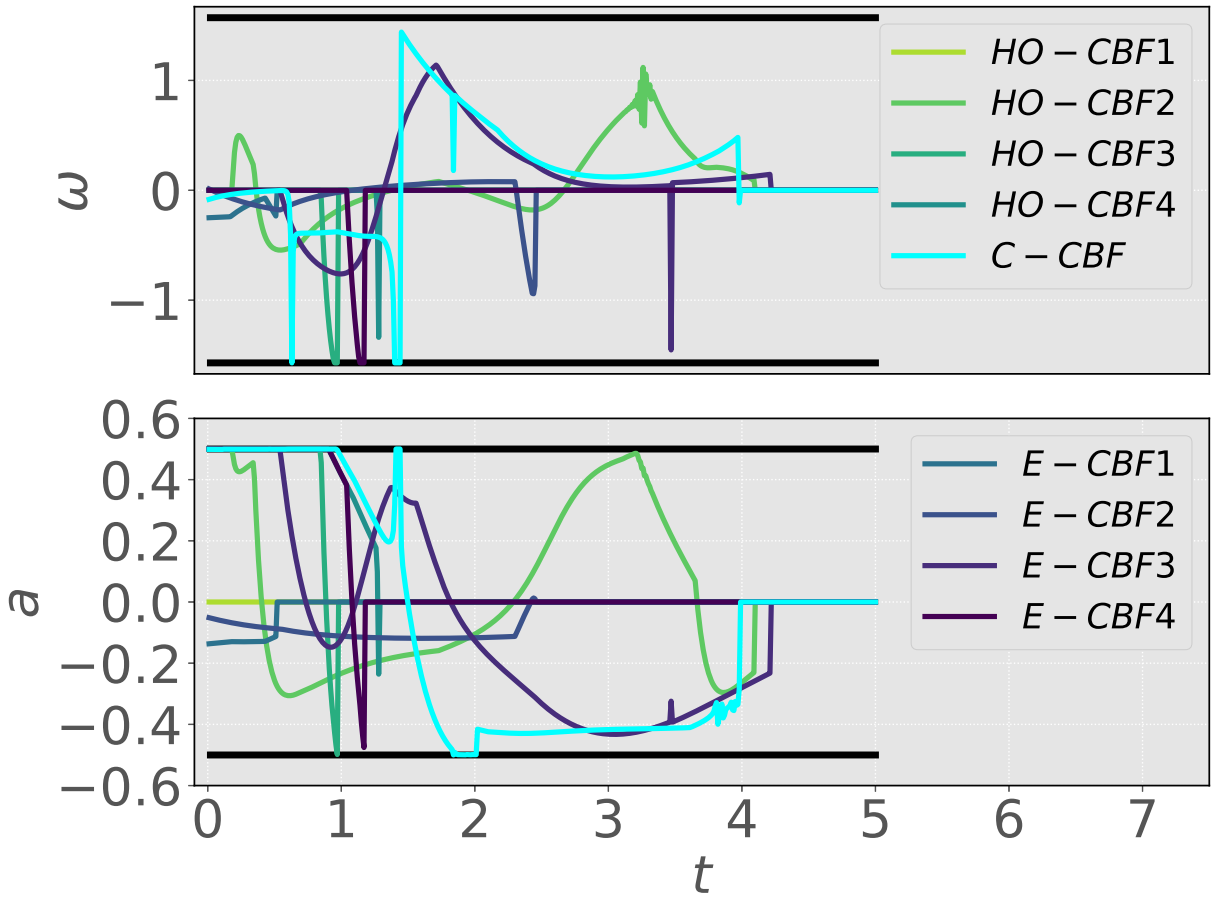

Figure 6.6: Control trajectories for the bicycle robot reach-avoid problem.

functions that allows the robot to safely reach the goal within the prescribed time. Figure 6.7 shows that all constraints were satisfied, and that feasibility of the C-CBF condition is preserved despite six of the eight constraints having relative-degree two with respect to the system dynamics (and thus contributing nothing to the $\frac{\partial H}{\partial \boldsymbol{x}} g(\boldsymbol{x})$ term in the C-CBF dynamics). Smoothly weighting the various constraint functions, as highlighted in Figure 6.8, allows the controller to take smooth control actions without sudden switching or oscillatory behavior, and thus the C-CBF controlled vehicle reaches the goal while satisfying every constraint throughout the duration of the maneuver.

6.4.2 Multi-Agent Studies

Two studies are considered in this subsection. The first is a multi-agent reach-avoid problem in which 3 non-communicating bicycle robots seek to reach target locations by navigating through a narrow corridor amongst non-responsive agents. In the second, a hardware experiment is conducted in the laboratory environment in which a ground rover seeks to reach a goal location in the

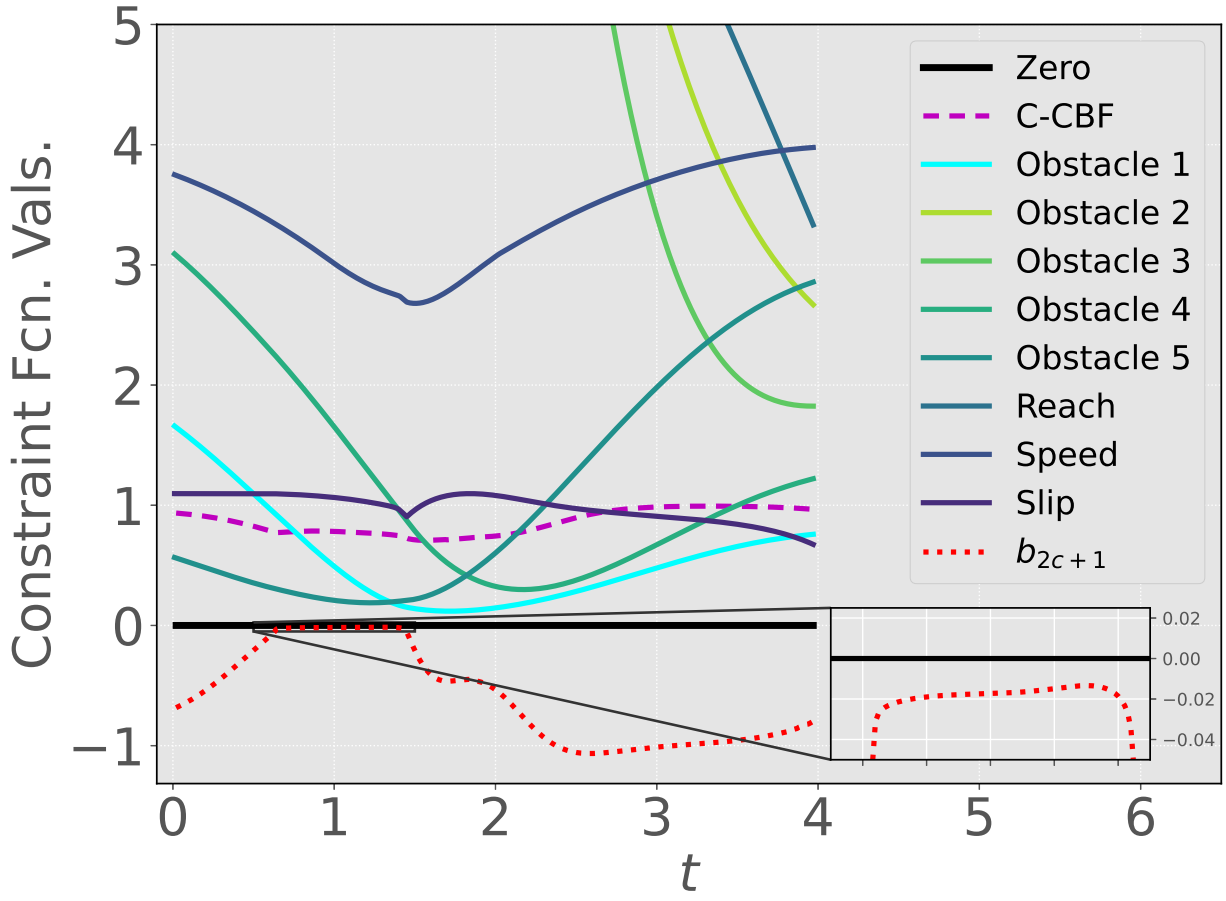

Figure 6.7: Values of the constraint functions h_i, $\forall i \in [8]$ (solid), the C-CBF H (dashed), and constraint function b_{2c+1} given by (6.40) (dotted) with respect to time for the C-CBF controlled bicycle robot in the reach-avoid problem.

presence of two non-communicating rovers. In all of the studies in this subsection, the adaptation law (6.25) is used to enforce the C-CBF condition.

6.4.2.1 Warehouse Goal-Seeking

Consider a collection of 3 non-communicative (i.e., do not share information regarding goals, control inputs, etc.), but responsive (i.e., seek to preserve safety) robots ($i \in \mathcal{A}_r$) in a warehouse environment seeking to traverse a narrow corridor intersected by a passageway occupied with 6 non-responsive (i.e., may not seek to preserve safety) agents ($i \in \mathcal{A}_{nr}$). The non-responsive agents may be e.g. humans walking or some other dynamic obstacles. The dynamics model for all agents was taken to be the dynamic bicycle model (6.55).

The challenges of this scenario relate to preserving safety despite multiple non-communicative and non-responsive agents present in a constrained environment. A robot is safe if it 1) obeys the

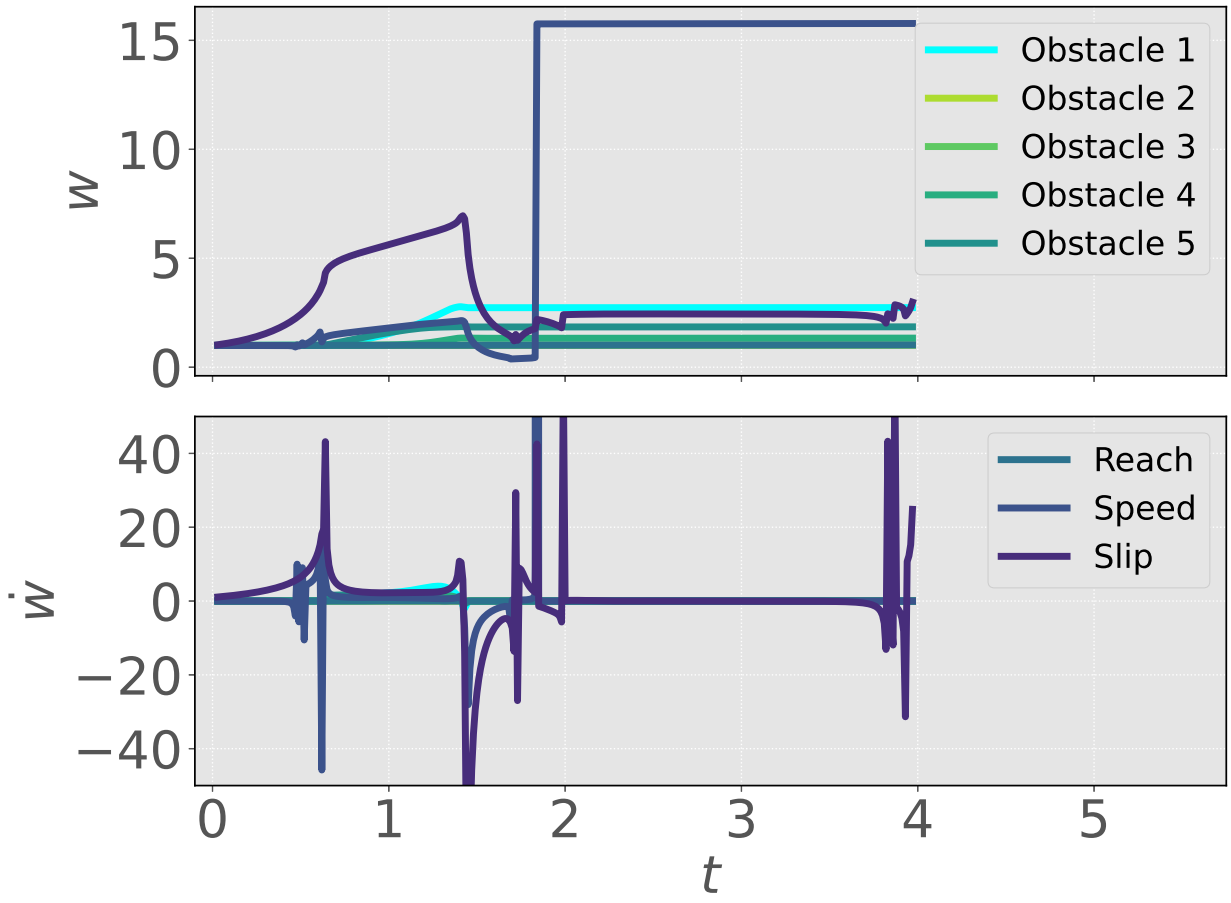

Figure 6.8: C-CBF weights $\boldsymbol{w}$ and their derivatives $\dot{\boldsymbol{w}}$ using adaptation law (6.35) for the bicycle robot reach-avoid problem.

speed restriction, 2) remains inside the corridor area, and 3) avoids collisions with all other robots. Speed is addressed with the following candidate CBF:

$$h_v(\boldsymbol{z}_i) = s_M - v_i, \tag{6.56}$$

where $s_M > 0$, while for corridor safety and collision avoidance we used forms of the relaxed future-focused CBF introduced in Chapter 2 for roadway intersections, namely

$$h_c(\boldsymbol{z}_i) = (m_L(x_i + \dot{x}_i) + b_L - (y_i + \dot{y}_i))(m_R(x_i + \dot{x}_i) + b_R - (y_i + \dot{y}_i)) \tag{6.57}$$

$$h_r(\boldsymbol{z}_i, \boldsymbol{z}_j) = D(\boldsymbol{z}_i, \boldsymbol{z}_j, t + \hat{\tau})^2 + \epsilon D(\boldsymbol{z}_i, \boldsymbol{z}_j, t)^2 - (1 + \epsilon)(2R)^2, \tag{6.58}$$

where (6.57) prevents collisions with the corridor walls (defined as lines in the xy-plane via $m_L, b_L, m_R, b_R \in \mathbb{R}$), and (6.58) prevents inter-robot collisions and is defined $\forall i \in \mathcal{A}_n \setminus \mathcal{A}_{n,n}$,

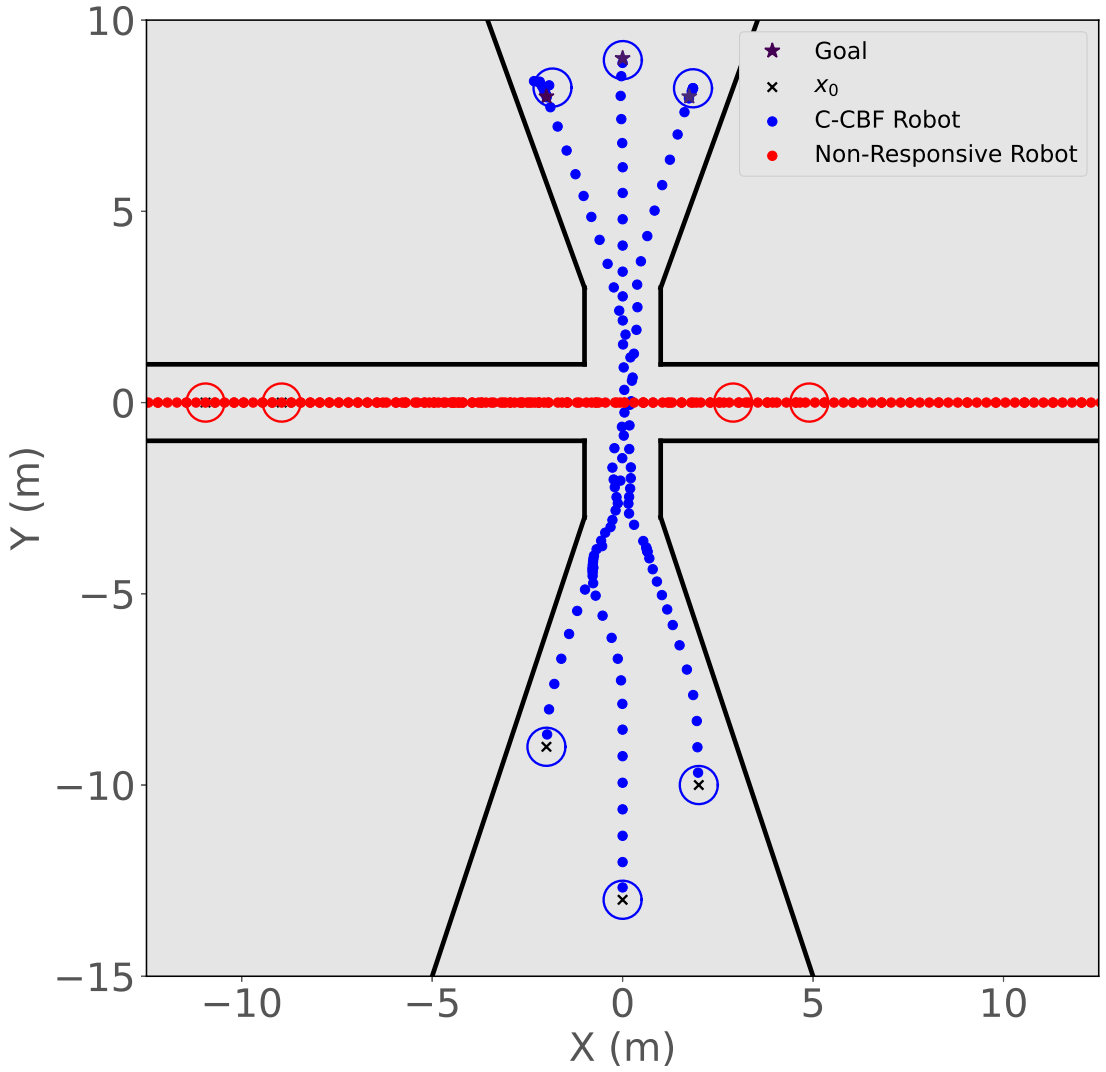

Figure 6.9: XY paths for the warehouse robots (blue) and non-responsive agents (red) in the warehouse control problem.

$\forall j \in \mathcal{A}_n$, where $\epsilon > 0$, $D(\boldsymbol{z}_i, \boldsymbol{z}_j, t_a)$ is the Euclidean distance between agents i and j at arbitrary time t_a, and $\hat{\tau}$ denotes the time in the interval $[0, T]$ at which the minimum inter-agent distance will occur under constant velocity future trajectories. As such, (6.56), (6.57), and (6.58) define the sets

$$
\begin{aligned}
S_{v,i} &= \{\boldsymbol{z}_i \in \mathbb{R}^n \mid h_v(\boldsymbol{z}_i) \geq 0\}, \\
S_{c,i} &= \{\boldsymbol{z}_i \in \mathbb{R}^n \mid h_c(\boldsymbol{z}_i) \geq 0\}, \\
S_{r,i} &= \bigcap_{j=1, j\neq i}^{A} \{\boldsymbol{z} \in \mathbb{R}^N \mid h_r(\boldsymbol{z}_i, \boldsymbol{z}_j) \geq 0\},
\end{aligned}
$$

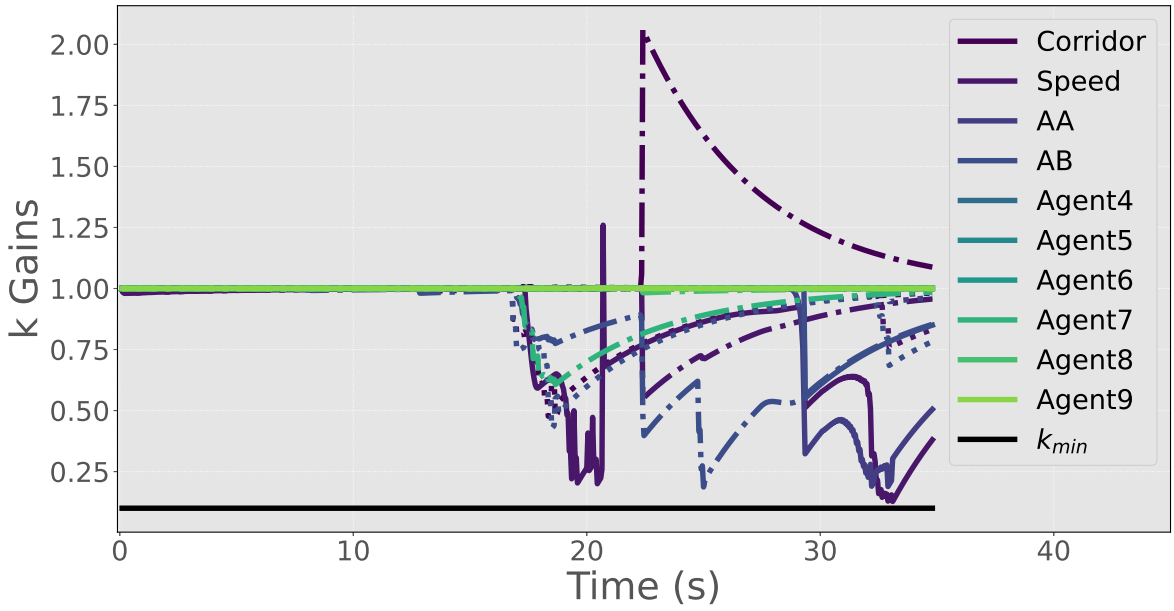

Figure 6.10: Gains $\boldsymbol{w}$ for the C-CBF controllers in the warehouse study. Robot 1 denoted with solid lines, dotted for robot 2, dash-dots for robot 3. AgentA and AgentB denote the other two non-communicative robots from the perspective of one (e.g. AgentA=Agent1 and AgentB=Agent3 for robot 2).

the intersection of which constitutes the safe set for agents i, i.e. $S_i(t) = S_{v,i} \cap S_{c,i} \cap S_{r,i}$.

The robots $i \in \mathcal{A}_r$ are controlled using a C-CBF-QP controller of the form (6.46) with constituent functions h_c, h_s, h_r, an Linear-Quadratic Regulator (LQR) based nominal control input (see Appendix A), and initial gains $\boldsymbol{w}(0) = \mathbf{1}_{10\times 1}$. The non-responsive agents used a similar LQR controller to move through the passageway in pairs of two, with the first two pairs passing through the intersection without stopping and the last pair stopping at the intersection before proceeding.

As shown in Figure 6.9, the non-communicative robots traverse both the narrow corridor and the busy intersection to reach their goal locations safely. The trajectories of the gains $\boldsymbol{w}$ for each warehouse robot are shown in Figure 6.10, while their control inputs are depicted in Figure 6.11. The CBF time histories for the constituent and consolidated functions are highlighted in Figures 6.12 and 6.13 respectively, and show that the C-CBF controllers maintained safety at all times.

6.4.2.2 Laboratory Experiment

For experimental validation of our approach, an AION R1 UGV ground rover was used as an ego vehicle in the laboratory setting. It was required to reach a goal location in the presence of two non-responsive rovers: one static and one dynamic. The rovers were modelled as bicycles using (6.55), and sent angular rate ω_i and velocity v_i (numerically integrated based on the controller's acceleration output) commands to the rovers' on-board PID controllers. The ego rover used the proposed C-CBF-QP controller (6.46) with constituent candidate CBFs (6.56) (with $s_M = 1$ m/s)

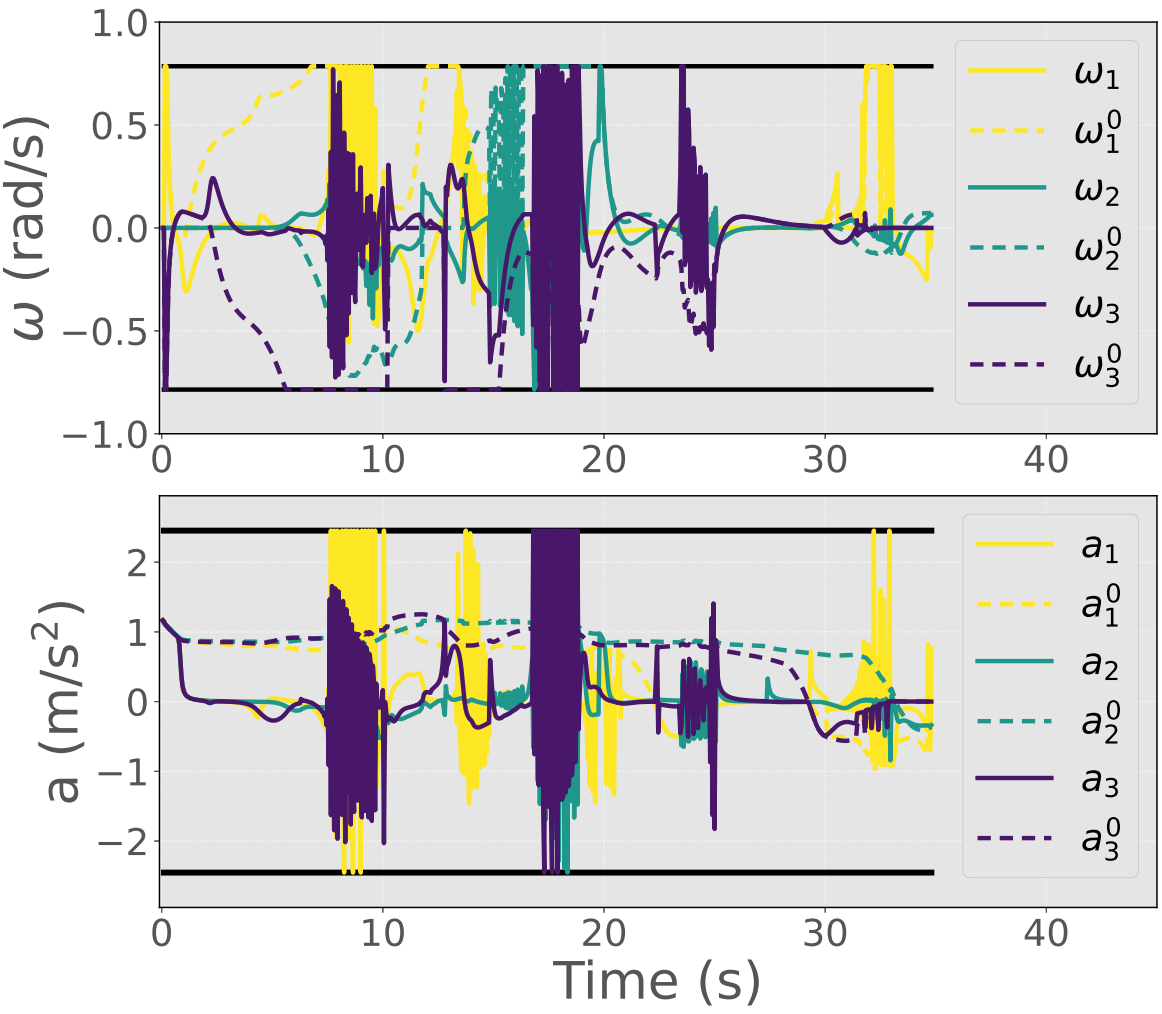

Figure 6.11: Warehouse robot controls: accel. (a) and slip angle rate (ω).

and the Relaxed Future-Focused Control Barrier Function (RFF-CBF) defined in (6.58) for collision avoidance. The nominal input to the C-CBF controller was the LQR law from the warehouse robot example, as was the controller used by the dynamic non-responsive rover. A Vicon motion capture system was used for position feedback, and the state estimation was performed by extended Kalman filter via the on-board PX4.

For the setup, the static rover was placed directly between the ego rover and its goal, while the dynamic rover was stationary until suddenly moving across the ego's path as it approached its target. As highlighted in Figure 6.14, the ego rover first headed away from the static rover and then decelerated and swerved to avoid a collision with the second rover before correcting course and reaching its goal. Videos and code for both this experiment and the prior simulations are available on Github[4].

[4]Link to Github repo: github.com/6lackmitchell/CCBF-Control

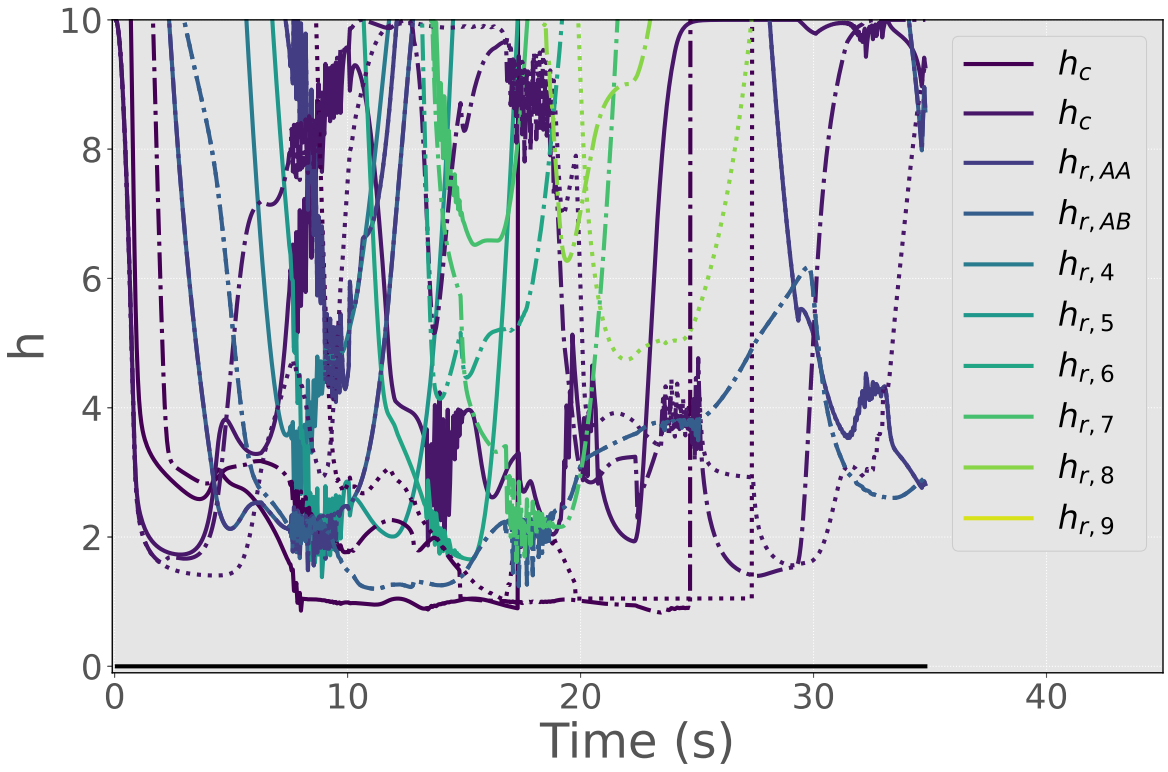

Figure 6.12: Evolution of warehouse robot constituent CBF candidates, $h_s \; \forall s \in [1..c]$, synthesized to construct C-CBF.

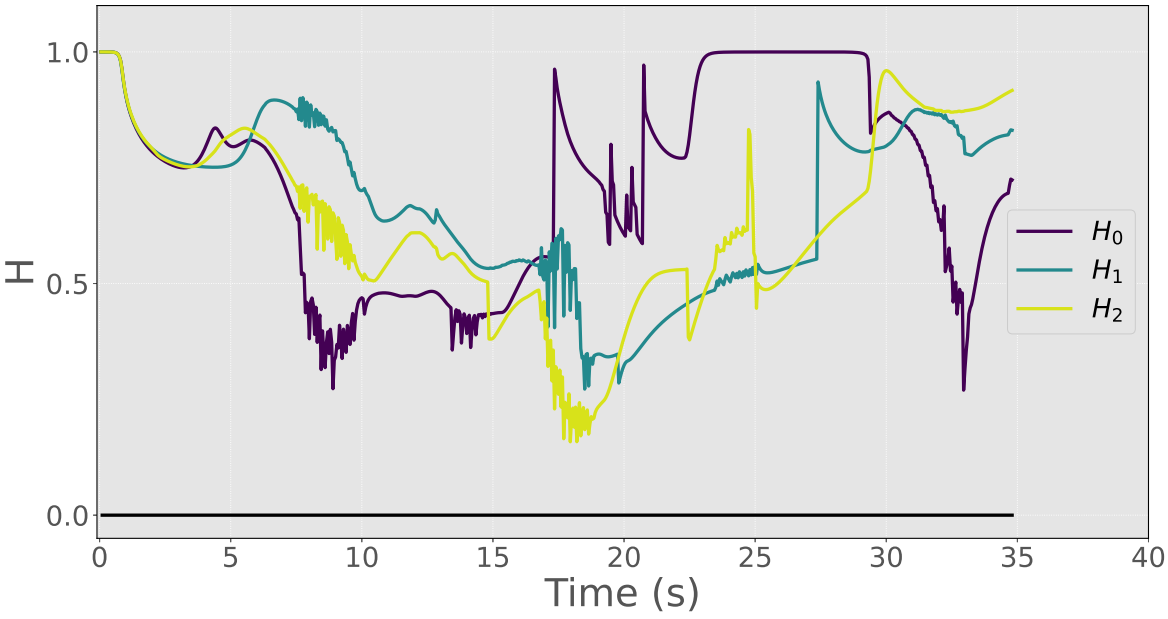

Figure 6.13: Evolution of C-CBF H for warehouse robots 1, 2, and 3.

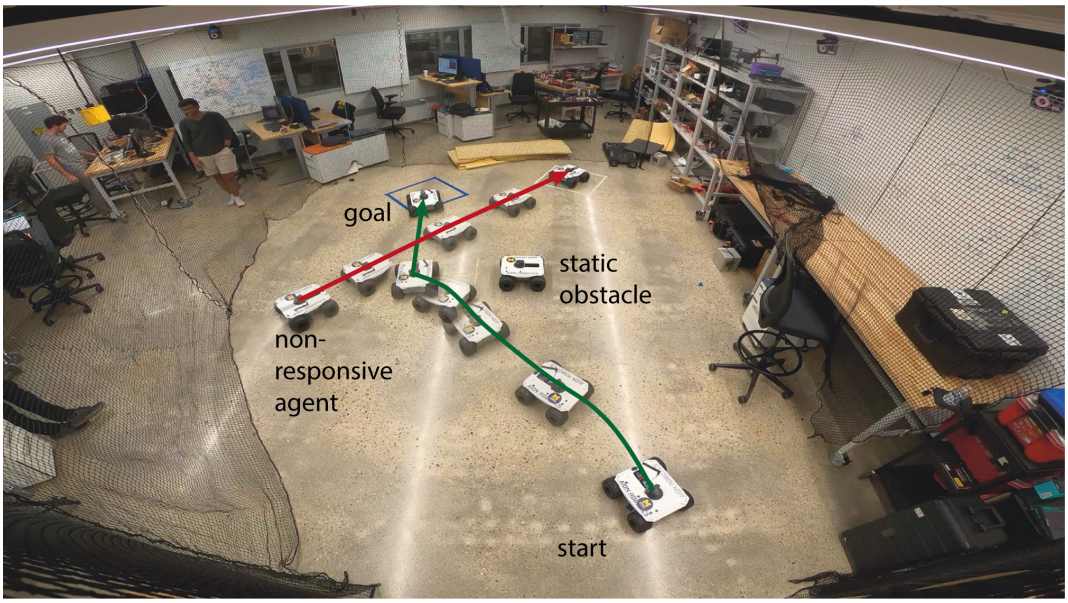

Figure 6.14: A rover avoids a static and dynamic rover using our proposed C-CBF controller en route to a target in the laboratory setting.

6.5 Conclusion

In this chapter, a class of consolidated control barrier function candidates was proposed for control design of a class of nonlinear, control-affine systems under multiple spatiotemporal and input constraints. It was shown that the C-CBF candidate could be rendered valid online in the case of unbounded control authority by adapting the weights of its constituent constraint functions according to a QP-based adaptation law. Then, using interior point methods from the theory of continuous-time optimization, a second weight adaptation law was proposed for the case of limited control authority in the form of an auxiliary dynamical system, the solution of which is guaranteed to lie within the feasible region of the underlying optimization problem whenever it contains an interior point. Single- and multi-agent case studies in both simulation and hardware experimentation demonstrated the efficacy of the methods for online control design under multiple spatiotemporal constraints.

CHAPTER 7

Conclusion

7.1 Conclusions

This dissertation advances the viability of Control Barrier Function (CBF)-based control synthesis for safety-critical systems in complex and uncertain environments.

First, in Chapter 2 a safe, efficient, predictive control framework was proposed for autonomous vehicles to address a deficiency in existing CBF-based approaches, namely that their influence leads to myopically present-focused behavior. Classes of Future-Focused Control Barrier Functions (FF-CBFs) and Relaxed Future-Focused Control Barrier Functions (RFF-CBFs) were introduced to encode that present control accounts take future safety predicted under a zero-control policy into account, and their use on an unsignaled intersection crossing problem was shown to significantly reduce the frequency of deadlocks. In the context of decentralized multi-agent control design, the FF-CBF was shown to preserve safety under perfect state measurements in the presence of unknown actions taken by non-communicating vehicles without requiring additional robustness measures.

Chapter 3 studied the problem of fixed-time system identification for the purpose of reducing conservatism in safe control design under bounded, parametric model uncertainty. As a solution, it proposed two parameter adaptation laws for identifying the unknown perturbation to the system dynamics within a fixed-time when perfect rate and/or state measurements are available. An expression for the time-varying, monotonically decreasing parameter estimation error bound was derived, and a new, robust, adaptive CBF condition was introduced for preserving safety. In Chapter 4, an adaptation law from Chapter 3 was proven to be robust to an additive, bounded perturbation to the system dynamics; namely, it was shown that the parameter estimates would converge to a characterized neighborhood of the true values within a fixed-time despite the effect of bounded measurement noise or additional non-parametric disturbances. Emphasizing its versatility, a form of that same law was then proposed for learning a more general class of, bounded, nonlinear perturbations to the system dynamics via a novel form of Koopman operator theory (KOT)-based

fixed-time system identification for safe control design under the assumption that the choice of basis functions is sufficiently descriptive.

In pursuit of a comprehensive control framework for safety under uncertainty and having already studied various classes of model uncertainty in the deterministic setting, Chapter 5 considered the problem of risk-aware control for a class of nonlinear, control-affine, stochastic systems. Thus, the uncertainty under consideration was represented by an additive, Brownian motion process and thus modelled the effect of random perturbations to the system, though notably it was assumed that the state was measured exactly at all times. The main contribution was a novel class of Risk-Aware Control Barrier Functions (RA-CBFs), the use of which for control design results in a bound on the system becoming unsafe over a specified (finite) time interval. It was shown that the proposed approach reduces conservatism under explicitly defined conditions relating to the strength of the process noise when compared to the existing state-of-the-art, and a recursive approach was further introduced to reduce the upper bound on the system risk. The method was verified in simulation with a large-scale empirical study on a reach-avoid problem and in the context of autonomous vehicle merging onto a highway amongst dense traffic. Finally, Chapter 6 addressed a common oversight in CBF-based control design by introducing adaptation-based approaches to synthesizing a *valid* Consolidated Control Barrier Function (C-CBF) that serves to ensure that multiple spatiotemporal constraints are satisfied jointly at all times under both unbounded and limited control authority. Having studied system identification in Chapters 3 and 4, it was assumed in this case that the system model was known. Applications of the proposed methods are shown for both single- and multi-agent systems in simulation and laboratory experiments.

In summary, this dissertation is a step toward a full-stack framework for safe, online control synthesis in dynamic, unknown environments. Through future state prediction, future risk assessment, adaptation for system identification, and adaptation for verification, it is the hope of the author that the work in this dissertation is of interest and value to researchers and engineers searching for safe control solutions.

7.2 Future Work

7.2.1 System Identification with Koopman Operator Theory

In recent years, advancements to the field of KOT have ushered in a new era of data-driven nonlinear system identification for control. Many recent works have used a newly popular extended dynamic mode decomposition approach to learning a dynamical system model online via batch estimation [119, 122]. As shown in the comparative study in Chapter 4, however, analytical bounds on the system identification error may not be available, which may inhibit the viability of this class

of methods for safe control synthesis. Instead, the work in Chapter 4 of this dissertation proposed a form of recursive system identification, though not without its limitations.

Since KOT dictates that for a class of nonlinear dynamical systems there exists an analogous linear but importantly *infinite-dimensional* Koopman dynamical system, one of the main open problems in this field is in quantifying the error associated with projecting the infinite-dimensional Koopman operator onto a finite-dimensional subspace. Some recent work has sought to address this problem by deriving bounds on the operator projection error, e.g., for ergodic trajectories [128] or under finite data (though, notably, suffering from the curse of dimensionality as pointed out in [127]), but no existing methods exist for bounding this error in the continuous-time domain. In fact, in this dissertation it was assumed that there exists a finite-dimensional matrix representation of the infinite-dimensional Koopman operator that exactly captures the dynamics in the lifted space, i.e., that a Koopman-invariant subspace was captured with the chosen basis functions. In the future, the author hopes to remove this assumption by making what follows the subject of future study: 1) the problem of quantifying the finite-dimensional projection error in the context of recursive identification schemes, and 2) determining a priori a choice of basis functions associated with a Koopman invariant subspace, i.e., a finite-dimensional space over which the infinite-dimensional Koopman operator is captured exactly. In doing so, the loop on a robust framework for system identification for safe control could be considered closed.

7.2.2 Online Predictive Control for Safety-Critical Systems

Existing methods to CBF-based online, safe, predictive control, including the class of FF-CBFs introduced in Chapter 2 and the later development of the more general predictive CBFs by [239], seek to encode that state trajectories predicted over some future time interval remain within some set of states *predicted* to be safe. Approaches to dealing with scenarios in which the predicted trajectories become unsafe typically fall into two categories: 1) relaxing the constraint while the predicted safety violation is far enough in the future, or 2) switching to a backup control law [240, 197] to steer the system back to safety. And whereas existing results on CBFs indicate that the safe set can be reached from outside asymptotically [3] or in finite-time [241], the problem of certifying that the set of states predicted to remain safe will be reached from outside *before the system trajectories leave the actual safe set* is not well-studied.

This problem is relevant as well in risk-aware control for stochastic, safety-critical systems. In the class of RA-CBFs proposed in Chapter 5, the risk of becoming unsafe over a finite time interval was bounded via control design. In the context of FF-CBFs for predictive control, however, the system trajectories may exit the safe set without incurring actual safety violations, e.g., colliding with an obstacle. The probability of becoming unsafe in reality then becomes the probability that

the system trajectories leave the *predicted* safe set *and* that they do not recover to the predicted safe set before leaving the present safe set. Thus, the author is interested in pursuing extensions of risk-aware control design to predictive control frameworks while removing the assumption that perfect measurements are available via the consideration of stochastic estimators (e.g., extended Kalman filter) in order to simultaneously derive tighter bounds on the risk of the system becoming unsafe, reduce conservatism in the control design, and account for the imperfections associated with real-world sensing capabilities.

In addition, the class of stochastic uncertainty under consideration in Chapter 5 takes a very specific form: in effect an additive, Brownian motion perturbation with known covariance. In crowded, multi-agent environments, it may be more beneficial for each individual agent to consider some alternate probability distribution over the set of actions available to the remaining agents. Though this may require the use of learning-based tools like Gaussian processes, Bayesian optimization, kernel density estimation, etc. to infer the underlying distribution, doing so would provide a more accurate assessment of the risk associated with taking an action both in the present moment and over some future time interval. It is the objective of the author to study the effect of these learning-based methods for modeling system uncertainty in the context of risk-aware and predictive control.

7.2.3 Viability of CBF-based Control Laws

As discussed in Chapter 6, finding a viability domain for a CBF-based controller is a difficult problem. In particular, for the class of CBF-Quadratic Program (QP) control laws used throughout this dissertation guarantees of viability may require extensive offline analysis using, e.g., verification tools [176, 177], sampling methods [242], reachability analysis [243], etc. Methods proposed in recent years offering guarantees of feasibility for this class of QP-based control laws (e.g., [49, 46]) may more appropriately be sorted into a class of *feasibility enhancing* approaches due to the tendency to assume the existence of a feasible input at some level deeper than the standard QP, the work in Chapter 6 of this dissertation included. But whereas many other works use optimization explicitly for control, it is the belief of the author that implicit optimization via dynamical systems introduced by, e.g., interior point methods for continuous-time optimization, represent an interesting future avenue toward bridging the gap between online control synthesis and offline system verification.

Of particular interest are methods for synthesizing Lyapunov functions for time-varying systems. Considering that, as discussed in Section 6.3.2, a class of nonlinear, control-affine systems under the effect of the proposed C-CBF control law may be reformulated into a time-varying, autonomous system, there is an opportunity to investigate stability properties of the full system either

through 1) offline analysis, e.g. stability theorems like Barbalat's lemma, or via 2) online gain adaptation, though this may be more challenging given that the underlying system of interest is subject to spatiotemporal constraints. In addition, it may be possible to either learn a Lyapunov function for the full adaptively controlled dynamical system [244], or to certify the system for the specific choice of gains as unstable and to adjust the gains in an iterative process [245]. In effect, the author is interested in removing the possibly prohibitive assumption that the optimization problems laying the foundation for parameter adaptation in this line of work are always feasible, and a system-level verification or analysis would make this possible.

APPENDIX A

Linear Quadratic Regulator-based Control Law

For each vehicle, we assume that a desired state trajectory, $\boldsymbol{q}_i^*(t) = [x_i^* \ y_i^* \ \dot{x}_i^* \ \dot{y}_i^*]^\top$, is available. Then, we define the modified state vector and tracking error as $\boldsymbol{\zeta}_i(t) = [x_i \ y_i \ \dot{x}_i \ \dot{y}_i]^\top$, and $\tilde{\boldsymbol{\zeta}}_i(t) = \boldsymbol{\zeta}_i(t) - \boldsymbol{q}_i^*(t)$ respectively. We then compute the optimal LQR gain, K, for a planar double integrator model and compute $\boldsymbol{\mu} = [a_{x,i} \ a_{y,i}]^\top = -K\tilde{\boldsymbol{\zeta}}_i$. Then, we map $a_{x,i}$, $a_{y,i}$ to ω_i^0, a_i^0 via

$$\begin{bmatrix} \omega_i^0 \\ a_i^0 \end{bmatrix} = S^{-1} \begin{bmatrix} a_{x,i} + \dot{y}_i\dot{\psi}_i \\ a_{y,i} - \dot{x}_i\dot{\psi}_i \end{bmatrix},$$

where

$$S = \begin{bmatrix} -v_i \sin(\psi_i)\sec^2(\beta_i) & \cos(\psi_i) - \sin(\psi_i)\tan(\beta_i) \\ v_i \cos(\psi_i)\sec^2(\beta_i) & \sin(\psi_i) + \cos(\psi_i)\tan(\beta_i) \end{bmatrix},$$

the inverse of which exists as long as $v_i \neq 0$. Therefore, if $|v_i| < \epsilon$, where $0 < \epsilon \ll 1$, we assign $\omega_i^0 = 0$ and $a_i^0 = \sqrt{a_{x,i}^2 + a_{y,i}^2}$.

APPENDIX B

Proof of Lemma 4.2

Proof. First, observe that $\boldsymbol{x}^T\boldsymbol{y} = \|\boldsymbol{x}\|\|\boldsymbol{y}\|\cos(\theta_{xy})$ and $\|\boldsymbol{x}+\boldsymbol{y}\|^2 = \|\boldsymbol{x}\|^2 + \|\boldsymbol{y}\|^2 + 2\|\boldsymbol{x}\|\|\boldsymbol{y}\|\cos(\theta_{xy})$, where θ_{xy} is the angle between vectors $\boldsymbol{x}$ and $\boldsymbol{y}$, and rewrite (4.14) as $P(\boldsymbol{x},\boldsymbol{y}) = P_1(x,y,z) + P_2(x,y,z)$, where $x = \|\boldsymbol{x}\|$, $y = \|\boldsymbol{y}\|$, $z = \cos(\theta_{xy})$, and

$$P_1(x,y,z) = axyz\left(x^2+y^2+2xyz\right)^{\frac{1}{m}},$$
$$P_2(x,y,z) = \frac{bxyz}{\left(x^2+y^2+2xyz\right)^{\frac{1}{m}}}.$$

It is then true that for fixed x and y,

$$P(\boldsymbol{x},\boldsymbol{y}) \geq \min_z P_1(x,y,z) + \min_z P_2(x,y,z).$$

As such, proceed by solving for $\min_z P_1(x,y,z)$ and $\min_z P_2(x,y,z)$, and (omitting arguments when appropriate for conciseness). Observe that $x, y \geq 0$, which means that for all $z \geq 0$ it is true that $P_1, P_2 \geq 0$. Additionally, by the AM-GM inequality[1] it is true that $x^2+y^2+2xyz > 0$ for all $z \in (-1,0]$ and $x^2+y^2+2xyz \geq 0$ for $z = -1$, thus it is obvious that there exists $z \in [-1,0]$ such that $P_1, P_2 < 0$. As such, focus is placed on the case where $z \in [-1,0]$. It follows that

$$\frac{\partial P_1}{\partial z} = axy\left(x^2+y^2+2xyz\right)^{\frac{1}{m}} + \frac{2a}{m}x^2y^2z\left(x^2+y^2+2xyz\right)^{\frac{1}{m}-1}.$$

Setting $\frac{\partial P_1}{\partial z} = 0$, the candidate minimizer is $z_1^* = -\frac{x^2+y^2}{2xy(1+\frac{1}{m})}$. Since

$$\frac{\partial^2 P_1}{\partial z^2} = \frac{4a}{m}x^2y^2\left(x^2+y^2+2xyz\right)^{\frac{1}{m}-1} + \left(\frac{1}{m}-1\right)\frac{4a}{m}x^3y^3z\left(x^2+y^2+2xyz\right)^{\frac{1}{m}-2}$$

with $a > 0$, $m > 2$, it follows that $\frac{\partial^2 P_1}{\partial z^2} > 0$ for all $x, y > 0$ and $z \in (-1,0]$. Therefore, by second order sufficient conditions for optimality z_1^* is the unique minimizer for P_1 over $z \in (-1,0]$. It

[1]The arithmetic mean-geometric mean inequality states that $x+y \geq 2\sqrt{xy}$, for $x, y > 0$.

also follows from the AM-GM inequality that $z_1^* \leq -\frac{m}{m+1}$ and thus from $m > 2$ that $z_1^* \leq -\frac{2}{3}$. Then, consider in addition that $\|\boldsymbol{x}+\boldsymbol{y}\|^2 \geq x^2$ if and only if $\cos(\theta_{xy}) \geq -\frac{y}{2x}$. Since $x > 2y \geq 0$ it is true that $-\frac{y}{2x} \geq -\frac{1}{4} > z_1^*$, and thus $x^2+y^2+2xyz_1^* < x^2$. As such,

$$\min_{z\in[-1,1]} P_1(x,y,z) = axyz_1^* \left(x^2+y^2+2xyz_1^*\right)^{\frac{2}{m}} \geq -aB_y x^{1+\frac{2}{m}}. \tag{B.1}$$

Now the case of P_2. By

$$\frac{\partial P_2}{\partial z} = \frac{bxy}{(x^2+y^2+2xyz)^{\frac{1}{m}}} - \frac{2bx^2y^2z}{m\,(x^2+y^2+2xyz)^{1+\frac{1}{m}}},$$

and second order sufficient conditions for optimality, it follows that $z_2^* = -\frac{x^2+y^2}{2xy(1-\frac{1}{m})}$ is the unique minimizer of P_2 for fixed x, y. Now, by the AM-GM inequality and $m > 2$ it follows that $z_2^* < -1$. Since $\frac{\partial P_2}{\partial z} > 0$ for all $z \leq 0$, it follows that $z_2^* = -1$ is the minimizer of P_2 over the domain $z \in [-1,1]$. With $z_2^* = -1$ and $x > 2y$, it is then true that $\|\boldsymbol{x}+\boldsymbol{y}\| \geq \frac{1}{2}x$. As such,

$$\min_{z\in[-1,1]} P_2(x,y,z) = -\frac{bxy}{(x^2+y^2-2xy)^{\frac{1}{m}}} \geq -2^{\frac{2}{m}} bB_y x^{1-\frac{2}{m}}. \tag{B.2}$$

Thus, by $P(\boldsymbol{x},\boldsymbol{y}) \geq \min_z P_1(x,y,z) + \min_z P_2(x,y,z)$ it follows that (4.15) is obtained from (B.1), (B.2), $x = \|\boldsymbol{x}\|$, and $y = \|\boldsymbol{y}\|$. This completes the proof. □

BIBLIOGRAPHY

[1] J.C. Knight. Safety critical systems: challenges and directions. In *Proceedings of the 24th International Conference on Software Engineering. ICSE 2002*, pages 547–550, 2002.

[2] Peter Wieland and Frank Allgöwer. Constructive safety using control barrier functions. *IFAC Proceedings Vols.*, 40(12):462–467, 2007.

[3] Aaron D Ames, Xiangru Xu, Jessy W Grizzle, and Paulo Tabuada. Control barrier function based quadratic programs for safety critical systems. *IEEE Trans. on Automatic Control*, 62(8):3861–3876, 2017.

[4] Stephen Prajna, Ali Jadbabaie, and George J. Pappas. A framework for worst-case and stochastic safety verification using barrier certificates. *IEEE Trans. on Automatic Control*, 52(8):1415–1428, 2007.

[5] Lukas Schmid, Michael Pantic, Raghav Khanna, Lionel Ott, Roland Siegwart, and Juan Nieto. An efficient sampling-based method for online informative path planning in unknown environments. *IEEE Robotics and Automation Letters*, 5(2):1500–1507, 2020.

[6] Andreas Bircher, Mina Kamel, Kostas Alexis, Helen Oleynikova, and Roland Siegwart. Receding horizon path planning for 3d exploration and surface inspection. *Autonomous Robots*, 42:291–306, 2018.

[7] Sertac Karaman and Emilio Frazzoli. Sampling-based algorithms for optimal motion planning. *The international journal of robotics research*, 30(7):846–894, 2011.

[8] Hans Georg Bock and Karl-Josef Plitt. A multiple shooting algorithm for direct solution of optimal control problems. *IFAC Proceedings Volumes*, 17(2):1603–1608, 1984.

[9] Markus Giftthaler, Michael Neunert, Markus Stäuble, Jonas Buchli, and Moritz Diehl. A family of iterative gauss-newton shooting methods for nonlinear optimal control. In *2018 IEEE/RSJ International Conference on Intelligent Robots and Systems (IROS)*, pages 1–9. IEEE, 2018.

[10] Shang Erke, Dai Bin, Nie Yiming, Zhu Qi, Xiao Liang, and Zhao Dawei. An improved a-star based path planning algorithm for autonomous land vehicles. *International Journal of Advanced Robotic Systems*, 17(5):1729881420962263, 2020.

[11] Guang-rong Chen, Sheng Guo, Jun-zheng Wang, Hai-bo Qu, Ya-qiong Chen, and Bo-wen Hou. Convex optimization and a-star algorithm combined path planning and obstacle avoidance algorithm. *Control and Decision*, 35(12):2907–2914, 2020.

[12] Reza Mashayekhi, Mohd Yamani Idna Idris, Mohammad Hossein Anisi, and Ismail Ahmedy. Hybrid rrt: A semi-dual-tree rrt-based motion planner. *IEEE Access*, 8:18658–18668, 2020.

[13] Francesco Grothe, Valentin N Hartmann, Andreas Orthey, and Marc Toussaint. St-rrt*: Asymptotically-optimal bidirectional motion planning through space-time. In *2022 International Conference on Robotics and Automation (ICRA)*, pages 3314–3320. IEEE, 2022.

[14] Julian Berberich, Johannes Köhler, Matthias A Müller, and Frank Allgöwer. Data-driven model predictive control with stability and robustness guarantees. *IEEE Transactions on Automatic Control*, 66(4):1702–1717, 2020.

[15] Juraj Kabzan, Lukas Hewing, Alexander Liniger, and Melanie N Zeilinger. Learning-based model predictive control for autonomous racing. *IEEE Robotics and Automation Letters*, 4(4):3363–3370, 2019.

[16] Somil Bansal, Varun Tolani, Saurabh Gupta, Jitendra Malik, and Claire Tomlin. Combining optimal control and learning for visual navigation in novel environments. In *Conference on Robot Learning*, pages 420–429. PMLR, 2020.

[17] Jianguo Zhao, Chunyu Yang, and Weinan Gao. Reinforcement learning based optimal control of linear singularly perturbed systems. *IEEE Transactions on Circuits and Systems II: Express Briefs*, 69(3):1362–1366, 2021.

[18] Weiwei Bai, Tieshan Li, and Shaocheng Tong. Nn reinforcement learning adaptive control for a class of nonstrict-feedback discrete-time systems. *IEEE Transactions on Cybernetics*, 50(11):4573–4584, 2020.

[19] Joel AE Andersson, Joris Gillis, Greg Horn, James B Rawlings, and Moritz Diehl. Casadi: a software framework for nonlinear optimization and optimal control. *Mathematical Programming Computation*, 11:1–36, 2019.

[20] Bijan Sakhdari and Nasser L Azad. A distributed reference governor approach to ecological cooperative adaptive cruise control. *IEEE Transactions on Intelligent Transportation Systems*, 19(5):1496–1507, 2017.

[21] Marco M Nicotra and Emanuele Garone. The explicit reference governor: A general framework for the closed-form control of constrained nonlinear systems. *IEEE Control Systems Magazine*, 38(4):89–107, 2018.

[22] Arun Lakshmanan, Aditya Gahlawat, and Naira Hovakimyan. Safe feedback motion planning: A contraction theory and 1-adaptive control based approach. In *2020 59th IEEE Conference on Decision and Control (CDC)*, pages 1578–1583. IEEE, 2020.

[23] Sumeet Singh, Hiroyasu Tsukamoto, Brett T. Lopez, Soon-Jo Chung, and Jean-Jacques Slotine. Safe motion planning with tubes and contraction metrics. In *2021 60th IEEE Conference on Decision and Control (CDC)*, pages 2943–2948, 2021.

[24] Manuel Rauscher, Melanie Kimmel, and Sandra Hirche. Constrained robot control using control barrier functions. In *IEEE/RSJ International Conference on Intelligent Robots and Systems*, pages 279–285, 2016.

[25] Kaiwen Liu, Nan Li, Ilya Kolmanovsky, Denise Rizzo, and Anouck Girard. Model-free learning for safety-critical control systems: A reference governor approach. In *2020 American Control Conference (ACC)*, pages 943–949. IEEE, 2020.

[26] Dawei Sun, Susmit Jha, and Chuchu Fan. Learning certified control using contraction metric. In *Proceedings of the 2020 Conference on Robot Learning*, volume 155 of *Proceedings of Machine Learning Research*, pages 1519–1539. PMLR, 16–18 Nov 2021.

[27] Alexander Robey, Haimin Hu, Lars Lindemann, Hanwen Zhang, Dimos V. Dimarogonas, Stephen Tu, and Nikolai Matni. Learning control barrier functions from expert demonstrations. In *2020 59th IEEE Conference on Decision and Control (CDC)*, pages 3717–3724, 2020.

[28] Elmer Gilbert and Ilya Kolmanovsky. Nonlinear tracking control in the presence of state and control constraints: a generalized reference governor. *Automatica*, 38(12):2063–2073, 2002.

[29] Ilya Kolmanovsky, Emanuele Garone, and Stefano Di Cairano. Reference and command governors: A tutorial on their theory and automotive applications. In *2014 American Control Conference*, pages 226–241, 2014.

[30] Pan Zhao, Arun Lakshmanan, Kasey Ackerman, Aditya Gahlawat, Marco Pavone, and Naira Hovakimyan. Tube-certified trajectory tracking for nonlinear systems with robust control contraction metrics. *IEEE Robotics and Automation Letters*, 7(2):5528–5535, 2022.

[31] Mrdjan Jankovic. Robust control barrier functions for constrained stabilization of nonlinear systems. *Automatica*, 96:359–367, 2018.

[32] A. J. Taylor and A. D. Ames. Adaptive safety with control barrier functions. In *2020 American Control Conf.*, pages 1399–1405, 2019.

[33] Kaiwen Liu, Nan Li, Ilya Kolmanovsky, Denise Rizzo, and Anouck Girard. Tanker truck rollover avoidance using learning reference governor. *SAE International Journal of Advances and Current Practices in Mobility*, 3(3):1385–1394, apr 2021.

[34] Lars Lindemann, Haimin Hu, Alexander Robey, Hanwen Zhang, Dimos Dimarogonas, Stephen Tu, and Nikolai Matni. Learning hybrid control barrier functions from data. In *Proceedings of the 2020 Conference on Robot Learning*, volume 155 of *Proceedings of Machine Learning Research*, pages 1351–1370. PMLR, 16–18 Nov 2021.

[35] Lukas Brunke, Melissa Greeff, Adam W Hall, Zhaocong Yuan, Siqi Zhou, Jacopo Panerati, and Angela P Schoellig. Safe learning in robotics: From learning-based control to safe reinforcement learning. *Annual Review of Control, Robotics, and Autonomous Systems*, 5:411–444, 2022.

[36] Alexander Bertino, Peiman Naseradinmousavi, and Miroslav Krstic. Experiment and design of prescribed-time safety filter for a 7-dof robot manipulator using cbf-qp. *IFAC-PapersOnLine*, 55(37):481–487, 2022. 2nd Modeling, Estimation and Control Conference MECC 2022.

[37] Kunal Garg and Dimitra Panagou. Control-lyapunov and control-barrier functions based quadratic program for spatio-temporal specifications. In *2019 IEEE 58th Conference on Decision and Control (CDC)*, pages 1422–1429, 2019.

[38] Hongguang Lyu and Yong Yin. Colregs-constrained real-time path planning for autonomous ships using modified artificial potential fields. *The Journal of navigation*, 72(3):588–608, 2019.

[39] Yanjun Huang, Haitao Ding, Yubiao Zhang, Hong Wang, Dongpu Cao, Nan Xu, and Chuan Hu. A motion planning and tracking framework for autonomous vehicles based on artificial potential field elaborated resistance network approach. *IEEE Transactions on Industrial Electronics*, 67(2):1376–1386, 2019.

[40] Quan Nguyen and Koushil Sreenath. Exponential control barrier functions for enforcing high relative-degree safety-critical constraints. In *American Control Conference*, pages 322–328. IEEE, 2016.

[41] Manavendra Desai and Azad Ghaffari. Auxiliary control to avoid undesirable equilibria in constrained quadratic programs for trajectory tracking applications. *IEEE Transactions on Robotics*, pages 1–15, 2023.

[42] Max H. Cohen and Calin Belta. Approximate optimal control for safety-critical systems with control barrier functions. In *2020 59th IEEE Conference on Decision and Control (CDC)*, pages 2062–2067, 2020.

[43] Hardik Parwana and Dimitra Panagou. Trust-based rate-tunable control barrier functions for non-cooperative multi-agent systems. *arXiv preprint arXiv:2204.04555*, 2022.

[44] Jun Zeng, Bike Zhang, Zhongyu Li, and Koushil Sreenath. Safety-critical control using optimal-decay control barrier function with guaranteed point-wise feasibility. In *2021 American Control Conference (ACC)*, pages 3856–3863, 2021.

[45] Kaiyuan Xu, Wei Xiao, and Christos G. Cassandras. Feasibility guaranteed traffic merging control using control barrier functions. In *2022 American Control Conference (ACC)*, pages 2309–2314, 2022.

[46] Wei Xiao, Calin A. Belta, and Christos G. Cassandras. Sufficient conditions for feasibility of optimal control problems using control barrier functions. *Automatica*, 135:109960, 2022.

[47] Matheus F. Reis, A. Pedro Aguiar, and Paulo Tabuada. Control barrier function-based quadratic programs introduce undesirable asymptotically stable equilibria. *IEEE Control Systems Letters*, 5(2):731–736, 2021.

[48] Xiao Tan and Dimos V Dimarogonas. On the undesired equilibria induced by control barrier function based quadratic programs. *arXiv preprint arXiv:2104.14895*, 2021.

[49] Jun Zeng, Bike Zhang, and Koushil Sreenath. Safety-critical model predictive control with discrete-time control barrier function. In *2021 American Control Conference (ACC)*, pages 3882–3889, 2021.

[50] Maria Charitidou and Dimos V. Dimarogonas. Barrier function-based model predictive control under signal temporal logic specifications. In *2021 European Control Conference (ECC)*, pages 734–739, 2021.

[51] Zahra Marvi and Bahare Kiumarsi. Safety planning using control barrier function: A model predictive control scheme. In *2019 IEEE 2nd Connected and Automated Vehicles Symposium (CAVS)*, pages 1–5, 2019.

[52] Ugo Rosolia and Aaron D. Ames. Multi-rate control design leveraging control barrier functions and model predictive control policies. *IEEE Control Systems Letters*, 5(3):1007–1012, 2021.

[53] Ruben Grandia, Andrew J. Taylor, Aaron D. Ames, and Marco Hutter. Multi-layered safety for legged robots via control barrier functions and model predictive control. In *2021 IEEE International Conference on Robotics and Automation (ICRA)*, pages 8352–8358, 2021.

[54] Tarek Madani and Abdelaziz Benallegue. Backstepping control for a quadrotor helicopter. In *2006 IEEE/RSJ International Conference on Intelligent Robots and Systems*, pages 3255–3260. IEEE, 2006.

[55] Chiman Kwan and Frank L Lewis. Robust backstepping control of nonlinear systems using neural networks. *IEEE Transactions on Systems, Man, and Cybernetics-Part A: Systems and Humans*, 30(6):753–766, 2000.

[56] José de Jesús Rubio. Robust feedback linearization for nonlinear processes control. *ISA transactions*, 74:155–164, 2018.

[57] Arshad Mahmood and Yoonsoo Kim. Decentrailized formation flight control of quadcopters using robust feedback linearization. *Journal of the Franklin Institute*, 354(2):852–871, 2017.

[58] Shafiqul Islam and Xiaoping P Liu. Robust sliding mode control for robot manipulators. *IEEE Transactions on industrial electronics*, 58(6):2444–2453, 2010.

[59] Spyros Tzafestas, Mark Raibert, and Costas Tzafestas. Robust sliding-mode control applied to a 5-link biped robot. *Journal of Intelligent and Robotic Systems*, 15:67–133, 1996.

[60] Khoi B Ngo, Robert Mahony, and Zhong-Ping Jiang. Integrator backstepping using barrier functions for systems with multiple state constraints. In *Proceedings of the 44th IEEE Conference on Decision and Control*, pages 8306–8312. IEEE, 2005.

[61] Liang Sun, Wei Huo, and Zongxia Jiao. Adaptive backstepping control of spacecraft rendezvous and proximity operations with input saturation and full-state constraint. *IEEE Transactions on Industrial Electronics*, 64(1):480–492, 2016.

[62] Hassan Almubarak, Nader Sadegh, and Evangelos A Theodorou. Safety embedded control of nonlinear systems via barrier states. *IEEE Control Systems Letters*, 6:1328–1333, 2021.

[63] Hassan Almubarak, Kyle Stachowicz, Nader Sadegh, and Evangelos A Theodorou. Safety embedded differential dynamic programming using discrete barrier states. *IEEE Robotics and Automation Letters*, 7(2):2755–2762, 2022.

[64] Marco A Gomez, Christopher D Cruz-Ancona, and Leonid Fridman. Safe sliding mode control. In *2022 19th International Conference on Electrical Engineering, Computing Science and Automatic Control (CCE)*, pages 1–6. IEEE, 2022.

[65] Xiangru Xu, Paulo Tabuada, Jessy W Grizzle, and Aaron D Ames. Robustness of control barrier functions for safety critical control. *IFAC-PapersOnLine*, 48(27):54–61, 2015.

[66] Shishir Kolathaya and Aaron D. Ames. Input-to-state safety with control barrier functions. *IEEE Control Systems Letters*, 3(1):108–113, 2019.

[67] Anil Alan, Andrew J. Taylor, Chaozhe R. He, Gábor Orosz, and Aaron D. Ames. Safe controller synthesis with tunable input-to-state safe control barrier functions. *IEEE Control Systems Letters*, 6:908–913, 2022.

[68] Ryan K. Cosner, Andrew W. Singletary, Andrew J. Taylor, Tamas G. Molnar, Katherine L. Bouman, and Aaron D. Ames. Measurement-robust control barrier functions: Certainty in safety with uncertainty in state. In *2021 IEEE/RSJ International Conference on Intelligent Robots and Systems (IROS)*, pages 6286–6291, 2021.

[69] Devansh R. Agrawal and Dimitra Panagou. Safe and robust observer-controller synthesis using control barrier functions. *IEEE Control Systems Letters*, 7:127–132, 2023.

[70] Richard Cheng, Mohammad Javad Khojasteh, Aaron D. Ames, and Joel W. Burdick. Safe multi-agent interaction through robust control barrier functions with learned uncertainties. In *2020 59th IEEE Conference on Decision and Control (CDC)*, pages 777–783, 2020.

[71] Jason J. Choi, Donggun Lee, Koushil Sreenath, Claire J. Tomlin, and Sylvia L. Herbert. Robust control barrier–value functions for safety-critical control. In *2021 60th IEEE Conference on Decision and Control (CDC)*, pages 6814–6821, 2021.

[72] Jyot Buch, Shih-Chi Liao, and Peter Seiler. Robust control barrier functions with sector-bounded uncertainties. *IEEE Control Systems Letters*, 6:1994–1999, 2022.

[73] Yousef Emam, Gennaro Notomista, Paul Glotfelter, and Magnus Egerstedt. Data-driven adaptive task allocation for heterogeneous multi-robot teams using robust control barrier functions. In *2021 IEEE International Conference on Robotics and Automation (ICRA)*, pages 9124–9130, 2021.

[74] Kunal Garg and Dimitra Panagou. Robust control barrier and control lyapunov functions with fixed-time convergence guarantees. In *2021 American Control Conference (ACC)*, pages 2292–2297, 2021.

[75] Mario Luca Fravolini, Nicholas Cartocci, Kadriye Merve Dogan, and Tansel Yucelen. A safe learning model reference adaptive controller for uncertain aircrafts models. In *AIAA Scitech 2021 Forum*, page 0532, 2021.

[76] Ehsan Arabi, Benjamin C Gruenwald, Tansel Yucelen, and Nhan T Nguyen. A set-theoretic model reference adaptive control architecture for disturbance rejection and uncertainty suppression with strict performance guarantees. *International Journal of Control*, 91(5):1195–1208, 2018.

[77] Yashar Mousavi, Alireza Alfi, Ibrahim Beklan Kucukdemiral, and Afef Fekih. Tube-based model reference adaptive control for vibration suppression of active suspension systems. *IEEE/CAA Journal of Automatica Sinica*, 9(4):728–731, 2022.

[78] Brian DO Anderson and Arvin Dehghani. Challenges of adaptive control–past, permanent and future. *Annual reviews in control*, 32(2):123–135, 2008.

[79] David D Fan, Jennifer Nguyen, Rohan Thakker, Nikhilesh Alatur, Ali-akbar Agha-mohammadi, and Evangelos A Theodorou. Bayesian learning-based adaptive control for safety critical systems. In *2020 IEEE international conference on robotics and automation (ICRA)*, pages 4093–4099. IEEE, 2020.

[80] Christopher König, Matteo Turchetta, John Lygeros, Alisa Rupenyan, and Andreas Krause. Safe and efficient model-free adaptive control via bayesian optimization. In *2021 IEEE International Conference on Robotics and Automation (ICRA)*, pages 9782–9788. IEEE, 2021.

[81] Armin Lederer, Alejandro J Ordóñez Conejo, Korbinian A Maier, Wenxin Xiao, Jonas Umlauft, and Sandra Hirche. Gaussian process-based real-time learning for safety critical applications. In *International Conference on Machine Learning*, pages 6055–6064. PMLR, 2021.

[82] Alexander H Chang, Christian M Hubicki, Jeffrey J Aguilar, Daniel I Goldman, Aaron D Ames, and Patricio A Vela. Learning terrain dynamics: A gaussian process modeling and optimal control adaptation framework applied to robotic jumping. *IEEE Transactions on Control Systems Technology*, 29(4):1581–1596, 2020.

[83] Kai Zhao, Yongduan Song, and Zhixi Shen. Neuroadaptive fault-tolerant control of nonlinear systems under output constraints and actuation faults. *IEEE transactions on neural networks and learning systems*, 29(2):286–298, 2016.

[84] Isura Ranatunga, Sven Cremer, Frank L Lewis, and Dan O Popa. Neuroadaptive control for safe robots in human environments: A case study. In *2015 IEEE International Conference on Automation Science and Engineering (CASE)*, pages 322–327. IEEE, 2015.

[85] Vahid Azimi and Patricio A. Vela. Robust adaptive quadratic programming and safety performance of nonlinear systems with unstructured uncertainties. In *2018 IEEE Conference on Decision and Control (CDC)*, pages 5536–5543, 2018.

[86] Brett T. Lopez, Jean-Jacques E. Slotine, and Jonathan P. How. Robust adaptive control barrier functions: An adaptive and data-driven approach to safety. *IEEE Control Systems Letters*, 5(3):1031–1036, 2021.

[87] Pan Zhao, Yanbing Mao, Chuyuan Tao, Naira Hovakimyan, and Xiaofeng Wang. Adaptive robust quadratic programs using control lyapunov and barrier functions. In *2020 59th IEEE Conference on Decision and Control (CDC)*, pages 3353–3358, 2020.

[88] Max H. Cohen and Calin Belta. High order robust adaptive control barrier functions and exponentially stabilizing adaptive control lyapunov functions. In *2022 American Control Conference (ACC)*, pages 2233–2238, 2022.

[89] Yujie Wang and Xiangru Xu. Observer-based control barrier functions for safety critical systems. In *2022 American Control Conference (ACC)*, pages 709–714, 2022.

[90] Anil Alan, Tamas G. Molnar, Ersin Daş, Aaron D. Ames, and Gábor Orosz. Disturbance observers for robust safety-critical control with control barrier functions. *IEEE Control Systems Letters*, 7:1123–1128, 2023.

[91] Feng Ding, Xuehai Wang, Qijia Chen, and Yongsong Xiao. Recursive least squares parameter estimation for a class of output nonlinear systems based on the model decomposition. *Circuits, Systems, and Signal Processing*, 35:3323–3338, 2016.

[92] Meihang Li and Ximei Liu. The least squares based iterative algorithms for parameter estimation of a bilinear system with autoregressive noise using the data filtering technique. *Signal Processing*, 147:23–34, 2018.

[93] Ana SR Brásio, Andrey Romanenko, and Natércia CP Fernandes. Using sequential quadratic programming for system identification. *Applied Mathematics & Information Sciences*, 9(1):19, 2015.

[94] ME Furlong, GE Hearn, SM Veres, and E Rogers. Nonlinear system identification tools applied to the modelling of submarine dynamics. *IFAC Proceedings Volumes*, 36(4):49–54, 2003.

[95] Ali Akramizadeh, A Akbar Farjami, and Hamid Khaloozadeh. Nonlinear hammerstein model identification using genetic algorithm. In *Proceedings 2002 IEEE International Conference on Artificial Intelligence Systems (ICAIS 2002)*, pages 351–356. IEEE, 2002.

[96] Wei-Der Chang. Nonlinear system identification and control using a real-coded genetic algorithm. *Applied Mathematical Modelling*, 31(3):541–550, 2007.

[97] Alireza Alfi and Hamidreza Modares. System identification and control using adaptive particle swarm optimization. *Applied Mathematical Modelling*, 35(3):1210–1221, 2011.

[98] Sheng Chen, Xia Hong, Bing L Luk, and Chris J Harris. Non-linear system identification using particle swarm optimisation tuned radial basis function models. *International Journal of Bio-Inspired Computation*, 1(4):246–258, 2009.

[99] J Prawin and A Rama Mohan Rao. Nonlinear identification of mdof systems using volterra series approximation. *Mechanical Systems and Signal Processing*, 84:58–77, 2017.

[100] Christophe Andrieu, Arnaud Doucet, and Roman Holenstein. Particle markov chain monte carlo methods. *Journal of the Royal Statistical Society: Series B (Statistical Methodology)*, 72(3):269–342, 2010.

[101] Bryson C Bates and Edward P Campbell. A markov chain monte carlo scheme for parameter estimation and inference in conceptual rainfall-runoff modeling. *Water resources research*, 37(4):937–947, 2001.

[102] Jianye Ching, James L Beck, and Keith A Porter. Bayesian state and parameter estimation of uncertain dynamical systems. *Probabilistic engineering mechanics*, 21(1):81–96, 2006.

[103] Fabien Campillo and Vivien Rossi. Convolution particle filter for parameter estimation in general state-space models. *IEEE Transactions on Aerospace and Electronic Systems*, 45(3):1063–1072, 2009.

[104] Lennart Ljung. Perspectives on system identification. *Annual Reviews in Control*, 34(1):1–12, 2010.

[105] Daniel Gedon, Niklas Wahlström, Thomas B Schön, and Lennart Ljung. Deep state space models for nonlinear system identification. *IFAC-PapersOnLine*, 54(7):481–486, 2021.

[106] Enoch Yeung, Soumya Kundu, and Nathan Hodas. Learning deep neural network representations for koopman operators of nonlinear dynamical systems. In *2019 American Control Conference (ACC)*, pages 4832–4839. IEEE, 2019.

[107] Xiangjun Jin, Jie Shao, Xin Zhang, Wenwei An, and Reza Malekian. Modeling of nonlinear system based on deep learning framework. *Nonlinear Dynamics*, 84:1327–1340, 2016.

[108] Maziar Raissi. Deep hidden physics models: Deep learning of nonlinear partial differential equations. *The Journal of Machine Learning Research*, 19(1):932–955, 2018.

[109] Nima Mohajerin, Melissa Mozifian, and Steven Waslander. Deep learning a quadrotor dynamic model for multi-step prediction. In *2018 IEEE international conference on robotics and automation (ICRA)*, pages 2454–2459. IEEE, 2018.

[110] Ali Punjani and Pieter Abbeel. Deep learning helicopter dynamics models. In *2015 IEEE International Conference on Robotics and Automation (ICRA)*, pages 3223–3230. IEEE, 2015.

[111] Zheng Wang, Dunhui Xiao, Fangxin Fang, Rajesh Govindan, Christopher C Pain, and Yike Guo. Model identification of reduced order fluid dynamics systems using deep learning. *International Journal for Numerical Methods in Fluids*, 86(4):255–268, 2018.

[112] Georgy E Manucharyan, Lia Siegelman, and Patrice Klein. A deep learning approach to spatiotemporal sea surface height interpolation and estimation of deep currents in geostrophic ocean turbulence. *Journal of Advances in Modeling Earth Systems*, 13(1):e2019MS001965, 2021.

[113] James B Heaton, Nick G Polson, and Jan Hendrik Witte. Deep learning for finance: deep portfolios. *Applied Stochastic Models in Business and Industry*, 33(1):3–12, 2017.

[114] Thomas Fischer and Christopher Krauss. Deep learning with long short-term memory networks for financial market predictions. *European journal of operational research*, 270(2):654–669, 2018.

[115] Hector Rios, Denis Efimov, Jaime A. Moreno, Wilfrid Perruquetti, and Juan G. Rueda-Escobedo. Time-varying parameter identification algorithms: Finite and fixed-time convergence. *IEEE Transactions on Automatic Control*, 62:3671–3678, 7 2017.

[116] Jing Na, Guido Herrmann, Xuemei Ren, Muhammad Nasiruddin Mahyuddin, and Phil Barber. Robust adaptive finite-time parameter estimation and control of nonlinear systems. *IEEE International Symposium on Intelligent Control - Proceedings*, pages 1014–1019, 2011.

[117] Jing Na, Muhammad Nasiruddin Mahyuddin, Guido Herrmann, Xuemei Ren, and Phil Barber. Robust adaptive finite-time parameter estimation and control for robotic systems. *International Journal of Robust and Nonlinear Control*, 25:3045–3071, 11 2015.

[118] Matthew O Williams, Ioannis G Kevrekidis, and Clarence W Rowley. A data–driven approximation of the koopman operator: Extending dynamic mode decomposition. *Journal of Nonlinear Science*, 25(6):1307–1346, 2015.

[119] Daniel Bruder, Xun Fu, R. Brent Gillespie, C. David Remy, and Ram Vasudevan. Data-driven control of soft robots using koopman operator theory. *IEEE Transactions on Robotics*, 37(3):948–961, 2021.

[120] Masih Haseli and Jorge Cortés. Data-driven approximation of koopman-invariant subspaces with tunable accuracy. In *2021 American Control Conference (ACC)*, pages 470–475, 2021.

[121] Daniel Bruder, C. David Remy, and Ram Vasudevan. Nonlinear system identification of soft robot dynamics using koopman operator theory. In *2019 International Conference on Robotics and Automation (ICRA)*, pages 6244–6250, 2019.

[122] Stefan Klus, Feliks Nüske, Sebastian Peitz, Jan-Hendrik Niemann, Cecilia Clementi, and Christof Schütte. Data-driven approximation of the koopman generator: Model reduction, system identification, and control. *Physica D: Nonlinear Phenomena*, 406:132416, 2020.

[123] Zlatko Drmač, Igor Mezić, and Ryan Mohr. Identification of nonlinear systems using the infinitesimal generator of the koopman semigroup—a numerical implementation of the mauroy–goncalves method. *Mathematics*, 9(17):2075, Aug 2021.

[124] Alexandre Mauroy and Jorge Goncalves. Koopman-based lifting techniques for nonlinear systems identification. *IEEE Transactions on Automatic Control*, 65(6):2550–2565, 2020.

[125] Stefan Klus, Péter Koltai, and Christof Schütte. On the numerical approximation of the perron-frobenius and koopman operator. *Journal of Computational Dynamics*, 3(1):51–79, 2016.

[126] Milan Korda and Igor Mezić. On convergence of extended dynamic mode decomposition to the koopman operator. *Journal of Nonlinear Science*, 28:687–710, 2018.

[127] Manuel Schaller, Karl Worthmann, Friedrich Philipp, Sebastian Peitz, and Feliks Nüske. Towards reliable data-based optimal and predictive control using extended dmd. *arXiv preprint arXiv:2202.09084*, 2022.

[128] Feliks Nüske, Sebastian Peitz, Friedrich Philipp, Manuel Schaller, and Karl Worthmann. Finite-data error bounds for koopman-based prediction and control. *Journal of Nonlinear Science*, 33(1):14, 2023.

[129] Milan Korda and Igor Mezić. Linear predictors for nonlinear dynamical systems: Koopman operator meets model predictive control. *Automatica*, 93:149–160, 2018.

[130] Carl Folkestad and Joel W Burdick. Koopman nmpc: Koopman-based learning and nonlinear model predictive control of control-affine systems. In *2021 IEEE International Conference on Robotics and Automation (ICRA)*, pages 7350–7356. IEEE, 2021.

[131] Alexandre Mauroy, Y Susuki, and I Mezić. *Koopman operator in systems and control*. Springer, 2020.

[132] Petar Bevanda, Stefan Sosnowski, and Sandra Hirche. Koopman operator dynamical models: Learning, analysis and control. *Annual Reviews in Control*, 52:197–212, 2021.

[133] Horacio M. Calderón, Erik Schulz, Thimo Oehlschlägel, and Herbert Werner. Koopman operator-based model predictive control with recursive online update. In *2021 European Control Conference (ECC)*, pages 1543–1549, 2021.

[134] Sanjay P Bhat and Dennis S Bernstein. Finite-time stability of continuous autonomous systems. *SICON*, 38(3):751–766, 2000.

[135] Andrey Polyakov. Nonlinear feedback design for fixed-time stabilization of linear control systems. *IEEE Transactions on Automatic Control*, 57(8):2106, 2012.

[136] Edward E Rigdon. Demonstrating the effects of unmodeled random measurement error. *Structural Equation Modeling: A Multidisciplinary Journal*, 1(4):375–380, 1994.

[137] Sandeep Gorantla, Jeel Chatrola, Jay Bhagiya, Adnane Saoud, and Pushpak Jagtap. Funnel-based reachability control of unknown nonlinear systems using gaussian processes. *arXiv preprint arXiv:2209.14015*, 2022.

[138] Felix Berkenkamp and Angela P Schoellig. Safe and robust learning control with gaussian processes. In *2015 European Control Conference (ECC)*, pages 2496–2501. IEEE, 2015.

[139] Armin Lederer, Jonas Umlauft, and Sandra Hirche. Uniform error bounds for gaussian process regression with application to safe control. In H. Wallach, H. Larochelle, A. Beygelzimer, F. d'Alché-Buc, E. Fox, and R. Garnett, editors, *Advances in Neural Information Processing Systems*, volume 32. Curran Associates, Inc., 2019.

[140] Pushpak Jagtap, George J. Pappas, and Majid Zamani. Control barrier functions for unknown nonlinear systems using gaussian processes. In *59th IEEE Conference on Decision and Control*, pages 3699–3704, 2020.

[141] Mouhyemen Khan and Abhijit Chatterjee. Gaussian control barrier functions: Safe learning and control. In *59th IEEE Conference on Decision and Control (CDC)*, pages 3316–3322, 2020.

[142] Mouhyemen Khan, Tatsuya Ibuki, and Abhijit Chatterjee. Safety uncertainty in control barrier functions using gaussian processes. In *2021 IEEE International Conference on Robotics and Automation*, pages 6003–6009, 2021.

[143] Yifan Hu, Junjie Fu, and Guanghui Wen. Decentralized robust collision avoidance for cooperative multirobot systems: A gaussian process-based control barrier function approach. *IEEE Transactions on Control of Network Systems*, 2022.

[144] Mouhyemen A Khan, Tatsuya Ibuki, and Abhijit Chatterjee. Gaussian control barrier functions: Non-parametric paradigm to safety. *IEEE Access*, 10:99823–99836, 2022.

[145] Mohammad Javad Khojasteh, Vikas Dhiman, Massimo Franceschetti, and Nikolay Atanasov. Probabilistic safety constraints for learned high relative degree system dynamics. In *Proceedings of the 2nd Conference on Learning for Dynamics and Control*, volume 120 of *Proceedings of Machine Learning Research*, pages 781–792. PMLR, 10–11 Jun 2020.

[146] Soumith Udatha, Yiwei Lyu, and John Dolan. Safe reinforcement learning with probabilistic control barrier functions for ramp merging. *arXiv preprint arXiv:2212.00618*, 2022.

[147] Yiwei Lyu, Wenhao Luo, and John M. Dolan. Probabilistic safety-assured adaptive merging control for autonomous vehicles. In *2021 IEEE International Conference on Robotics and Automation*, pages 10764–10770, 2021.

[148] Wenhao Luo, Wen Sun, and Ashish Kapoor. Multi-robot collision avoidance under uncertainty with probabilistic safety barrier certificates. *Advances in Neural Information Processing Systems*, 33:372–383, 2020.

[149] Mohamadreza Ahmadi, Xiaobin Xiong, and Aaron D Ames. Risk-averse control via cvar barrier functions: Application to bipedal robot locomotion. *IEEE Control Systems Letters*, 6:878–883, 2021.

[150] Andrew Singletary, Mohamadreza Ahmadi, and Aaron D Ames. Safe control for nonlinear systems with stochastic uncertainty via risk control barrier functions. *IEEE Control Systems Letters*, 7:349–354, 2022.

[151] Astghik Hakobyan and Insoon Yang. Wasserstein distributionally robust motion planning and control with safety constraints using conditional value-at-risk. In *2020 IEEE International Conference on Robotics and Automation (ICRA)*, pages 490–496. IEEE, 2020.

[152] Samantha Samuelson and Insoon Yang. Safety-aware optimal control of stochastic systems using conditional value-at-risk. In *2018 Annual American Control Conference (ACC)*, pages 6285–6290. IEEE, 2018.

[153] Mohamadreza Ahmadi, Xiaobin Xiong, and Aaron D Ames. Risk-sensitive path planning via cvar barrier functions: Application to bipedal locomotion. *arXiv preprint arXiv:2011.01578*, 2020.

[154] Cesar Santoyo, Maxence Dutreix, and Samuel Coogan. A barrier function approach to finite-time stochastic system verification and control. *Automatica*, 125:109439, 2021.

[155] Shakiba Yaghoubi, Keyvan Majd, Georgios Fainekos, Tomoya Yamaguchi, Danil Prokhorov, and Bardh Hoxha. Risk-bounded control using stochastic barrier functions. *IEEE Control Systems Letters*, 5(5):1831–1836, 2021.

[156] Shakiba Yaghoubi, Georgios Fainekos, Tomoya Yamaguchi, Danil Prokhorov, and Bardh Hoxha. Risk-bounded control with kalman filtering and stochastic barrier functions. In *2021 60th IEEE Conference on Decision and Control (CDC)*, pages 5213–5219, 2021.

[157] Chuanzheng Wang, Yiming Meng, Stephen L. Smith, and Jun Liu. Safety-critical control of stochastic systems using stochastic control barrier functions. In *60th IEEE Conference on Decision and Control*, pages 5924–5931, 2021.

[158] Albert Chern, Xiang Wang, Abhiram Iyer, and Yorie Nakahira. Safe control in the presence of stochastic uncertainties. In *60th IEEE Conference on Decision and Control*, pages 6640–6645, 2021.

[159] Andrew Clark. Control barrier functions for stochastic systems. *Automatica*, 130:109688, 2021.

[160] Chuyuan Tao, Hyung-Jin Yoon, Hunmin Kim, Naira Hovakimyan, and Petros Voulgaris. Path integral methods with stochastic control barrier functions. *arXiv preprint arXiv:2206.11985*, 2022.

[161] Sergei Aleksandrovich Nazin, Boris Teodorovich Polyak, and MV Topunov. Rejection of bounded exogenous disturbances by the method of invariant ellipsoids. *Automation and Remote Control*, 68(3):467–486, 2007.

[162] John Abedor, Krishan Nagpal, and Kameshwar Poolla. A linear matrix inequality approach to peak-to-peak gain minimization. *International Journal of Robust and Nonlinear Control*, 6(9-10):899–927, 1996.

[163] BT Polyak, PS Shcherbakov, and MV Topunov. Invariant ellipsoids approach to robust rejection of persistent disturbances. *IFAC Proceedings Volumes*, 41(2):3976–3981, 2008.

[164] Weehong Tan and Andrew Packard. Stability region analysis using polynomial and composite polynomial lyapunov functions and sum-of-squares programming. *IEEE Transactions on Automatic Control*, 53(2):565–571, 2008.

[165] Antonis Papachristodoulou and Stephen Prajna. A tutorial on sum of squares techniques for systems analysis. In *Proceedings of the 2005, American Control Conference, 2005.*, pages 2686–2700. IEEE, 2005.

[166] Suseong Kim, Davide Falanga, and Davide Scaramuzza. Computing the forward reachable set for a multirotor under first-order aerodynamic effects. *IEEE Robotics and Automation Letters*, 3(4):2934–2941, 2018.

[167] Yifei Simon Shao, Chao Chen, Shreyas Kousik, and Ram Vasudevan. Reachability-based trajectory safeguard (rts): A safe and fast reinforcement learning safety layer for continuous control. *IEEE Robotics and Automation Letters*, 6(2):3663–3670, 2021.

[168] Joseph Breeden and Dimitra Panagou. High relative degree control barrier functions under input constraints. In *2021 60th IEEE Conference on Decision and Control (CDC)*, pages 6119–6124, 2021.

[169] Wei Xiao, Calin Belta, and Christos G. Cassandras. Adaptive control barrier functions. *IEEE Transactions on Automatic Control*, 67(5):2267–2281, 2022.

[170] Wenceslao Shaw Cortez, Xiao Tan, and Dimos V. Dimarogonas. A robust, multiple control barrier function framework for input constrained systems. *IEEE Control Systems Letters*, 6:1742–1747, 2022.

[171] Paul Glotfelter, Jorge Cortés, and Magnus Egerstedt. Nonsmooth barrier functions with applications to multi-robot systems. *IEEE Control Systems Letters*, 1(2):310–315, 2017.

[172] Yiwen Huang and Yan Chen. Switched Control Barrier Function With Applications to Vehicle Safety Control. volume 1 of *Dynamic Systems and Control Conference*, 10 2020.

[173] Lars Lindemann and Dimos V. Dimarogonas. Control barrier functions for signal temporal logic tasks. *IEEE Control Systems Letters*, 3(1):96–101, 2019.

[174] Manao Machida and Masumi Ichien. Consensus-based control barrier function for swarm. In *2021 IEEE International Conference on Robotics and Automation (ICRA)*, pages 8623–8628, 2021.

[175] Li Wang, Dongkun Han, and Magnus Egerstedt. Permissive barrier certificates for safe stabilization using sum-of-squares. In *2018 Annual American Control Conference (ACC)*, pages 585–590, 2018.

[176] Andrew Clark. Verification and synthesis of control barrier functions. In *60th IEEE Conference on Decision and Control (CDC)*, pages 6105–6112, 2021.

[177] Ellie Pond and Matthew Hale. Fast verification of control barrier functions via linear programming. *arXiv preprint arXiv:2212.00598*, 2022.

[178] Zhiyuan Cai, Huanhui Cao, Wenjie Lu, Lin Zhang, and Hao Xiong. Safe multi-agent reinforcement learning through decentralized multiple control barrier functions. *arXiv preprint arXiv:2103.12553*, 2021.

[179] Haitong Ma, Jianyu Chen, Shengbo Eben, Ziyu Lin, Yang Guan, Yangang Ren, and Sifa Zheng. Model-based constrained reinforcement learning using generalized control barrier function. In *2021 IEEE/RSJ International Conference on Intelligent Robots and Systems (IROS)*, pages 4552–4559, 2021.

[180] Mitchell Black, Mrdjan Jankovic, Abhishek Sharma, and Dimitra Panagou. Future-focused control barrier functions for autonomous vehicle control. In *2023 American Control Conference (ACC)*, 2023, to appear.

[181] Mitchell Black, Ehsan Arabi, and Dimitra Panagou. A fixed-time stable adaptation law for safety-critical control under parametric uncertainty. In *2021 European Control Conference (ECC)*, pages 1328–1333, 2021.

[182] Mitchell Black, Ehsan Arabi, and Dimitra Panagou. Fixed-time parameter adaptation for safe control synthesis. *Automatica*, 2022, under review.

[183] Mitchell Black and Dimitra Panagou. Safe control design for unknown nonlinear systems with koopman-based fixed-time identification. In *IFAC World Congress*, 2023, to appear.

[184] Mitchell Black, Georgios Fainekos, Bardh Hoxha, Danil Prokhorov, and Dimitra Panagou. Safety under uncertainty: Tight bounds with risk-bounded control barrier functions. *arXiv preprint arXiv:numbers*, 2022.

[185] Mitchell Black and Dimitra Panagou. Adaptation for validation of a consolidated control barrier function based control synthesis. *arXiv preprint arXiv:2209.08170*, 2022.

[186] Mitchell Black and Dimitra Panagou. Consolidated control barrier functions: Synthesis and online verification via adaptation. *Submitted to IEEE Trans. on Automatic Control*, 2023, under review.

[187] R. A. Freeman and P. V. Kokotovic. Inverse optimality in robust stabilization. *SIAM Journal on Control and Optimization*, 34(4):1365–1391, 1996.

[188] F. Blanchini. Set invariance in control. *Automatica*, 35(11):1747 – 1767, 1999.

[189] Mitchell Black, Kunal Garg, and Dimitra Panagou. A quadratic program based control synthesis under spatiotemporal constraints and non-vanishing disturbances. In *2020 59th IEEE Conference on Decision and Control (CDC)*, pages 2726–2731, 2020.

[190] Mrdjan Jankovic and Mario Santillo. Collision avoidance and liveness of multi-agent systems with cbf-based controllers. In *2021 60th IEEE Conference on Decision and Control (CDC)*, pages 6822–6828, 2021.

[191] Rajesh. Rajamani. *Vehicle Dynamics and Control*. Springer US, 2012.

[192] Jason Kong, Mark Pfeiffer, Georg Schildbach, and Francesco Borrelli. Kinematic and dynamic vehicle models for autonomous driving control design. In *2015 IEEE Intelligent Vehicles Symposium (IV)*, pages 1094–1099, 2015.

[193] Mario Santillo and Mrdjan Jankovic. Collision free navigation with interacting, non-communicating obstacles. In *2021 American Control Conference (ACC)*, pages 1637–1643, 2021.

[194] Fernando Castaneda, Jason J Choi, Bike Zhang, Claire J Tomlin, and Koushil Sreenath. Gaussian process-based min-norm stabilizing controller for control-affine systems with uncertain input effects and dynamics. In *2021 American Control Conference (ACC)*, pages 3683–3690. IEEE, 2021.

[195] He Yuqing and Han Jianda. Generalized point wise min-norm control based on control lyapunov functions. In *2007 Chinese Control Conference*, pages 404–408. IEEE, 2007.

[196] Thomas Gurriet, Mark Mote, Andrew Singletary, Petter Nilsson, Eric Feron, and Aaron D. Ames. A scalable safety critical control framework for nonlinear systems. *IEEE Access*, 8:187249–187275, 2020.

[197] Yuxiao Chen, Mrdjan Jankovic, Mario Santillo, and Aaron D Ames. Backup control barrier functions: Formulation and comparative study. In *2021 60th IEEE Conference on Decision and Control (CDC)*, pages 6835–6841, 2021.

[198] Brett T. Lopez, Jean-Jacques E. Slotine, and Jonathan P. How. Robust adaptive control barrier functions: An adaptive and data-driven approach to safety. *IEEE Control Systems Letters*, 5(3):1031–1036, 2021.

[199] Lennart Ljung. *System identification : theory for the user*. Information and science. Prentice-Hall, Englewood Cliffs, NJ, 1987.

[200] Marc. Bodson. *Adaptive control: stability, convergence, and robustness*. Prentice Hall advanced reference series. Prentice Hall, 1989.

[201] P.O. Arambel and G. Tadmor. Identifiability and persistent excitation in full matrix fraction parameter estimation. *Automatica*, 33(4):689–692, 1997.

[202] Tony Roskilly and Rikard Mikalsen. *Marine systems identification, modeling and control*. Butterworth-Heinemann, 2015.

[203] Veronica Adetola and Martin Guay. Finite-time parameter estimation in adaptive control of nonlinear systems. *IEEE Transactions on Automatic Control*, 53(3):807–811, 2008.

[204] Gilbert Strang. *Introduction to Linear Algebra*. Wellesley-Cambridge Press, 5 edition, 2016.

[205] Sergey Parsegov, Andrey Polyakov, and Pavel Shcherbakov. Nonlinear fixed-time control protocol for uniform allocation of agents on a segment. pages 7732–7737, 12 2012.

[206] David G Luenberger. *Optimization by vector space methods*. Decision and control. Wiley, New York, NY, 1969.

[207] Randal W. Beard. Quadrotor dynamics and control. Technical report, 2008.

[208] N. Sydney, B. Smyth, and D. A. Paley. Dynamic control of autonomous quadrotor flight in an estimated wind field. In *52nd IEEE Conference on Decision and Control*, pages 3609–3616, 2013.

[209] Nguyen Khoi Tran, Eitan Bulka, and Meyer Nahon. Quadrotor control in a wind field. In *2015 International Conference on Unmanned Aircraft Systems (ICUAS)*, pages 320–328. IEEE, 2015.

[210] Y. Guo, B. Jiang, and Y. Zhang. A novel robust attitude control for quadrotor aircraft subject to actuator faults and wind gusts. *IEEE/CAA Journal of Automatica Sinica*, 5(1):292–300, 2018.

[211] Zahra Marvi and Bahare Kiumarsi. Safety planning using control barrier function: A model predictive control scheme. In *2019 IEEE 2nd Connected and Automated Vehicles Symposium (CAVS)*, pages 1–5, 2019.

[212] Richard Cheng, Gábor Orosz, Richard M Murray, and Joel W Burdick. End-to-end safe reinforcement learning through barrier functions for safety-critical continuous control tasks. In *Proceedings of the AAAI Conference on Artificial Intelligence*, volume 33, pages 3387–3395, 2019.

[213] Angela P. Schoellig, Clemens Wiltsche, and Raffaello D'Andrea. Feed-forward parameter identification for precise periodic quadrocopter motions. In *2012 American Control Conference (ACC)*, pages 4313–4318, 2012.

[214] Mouhyemen Khan, Munzir Zafar, and Abhijit Chatterjee. Barrier functions in cascaded controller: Safe quadrotor control. In *2020 American Control Conference (ACC)*, pages 1737–1742, 2020.

[215] Kunal Garg and Dimitra Panagou. Characterization of domain of fixed-time stability under control input constraints. In *2021 American Control Conference (ACC)*, pages 2272–2277, 2021.

[216] Mrdjan Jankovic. Robust control barrier functions for constrained stabilization of nonlinear systems. *Automatica*, 96:359–367, 2018.

[217] Steven L Brunton, Bingni W Brunton, Joshua L Proctor, and J Nathan Kutz. Koopman invariant subspaces and finite linear representations of nonlinear dynamical systems for control. *PloS one*, 11(2):e0150171, 2016.

[218] Behdad Davoudi, Ehsan Taheri, Karthik Duraisamy, Balaji Jayaraman, and Ilya Kolmanovsky. Quad-rotor flight simulation in realistic atmospheric conditions. *AIAA Journal*, 58(5):1992–2004, 2020.

[219] Dingjiang Zhou and Mac Schwager. Vector field following for quadrotors using differential flatness. In *2014 IEEE International Conference on Robotics and Automation (ICRA)*, pages 6567–6572, 2014.

[220] I. Blake and W. Lindsey. Level-crossing problems for random processes. *IEEE Trans. on Information Theory*, 19(3):295–315, 1973.

[221] Mitchell Black, Georgios Fainekos, Bardh Hoxha, Danil Prokhorov, and Dimitra Panagou. Safety under uncertainty: Tight bounds with risk-aware control barrier functions. In *2023 International Conference on Robotics and Automation (ICRA)*, 2023, to appear.

[222] Ioannis Karatzas and Steven E. Shreve. *Brownian Motion and Stochastic Calculus*. Springer New York, NY, second edition edition, 1998.

[223] Bernt Øksendal. *Stochastic Differential Equations: An Introduction with Applications*. Springer, sixth edition edition, 2003.

[224] Ernesto Kofman, José A. De Doná, and Maria M. Seron. Probabilistic set invariance and ultimate boundedness. *Automatica*, 48(10):2670–2676, 2012.

[225] Harold J. Kushner. *Stochastic Stability and Control*, volume 33 of *Mathematics in Science and Engineering*. Elsevier, 1967.

[226] Kelvin Shuangjian Zhang, Gabriel Peyré, Jalal Fadili, and Marcelo Pereyra. Wasserstein control of mirror langevin monte carlo. In *Proceedings of 33rd Conference on Learning Theory*, volume 125, pages 3814–3841, 09–12 Jul 2020.

[227] Aaron D. Ames, Xiangru Xu, Jessy W. Grizzle, and Paulo Tabuada. Control barrier function based quadratic programs for safety critical systems. *IEEE Trans. on Automatic Control*, 62(8):3861–3876, 2017.

[228] Martin Treiber, Ansgar Hennecke, and Dirk Helbing. Congested traffic states in empirical observations and microscopic simulations. *Phys. Rev. E*, 62:1805–1824, Aug 2000.

[229] Mokhtar S Bazaraa, Hanif D Sherali, and Chitharanjan M Shetty. *Nonlinear programming: theory and algorithms*. John Wiley & Sons, 2013.

[230] Dimitri P Bertsekas. Convexification procedures and decomposition methods for nonconvex optimization problems. *Journal of Optimization Theory and Applications*, 29(2):169–197, 1979.

[231] Mahyar Fazlyab, Santiago Paternain, Victor M. Preciado, and Alejandro Ribeiro. Prediction-correction interior-point method for time-varying convex optimization. *IEEE Transactions on Automatic Control*, 63(7):1973–1986, 2018.

[232] Joseph Breeden and Dimitra Panagou. Robust control barrier functions under high relative degree and input constraints for satellite trajectories. *Automatica*, (to be published) 2023.

[233] Wei Xiao and Calin Belta. Control barrier functions for systems with high relative degree. 2019.

[234] Mrdjan Jankovic, Mario Santillo, and Yan Wang. Multi-agent systems with cbf-based controllers – collision avoidance and liveness from instability. *arXiv preprint arXiv:2207.04915*, 2022.

[235] Thomas F. Coleman and Danny C. Sorensen. A note on the computation of an orthonormal basis for the null space of a matrix. *Mathematical Programming*, 29:234–242, 6 1984.

[236] Shengbo Wang, Kaibo Shi, Tingwen Huang, et al. Suboptimal safety-critical control for continuous systems using prediction-correction online optimization. *arXiv preprint arXiv:2203.15305*, 2022.

[237] Hassan K Khalil and JW Grizzle. *Nonlinear systems*, volume 3. Prentice hall Upper Saddle River, NJ, 2002.

[238] Wei Xiao and Calin Belta. High-order control barrier functions. *IEEE Transactions on Automatic Control*, 67(7):3655–3662, 2022.

[239] Joseph Breeden and Dimitra Panagou. Predictive control barrier functions for online safety critical control. *arXiv preprint arXiv:2204:00208*, 2022.

[240] Devansh Agrawal, Ruichang Chen, and Dimitra Panagou. Gatekeeper: Safety critical control of nonlinear systems with limited perception in unknown and dynamic environments. *arXiv preprint arXiv:2211.14361*, 2022.

[241] Mohit Srinivasan, Samuel Coogan, and Magnus Egerstedt. Control of multi-agent systems with finite time control barrier certificates and temporal logic. In *2018 IEEE Conference on Decision and Control (CDC)*, pages 1991–1996, 2018.

[242] Kunal Garg, Alvaro A Cardenas, and Ricardo G Sanfelice. Sampling-based computation of viability domain to prevent safety violations by attackers. In *2022 IEEE Conference on Control Technology and Applications (CCTA)*, pages 720–725. IEEE, 2022.

[243] Sander Tonkens and Sylvia Herbert. Refining control barrier functions through hamilton-jacobi reachability. In *2022 IEEE/RSJ International Conference on Intelligent Robots and Systems (IROS)*, pages 13355–13362, 2022.

[244] Hadi Ravanbakhsh and Sriram Sankaranarayanan. Learning control lyapunov functions from counterexamples and demonstrations. *Autonomous Robots*, 43:275–307, 2019.

[245] Andrew J Taylor, Victor D Dorobantu, Hoang M Le, Yisong Yue, and Aaron D Ames. Episodic learning with control lyapunov functions for uncertain robotic systems. In *2019 IEEE/RSJ International Conference on Intelligent Robots and Systems (IROS)*, pages 6878–6884. IEEE, 2019.